URANIUM (VI) INTERACTIONS WITH MINERAL SURFACES: CONTROLLING FACTORS AND SURFACE COMPLEXATION MODELLING

A thesis submitted in fulfilment of the requirements for the award of the degree of

DOCTOR OF PHILOSOPHY

from the

UNIVERSITY OF NEW SOUTH WALES

by

Timothy Ernest Payne, MEnvStud

SCHOOL OF CIVIL AND ENVIRONMENTAL ENGINEERING

August 1999

ACKNOWLEDGEMENTS

I am indebted to Professor T. David Waite who supervised this thesis, and is largely responsible for the systematic approach to sorption studies which has been adopted. I am also grateful to Dr James Davis of the United States Geological Survey, who has played a major role in the development of surface complexation modelling, and provided many valuable suggestions for the U sorption study. The financial support of the United States Nuclear Regulatory Commission for much of the work is also acknowledged.

The experimental work was carried out at the Lucas Heights Research Laboratories of the Australian Nuclear Science and Technology Organisation (ANSTO). I gratefully acknowledge the support of ANSTO for this PhD project. Particular credit is due to Peter Duerden and Dr Peter Airey who have directed the Koongarra natural analogue study and have provided great personal encouragement. ANSTO provides an excellent environment for research, and many ANSTO friends have made valuable contributions to the study. I particularly thank Dr Greg Lumpkin, whose skills with the AEM provided some key data about the association of U with mineral surfaces. Other ANSTO personnel deserving special mention include Robert Edis, David Garton, Robin Lowerson, and the dedicated staff of the ANSTO library.

I am grateful to my wife Narelle, who has endured countless days of my absence on account of this thesis. Without her love, patience and support this work would have foundered long before its completion.

DEDICATION

This thesis is dedicated to the memory of Charles George Payne.

ABSTRACT

The objective of the work described in this thesis was to improve the scientific basis for modelling the migration of U in the sub-surface environment. The project involved:

- studying the sorption of U on model minerals (Georgia kaolinite and ferrihydrite) in laboratory experiments
- carrying out experimental studies of U sorption on complex natural substrates
- studying the mechanisms influencing U retardation in the natural environment, including transformation processes of iron oxides
- identifying chemical factors which control U sorption on model and natural substrates
- developing a mechanistic model for U sorption on ferrihydrite and kaolinite using the surface complexation adsorption model , and
- assessing and modelling the effect of complexing ligands on uranyl adsorption.

Uranium (VI) sorption on geological materials is influenced by a large number of factors including: pH, ionic strength, partial pressure of CO_2, adsorbent loading, total amount of U present, and the presence of inorganic and organic ligands. The sorption of UO_2^{2+} typically increases with increasing pH (the 'low pH sorption edge') up to about pH 7. In systems equilibrated with air, there is a sharp decrease in sorption above this pH value (the 'high pH edge'), due to strong complexation between uranyl and carbonate.

The adsorption model being used for ferrihydrite is a surface complexation model with a diffuse double layer, and both strong and weak sites for U sorption. Based on the analysis of EXAFS data, the U surface complexes were modelled as mononuclear bidentate surface complexes of the form $(>FeO_2)UO_2^0$. Ternary surface complexes involving carbonate with the form $(>FeO_2)UO_2CO_3^{2-}$ were also required for the best simulation of U sorption data. There was a slight decrease in U sorption on ferrihydrite in systems that contained sulfate. It was necessary to consider competition between UO_2^{2+} and SO_4^{2-} for surface sites, as well as complexation

between UO_2^{2+} and SO_4^{2-} to model the data. The presence of citrate considerably reduced U sorption and caused dissolution of ferrihydrite. Complexation of citrate with both uranyl and ferric ions was taken into account in modelling this system. The model required the optimisation of the formation constant for a postulated mixed metal (U/Fe/citrate) aqueous complex. Humic acid increased U uptake at pH values below 7, with little effect at higher pH values.

In terms of the amount of U sorbed per gram of adsorbent, U uptake on kaolinites KGa-1 and KGa-1B was much weaker than U uptake on ferrihydrite under similar experimental conditions. Electron microscope examination showed that titanium-rich impurity phases played a major role in the sorption of U by these standard kaolinites. A relatively simple model for uranyl sorption on the model kaolinites was able to account for U sorption under a wide range of experimental conditions. The model involved only three surface reactions on two sites (>TiOH and >AlOH), with a non-electrostatic surface complexation model. The relative amounts of the sites were estimated from AEM results. Precipitation was taken into account in modelling the experimental data obtained with high U concentrations. The effects of sulfate and citrate on U sorption by kaolinite were also assessed and modelled. Sulfate had a small effect on U sorption, which may be explained by aqueous complexation. Citrate had a greater effect, and this was not wholly explained by the formation of aqueous U-citrate complexes. The most likely explanation would also involve competition for surface sites between U and citrate.

Uranyl uptake on ferrihydrite was greatly increased by the presence of phosphate. This was not due to precipitation, and was attributed to the formation of a ternary surface complex with a proposed structure of $(>FeO_2)UO_2PO_4^{3-}$. The log K value for the formation of this complex was optimised using FITEQL. Phosphate also increased uptake of uranyl on kaolinite, and this was also attributed to the formation of ternary uranyl phosphate surface species.

Uranium sorption on weathered schist samples from the vicinity of the Koongarra U deposit in northern Australia was generally similar to the model minerals (in terms of the effects of pH, ionic strength, total U, etc). Many

experiments with the natural materials were spiked with an artificial U isotope (^{236}U), which allowed adsorption (of ^{236}U) and desorption (of ^{238}U) to be distinguished, and provided a means of estimating the 'labile' or 'accessible' portion of the natural U content. A significant advantage of this method is that (unlike chemical extractions) it does not rely on the assumptions about the phases extracted by 'selective' reagents.

Uranium sorption experiments were also carried out with Koongarra samples which had been treated with citrate / dithionite / bicarbonate (CDB) reagent to remove iron oxides. Uranium sorption was greatly decreased by the CDB extraction, which reduced the surface area of the samples by about 30-40%. To further elucidate the impact of iron minerals on U mobility in the natural environment, the transformation of synthetic ferrihydrite containing adsorbed natural uranium was studied. In these experiments, the ferrihydrite was partially converted to crystalline forms such as hematite and goethite. The uptake of an artificial uranium isotope (^{236}U) and the leaching of ^{238}U from the samples were then studied in adsorption / desorption experiments. The transformation of ferrihydrite to crystalline minerals substantially reduced the ability of the samples to adsorb ^{236}U from solution. Some of the previously adsorbed ^{238}U was irreversibly incorporated within the mineral structure during the transformation process. Therefore, transformation of iron minerals from amorphous to crystalline forms provides a possible mechanism for uranium immobilisation in the groundwater environment. In considering the overall effect on U migration, this must be balanced against the reduced ability of the transformed iron oxide to adsorb U.

The experiments with the model and natural substrates demonstrated that trace impurities (such as Ti-oxides) and mineral coatings (such as ferrihydrite) can play a dominant role in U adsorption in both environmental and model systems. Although the various substrates had different affinities for adsorbing U, the effects of chemical factors, including pH, ionic strength, and carbonate complexation were similar for the different materials. This suggests that a mechanistic model for U sorption on model minerals may eventually be incorporated in geochemical transport models, and used to describe U sorption in the natural environment.

ABBREVIATIONS

AEM	analytical electron microscopy
ANSTO	Australian Nuclear Science and Technology Organisation
ARAP	Alligator Rivers Analogue Project
ASARR	Analogue Studies in the Alligator Rivers Region
BET	Brunauer-Emmett-Teller method (a surface area technique)
CDB	citrate-dithionite-bicarbonate reagent
CIT	citrate ion
CMS	Clay Minerals Society
DDLM	diffuse double layer model
EDX	energy dispersive x-ray spectroscopy
EXAFS	extended X-ray absorption fine structure
FITEQL	computer program for determining chemical equilibrium constants
KGa-1, KGa-1B	kaolinite standards from Georgia, USA
HA	humic acid
HFO	hydrous ferric oxide (ferrihydrite)
KPA	kinetic phosphorescence analyser
MINTEQA2	a geochemical modelling computer program
NEA	Nuclear Energy Agency
OECD	Organisation for Economic Cooperation and Development
PRODEFA2	MINTEQA2 pre-processor (problem definition)
RCF	relative centrifugal force
SCM	surface complexation model
SEM	scanning electron microscope
SGMA	Stanford Generalised Model for Adsorption
TAO	Tamm's acid oxalate
TEM	transmission electron microscope
TOC	total organic carbon
TLM	triple layer model

Abbreviations (Continued)

USGS	United States Geological Survey
USNRC	United States Nuclear Regulatory Commission
WSOS/DOF	weighted sum of squares / degrees of freedom
XAFS	x-ray absorption fine structure
XRD	x-ray diffraction

CONTENTS

page

Acknowledgements i

Abstract ii

Abbreviations v

Contents vii

List of figures xiii

List of tables xxi

PART I. Background to this study of U sorption 1

1 INTRODUCTION 2

1.1 Overview 2

1.2 Context of this study 3

1.3 Koongarra study site 4

1.4 Approaches to modelling sorption in natural systems 6

2 SORPTION MECHANISMS AT THE SOLID-LIQUID INTERFACE 8

2.1 Historical perspective 8

2.2 Sorption isotherms 9

2.3 The development of geochemical and sorption modelling 13

2.4 The surface complexation model 15

2.5 Sorption models in contaminant migration and radioactive waste disposal 18

2.6 Aims of the Koongarra uranium sorption study 20

3 AQUEOUS URANIUM SPECIATION AND MINERAL SOLUBILITY 21
3.1 Sources of thermodynamic data 21
3.2 Uranium (VI) speciation 22
3.3 Solubility considerations 30

4 URANIUM SORPTION 40
4.1 Experimental studies of U sorption on single mineral phases 40
4.2 Models for U sorption on Fe-oxides 48
4.3 U sorption on complex geologic substrates 54
4.4 Developments between 1993 and 1998 56

PART II. Experimental studies of U sorption on model minerals and natural materials 59

5 EXPERIMENTAL METHODS FOR U SORPTION 60
5.1 Substrates for U sorption experiments 60
5.1.1 Model minerals 60
5.1.2 Koongarra substrates 61
5.2 Procedure for sorption experiments 62
5.3 Analytical techniques for dissolved U 65
5.4 Analytical electron microscopy 67
5.5 Reproducibility and sources of error in U sorption experiments 68
5.6 Sorption on container materials 70
5.7 Assessment of separation technique 71
5.8 Sample preparation for EXAFS 73

6 URANIUM (VI) UPTAKE ON FERRIHYDRITE 75

6.1 Kinetics of U sorption on ferrihydrite 75

6.2 Effect of experimental conditions on U sorption 77

6.2.1 pH and mass loading 77

6.2.2 Total U 79

6.2.3 Partial pressure of CO_2 and ionic strength 83

6.3 Comparison of U sorption with co-precipitation 86

6.4 Effect of complexing ligands on U sorption by ferrihydrite 87

6.4.1. Phosphate 88

6.4.2 Humic acid 98

6.4.3 Sulfate 100

6.4.4 Citrate 101

7 URANIUM (VI) UPTAKE ON KAOLINITE 106

7.1 Effect of pH and mass loading 106

7.2 Effect of total U – evidence for precipitation 108

7.3 Effect of ionic strength 113

7.4 Comparison of U sorption behaviour of KGa-1, KGa-1B and ferrihydrite 114

7.5 Effect of complexing ligands on U sorption by kaolinite 116

7.5.1 Phosphate 116

7.5.2 Humic acid, sulfate and citrate 121

7.6 Effect of trace inpurities on U sorption by kaolinite 124

7.6.1 U sorption in mixed ferrihydrite / kaolinite systems 124

7.6.2 Analytical electron microscopy 124

7.6.3 Implications of the presence of anatase in Georgia kaolinites 131

7.7 Summary of experiments with kaolinite 131

8 URANIUM(VI) SORPTION ON SUB-SURFACE MATERIAL FROM THE KOONGARRA WEATHERED ZONE 133

8.1 Sample characterisation by SEM 134

8.2 Sequential extraction study 135

8.3 Total and added U in experimental systems 141

8.4 Results of U sorption experiments with Koongarra substrates 143

8.5 Effect of the CDB extraction on U sorption by Koongarra materials 151

8.6 Isotope exchange and leaching results 154

8.7 Comparison of natural substrates with ferrihydrite and kaolinite 158

8.8 Discussion 159

9 TRANSFORMATION PROCESSES OF IRON MINERALS 161

9.1 Aim of the transformation study 161

9.2 Experimental study of transformation of Fe-oxides and effects on adsorbed U 162

9.3 Change in sorption behaviour of iron minerals of increasing crystallinity 164

9.4 Evidence for incorporation of ^{238}U in the transformed iron oxides 167

9.5 Amount of ^{238}U and Fe released from synthetic iron oxides by the TAO reagent 171

9.6 Conclusions and implications of transformation study 172

PART III. Uranium (VI) sorption on model minerals - controlling factors and surface complexation modelling.....173

10 FACTORS INFLUENCING U UPTAKE ON MINERAL SURFACES 174

10.1 Parameters having a major influence on U sorption..... 174

10.2 Comparison with previous studies 177

11 A SURFACE COMPLEXATION MODEL FOR U(VI) SORPTION BY FERRIHYDRITE..... 183

11.1 Structure of U surface complexes on ferrihydrite 183

11.2 Surface complexation model of U sorption..... 188

11.3 Implementation of the model using MINTEQA2 193

11.4 Comparison of model computations with experimental data 198

11.5 Surface speciation of adsorbed U..... 206

11.6 Modelling U sorption on ferrihydrite in the presence of sulfate 207

11.7 Modelling U sorption on ferrihydrite in the presence of citrate 218

11.8 Summary of SCM for U sorption on ferrihydrite 230

12 MODELLING INTERACTIONS OF URANYL WITH MODEL KAOLINITES..... 232

12.1 Modelling approach..... 232

12.2 Stoichiometry and sites of surface reactions 233

12.3 Modelling U sorption on kaolinite with FITEQL and MINTEQA2 237

12.4 Ternary uranyl – carbonato surface complex..... 248

12.5 Comparison of model output with experimental data 250

12.6 Surface speciation of adsorbed U..... 255

12.7 Comparison of U sorption models..... 257

12.8 Modelling the effect of sulfate and citrate on U sorption by kaolinite..260

12.9 Summary of SCM for U sorption on kaolinite 262

13 URANYL SORPTION IN PHOSPHATE-CONTAINING SYSTEMS 264
13.1 Possible mechanisms of surface interactions between uranyl and phosphate 264
13.2 Modelling the U-phosphate-ferrihydrite system 269
13.3 Modelling the U-phosphate-kaolinite system 281
13.4 Modelling the effects of phosphate on U sorption by model minerals 287

PART IV. Conclusions 289

14 OUTCOMES OF THE U-SORPTION STUDY 290
14.1 Conclusions 290
14.1.1 Chemical influences on uranium sorption 290
14.1.2 Modelling of U adsorption 290
14.1.3 Sorption phenomena in the natural environment 293
14.2 Summary of the work 294
14.3 Possible further work 295

PART V. References and appendices 297

15 REFERENCES 298

Appendix 1 U-sorption data-sets
Appendix 2 List of selected publications by the author
Appendix 3 Journal papers based on the U sorption data contained in this thesis

LIST OF FIGURES

1.1 Simplified cross section through the Koongarra No.1 orebody.....4

2.1 Hypothetical data and possible linear isotherm for U sorption.....10

2.2 Possible Langmuir isotherm and Freundlich isotherm for the hypothetical U sorption data shown in Figure 2.1.....12

3.1 Uranium speciation in 0.1 mol/L $NaNO_3$ in equilibrium with air. (ΣU = 1 μmol/L).....25

3.2 Uranium speciation in 0.1 mol/L $NaNO_3$ in equilibrium with air. (ΣU = 100 μmol/L).....25

3.3 Uranium speciation in 0.1 mol/L $NaNO_3$ in equilibrium with a gas phase having a pCO_2 of 0.01 atm. ΣU = 1 μmol/L.....26

3.4 Uranium speciation in 0.1 mol/L $NaNO_3$ in equilibrium with a gas phase having a pCO_2 of $10^{-6.5}$ atm. ΣU = 1 μmol/L.....26

3.5 U(VI) speciation in (0.1 mol/L $NaNO_3$ + 0.01 mol/L Na_2SO_4) in equilibrium with air. ΣU = 1 μmol/L.....27

3.6 U(VI) speciation in 0.1 mol/L $NaNO_3$, with added PO_4 of 100 μmol/L. ΣU = 1 μmol/L (precipitation excluded).....28

3.7 Uranium speciation in the presence of citrate a) 0.01 mol/L b) 100 μmol/L. In each case, total U is 1 μmol/L.....29

3.8 Aqueous U in systems controlled by the solubility of $UO_2(OH)_2$ using various log K values for the reaction $UO_2(OH)_2 \Leftrightarrow UO_2^{2+} + 2OH^-$.....33

3.9 Solubility of U(VI) in phosphate-containing systems (ΣP=100 μmol/L) with various solubility limiting phases.....35

3.10 Uranium mineral solubility calculations in systems used for solubility determinations of $UO_2HPO_4.4H_2O$ by Moskvin *et al.* [1964] and systems used for measurements of U complexation by Dongarra and Langmuir [1980]..... 37

4.1 Experimental data for U sorption on goethite [Tripathi, 1983] and model curves.....51

List of Figures (continued)

4.2 Implementation of the U sorption model of Hsi and Langmuir [1985].....52

4.3 The model of Tripathi [1983] predicts a shift of the U sorption edge to lower pH values with a decrease in ionic strength.....53

5.1 Calibration curve for KPA in the concentration range below 25 ppb 66

5.2 Uranium α-spectrum obtained after adsorption/desorption experiment 67

5.3 Reproducibility of data obtained for U sorption on ferrihydrite 69

5.4 U uptake on polypropylene centrifuge tubes in presence and absence of ferrihydrite 71

5.5 Uranium associated with solid determined by centrifugation or by membrane filtration using pre-conditioned membranes 73

6.1 Kinetics of U sorption on ferrihydrite at pH 5.0 and 4.5.....76

6.2 U(VI) sorption on ferrihydrite – effect of pH and mass loading of ferrihydrite78

6.3 U(VI) sorption to ferrihydrite for a range of ΣU.....80

6.4 U sorption data on ferrihydrite presented as 'isotherms', obtained by re-calculating selected data points from Figure 6.3 81

6.5 U uptake as a function of ΣU at fixed pH values of 4.5 and 5.25.....82

6.6 U sorption isotherms for systems shown in Figure 6.5 83

6.7 Effect of pCO_2 on sorption of U by ferrihydrite.....84

6.8 Effect of ionic strength on U sorption edges.....85

6.9 Comparison of the percentage of U bound by ferrihydrite in sorption and co-precipitation experiments 87

6.10 Effect of phosphate on the sorption of uranium by ferrihydrite 90

6.11 Effect of phosphate and ΣU on U(VI) adsorption by ferrihydrite 91

6.12 Effect of phosphate and ionic strength on U(VI) adsorption by ferrihydrite .....
.....92

6.13 U(VI) adsorption by ferrihydrite: effect of ionic strength on the high-pH edge in the presence and absence of phosphate.....93

6.14 Uptake of phosphate (100 μmol/L) on ferrihydrite in the presence of

List of Figures (continued)

various ΣU 94

6.15 Percentage of U adsorbed by ferrihydrite as a function of ΣU - effect of added total phosphate of 100 μmol/L 96

6.16 Adsorption isotherm for U in phosphate-free systems, and in systems containing fixed total phosphate of 100 μmol/L 97

6.17 Percentage of P adsorbed as a function of ΣP in uranyl free systems at pH 5.25 and 8.25 97

6.18 Effect of humic acid on the sorption of uranyl by ferrihydrite 99

6.19 Effect of sulfate on U adsorption by ferrihydrite 101

6.20 Effect of 0.01 mol/L citrate on U sorption by ferrihydrite 103

6.21 Dissolved Fe in the U sorption experiments shown in Figure 6.20 103

6.22 Adsorption of U in systems containing insufficient citrate to entirely dissolve the ferrihydrite. The resulting sorption curve exhibits an unusual 'double-hump'104

6.23 Amount of dissolved Fe in the U sorption experiments shown in Figure 6.22 105

7.1 Uranium sorption on kaolinite (KGa-1B) – pH dependence and effect of solid mass loading 107

7.2 Uranium sorption on kaolinite (KGa-1B) – pH dependence and effect of solid mass loading for ΣU of 10 μmol/L 108

7.3 Effect of ΣU on U sorption by kaolinite KGa-1B 109

7.4 Uranium uptake on KGa-1 - effect of ΣU 110

7.5 Total dissolved U in experiments with kaolinite 110

7.6 Uranium associated with solid phases in experiments with kaolinite (4g/L) and with ΣU of 1 mmol/L 112

7.7 U-uptake by kaolinite KGa-1B - effect of ionic strength 114

7.8 U-uptake by kaolinites KGa-1 and KGa-1B 115

7.9 pH-edges for U uptake on kaolinite and ferrihydrite for various ΣU 117

7.10 Effect of phosphate on U uptake by kaolinite (KGa-1B) 117

7.11 Comparison of U sorption on ferrihydrite and kaolinite (KGa-1B) in the presence of added phosphate 119

List of Figures (continued)

7.12 Effect of phosphate on U uptake by kaolinite (KGa-1B)..... 120

7.13 Uranium and P uptake by kaolinite at mass loadings of 4 g/L and 40 g/L..... 120

7.14 Effect of humic acid on U uptake by kaolinite (KGa-1B)..... 121

7.15 Effect of sulfate and citrate ligands on U sorption by KGa-1B kaolinite ... 122

7.16 Effect of the addition of citrate on U sorption by kaolinite 123

7.17 Adsorption of U on ferrihydrite, kaolinite and a mixed substrate comprising both minerals..... 125

7.18 Electron microscopy results for U sorption experiments with KGa-1 kaolinite 128

7.19 Electron microscopy results for anatase..... 129

7.20 Electron microscopy results for U-rich precipitate 130

8.1 Uptake of ^{236}U spike as a function of pH in experiments with Koongarra natural substrates..... 144

8.2 Uptake of ^{236}U on the W1 sample at two mass loadings 145

8.3 Effect of increased total U on the results of U sorption experiments with the natural substrates..... 147

8.4 Effect of elevated pCO_2 on sorption experiments with the Koongarra natural substrates..... 148

8.5 Effect of ionic strength on U sorption by Koongarra natural substrates.... 150

8.6 Results of sorption experiments with Koongarra W2c substrate in systems with and without added magnesium 151

8.7 Effect of the CDB treatment on the adsorption of U by the Koongarra samples 153

8.8 Summary isotope exchange plots for adsorption / desorption experiments with Koongarra natural substrates in air-equilibrated systems..... 155

8.9 Summary isotope exchange plots for adsorption / desorption experiments for Koongarra natural substrates in systems equilibrated with 1% CO_2 156

List of Figures (continued)

8.10 Comparison of U-sorption data on natural substrates with data for model minerals (kaolinite and ferrihydrite)..... 159

9.1 X-ray diffraction patterns (Cu Kα radiation) for Fe-oxide samples A, B and C 165

9.2 Adsorption of ^{236}U on Fe-oxide samples A, B and C 166

9.3 Adsorption of ^{236}U and desorption of ^{238}U on Fe-oxide samples A, B and C 168

9.4 Isotope exchange between ^{238}U and ^{236}U in experiments with Fe-oxide sample C 170

11.1 Structure of uranyl salts and complexes 185

11.2 Model structure for the surface complex of UO_2^{2+} on ferrihydrite 187

11.3 U(VI) sorption on ferrihydrite for a range of ΣU. Curves were calculated using MINTEQA2 with the suite of surface reactions in Table 11.2 199

11.4 Effect of solid mass loading on U sorption by ferrihydrite. Model curves were calculated using the reactions in Table 11.2 200

11.5 Uranium adsorption by ferrihydrite at two partial pressures of CO_2. Curves were calculated using MINTEQA2 and the reactions in Table 11.2..... 201

11.6 Effect of ionic strength on U sorption. Curves calculated using the reactions in Table 11.2..... 202

11.7 U sorption as a function of ΣU at pH values of 4.5 and 5.25 and corresponding model curve. 203

11.8 U sorption isotherms – comparison of experimental data and model calculations. 204

11.9 Surface speciation of adsorbed U(VI). 206

11.10 Modelling the effect of sulfate on U sorption by ferrihydrite..... 209

11.11 Data and model for sulfate adsorption on ferrihydrite 210

11.12 Modelling of sulfate adsorption on ferrihydrite assuming a high surface site density of 0.875 mol site/ mol Fe 215

11.13 Experimental data and models for U sorption on ferrihydrite in absence and presence of sulfate 217

List of Figures (continued)

11.14 Structure of complexes in the UO_2^{2+} / Fe^{3+} / citrate system 218

11.15 Dissolution of ferrihydrite in the presence and absence of citrate 221

11.16 Modelling U adsorption in the Fe-U-citrate system (ΣCIT = 0.01 mol/L) using Model 1 (containing only Fe^{3+}–citrate and UO_2^{2+}-citrate complexes) 223

11.17 Modelling U adsorption in the Fe-U-citrate system. Experimental results for ΣCIT = 100 μmol/L with simulation results from Model 1 (containing only Fe-citrate and U-citrate complexes) 224

11.18 Sorption data for the U-citrate-ferrihydrite system together with predictions for Model 2 227

11.19 Computed uranium surface and aqueous speciation for the system shown in Figure 11.17 228

11.19 Possible structure for the mixed metal complex uranyl aluminium citrate 229

12.1 Adsorption edges and Kurbatov plots for uranyl adsorption on ferrihydrite and KGa-1B kaolinite 235

12.2 Schematic structure of kaolinite, showing the alternating silica-type and gibbsite-type layers 236

12.3 FITEQL model for KGa-1 data 245

12.4 FITEQL model for KGa-1B data 245

12.5 MINTEQA2 model for KGa-1 data over the pH range 2 to 10, using the sorption reactions for the TiOH and AlOH sites shown in Table 12.3 247

12.6 MINTEQA2 model for KGa-1B data 247

12.7 Model simulations for sorption data with KGa-1, showing the effect of the ternary uranyl carbonate complex on the >TiOH site 249

12.8 Model simulations for sorption data with KGa-1B showing the effect of the ternary uranyl carbonate complex on the >TiOH site 249

12.9 Model simulation of KGa-1 uranyl sorption data using reactions in Table 12.4 251

List of Figures (continued)

12.10 Model simulation of KGa-1B uranyl sorption data using reactions in Table 12.4. 251

12.11 Modelling the effect of variable mass loading of the KGa-1B kaolinite in experiments with total U of 1 μmol/L..... 252

12.12 Modelling the effect of variable mass loading of the KGa-1B kaolinite in experiments with total U of 10 μmol/L..... 252

12.13 Modelling the effect of ionic strength on U sorption by the KGa-1B kaolinite253

12.14 Simulation results for experiments with ΣU of 100 μmol/L and 1 mmol/L. In the experiments with ΣU of 1 mmol/L, sorption plays no role in removing U from solution..... 254

12.15 Surface speciation of adsorbed U in system containing 4 g/L of KGa-1B, with ΣU of 1 μmol/L..... 255

12.16 Surface speciation of adsorbed U in system containing 4 g/L of Kga-1B, with ΣU of 10 μmol/L 256

12.17 Modelling the effect of sulfate (10 mmol/L) on U sorption by kaolinite 260

12.18 Modelling the effect of citrate on U sorption. In this simulation, only U-citrate complexation was considered..... 261

13.1 U uptake on ferrihydrite with added ΣP of 100 μmol/L. The model curves are calculated on the basis that U removal from solution occurs by precipitation of $(UO_2)_3(PO_4)_2$..... 266

13.2 Modelling the ferrihydrite-phosphate system with FITEQL 272

13.3 Modelling U sorption on ferrihydrite in the presence of phosphate with a ternary uranyl-phosphate surface complex 276

13.4 Sorption model including ternary surface uranyl phosphate complex as implemented by MINTEQA2 for ΣU of 1 μmol/L 277

13.5 Sorption model including ternary surface uranyl phosphate complex as implemented by MINTEQA2 for ΣU of 100 μmol/L 278

13.6 Simulation of U adsorption in the presence of phosphate at fixed pH of 4.5. (I = 0.02)..... 280

13.7 Experimental data and model simulations from Figure 13.6 in isotherm

format 280

13.8 The model predicts that the presence of uranyl should slightly increase the uptake of phosphate on the ferrihydrite surface 281

13.9 Model simulation of the uptake of phosphate on Georgia kaolinite KGa-1B 283

13.10 Modelling U uptake on kaolinite (4 g/L) in the presence and absence of 100 μmol/L phosphate (ΣU = 1 μmol/L), with a ternary surface complex on the titanol site 286

13.11 Modelling U uptake on kaolinite (40 g/L) in the presence and absence of 100 μmol/L phosphate (ΣU = 1 μmol/L) 287

LIST OF TABLES

3.1 Formation constants for aqueous complexes....23

4.1 Summary of models for U sorption on goethite 50

7.1 Chemical composition of KGa-1 and KGa-1B kaolinite samples.... 115

7.2. Summary of AEM data for samples from U-sorption experiments.... 127

8.1 Summary of Koongarra samples used in sorption experiments 135

8.2 Extraction scheme used for Koongarra samples.... 137

8.3 Elemental distribution in Koongarra samples as determined by a sequential extraction 139

8.4 Uranium distribution and $^{234}U/^{238}U$ in Koongarra samples as determined by a sequential extraction.... 140

8.5 Representative calculations of total U in experimental systems, with ΣU estimated by TAO –extraction.... 142

8.6 Estimates of accessible natural ^{238}U in Koongarra substrates by isotope exchange compared with estimates from TAO-extraction.... 157

8.7 Summary of experimental conditions for the data sets compared in Figure 8.10 158

9.1 Percentages of Fe and ^{238}U dissolved by TAO from iron mineral samples 171

10.1 Factors which have been shown to influence U sorption on ferrihydrite and kaolinite.... 175

10.2 Ligand effects on U sorption.... 176

11.1 Ferrihydrite surface reactions and correction of log K values to I = 0 192

11.2 Surface reactions expressed in terms of MINTEQ components 197

11.3 FITEQL input for modelling sulfate sorption on ferrihydrite 212

11.4 Reactions in the Fe^{3+} – UO_2^{2+} – citrate system.... 220

12.1 Kaolinite model input parameters.... 238

List of Tables (continued)

12.2 Tableau for FITEQL input for experimental data with KGa-1B 242

12.3 Derivation of average values of log K for surface complexes..... 244

12. 4 Surface complexation reactions used to described the experimental sorption data obtained with model kaolinites KGa-1 and KGa-1B..... 250

12.5 Suite of uranyl surface co-ordination reactions and associated log K values for kaolinite [Turner and Sassman, 1996]..... 257

12.6 Comparison of models for U sorption on ferrihydrite and model kaolinites..... 259

13.1 Input file for FITEQL optimisation of proposed ternary uranyl-phosphate surface complexes on ferrihydrite..... 275

PART I.

Background to this study of U sorption

1 INTRODUCTION

1.1 Overview

The migration of pollutants in the sub-surface environment has become a topic of increasing concern as the community has become more aware of the adverse consequences of groundwater pollution. However, many of the processes influencing elemental mobility in geological systems are poorly understood. Some geochemical processes (such as precipitation or adsorption) have been studied in simple systems, but theoretical modelling and the application of the results to more complex systems has been limited.

The objective of this work is to advance the understanding of the mobility of uranium in groundwater environments. The sorption[1] and retention of U on mineral surfaces is central to the study. Uranium migration in the weathered zone of the Koongarra uranium deposit (Northern Australia) will be given particular attention. Whilst this system is the focus of much of the work, the intention is to develop insights and models which are broadly applicable to pollutant migration in natural waters. In particular, the work involved the use of the Surface Complexation Model (SCM) for trace metal uptake on mineral surfaces. In the SCM, sorption reactions are written as chemical reactions between aqueous species and surface sites, with equilibrium constants assigned to each reaction.

The approach involved laboratory experiments aimed at identifying the main factors controlling the sorption of U by model minerals (kaolinite and ferrihydrite). Further sorption data were then collected for complex natural substrates, with the objective of studying the mechanisms influencing U retardation in the natural environment. The effects of transformations of iron oxide minerals were then examined. Detailed consideration was given to developing a SCM for U sorption on

[1]The term 'sorption' is used in this thesis for surface reactions which involve both adsorption (uptake) and desorption (release) of solutes. The terms 'adsorption' and 'desorption' are used when specific meaning is intended.

the model minerals in simple systems with an inert background electrolyte ($NaNO_3$). These models were then extended to include the effects of various ligands including carbonate, phosphate, citrate and sulfate.

1.2 Context of this study

This study was undertaken as part of the ASARR (Analogue Studies in the Alligator Rivers Region) project. In this project, the Koongarra uranium ore body was studied as a 'natural analogue' for processes relevant to the performance of nuclear waste repositories. The ultimate aim was to develop quantitative models for the migration of radionuclides after their disposal in a waste repository. As it is not generally possible to study the behaviour of anthropogenic radionuclides in the environment, natural systems exhibiting some of the properties of radioactive waste, such as uranium deposits, have been selected for the study of many of the relevant processes. This approach allows processes occurring over long geological timescales, and of considerable spatial extent to be studied. The applications of natural analogues for nuclear waste repositories have been extensively reviewed [Miller *et al.*, 1994].

Detailed studies of Koongarra have been undertaken since its value as a natural analogue was recognised in the early 1980's. This work has been reviewed by several authors (e.g. Airey [1986], Duerden [1992]). During these studies, the requirement for predictive models of U sorption became apparent to the participants in the project. The present work developed out of that specific need. However, the results should be broadly applicable in many situations involving sorption interactions on mineral surfaces.

In order to more fully set the scene for the study, the knowledge of metal sorption that existed when the work commenced is summarised in Chapter Two, which surveys the development of models of sorption on geologic materials which had occurred until about 1990. The next two chapters focus on the aqueous chemistry of U and previous studies of U uptake on mineral surfaces. This material forms the basis of knowledge upon which the present study aims to build.

1.3 Koongarra study site

Koongarra is located in the Alligator Rivers region of the Northern Territory about 225 km east of Darwin. There are two major ore bodies, located in a zone of deeply dipping Cahill formation schists adjacent to a reverse fault. The No.1 ore body shows extensive evidence of radionuclide movement in groundwaters, and one of its main geological features is the characteristic 'dispersion fan'. This is an area containing elevated concentrations of U and other radionuclides which have been transported from the zone of original U accumulation (the primary ore zone) into the surrounding rocks (Figure 1.1).

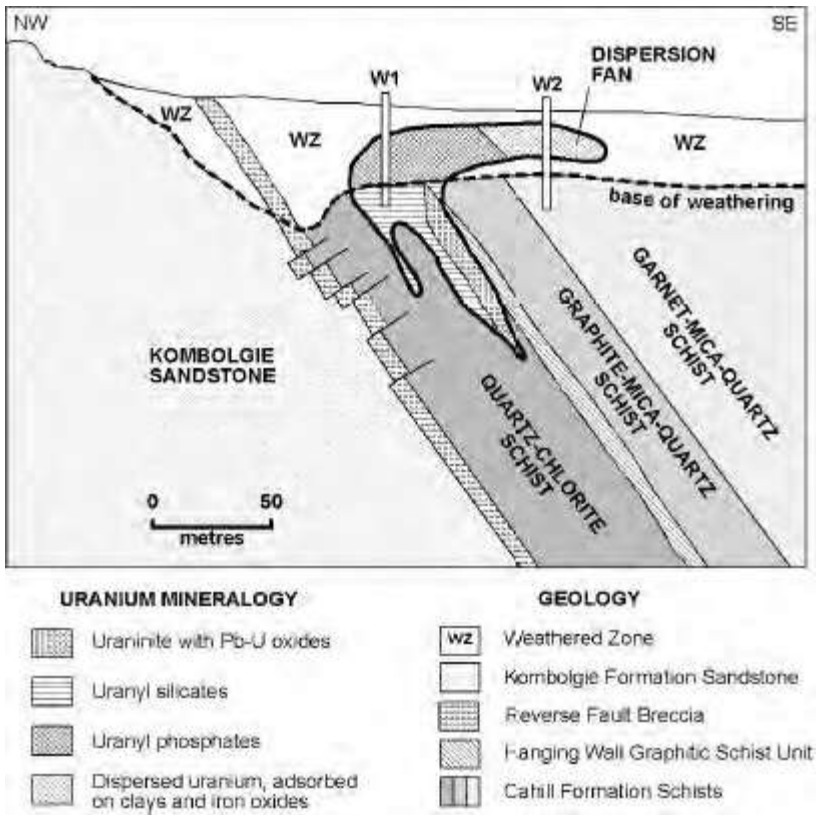


FIGURE 1.1 Simplified cross-section through the Koongarra No. 1 orebody showing the geology and distribution of uranium minerals (from Snelling [1994]). The approximate locations of boreholes W1 and W2 from which cores were taken for sorption experiments are shown. Borehole W7 is further downgradient from W2.

The evolution of the Koongarra No.1 ore body has been discussed in detail by Snelling [1994]. The primary ore body formed about 1800 million years ago when U originating from basement granitoids and sediments was precipitated after a sequence of adsorption and redox reactions, which probably involved graphite, chlorite and pyrite. The primary mineralisation occurs in a series of uraninite lenses, which extend from the base of the weathered zone (about 25 - 30 m below the surface) to about 100 m depth. The mobilisation of U away from the primary ore body occurred when the weathering front, which is slowly moving downwards, intersected the primary U mineralisation. This event occurred between 1 and 3 million years ago [Airey *et al.*, 1986]. Groundwater then dissolved uraninite and other minerals in the primary ore and transported the U into the surrounding rocks. This process has continued to the present day and has led to the formation of the dispersion fan (Figure 1.1).

The Koongarra reverse fault forms the contact with the Kombolgie sandstone formation. There is apparently some transport of water across the fault, which has led to in-situ alteration of primary U minerals near the fault. On the down-gradient side of the ore-body, primary U mineralisation is adjacent to a graphitic confining layer. In the weathered zone immediately above the primary ore, where groundwater U concentrations are relatively high, uranyl phosphate minerals (such as saleeite ($Mg(UO_2)_2(PO_4)_2.8\text{-}10H_2O$) are abundant. Further down-gradient in the dispersion fan, where U concentrations are lower, adsorption of U on Fe-oxides and clays appears to be important in reducing U mobility.

Iron oxides and clay minerals occur throughout the weathered zone and are a product of the weathering of chlorite, which is a major component of the host chlorite schists [Murakami *et al.*, 1994]. During weathering, the iron-rich chlorite is converted to vermiculite then kaolinite in a sequence of reactions which also leads to the precipitation of iron minerals including goethite, hematite and ferrihydrite. Ferrihydrite is an amorphous Fe-oxide with a very high specific surface area, and is believed to play a major role in adsorbing U in the weathered part of the system [Yanase *et al.*, 1991]. While ferrihydrite is known to strongly adsorb numerous trace metals, it is thermodynamically unstable and readily converts to other Fe-oxides such as hematite

and goethite [Schwertmann and Cornell, 1991] which have a lower surface area and sorption capacity. Clay minerals such as kaolinite may also be important sorbing phases in the Koongarra system [Giblin, 1980].

1.4 Approaches to modelling sorption in natural systems

A number of approaches to modelling pollutant interactions with complex geological materials have been advocated. It has recently been suggested that these may be broadly categorised into two types of strategies: 'top-down' and 'bottom-up' [Altmann, 1997]. In the 'top-down' strategy, the behaviour of the complex system is modelled on the basis of bulk system parameters (e.g. the surface area and cation exchange capacity of the geologic substrate). In this approach, no attempt is made to quantify the relative importance of constituent mineral phases, such as clays, iron-oxides or humic materials.

In the alternative 'bottom-up' strategy, one identifies all significant components of the system and attempts to systematically understand and model the interactions of each component with the pollutant(s) of interest. This involves detailed study of both the mineralogy of the solid phase and the chemistry of the aqueous phase. Inevitably some simplifications are required in this approach, because the number of potential interactions is unlimited. However, this strategy is more fundamental and appears more generally applicable than the 'top-down' method which necessarily relates to specific geological materials and groundwater chemistry.

In order to apply the more fundamental 'bottom-up' approach to modelling U migration in the Koongarra system, the initial focus will be on minerals which are thought to play major roles in this environment. Iron minerals are a logical starting point, because previous work has suggested that iron minerals (particularly ferrihydrite) dominate the initial sorption of uranyl from groundwaters at Koongarra [Payne and Waite, 1991; Yanase *et al.*, 1991], and at the nearby Ranger uranium deposit [Lowson *et al.*, 1986]. However, the relative importance of various minerals in sorbing U in the Koongarra system has not yet been conclusively demonstrated. Giblin [1980] considered that U sorption on kaolinite was an important concentration

mechanism for U in the Alligator Rivers Region deposits.

The questions being addressed in this study include:

- What are the factors controlling U sorption by ferrihydrite and kaolinite, which are being used as model mineral sorbents?
- What are the similarities and differences between U sorption on complex natural materials such as soils, compared to the model minerals?
- Can U sorption on the model minerals in simple electrolytes be modelled adequately by the SCM for a range of aqueous conditions?
- Can the SCM model be extended to include the effects of complexing ligands?
- What is the role of other processes (apart from sorption), such as mineral transformations?

2 SORPTION MECHANISMS AT THE SOLID-WATER INTERFACE

2.1 Historical perspective

It is only in comparatively recent years that the adsorption of pollutants on natural mineral surfaces has become the subject of intense quantitative study. Thirty years ago, the knowledge of sorption processes at the mineral / water interface was very limited. In a standard geochemistry textbook of the late 1960's, Krauskopf [1967] observed that:

> Despite the importance of adsorption and ion exchange, our knowledge regarding them is still largely empirical. So many variables are involved, and some are so difficult to control, that experiments all too often lead only to broad generalisations rather than to specific rules...we shall often mention adsorption and ion exchange as important geologic processes, but we shall seldom be able to predict just what their effects should be in particular situations.

By 1990 the situation was much more advanced. In that year, a detailed account of the application of the SCM to the sorption of a wide range of metal ions and anions on hydrous iron (III) oxide surfaces was published [Dzombak and Morel, 1990]. These authors reviewed the remarkable advance of the SCM in less than three decades, during which time the model had been developed with contributions from numerous workers in a range of disciplines.

Given the vast advances since the late 1960's, it is instructive to review the developments in geochemistry and aquatic surface chemistry which have transformed the understanding of sorption processes from descriptive generalisations to the status of a quantitative predictive model.

2.2 Sorption isotherms

It should not be concluded from the foregoing that nothing was known about sorption phenomena before 1967. However, the existing information was fragmentary and qualitative. Many workers utilised 'isotherms', such as the Langmuir or Freundlich isotherms, to describe their sorption data. Isotherms were originally derived to describe adsorption of gases at the gas / solid interface, and consisted of plots of the fractional coverage (θ) of a surface against the partial pressure (p) of the adsorbate in the gas phase (at constant temperature, hence described as an 'isotherm'). In aqueous chemistry, isotherms are plots of sorption density (Γ) against dissolved sorbate concentration at constant temperature. In order to be of value, it is essential that pH also be constant.

The most simple isotherm is one in which the sorption density is proportional to the dissolved sorbate concentration. This is the *linear* isotherm:

$$\Gamma = K_d[J] \qquad (2.1)$$

where [J] is the concentration of an adsorbing solute J and K_d is the *distribution coefficient*.

If two simple experiments of U sorption on a mineral phase were carried out, and both Γ and [U] were measured, one might obtain the points indicated as P1 and P2 on Figure 2.1. A linear isotherm with a K_d value of 10^5 mL/g seems to provide a fair description of the two data points[1]. However, further experimentation at a higher U concentration might result in a data point (P3) which is not on the linear isotherm. Although this example is hypothetical, it reflects a typical trend in sorption data, where sorption tends to be relatively weaker at higher metal concentrations and a linear isotherm is not applicable.

[1] The commonly encountered units for Γ (mol/g) and K_d (mL/g) are used in this thesis.

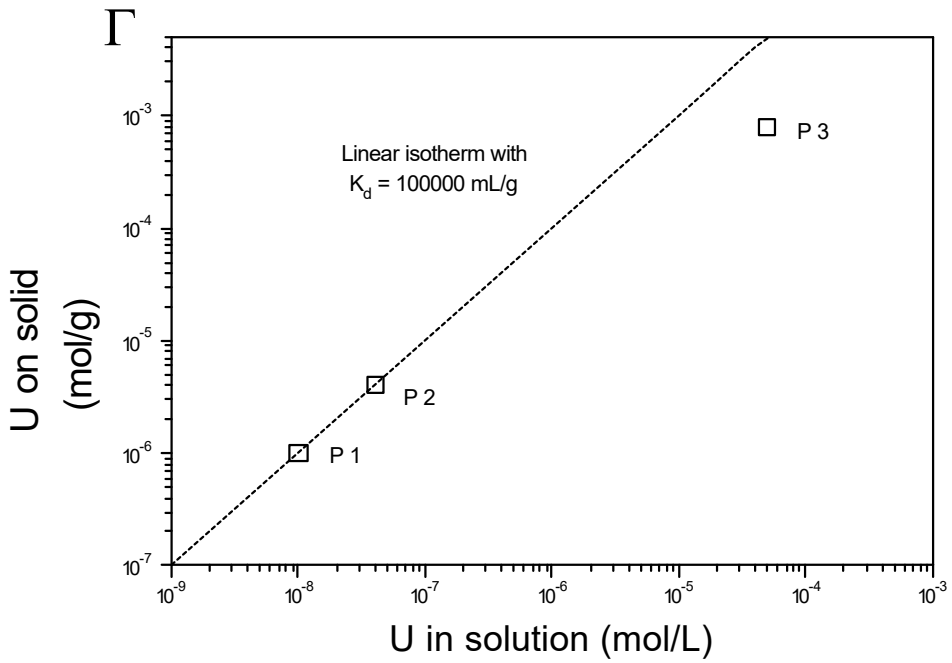


FIGURE 2.1 Hypothetical data and possible linear isotherm for U sorption.

Numerous more complex isotherms have been used to describe experimental adsorption data. The Langmuir isotherm, developed In the early 1900's, was derived by considering the reaction:

$$> S - + J \Leftrightarrow > S - J \qquad (2.2)$$

where >S- is a surface site and >S-J represents J adsorbed on the surface site. The expression for the equilibrium constant of this reaction is:

$$K_{ads} = \frac{[> S - J]}{[> S -][J]} \qquad (2.3)$$

where the square brackets imply concentration (mol/L). The total concentration of

surface sites [$>S_{TOT}$] is given by:

$$[>S_{TOT}] = [>S\text{–}] + [>S-J] \tag{2.4}$$

The ratio between occupied and total surface sites is:

$$\frac{\Gamma}{\Gamma_{MAX}} = \frac{[>S-J]}{[S_{TOT}]} = \frac{[>S-J]}{[>S\text{–}] + [>S-J]} \tag{2.5}$$

Dividing both top and bottom of this equation by [>S-J], then substituting (from Equation 2.3)

$$\frac{[>S-J]}{[>S\text{–}]} = K_{ads}[J] \tag{2.6}$$

and rearranging, Equation 2.5 becomes

$$\Gamma = \Gamma_{MAX}\left(\frac{K_{ads}[J]}{1+K_{ads}[J]}\right) \tag{2.7}$$

which is the well-known Langmuir isotherm. This equation becomes linear at low [J], corresponding to a linear isotherm with a K_d equal to $\Gamma_{MAX}.K_{ads}$. At high [J], the value of Γ approaches Γ_{MAX}. These features will be observed on Figure 2.2.

Another common isotherm is the Freundlich isotherm, which has the equation:

$$\Gamma = A[J]^{\alpha} \tag{2.8}$$

with A and α adjustable constants. The Freundlich isotherm is linear on a log-log graph (Figure 2.2), and is often regarded as being merely a fitting equation.

However, it can be derived by assuming that the free energy of adsorption (ΔG_{ads}) increases linearly with the log concentration of adsorbate [Morel and Hering, 1993]. Adsorption data for trace metals tend to correspond more closely to the Freundlich isotherm than to other simple isotherms [Dzombak and Morel, 1990], usually with the value of α being slightly below 1.0, indicating a decrease in sorption affinity with increasing sorption density. The linear isotherm is a special case of the Freundlich isotherm with α = 1.0.

Numerous other isotherms have been developed and applied in environmental chemistry, and an excellent review of the subject, together with a discussion of the errors inherent in estimating the associated adjustable parameters is given by Kinniburgh [1986].

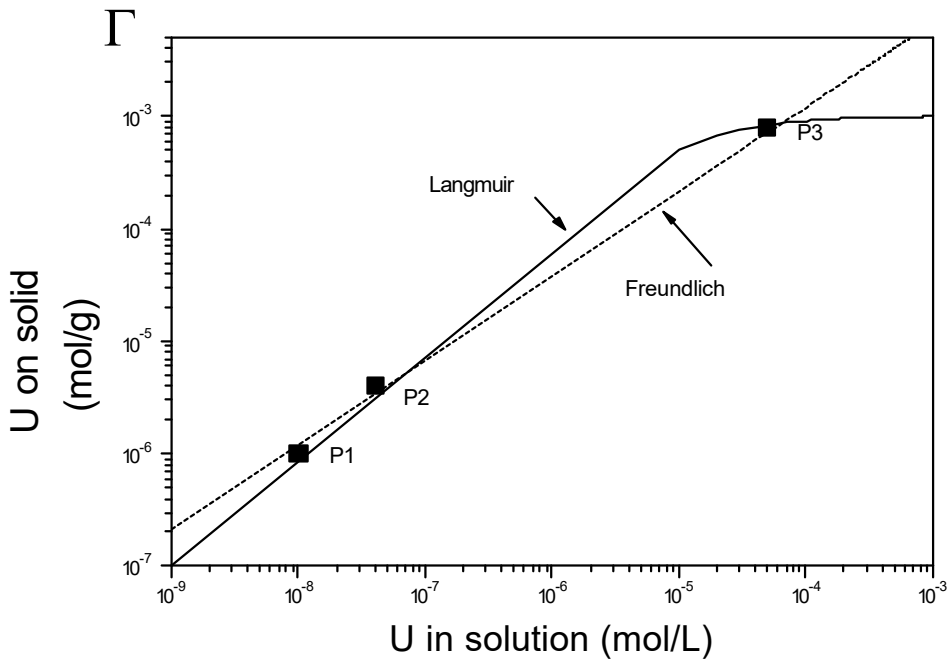


FIGURE 2.2 Possible Langmuir isotherm (Γ_{MAX} = 10^{-3} mol/L) and Freundlich isotherm (α = 0.75) for the hypothetical U sorption data shown in Figure 2.1.

2.3 The development of geochemical and sorption modelling

The simple partitioning approaches outlined above do not involve modelling of surface chemistry, and no mechanisms for surface reactions are postulated. However, most reactions at the solid / liquid interface are strongly dependent on factors such as pH, ionic strength and the presence of competing ions. Thus, isotherm expressions, which simply relate the amount of metal adsorbed to the total metal concentration in solution, would require a large amount of data and an unwieldy set of fitting parameters to model sorption over a wide range of conditions [Dzombak and Morel, 1990]. As observed by Bowden *et al.* [1977], the limitations of simple models such as the Langmuir or Freundlich isotherms become apparent if 'fixed' parameter values must be changed to accommodate changes in pH or salt concentration, or the presence of competing or complexing ligands. A more systematic approach to aquatic sorption modelling necessitates a mechanistic understanding of adsorption reactions, and more broadly, of aquatic chemistry in general.

Aquatic chemistry has developed rapidly in the past few decades, during which many authors have placed aquatic reactions (including sorption) in a systematic thermodynamic framework, emphasising the application of the principles of chemical equilibrium to reactions in the aqueous phase. The mathematical description of aquatic systems is based on defining a set of *components*, which are the chemical building blocks from which the stoichiometry of the system can be uniquely formulated (e.g. UO_2^{2+}, H^+, CO_3^{2-}, NO_3^-). Chemical *species* are formed from the components, each having a particular stoichiometric formula (e.g. $UO_2NO_3^+$). The components are not necessarily important species in the system of interest, and are chosen for computational simplicity. For example, in many natural groundwaters HCO_3^- is the main carbonate-containing species, but it is conveniently expressed in terms of its components H^+ and CO_3^{2-}. Conservation of mass requires that the total amounts of elements in a system are fixed - this provides the essential *mole balance constraint*. Finally, there are

chemical *mass-action* equations involving various species in a system, with associated equilibrium constants, such as:

$$UO_2^{2+} + NO_3^- \Leftrightarrow UO_2NO_3^+ \qquad (2.9)$$

In this case, K is defined by

$$K = \frac{\{UO_2NO_3^+\}}{\{UO_2^{2+}\}\,\{NO_3^-\}} \qquad (2.10)$$

where the round brackets denote activity. For this example, the numerical value of log K (I=0) is 0.3.

Thus, each aquatic system is described by a number of linear mass balance equations and non-linear mass-action equations. This type of approach permits multi-component chemical equilibrium problems to be formulated, and the resulting system of equations is readily solved iteratively using a computer. A recent text [Morel and Hering, 1993] summarises the current status of aquatic chemistry in a systematic fashion.

An important development in the last few decades has been the acquisition of the thermodynamic data required to compute solution / mineral equilibria and chemical speciation in aqueous solutions. This has been a continuing process, which has occurred at different rates for various elements. Many chemical equilibria involving elements forming simple aqueous ions have been well established for some decades. However, the aqueous chemistry of ions with complex solution chemistry (such as UO_2^{2+}) has developed much more slowly, despite the expenditure of considerable effort. In the late 1980's all existing thermodynamic data for U species was assessed by an international team of scientists under the auspices of the NEA [Grenthe *et al*., 1992].

During the 1970's and 1980's a number of computer codes for calculating the equilibrium distribution of species in a system (often including adsorbed species) were developed. These are generally based on the type of mathematical formalism

outlined above, and include such codes as MINTEQA2, MINEQL, PHREEQE and EQ3/6 [Waite, 1989]. While these codes greatly simplify the computations, satisfactory results can only be obtained if care is taken to ensure the accuracy and internal consistency of the associated thermodynamic databases. This is not a simple matter, as the databases supplied with the programs are inevitably dated, often poorly documented and in some instances, simply erroneous. For example, it has been recently pointed out that MINTEQA2 has numerous errors in the organic ligand section of its database due to the incorrect formulation of the reactions in terms of system components [Serkiz *et al.*, 1996].

Another significant advance has been the development of FITEQL [Herbelin and Westall, 1994], which is a computer program for determining chemical equilibrium constants from experimental data. This program can be used for estimating log K values for sorption reactions and other reactions of interest in experimental systems (see Chapter 11).

2.4 The surface complexation model

The evolution of the SCM may be traced back to detailed studies of the origin of surface charge on oxides which appeared in the 1960's. In a key paper, Parks and DeBruyn [1962] concluded that the surface charge on hematite develops as a result of reactions of surface hydroxyl groups, which they expressed as:

$$> Fe(OH)_2^+ \quad \Leftrightarrow \quad > FeO_2^- + 2H^+ \qquad (2.11)$$

These investigations were continued in subsequent years, and the theory was generalised to other oxide surfaces [Parks, 1967].

The SCM emerged during the early 1970's, and was distinguished as being the "surface complex formation model in which hydrous (metal) oxide surface groups >Me-OH are treated...as complex forming species" [Stumm *et al.*, 1976].

In this model, the acidity constant K_{a1}^{app} for the deprotonation reaction of a surface site:

$$> XOH_2^+ \quad \Leftrightarrow \quad > XOH^0 + H^+ \tag{2.12}$$

is given by

$$K_{a1}^{app} = \frac{[XOH^0]\{H^+\}}{[> XOH_2^+]} \tag{2.13}$$

The activity coefficients of the surface species are assumed to be equal. K_{a1}^{app} is an apparent equilibrium constant because it is dependent on the surface charge. There are analogous equations for the removal of the second proton:

$$> XOH^0 \quad \Leftrightarrow \quad > XOH^- + H^+ \tag{2.14}$$

$$K_{a2}^{app} = \frac{[XOH^-]\{H^+\}}{[> XOH^0]} \tag{2.15}$$

As formulated by Stumm and co-workers, K_{a1}^{app} is related to the intrinsic acidity constant of the acid group in a hypothetical completely chargeless surrounding K_{a1}^{int} by

$$K_{a1}^{int} = K_{a1}^{app} \exp\left(\frac{-F\Psi}{RT}\right) \tag{2.16}$$

where Ψ is the effective potential difference between the surface site and the bulk solution. Equation 2.16 demonstrates that the SCM accounts for the contribution of the surface charge to the free energy of deprotonation. More generally, the SCM takes into account the effect of surface charge on the sorption of any species, in which case Equation 2.16 becomes

$$K^{int} = K^{app} \exp\left(\frac{\Delta Z\, F\, \Psi}{RT}\right) \qquad (2.17)$$

where ΔZ is the change in the charge of the surface species due to the sorption reaction.

In order to apply Equation 2.17, an expression for Ψ is required. Assuming the diffuse layer model for the solution side of the interface in a symmetrical electrolyte with a valence *Z*, the surface charge density σ (C/m^2) is related to the potential at the surface by:

$$\sigma = 0.1174 c^{1/2} \sinh (Z\, \Psi \times 19.46) \qquad (2.18)$$

where c is the molar electrolyte concentration [Dzombak and Morel, 1990]. The net charge on an oxide surface arises from proton transfer reactions together with surface coordination reactions by other cations and anions. The net charge density is given by

$$\sigma = F\, [\Gamma_H\, ^* \, - \, \Gamma_{OH}\, ^* + \sum (Z_M \Gamma_M\, ^*) + \sum (Z_A \Gamma_A\, ^*)] \qquad (2.19)$$

Here Γ^* is the sorption density (in mol/m^2), and Z_M and Z_A are the valences of the sorbing cations and anions. Equations 2.17 - 2.19 form the basis for the SCM with a diffuse double layer at the oxide surface.

Subsequent to the development of the basic SCM, a number of features have been refined, and there has been continuing debate over the description of the electrical double layer, for which at least five distinct models had emerged by 1980 [Westall and Hohl, 1980]. Many recent papers have adopted the diffuse double layer model [Dzombak and Morel, 1990], which was outlined above. The slightly more complex triple layer model [Davis *et al.*, 1978] is also commonly used in modelling trace metal sorption. A detailed discussion of two uranyl sorption models for iron

oxides that utilise double- or triple-layer SCM's is given in Section 4.2. In cases where the chemical contribution to the free energy of adsorption dominates over the electrostatic contribution, a simple non-electrostatic SCM may be justified. Davis and Kent [1990] have discussed the applications of the various double-layer models in surface complexation modelling.

As shown above, the key feature of the SCM is that electrostatic as well as chemical terms are incorporated in modelling sorption. Some of the originators of the SCM approach have provided comprehensive accounts of the SCM and its applications in aquatic chemistry and geochemistry [Stumm, 1992; Davis and Kent, 1990]. These authors provide many examples of models for the adsorption of trace metals (such as Cr, Cd, Cu, Zn, Pb and Ni) on simple oxides and other minerals.

Only a brief overview of the development of the SCM has been presented here, and a detailed account appears in Dzombak and Morel [1990]. These authors summarised the fundamental concepts of the SCM:

- Sorption on oxides takes place at specific coordination sites.
- Sorption reactions on oxides can be described quantitatively via mass law equations.
- Surface charge results from the sorption reactions themselves.
- The effect of surface charge on sorption can be taken into account by applying a correction factor derived from the electrical double layer theory to mass law constants for surface reactions.

2.5 Sorption models in contaminant migration and radioactive waste disposal

Given the progress in recent decades with the SCM approach and associated geochemical modelling, it might be reasonable to expect a rapid application of the SCM to predicting pollutant migration in the environment. In general, this has not yet occurred. This is partly due to the considerable data requirements of the SCM. For

each adsorbing metal and surface site type, a suite of possible surface reactions and associated formation constants is required. Assembling such a data set is a sizeable task. In general, the structure of surface complexes is unknown, hence the stoichiometry of surface reactions has been largely derived from guesswork and 'chemical intuition'. As will be shown in Chapter 4, this has led to a variety of surface complexes being suggested for similar adsorption reactions (e.g. the adsorption of UO_2^{2+} on Fe-oxide surfaces). The lack of structural information about surface complexes has not prevented the derivation of precise formation constants (log K values) for numerous postulated surface complexes, some of which are probably non-existent. In view of the data-requirements of the SCM, its application to complex natural systems is in its infancy.

Another problem restricting the adoption of the SCM in pollutant migration is its complexity, compared to the equations that are presently used to describe partitioning of contaminants between solid and aqueous phases in transport modelling. The 'constant K_d' approach has been widely applied, particularly in the context of nuclear waste disposal. In this case, the retardation of a pollutant front in simple porous media is given by:

$$\frac{\bar{v}}{\bar{v}_c} = 1 + \frac{\rho_b}{n} \bullet K_d \qquad (2.20)$$

where ρ_b is the bulk density, n the porosity, $\bar{v}$ the average linear velocity of the groundwater and $\bar{v}_c$ the velocity of the point on the concentration profile of the retarded constituent where the concentration is half that of the input concentration [Freeze and Cherry, 1979]. The K_d is defined by Equation 2.1, and a linear isotherm is therefore implicitly assumed. The ratio $\bar{v}/\bar{v}_c$ is the 'retardation factor' and represents the retardation of the movement of the pollutant relative to the flowing groundwater. It is understandable that simplified transport equations (such as Equation 2.20) have been widely used in contaminant modelling, given that the mechanistic sorption models such as the SCM are more complex and the required

data are lacking. Furthermore, many of the other parameter values in transport modelling are often poorly constrained (for example the value of $\bar{v}$) and some may consider that improvements to sorption modelling are therefore of rather academic interest.

However, applying a constant K_d value amounts to using a linear isotherm to describe sorption. As has already been shown, this is an excessively simple approach (see Figures 2.1 and 2.2) and in the context of radionuclide migration may result in predictions which are *non-conservative* (i.e. over-estimating retardation). If one only had the data points P1 and P2 (Figure 2.1) and assumed a constant K_d for U, then the extrapolation to higher U concentrations would lead to an overestimate of K_d and under-prediction of U migration.

An additional major shortcoming of the 'constant K_d ' approach is that the dependence of sorption on chemical factors is ignored. As will be shown, the sorption of species such as U is extremely sensitive to aqueous chemistry, and this needs to be accounted for in transport modelling.

2.6 Aims of the Koongarra uranium sorption study

The impetus for the commencement of the present work was the requirement to improve the modelling of radionuclide migration and to apply the results in repository safety assessment. The development and demonstration of surface complexation models for radionuclide sorption in the natural environment forms an important part of this effort. The natural analogue project at Koongarra provided an opportunity to study U sorption on a range of model and natural substrates, and to extend the results to a natural system. The aim was to demonstrate that a more sophisticated treatment of radionuclide sorption could be achieved, and that the results could be applied to the 'real world'. The ultimate goal was to increase confidence in predictions of radionuclide migration and the performance of radioactive waste repositories. The present work forms a part of that objective.

3 AQUEOUS URANIUM SPECIATION AND MINERAL SOLUBILITY

3.1 Sources of thermodynamic data

Since the 1950s, there have been numerous papers which have considered the aqueous speciation of U(VI) in various systems. The geochemical importance of U speciation was conclusively demonstrated in a classic paper by Hostetler and Garrels [1962]. Despite the uncertainty (or absence) of much of the relevant thermodynamic data, these authors were able to conclude that U(VI) is transported mainly in the form of highly stable uranyl di- and tri-carbonate complexes. They also devised a mechanism for the formation of carnotite ($K_2(UO_2)_2(VO_4)_2 .3H_2O$). In 1978, another key paper on the aqueous chemistry of U appeared [Langmuir, 1978], emphasising U speciation in natural waters. Although it was subsequently shown to be erroneous in some respects (particularly regarding the importance of U-phosphate complexes), this paper formed a basis for many subsequent studies, and allowed for experimental U sorption data to be interpreted quantitatively. Tripathi [1983] carried out an exhaustive review of the existing thermodynamic data for U, and applied the resulting thermodynamic data-base to modelling U(VI) sorption on goethite.

In the late 1980's all existing thermodynamic data for U was assessed by an international team of scientists under the auspices of the NEA [Grenthe *et al*., 1992]. This team reviewed and assessed over 500 relevant publications, and selected preferred values for a large number of thermodynamic constants. This was a complex undertaking, and not simply a matter of choosing the 'best' values from the individual publications. Relationships between the constants necessitated checking (and in many cases, re-calculating) thermodynamic constants to ensure internal consistency with other constants in the compilation. Despite the enormous effort invested in this exercise, some errors have been reported [Grenthe *et al*., 1995], and there are many areas of considerable uncertainty. While most of these relate to species which are not of major relevance to the present work, there are a few species (e.g. $UO_2(OH)_2^0$) for

which the uncertainty in existing thermodynamic data does affect speciation calculations.

When the work described in this thesis was partially completed, a paper describing some of the U sorption results and presenting a model for U sorption on ferrihydrite was published [Waite *et al.*, 1994]. The U speciation in this paper was based on the thermodynamic compilation of Grenthe *et al.* [1992], although there were some modifications, with some data obtained from Tripathi [1983]. The reaction:

$$UO_2^{2+} + 2OH^- \Leftrightarrow UO_2(OH)_2^0 \qquad (3.1)$$

was assigned a log K of 16.0, because Grenthe *et al.* [1992] only suggested an upper limit (<17.7). It should be noted that a revised value for this reaction was not offered by Grenthe *et al.* [1995], despite concerns expressed about the inadequacy of their 1992 value.

The widely accepted OECD/NEA data-base [Grenthe *et al.,* 1992] was adopted for the work described in this thesis, supplemented with other data only when necessary (e.g. for $UO_2(OH)_2^0$). Therefore, the thermodynamic data used in this thesis is consistent with Waite *et al.* [1994] and Grenthe *et al.* [1992] unless otherwise specified. The formation constants for aqueous complexes are summarised in Table 3.1.

3.2 Uranium(VI) speciation

Most of the experiments described in this thesis were undertaken in systems which were open to the atmosphere, with a background electrolyte of 0.1 mol/L $NaNO_3$. This ensured a constant ionic strength for the experiments, which is desirable unless ionic strength is itself the variable under investigation. Under these conditions, U is present in its +6 oxidation state, as the uranyl cation (UO_2^{2+}).

TABLE 3.1 Formation constants for aqueous complexes.

	log K (I = 0)
$UO_2^{2+} + H_2O \Leftrightarrow UO_2OH^+ + H^+$	-5.2
$UO_2^{2+} + 2H_2O \Leftrightarrow UO_2(OH)_{2,aq} + 2H^+$	-12.0
$UO_2^{2+} + 3H_2O \Leftrightarrow UO_2(OH)_3^- + 3H^+$	-20.0
$UO_2^{2+} + 4H_2O \Leftrightarrow UO_2(OH)_4^{2-} + 4H^+$	-33.0
$2UO_2^{2+} + H_2O \Leftrightarrow (UO_2)_2OH^{3+} + H^+$	-2.8
$2UO_2^{2+} + 2H_2O \Leftrightarrow (UO_2)_2(OH)_2^{2+} + 2H^+$	-5.63
$3UO_2^{2+} + 4H_2O \Leftrightarrow (UO_2)_3(OH)_4^{2+} + 4H^+$	-11.9
$3UO_2^{2+} + 5H_2O \Leftrightarrow (UO_2)_3(OH)_5^+ + 5H^+$	-15.56
$3UO_2^{2+} + 7H_2O \Leftrightarrow (UO_2)_3(OH)_7^- + 7H^+$	-31.0
$H_2O \Leftrightarrow OH^- + H^+$	-14.00
$UO_2^{2+} + CO_3^{2-} \Leftrightarrow UO_2CO_{3,aq}$	9.7
$UO_2^{2+} + 2CO_3^{2-} \Leftrightarrow UO_2(CO_3)_2^{2-}$	17.0
$UO_2^{2+} + 3CO_3^{2-} \Leftrightarrow UO_2(CO_3)_3^{4-}$	21.63
$2UO_2^{2+} + CO_3^{2-} + 3H_2O \Leftrightarrow (UO_2)_2CO_3(OH)_3^- + 3H^+$	-1.18
$H^+ + CO_3^{2-} \Leftrightarrow HCO_3^-$	10.33
$2H^+ + CO_3^{2-} \Leftrightarrow H_2CO_3^*$	16.68
$CO_{2(g)} + H_2O \Leftrightarrow H_2CO_3^*$	-1.47
$UO_2^{2+} + NO_3^- \Leftrightarrow UO_2NO_3^+$	0.3
$UO_2^{2+} + SO_4^{2-} \Leftrightarrow UO_2SO_{4,aq}$	3.15
$UO_2^{2+} + 2SO_4^{2-} \Leftrightarrow UO_2(SO_4)_2^{2-}$	4.14
$SO_4^{2-} + H^+ \Leftrightarrow HSO_4^-$	1.99
$UO_2^{2+} + PO_4^{3-} \Leftrightarrow UO_2PO_4^-$	13.23
$UO_2^{2+} + PO_4^{3-} + H^+ \Leftrightarrow UO_2HPO_{4,aq}$	19.59
$UO_2^{2+} + PO_4^{3-} + 2H^+ \Leftrightarrow UO_2H_2PO_4^+$	22.82
$UO_2^{2+} + PO_4^{3-} + 3H^+ \Leftrightarrow UO_2H_3PO_4^{2+}$	22.46
$UO_2^{2+} + 2PO_4^{3-} + 4H^+ \Leftrightarrow UO_2(H_2PO_4)_{2,aq}$	44.04
$UO_2^{2+} + 2PO_4^{3-} + 5H^+ \Leftrightarrow UO_2(H_2PO_4)(H_3PO_4)^+$	45.05
$PO_4^{3-} + H^+ \Leftrightarrow HPO_4^{2-}$	12.35
$PO_4^{3-} + 2H^+ \Leftrightarrow H_2PO_4^-$	19.55
$PO_4^{3-} + 3H^+ \Leftrightarrow H_3PO_{4,aq}$	21.70
$UO_2^{2+} + CIT^{3-} \Leftrightarrow UO_2CIT^-$	8.7[a]
$2UO_2^{2+} + 2\ CIT^{3-} \Leftrightarrow (UO_2)_2(CIT)_2^{2-}$	21.3[a]

From Waite *et al.* [1994] and Grenthe *et al.* [1992]

[a]CIT refers to the citrate ion. These data are from Smith and Martell [1993].

The speciation of U(VI) as a function of pH in systems exposed air (pCO_2 of $10^{-3.5}$ atm) is shown in Figure 3.1. The speciation of U(VI) was computed using the geochemical computer code MINTEQA2 [Allison *et al.*, 1990], having modified and updated its existing data-base (using the data in Table 3.1). The speciation was calculated for a typical experiment with total U (ΣU) of 10^{-6} mol/L in 0.1 mol/L $NaNO_3$.

Uranium speciation is dominated by a series of hydrolysed uranyl species, with uranyl carbonate complexes becoming dominant at high pH values. The computations described in this section differ slightly from Waite *et al.* [1994] because complexation with NO_3^- (which is a weak U(VI) complexant) was omitted in the 1994 paper. The $UO_2NO_3^+$ species is of some importance in $NaNO_3$ solutions below pH 7 (Figure 3.1).

At higher ΣU, polynuclear U complexes become more important (Figure 3.2). In this example, possible precipitation of solid U phases was excluded, although this was considered in the subsequent modelling of experimental results (and is discussed further below).

The speciation diagrams show that equilibration with atmospheric CO_2 plays a major role in determining U(VI) speciation. Due to the importance of carbonate speciation, some experiments were carried out in a glove box with an atmosphere containing an elevated pCO_2 of 10^{-2} atm., which is similar to many shallow groundwater environments. Under these conditions, carbonate complexes begin to dominate U speciation at lower pH values (Figure 3.3).

Some studies of U sorption reported in the literature have been carried out under nitrogen. If pCO_2 is zero, complexation of UO_2^{2+} with carbonate is absent. Figure 3.4 shows the results of calculations for systems where the pCO_2 is 1000 times below that of ordinary air. These calculations imply that incomplete exclusion of CO_2 will alter U-speciation, particularly at high pH values. It will be observed that $UO_2(OH)_3^-$ is dominant in part of the pH range in this system, and it would be even more dominant if carbonate was completely absent.

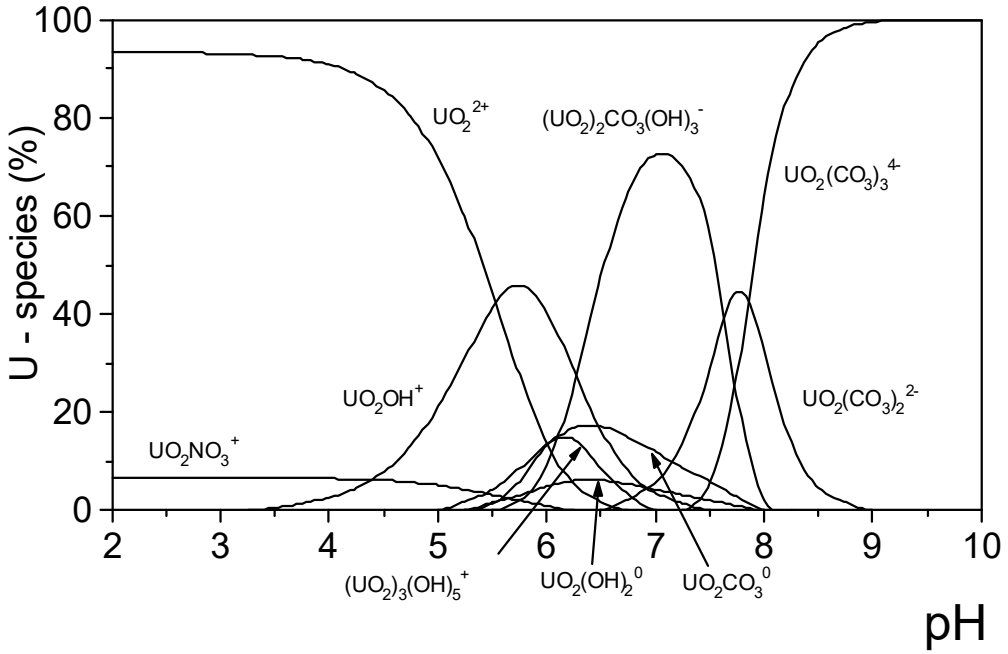


FIGURE 3.1 Uranium speciation in 0.1 mol/L $NaNO_3$ in equilibrium with air ($pCO_2 = 10^{-3.5}$ atm.). $\Sigma U = 1$ µmol/L.

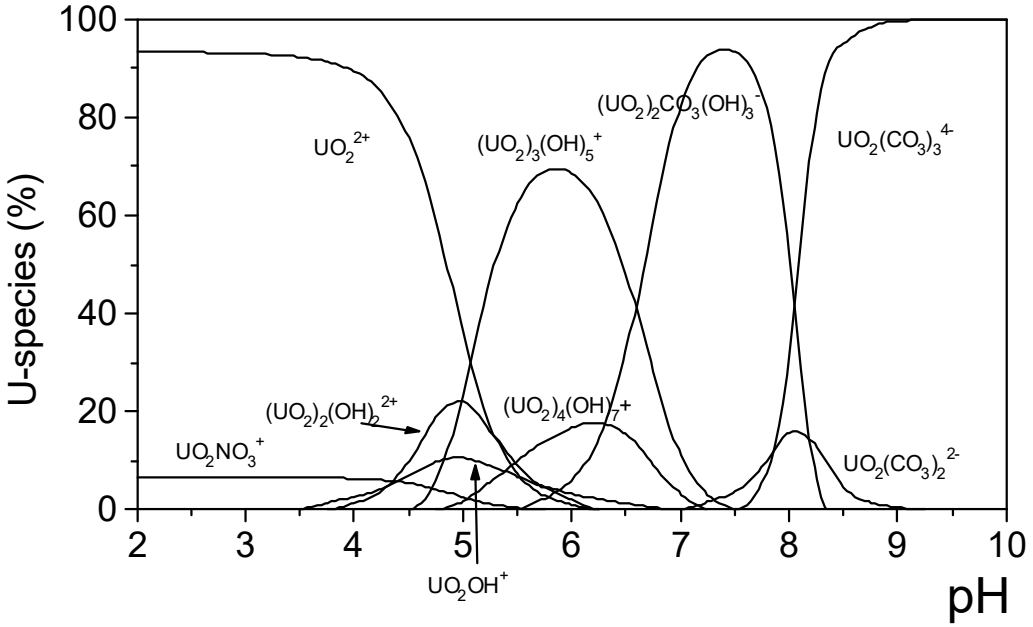


FIGURE 3.2 Uranium speciation in 0.1 mol/L $NaNO_3$ in equilibrium with air. $\Sigma U = 100$ µmol/L.

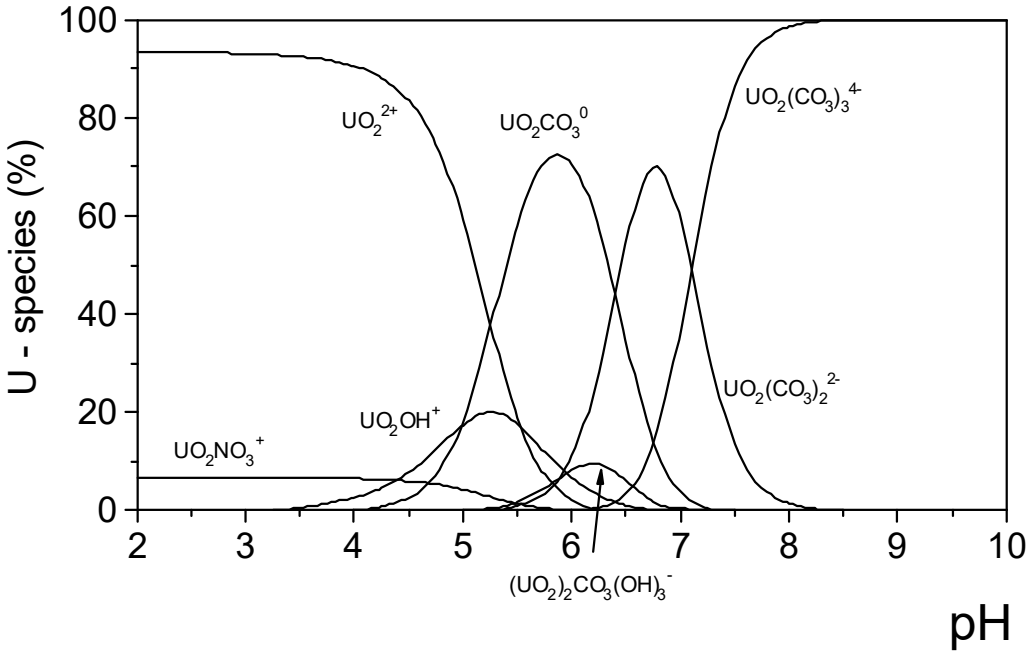


FIGURE 3.3 Uranium speciation in 0.1 mol/L $NaNO_3$ in equilibrium with a gas phase having a pCO_2 of 0.01 atm. ΣU = 1 μmol/L.

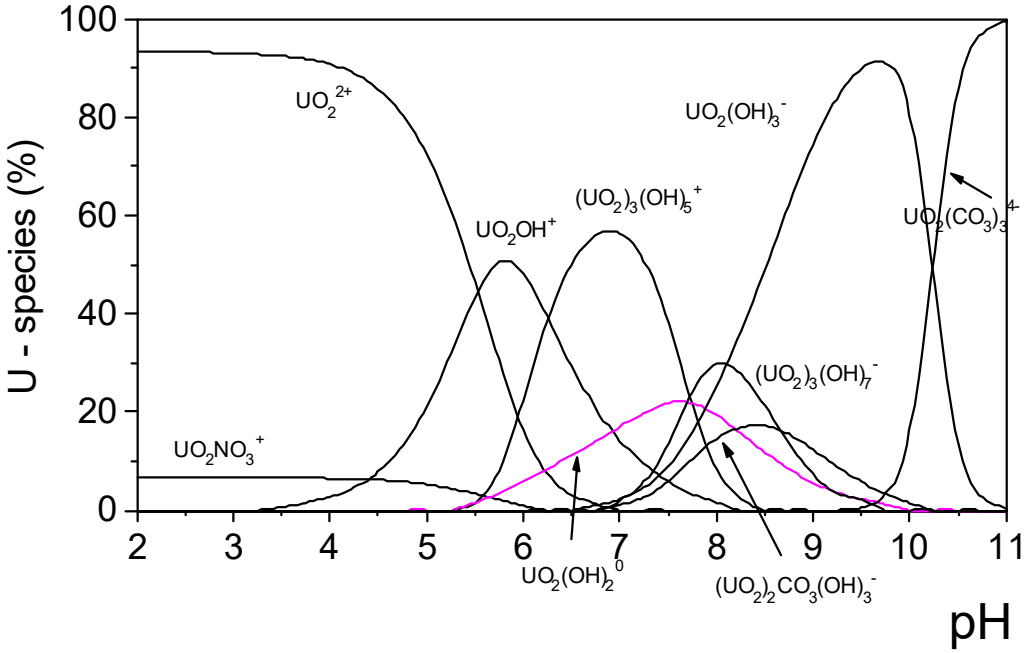


FIGURE 3.4 Uranium speciation in 0.1 mol/L $NaNO_3$ in equilibrium with a gas phase having a pCO_2 of $10^{-6.5}$ atm. ΣU = 1 μmol/L.

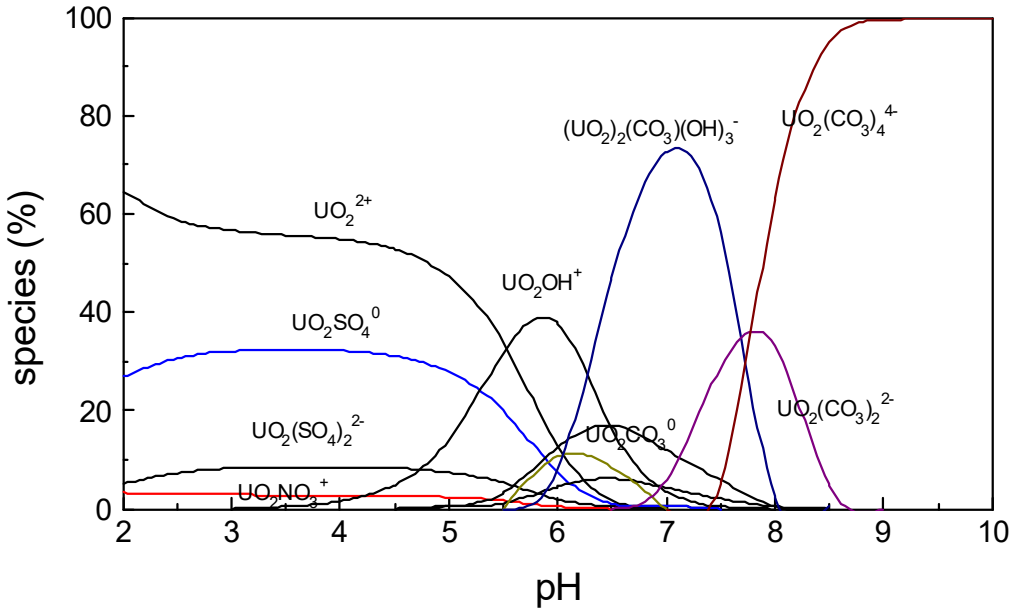


FIGURE 3.5 U(VI) speciation in (0.1 mol/L $NaNO_3$ + 0.01 mol/L Na_2SO_4) in equilibrium with air. ΣU = 1 μmol/L.

In systems containing additional complexing ligands, the speciation of U may be significantly modified. Sulfate is a fairly weak complexant for uranyl, but if sufficient amounts are present will affect U-speciation up to approximately pH 6.0 (Figure 3.5). The effect of phosphate is much greater (Figure 3.6), with ΣP of 100 μmol/L resulting in a substantial modification of U(VI) speciation compared to the ligand-free case. Precipitation (discussed below) is also possible in phosphate-containing systems.

The citrate ligand is a strong complexant for UO_2^{2+}. Figure 3.7 shows uranyl speciation in 0.1 M $NaNO_3$ (equilibrated in air) for two different total citrate concentrations. The thermodynamic data were obtained from Smith and Martell [1993] and are given in Table 3.1. These diagrams show that UO_2CIT^- is a very stable species and dominates U speciation over a wide pH range in these systems.

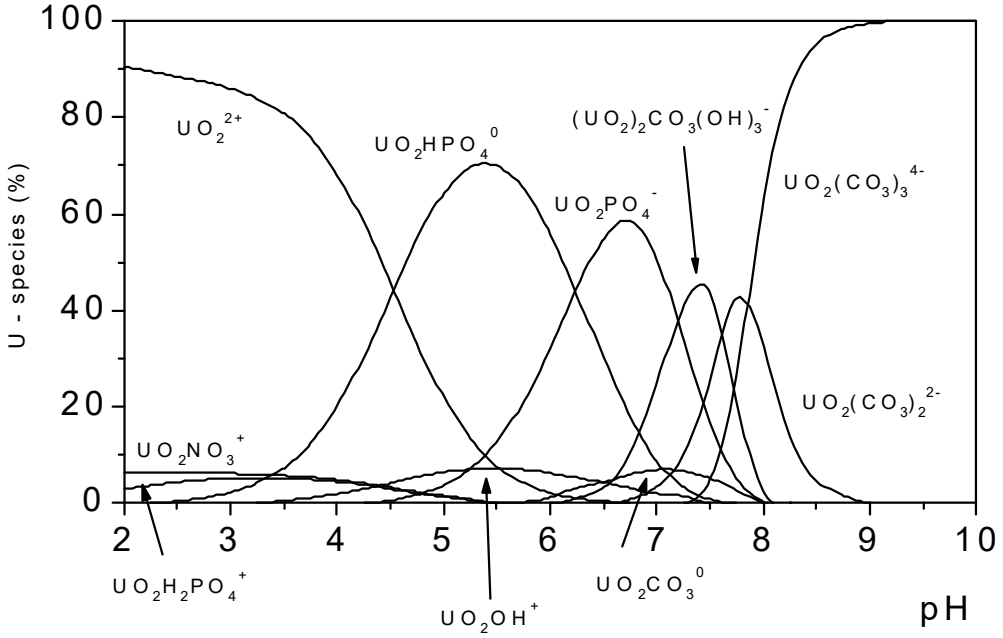


FIGURE 3.6 U(VI) speciation in 0.1 mol/L $NaNO_3$, with added PO_4 of 100 μmol/L. ΣU = 1 μmol/L (precipitation excluded).

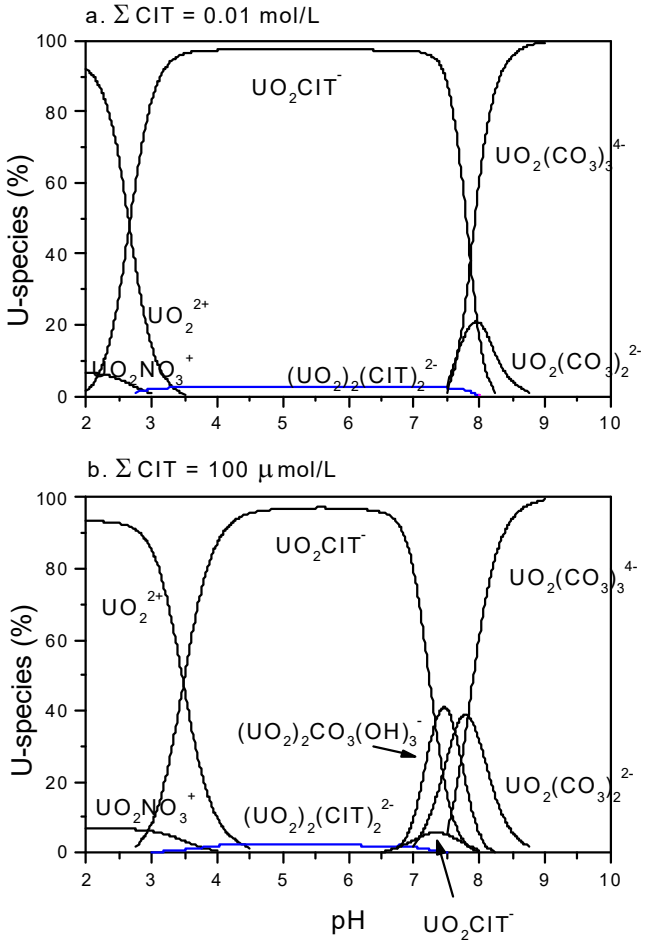


FIGURE 3.7 Uranium speciation in the presence of citrate a) 0.01 mol/L b) 100 µmol/L. In each case, total U is 1 µmol/L.

3.3 Solubility considerations

The experimental work described in this study was undertaken primarily to study sorption reactions at mineral surfaces. However, other possible mechanisms of U removal from solution must taken into account when considering the experimental data. The purpose of this section is to consider some limitations that may be imposed by solubility.

Consider a system containing aqueous U, a mineral M, and a ligand L. There are several possible mechanisms for removal of U from the aqueous phase. These include:

- adsorption of U on M
- co-adsorption of U and L on M (formation of a ternary surface complex)
- surface precipitation of U on M (possibly together with L)
- precipitation of uranyl hydroxide
- precipitation of a U-L phase
- adsorption of U on a new phase resulting from modification of M in the presence of L

The first three processes occur on the surface of the existing mineral (M). In contrast, the remaining processes involve the formation of new solids during the course of the experiment. The possible change of the identity of the sorbing solid phase introduces an extra degree of complexity in interpreting the experimental results.

One way of handling this problem is to choose experimental conditions that prevent the formation of new minerals by precipitation or transformation processes. This approach was adopted by Tripathi [1983], and simplifies the interpretation of the subsequent experimental data. However, it limits the range of experimental conditions that can be studied. Furthermore, it is reliant on the accuracy of the thermodynamic data and the correct identification of likely precipitating phases. Because much of the

solubility data is for crystalline phases, which are generally quite insoluble and may not form during the course of a sorption experiment of limited duration, this approach may be considered overly cautious.

The approach adopted in the present work is to carry out experiments over a wide range of conditions, including those in which precipitation is possible. This allows experimental concentration ranges to be selected for optimum analytical accuracy, and it would be expected that precipitation may be observed in some experiments. Under such circumstances, it is important to consider the formation of new minerals (by precipitation or other processes) and the following sections consider the possibilities mentioned above.

Precipitation of uranyl hydroxides

As observed by Grenthe *et al.* [1992], there have been numerous studies on the thermodynamic properties of uranium oxides and hydroxides. However, many of these are not highly relevant to the present work, because they focus on the solubility of well-defined crystalline minerals. In studies of crystalline solids, the presence of amorphous phases (such as newly formed precipitates) tends to invalidate the results. However, such phases are likely to be present in systems that may contain freshly formed precipitates, such as the experimental systems studied in the present work.

Waite *et al.* [1994] assumed that the formation of well crystallised β-$UO_2(OH)_2$ as given by the reaction:

$$\beta - UO_2 \Leftrightarrow UO_2^{2+} + 2OH^- \quad (\log K = -23.07) \qquad (3.2)$$

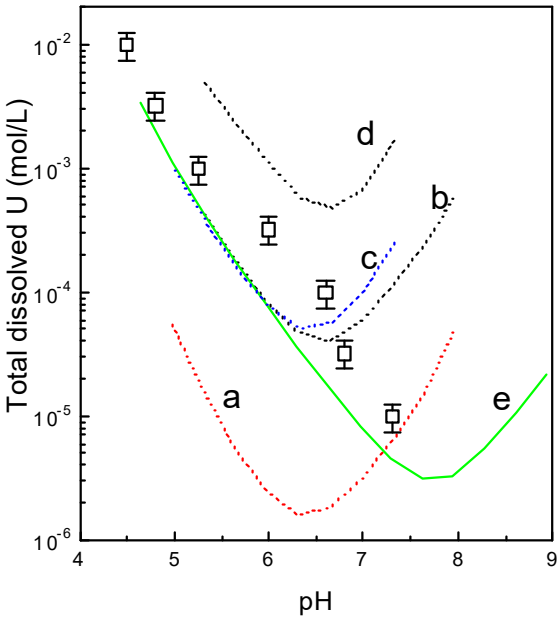
was kinetically hindered, and that it did not control the solubility of U in sorption experiments. They suggested that an amorphous phase was more likely to form under the experimental conditions. Tripathi [1983], who studied adsorption of U(VI) onto goethite (i.e. experimental systems very similar to those of the present work), carried

out a very thorough review of solubility data. He concluded that the structure of the solids for which solubility data had been computed was generally uncertain, and selected a generic value for the solubility product (K_{S0}) for 'uranyl hydroxide' . This was computed as $\{UO_2^{2+}\}\{OH^-\}^2$, and was not assigned to any specific solid phase. As noted above, such an approach is reasonable for this type of work, in which the exact identity of the solid phase is not crucial. Tripathi assembled a range of log K_{S0} values, most of which[1] were between -20.87 and -23.4, and after re-calculation of the data accepted a value of log K_{S0} of -22.43. This was similar to values obtained by other workers (such as -22.4 by Jensen [1982], although the data-selection in this case is not as well documented). Another review of U(VI) solubility was carried out by Allard *et al.* [1984], whose objective was to determine the likely mobility of actinides in the environment. For this purpose, the identity of precipitating solids was again not important, and their selected solubility product was -22.4 (with an upper limit of -22.0).

The various solubility constants for uranyl hydroxide (and U speciation schemes) were used to calculate the solubility of uranyl hydroxide in air-equilibrated systems using MINTEQA2 (Figure 3.8). A representative curve for a system equilibrated with N_2 is also shown. The minimum solubility in air-equilibrated systems occurs between pH 6.5 and 7.0, and is about 2×10^{-6} mol/L for β-$UO_2(OH)_2$, and close to 4×10^{-5} mol/L using the log K_{S0} values of Tripathi [1983] or Allard *et al.* [1984]. The calculated solubility is extremely sensitive to the value of log K_{S0},. While the selected log K_{S0} values of Jensen [1982], Tripathi [1983] and Allard *et al.* [1984] appear very similar, even the slightly higher 'upper limit' value of Allard *et al.* [1984] raises the solubility by a factor of five (Figure 3.8). Given the wide range of solubility values in the data surveyed by Tripathi [1983], this indicates that the true solubility of U(VI) in any given experimental system may be subject to considerable uncertainty. Figure 3.8 also shows that the computed solubility of U(VI) at high pH values is much lower under nitrogen ($pCO_2 = 0$) compared to air.

[1]About 14 separate experimental data values were in this range. Two much higher values (-17.22 and -19.82) and a lower value (-25.5) were discarded by Tripathi.

The calculated curves on Figure 3.8 can be compared with experimental studies of the precipitation of uranyl hydroxide. Such studies are rare compared to studies of the solubility of crystalline U minerals. Brusilovskii [1958] studied the precipitation process by a primitive but direct method in which tubes with various amounts of U were shaken, periodically tested for pH and precipitation was 'watched for'. The experiments were carried out under nitrogen. While the experimental technique would appear to be fraught with potential errors, the data suggest a much greater U 'solubility' compared to experiments with a crystalline solid. The data appear consistent with the solubility proposed by Tripathi [1983], with a log K close to –22.43.



In air

a) log K = -23.07 'well crystallised β-$UO_2(OH)_2$' [Waite *et al.*, 1994]

b) log K = -22.43 [Tripathi, 1983]

c) log K = -22.4 (selected by Allard *et al.* [1984])

d) log K = -22.0 (highest value of Allard *et al* [1984])

For internal consistency, curves (c) and (d) were calculated with thermodynamic data of Allard *et al.* which differs slightly from the NEA data-base.

In N_2

e) log K = -22.43 [Tripathi, 1983].

FIGURE 3.8 Aqueous U in systems controlled by the solubility of $UO_2(OH)_2$ using various log K values for the reaction $UO_2(OH)_2 \Leftrightarrow UO_2^{2+} + 2OH^-$. Data points are for the occurrence of a visible precipitate as reported by Brusilovskii [1958].

Precipitation of uranyl-ligand solids

To demonstrate the possible precipitation of a uranyl-ligand solid, the uranyl-phosphate system is considered. Of the experimental systems considered in this thesis, this is one of the most likely to result in the occurrence of a precipitate. In a typical experiment, the solubility of several solids may be of relevance. Three uranyl-phosphate solids are included In the NEA data-dase [Grenthe *et al.,* 1992, p287]. After changing the reactions (and associated log K values) to the component format consistent with MINTEQA2, the reactions are:

$$UO_2HPO_4 \bullet 4H_2O \Leftrightarrow UO_2^{2+} + 4H_2O + H^+ + PO_4^{3-} \quad (\log K = -24.202) \qquad (3.3)$$

$$(UO_2)_3(PO_4)_2 \bullet 4H_2O \Leftrightarrow 3UO_2^{2+} + 4H_2O + 2PO_4^{3-} \quad (\log K = -49.364) \qquad (3.4)$$

$$UO_2(H_2PO_4)_2 \bullet 3H_2O \Leftrightarrow UO_2^{2+} + 3H_2O + 4H^+ + 2PO_4^{3-} \quad (\log K = -45.104) \qquad (3.5)$$

As well as the above three phases, it is necessary to also include sodium uranyl phosphate:

$$NaUO_2PO_4 \bullet xH_2O \Leftrightarrow Na^+ + UO_2^{2+} + PO_4^{3-} \quad (\log K = -23.64) \qquad (3.6)$$

This phase is considered because Na^+ is present in the experimental systems due to the use of 0.1 M $NaNO_3$ as a background electrolyte. Solubility curves for these phases are shown as a function of pH in Figure 3.9. These were calculated for an experimental system which contains $\Sigma U = \Sigma P = 10^{-4}$ mol/L. These correspond to the greatest amounts studied experimentally in the present work. In addition, the solubility of 'uranyl hydroxide' (based on log K_{S0} = –22.43) is shown.

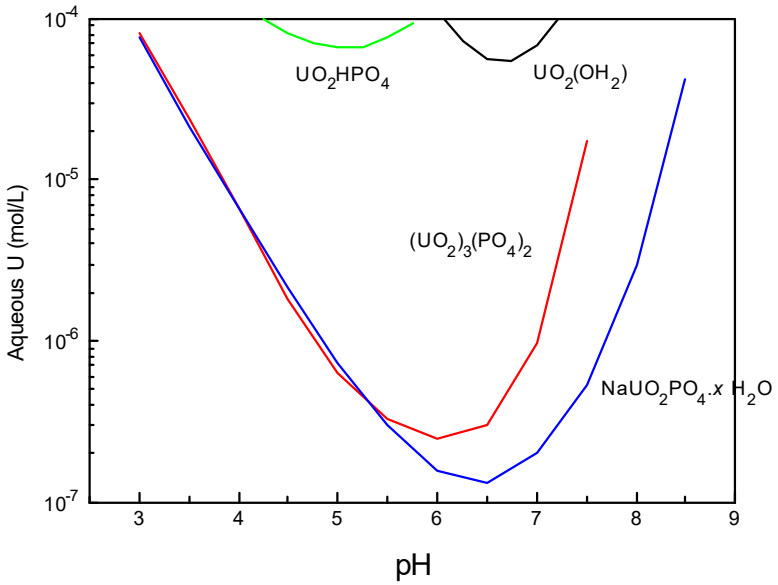


FIGURE 3.9 Solubility of U(VI) in phosphate-containing systems (ΣP=100 µmol/L) with various solubility limiting phases.

In this system, the solubility limits of normal uranyl orthophosphate and sodium autunite would limit U concentrations about 2 – 3 orders of magnitude below the limits imposed by the other phases. However, experimental studies of precipitation in U-phosphate systems usually result in the formation of $UO_2HPO_4.xH_2O$ [Schreyer and Baes, 1954; Sandino and Bruno, 1992] in the first instance. Typically, $(UO_2)_3(PO_4)_2.xH_2O$ is then obtained by various heating and drying steps. In the phosphoric acid solutions studied by Schreyer and Baes [1954], there was a tendency towards the transformation to $(UO_2)_3(PO_4)_2$ in more dilute systems, although this occurred over a long timescale.

The saturation index of a mineral in an aqueous system (SI) gives an indication of the potential for it to dissolve or precipitate. The index is defined as log (Q/K) where Q is the reaction quotient. If SI = 0, the mineral is at saturation. Values

above, or below, zero indicate a tendency to precipitate or dissolve, respectively (see Langmuir [1997]). The experimental systems studied by Moskvin *et al.* [1967] were clearly supersaturated with both sodium-autunite and $(UO_2)_3(PO_4)_2.xH_2O$ in most cases (see the data-points in dotted boxes on Figure 3.10). However $UO_2HPO_4.xH_2O$ was again the solid phase which was believed to be present. Similarly, the experiments of Dongarra and Langmuir [1980] were massively super-saturated with respect to $(UO_2)_3(PO_4)_2.xH_2O$ (as also noted by Tripathi [1983]). Calculations with the data-base in Table 3.1 resulted in log Q/K of between 4.6 and 5.7 (Figure 3.10). However, there is no indication in the account of this study that any precipitation occurred. Thus, it appears fairly unlikely that normal uranyl phosphate would control the solubility of U in short term experiments. Nonetheless, precipitation should be at least considered as an explanation of observed results in systems in which the solubility limit of $(UO_2)_3(PO_4)_2.xH_2O$ is exceeded.

In conclusion, it can be stated that experimental sorption results need to be interpreted carefully, with the possibility of precipitation taken into account. If this possibility is ignored and solubility limits are exceeded, the loss of U from the aqueous phase may be erroneously ascribed to a sorption reaction when it is in fact due to precipitation. On the other hand, it is well known that super saturation of a system with a particular phase does not guarantee that it will precipitate or control solubility. A typical example is the Fe/OH system, where ferrihydrite (an amorphous mineral) always forms rapidly upon neutralisation of an acidic Fe^{3+} solution, but eventually transforms towards more stable crystalline phases, such as goethite or hematite (this is discussed in more detail below). When ferrihydrite is present, the system is supersaturated with respect to the more stable Fe-oxides, but they play no role in limiting the aqueous Fe concentration.

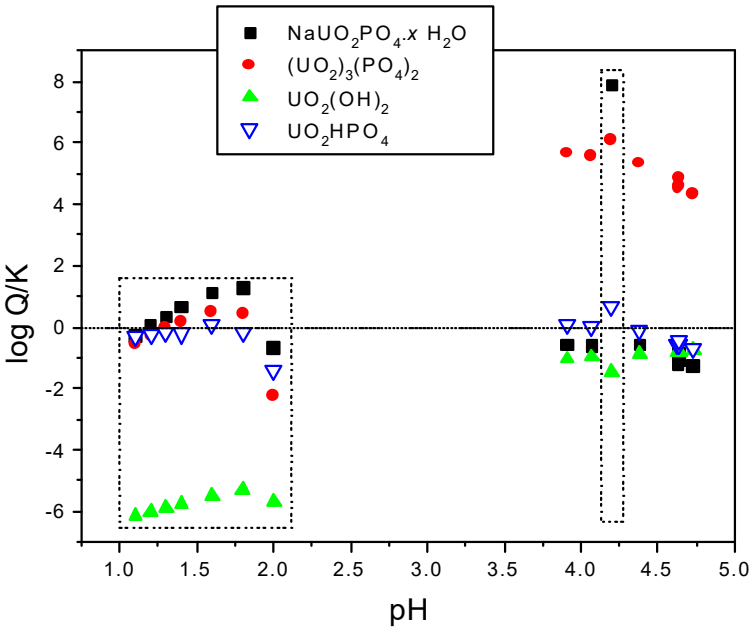


FIGURE 3.10 Uranium mineral solubility calculations in systems used for solubility determinations of $UO_2HPO_4.4H_2O$ by Moskvin *et al.* [1967] and systems used for measurements of U complexation by Dongarra and Langmuir [1980]. Many of these systems appear to be highly supersaturated with respect to $(UO_2)_3(PO_4)_2.xH_2O$. The experiments of Moskvin (in dotted boxes) were also apparently supersaturated with $NaUO_2PO_4.xH_2O$.

Adsorption of U on a new phase derived from the mineral sorbent

The final matter considered in this chapter relates to interactions that may affect the composition and surface chemistry of the substrate upon which U is being adsorbed. For example, consider ferrihydrite, which is widely used in sorption studies and is used as a model substrate in this thesis. Ferrihydrite is thermodynamically unstable and converts to other, more stable ferric oxide phases, such as hematite and goethite, which have different sorption properties. This process is fairly slow at room temperature, and significant amounts of the more crystalline phases only appear after 10-15 days of aging [Dzombak and Morel, 1990].

The effect of aging and transformation on the adsorption behaviour of iron oxides has been studied by several workers. Shuman [1977] showed that Zn retention by an aged Fe oxide was much lower than for a fresh Fe oxide, and similar results have been found for the sorption of some other elements. However, this effect is dependent upon the conditions under which aging is carried out. Aging of hydrous ferric oxide at room temperature had little effect on Pb sorption [Gadde and Laitinen, 1974]. Detailed sorption experiments with several Fe oxides showed that uranium uptake by amorphous ferric oxyhydroxide was much greater than by hematite or goethite [Hsi *et al.,* 1985]. It was suggested that U adsorbed on amorphous Fe oxides would later be desorbed when crystallization occurred with aging. This raised the key issue of whether adsorbed radionuclides are retained or released during the transformation of amorphous Fe oxides. This matter will be considered in Chapter 9.

In a system containing a ligand such as phosphate, it may also be necessary to consider the possible conversion of ferrihydrite to another phase such as ferric phosphate. Benjamin and Bloom [1981] studied adsorption of Zn on ferrihydrite in the presence of phosphate. Their experimental system contained equal amounts of phosphate and Fe (1 mmol/L), and it was proposed that a secondary surface phase formed in the presence of strongly sorbing anions (such as phosphate), and that this phase adsorbed trace metals more strongly than the original ferrihydrite. They hypothesised that adsorption was the dominant mechanism at low surface coverage

and there was some surface density at which an iron-anion surface precipitate starts forming. The possibility of surface precipitation is discussed by Dzombak and Morel [1990], who included it in their overall SCM for adsorption at the ferrihydrite surface.

Although the number of possible processes raised in this chapter may appear daunting, the uncertainty in interpretation may be reduced by suitable experimental design. This may mean studying U sorption at low concentrations where solubility limits are not exceeded. Furthermore, the systematic variation of experimental parameters (as carried out in the experimental work to be described in this thesis) can eliminate some possible explanations of the data. For example, if precipitation of a uranyl solid (rather than sorption) is suspected to occur in an experiment with ferrihydrite, the measurement could be repeated with a lower ferrihydrite loading. If, in this second experiment, dissolved U is greater at equilibrium, it is improbable that precipitation was controlling U concentrations in the former system, since this would normally not be sensitive to mass loading. Finally, it is essential in the modelling phase of any sorption study to routinely calculate saturation indices for possible precipitating phases and to establish (by physical examination if necessary) the exact nature of metal removal from the aqueous phase, whether by precipitation, adsorption, or some other process.

4 URANIUM SORPTION

Studies of U(VI) sorption on model minerals (Fe-oxides, clays, etc) and complex natural materials (soils and rocks) which were carried out prior to the commencement of the present work are discussed in the first three sections of this chapter. The final section briefly surveys some recent papers and reports published in the time period from 1993 to 1998, during which the present work was in progress.

In interpreting previous work, it is important to consider the range of experimental conditions which was studied, particularly if the results were used to develop a theoretical model of U-sorption. Experimental studies which have involved systematic variation of a range of variables are invariably more useful for modelling purposes. Key variables include pH, U concentration, ionic strength and the presence of complexing ligands. Some previous studies are virtually useless, as they lack sufficient pH control or measurement. However, another common problem is the use of fixed, and in some cases, very high, total U. Experiments with high ΣU (greater than 100 μmol/L - see Figure 3.8) are likely to be affected by precipitation, which has not always been taken into account in the data interpretation. In addition, sorption isotherms are typically non-linear (Chapter 3), and it is therefore desirable to vary the total U in order to derive information about the sorption affinity and populations of various sorbing surface sites. Again, some previous studies have involved only a limited range of ΣU (or a fixed ΣU).

4.1 Experimental studies of U sorption on single mineral phases

U sorption on iron oxides

An early study of U sorption on Fe-oxides was reported by Starik *et al.* [1958], who showed that U sorption was pH-dependent, with a maximum between pH 5 and 8. The desorption of U at high pH in systems equilibrated with air was attributed to carbonate complexation.

Van der Weijden *et al.* [1976] considered the geochemical implications of the 'remarkable sorptive power' of ferric hydroxides for uranyl. Sorption was maximal in the pH range 5.5 to 8.5, being much lower on hematite then amorphous Fe-oxide. They suggested that U might be released during aging of amorphous Fe-oxides to more crystalline material (see Section 3.3).

The U / Fe systems studied by Giblin *et al.* [1981] contained equal amounts of Fe and U, which were precipitated together during the experiments. Both pH and Eh were varied, and some systems contained CO_2 at a partial pressure of 0.5 atm. (much higher than that found in most natural systems). Carbonate was found to increase U mobility, but the adsorption of the highly negative $UO_2(CO_3)_3^{4-}$ species was inferred. The authors considered that their data were principally a measure of solubility, impacted by the effects of sorption and mobile colloids.

One of the most detailed studies of U sorption was that of Tripathi [1983], who aimed to develop a model for U sorption on goethite. A number of experimental parameters was studied, including complexants such as phosphate and fluoride. The approach was very thorough, and included a prior analysis of the existing thermodynamic data for U. Tripathi attempted to carry out experiments under conditions in which precipitation was impossible, and removal from solution could be ascribed to sorption alone. He concluded that the adsorption edge for U (the pH range in which sorption increased from negligible to nearly 100%) was at pH 5-6. With increasing ΣU, the adsorption edge moved to higher pH values. Both fluoride and phosphate slightly decreased U adsorption. As other workers had observed, carbonate strongly reduced U adsorption above pH 7. This decrease did not occur when experiments were carried out under nitrogen. Tripathi tried several models to fit the sorption data, and concluded that "neither UO_2^{2+} nor any of its hydroxo complexes could be used to model the adsorption data" (Tripathi [1983], p88). He further concluded that the main surface uranium species was monomeric and contained more than two hydroxyls. The reaction forming this surface species was given as:

$$> FeOH + UO_2^{2+} + 3H_2O \Leftrightarrow > FeOH_2^+UO_2(OH)_3 + 2H^+ \quad (\log K = -7.0) \qquad (4.1)$$

For U sorption at higher sorption densities, a second surface reaction was included:

$$> FeOH + 3UO_2^{2+} + 8H_2O \Leftrightarrow \quad > FeOH(UO_2)_3(OH)_8^{2-} + 8H^+ \quad (\log K = -31.3) \quad (4.2)$$

Reaction 4.1 implies that $UO_2(OH)_3^-$ forms at the surface in the pH range of the sorption edge. In solution, this species only forms at higher pH values (see Figure 3.4). Tripathi felt this provided support for the hypothesis that metal hydrolysis was enhanced by adsorbent surfaces.

Ames *et al.* [1983b] reported on U sorption experiments with amorphous ferric oxyhydroxide in 0.01 M NaCl (pH 6.9 and 8.2) and in 0.01 M $NaHCO_3$ (pH 8.7) at 25°C and 60°C. They found that U uptake was much weaker in the $NaHCO_3$. Due to the absence of pH dependence studies, the experimental U adsorption data are insufficient to provide a rigorous test of a surface complexation model. The authors fitted the data using an isotherm approach.

Hsi and Langmuir [1985] studied uranyl sorption on Fe-oxides, including goethite and hematite. In this detailed experimental and modelling study, a range of parameters was varied, including pH, total carbonate (C_T) and ionic strength. Experimental results were qualitatively similar to the other studies, with sorption being greater on amorphous Fe-oxide than on goethite. Uranium uptake was weak on hematite, which had a much lower surface area. Competing ions (Ca and Mg) had no effect on U sorption. Hsi and Langmuir reported that U sorption on Fe-oxides was reversible (i.e. a similar equilibrium position was obtained whether the adsorption or desorption reaction was studied). The effect of various C_T was investigated, with sorption becoming progressively weaker with increasing C_T. In carbonate-free systems, the sorption of U on goethite was modelled assuming that adsorption involved chiefly the UO_2OH^+ and $(UO_2)_3(OH)_5^+$ aqueous complexes, with the latter species most likely forming a bidentate surface complex. A limitation of this study is

that only one ΣU (10^{-5} mol/L) was employed. Variation of this parameter would have enabled the authors to do a thorough test of the proposed sorption model.

Comparison of the experimental data obtained for U sorption on goethite by Hsi and Langmuir [1985] with the analogous data of Tripathi [1983] indicates the existence of a substantial discrepancy for similar experimental conditions. Whereas the pH_{50} (pH of 50% adsorption on the low pH edge) is about 4.0 for the former data-set, Tripathi obtained a pH_{50} near 6.0. The slight differences in experimental conditions appear insufficient to explain such a large displacement between the pH edges. Given that these two data-sets are amongst the most comprehensive for U sorption on any substrate, it is of some concern that the results are so dissimilar[1]. It is possible that there was a highly sorbing amorphous Fe-oxide contamination in the goethite used by Hsi and Langmuir [1985]. A possible criticism of the data of Tripathi is that the lowest pH studied was 5.0. This is not significantly below the pH region in which the low-pH U sorption edge was observed, and is a pH at which Hsi and Langmuir reported virtually all the U to be adsorbed by the solid. Therefore the sorption edge of Hsi and Langmuir [1985] occurred in a pH range for which Tripathi [1983] reported no data. Whatever the reason for the differences between these two studies, this comparison indicates that there may be significant experimental difficulties in obtaining reproducible experimental sorption data.

The uptake of U on precipitating and pre-formed amorphous Fe-oxides in the narrow pH range 6-8 was studied by Van der Weijden *et al.* [1985]. Similar results were obtained in both cases, with the adsorption maximum at about pH 6.5. No modelling was attempted.

Several studies of U sorption on hematite have been reported by Ho and co-workers. Ho and Doern [1985] reported that the sorption was reversible with respect to solution pH. The pH range of sorption was observed to coincide with the increased existence of multinuclear species in solution (see Figures 3.1 and 3.2) and this was

[1]A detailed comparison and attempt at modelling the two data-sets is discussed by Turner [1993]. Not surprisingly, it is impossible to produce a satisfactory model for both data-sets.

interpreted as indicating the adsorption of multinuclear uranyl species. In a subsequent paper, Ho and Miller [1985] showed that the presence of humic acid (HA) enhanced the adsorption of uranium at low pH and low HA concentrations. With increased pH and higher free HA concentrations, a surface blocking effect and complex formation with free HA tended to reduce U sorption. In a later paper, Ho and Miller [1986] reported on systems to which a fixed amount of carbonate had been added. The experiments were performed in a 1 mol/L $NaHCO_3$ with the pH adjusted by addition of dilute HCl. The authors thought that $(UO_2)_2CO_3(OH)_3^-$ was the active species involved in the sorption process, since the pH of maximum adsorption corresponded with its predominance in solution.

The sorption of uranyl on magnetite and several other oxides was studied by Gupta and Venkataramani [1988]. These authors presented a qualitatively different surface hydrolysis model, in which sorption occurs when free hydroxyl groups are available on the surface. They hypothesised the formation of dimer-like surface structures, in which a uranyl species is co-ordinated to two surface hydroxyl groups. The paper contains a limited amount of data for U sorption on magnetite, with the adsorption edge being between pH 4 to 5. The ΣU was quite high at 10^{-4} mol/L. A second paper by these authors was concerned with the effect of anions on U sorption [Venkataramani and Gupta, 1991]. With sulfate of 0.1 mol/L or 0.001 mol/L, sorption by magnetite was reduced. This was attributed primarily to the complexation of aqueous uranyl with SO_4^{2-} (see Figure 3.5).

An interesting study of the sorption of uranyl and neptunyl (NpO_2^+) ions was reported in a brief paper by Kohler *et al.* [1992]. The Fe-oxide solid phases were hematite and goethite. The data-sets for UO_2^{2+} related to an investigation of the pH-dependence of sorption at various partial pressures of CO_2 (0, $10^{-3.5}$, and 2×10^{-2} atm). The low-pH sorption edge was in a similar pH range for all three values of pCO_2 (pH 4 - 5). In the absence of CO_2, the uptake of U(VI) remained strong at high pH values. When experiments were carried out with pCO_2 of $10^{-3.5}$, U was desorbed at pH values above about 9. With elevated pCO_2, the high pH desorption occurred at a pH of about 8.0. Although only a limited amount of data interpretation was reported,

the modelling assumed the uptake of the dominant aqueous U species, i.e. UO_2OH^+, $(UO_2)_3(OH)_5^+$, $UO_2(CO_3)_2^{2-}$ and $UO_2(CO_3)_3^{4-}$. The experimental data could not be adequately modelled in the absence of the ternary uranyl-carbonato surface complexes.

The studies of U-sorption on Fe-oxides summarised above have some similar features, primarily in the general pH dependence, the effect of carbonate, and (to a very limited extent) the effect of ligands on U-sorption. The differences between studies can be partly explained by the identity of the various Fe-oxide phases. However, the two most comprehensive studies of U-sorption on the same substrate (those of Hsi and Langmuir [1985] and Tripathi [1983] on goethite) arrived at entirely different models for their data. Perhaps this is not surprising given the vast discrepancy in their experimental results (as mentioned above). These two models for U sorption by goethite are discussed in Section 4.2.

U sorption on kaolinite

A relatively small number of studies of U sorption by clays had been reported at the time of the commencement of the present study. Giblin [1980] studied the adsorption of U by kaolinite (ΣU of 100 μg/L) and found that sorption occurred above pH 5.0 (with a sorption maximum around pH 7) and decreased at high pH values. These trends are similar to those reported for U sorption on other substrates. The data were converted to K_d values, and these exceeded 10^4 mL/g across a wide pH range (the highest value was 35000 mL/g). The data were qualitatively explained as being due to adsorption of positively charged uranyl species on the negatively charged kaolinite surface. Giblin [1980] considered that this sorption process, in conjunction with a subsequent reduction of U(VI), could be responsible for concentrating U in the deposits of the Alligator Rivers region.

The uptake of U(VI) on several clays was investigated by Borovec [1981]. Experiments were carried out at pH 6.0, with total U concentrations in the range 10^{-5} to 10^{-2} mol/L. Borovec reported that the presence of competing divalent cations (Mg,

Ca, Zn, Ni, Cd, Co, or Mn) reduced U uptake, and that kaolinite was a weaker U sorber than illite or montmorillonite. The experimental data were modelled by a mixture of the Freundlich and Langmuir isotherms, together with K_d computations. The U concentrations used in this study were extremely high, and it is surprising that precipitation was not observed at the experimental pH (see Figure 3.8).

Kaolinite was included in some of the experimental systems reported by Giblin *et al.* [1981]. The experiments also included Fe, which presumably formed a colloidal phase or coated the kaolinite. Unfortunately, no experiments containing only kaolinite were undertaken. The data were interpreted by computing a 'uranium mobility' parameter, to which adsorbed, aqueous and colloidal species all contributed. Multiple regression of this parameter against pH and Eh was carried out. Giblin *et al.* [1981] concluded that the presence of hydrous ferric oxide coatings on the kaolinite surface "had no effect on the sorption of cationic uranium species". However, Giblin *et al.* [1981] did not obtain data for any similar systems with Fe absent in order to test this assertion. Giblin *et al.* noted that their conclusion conflicted with the argument of Jenne [1968] that adsorption by hydrous ferric oxide is a major control upon trace metal mobility in natural waters. The work of Giblin and co-workers strongly implicated kaolinite (rather than Fe-oxides) as being a major U-sorbing substrate in the natural environment.

Ames *et al.* [1983a] studied U sorption on kaolinite and seven other substrates. The pH was not systematically varied, and modelling was based on the Freundlich isotherm. Although only a limited amount of data was obtained for kaolinite, the authors reported a large discrepancy with the results of Giblin [1980], obtaining K_d values about two orders of magnitude smaller under apparently similar conditions. They also concluded that non-crystalline iron oxides *were* important in U mobility, and were able to sorb uranyl ions more efficiently than the other minerals studied.

This review of papers dealing with U-sorption by kaolinite indicates a lack of consensus about the role of kaolinite in adsorbing U in the environment. The importance of kaolinite relative to other U-sorbing phases, such as amorphous ferric

oxides appears to be surrounded by considerable confusion.

U sorption on other simple oxides

The present interest in U sorption is largely driven by an interest in the environmental behaviour of U. In the 1960's, research on U-surface interactions was partly motivated by a completely different objective – to find cheap ways of concentrating U from ocean water (which has a U content of 3.34 μg/L). Consequently, considerable effort was expended on examining various methods to achieve this end. Davies *et al.* [1964] experimented with solvent extraction, and both organic and inorganic adsorbents (various compounds of Zn, Ti and Pb). They concluded that the most suitable material for sorbing U from seawater would be $Ti(OH)_4$, and supported this conclusion with a somewhat fanciful economic assessment. A later paper [Keen, 1968] reported a very high K_d for U on hydrous titanium oxide of around 10^5 mL/g, which certainly suggests a strong surface interaction.

Maya [1982] further probed the interaction between U and the hydrous Ti-oxide surface. An examination by scanning electron microscopy (with elemental mapping) showed that the distributions of U and Ti were very similar, which indicated chemical binding of U to the substrate (as opposed to the formation of a U precipitate). In recent years the interest in U sorption on the surface of Ti-oxides has waned, which is probably attributable to economic factors.

There is a limited amount of information on the adsorption of U by other mineral substrates. Lieser *et al.* [1992] reported that sorption of U(VI) by hydrous silicon dioxide was pH-dependent and decreased dramatically at high pH due to the formation of aqueous carbonate complexes. Following the approach adopted by several others, these authors modelled sorption as the uptake of the dominant aqueous complexes of U, namely UO_2^{2+}, UO_2OH^+ and $(UO_2)_3(OH)_7^+$.

4.2 Models for U sorption on Fe-oxides

The purpose of this section is to examine the models of U sorption on goethite proposed by Hsi and Langmuir [1985] and Tripathi [1983]. As may be inferred from the discussion in Section 4.1, these are the most useful (i.e. testable) models previously available for U-sorption on a substrate that is relevant to the present study. An important attribute of these studies is that the authors provided the thermodynamic data-base used in their modelling, which (together with the postulated sorption reactions) enables their models to be re-created and examined.

Both of the sorption models used the triple layer model (TLM) to describe electrostatic interactions at the surface. A description of this model and comparison with the diffuse double layer model (described in Section 2.4) is available in Hayes *et al.* [1991]. The terminology adopted here will be that of Hayes *et al.* [1991]. Computations were carried out using MINTEQA2, with the set of equations and parameters shown in Table 4.1.[1]

The experimental data obtained by Tripathi [1983] are shown in Figure 4.1. Tripathi's modelling focussed on the data set obtained for ΣU of 250 ppb (1.05 μmol/L), and was implemented using used a computational model referred to as the Stanford Generalized Model for Adsorption (SGMA). It will be observed that the implementation of the sorption model with MINTEQA2 provides the same excellent fit to the 250 ppb data set as reported by Tripathi [1983] with the SGMA. The experimental data show a displacement of the edge to increasing pH values with higher ΣU. As discussed in Chapter 2, this may indicate that more than one surface site is involved in U sorption. However, the model only includes a single site type, and the fit to the experimental data is imperfect with ΣU of 4.2 μmol/L. This shortcoming

[1] In implementing the models, particular care was taken to correctly assign the MINTEQ components 813 and 814 which are used to calculate the charge density on the inner and outer planes (σ_0 and σ_b). The inner plane only involves protonation and deprotonation reactions. Therefore a surface complex such as [$FeOH_2^+$-$UO_2(OH)_3^-$] contributes +1 to σ_0 and –1 to σ_b, despite having no net charge.

was recognised by Tripathi [1983]. Nonetheless, the model fits the data quite well, and (most importantly) correctly predicts a decrease in the percentage sorbed with increasing amount of U in the system.

The fit of the MINTEQA2 simulation to the data of Hsi and Langmuir [1985] was also very satisfactory (Figure 4.2). However, there is an interesting feature of their modelling approach, which became apparent when computations were carried out with different values of ΣU. Instead of the model pH-edges moving to the right with increasing ΣU, the curves move to the left (Figure 4.2). That is, sorption should become stronger with increasing ΣU. This is clearly not in concordance with the experimental data obtained by Tripathi [1983] and does not correspond with the trend usually observed in metal sorption (see the discussion in Dzombak and Morel [1990]). The model trend is due to the inclusion of the multinuclear surface complex [FeO^--$(UO_2)_3(OH)_5^+$] in the suite of surface reactions. With greater ΣU this surface complex becomes increasingly dominant. For example, with ΣU of 100 μmol/L, the model predicts that this complex should account for 86% of the adsorbed U at pH 4.5. (Although a multinuclear surface complex was also proposed by Tripathi, it plays very little role in the modelling calculations summarised in Figure 4.1).

The relative importance of the multinuclear surface complex and the multinuclear solution phase complexes will depend on their log K values and the experimental conditions. However, it appears that the response of an experimental system to changes in ΣU could provide a useful test of the validity of the sorption model proposed by Hsi and Langmuir [1985].

It is instructive to compare the reasons for the differences between the two sorption models. Obviously the speciation schemes and experimental results were very dissimilar, so it is not surprising that the sorption models differ significantly. In addition, the study by Hsi and Langmuir [1985] did not include an investigation of the effect of ΣU.

TABLE 4.1 Summary of models for U sorption on goethite as implemented using MINTEQA2. Experiments were carried out in 0.1 M $NaNO_3$ under nitrogen.

		Triple layer model of Tripathi [1983]	Triple layer model of Hsi and Langmuir [1985]
Aqueous uranyl species and log K values (see Table 3.1 for formation equations)			
UO_2OH^+		-5.3	-5.1
$(UO_2)_2(OH)_2^{2+}$		-5.68	-5.62
$(UO_2)_3(OH)_5^+$		-15.82	-15.63
$(UO_2)_3(OH)_4^{2+}$		-11.88	Omitted
$(UO_2)_3(OH)_7^-$		-28.34	Omitted
$(UO_2)_4(OH)_7^+$		-21.9	Omitted
Adjustable model parameters			
Reaction	*Symbol*	*Value*	*Value*
$FeOH + H^+ \Leftrightarrow FeOH_2^+$	*Log* K^+	4.2	4.5
$FeOH \Leftrightarrow FeO^- + H^+$	*Log* K^-	-10.8	-12.0
$FeOH + Na^+ \Leftrightarrow (FeO^-\text{-}Na^+) + H^+$	*Log* K_{Cat}	-8.9	-10.1
$FeOH + NO_3^- + H^+ \Leftrightarrow (FeOH_2^+\text{-}NO_3^-)$	*Log* K_{An}	6.1	7.0
Inner layer capacitance	C_1	1.0 F/m^2	1.4 F/m^2
Outer layer capacitance	C_2	0.2 F/m^2	0.2 F/m^2
Site density	N_S	18 sites/nm^2	18 sites/nm^2
Experimental parameters			
Solid loading		0.41 g/L	1.00 g/L
Total U (ΣU)		See text	1 x 10^{-5} mol/L

U sorption reactions [Tripathi, 1983]

	Log K
$FeOH + UO_2^{2+} + 3H_2O \Leftrightarrow [FeOH_2^+\text{-}UO_2(OH)_3^-] + 2H^+$	-7.0
$FeOH + 3UO_2^{2+} + 8H_2O \Leftrightarrow [FeOH\text{-}(UO_2)_3(OH)_8^{2-}] + 8H^+$	-31.3

U sorption reactions [Hsi and Langmuir, 1985]

	Log K
$FeOH + UO_2^{2+} + H_2O \Leftrightarrow [FeO^-\text{-}UO_2(OH)^+] + 2H^+$	-8.0
$FeOH + 3UO_2^{2+} + 5H_2O \Leftrightarrow [FeO^-\text{-}(UO_2)_3(OH)_5^+] + 6H^+$	-15.0

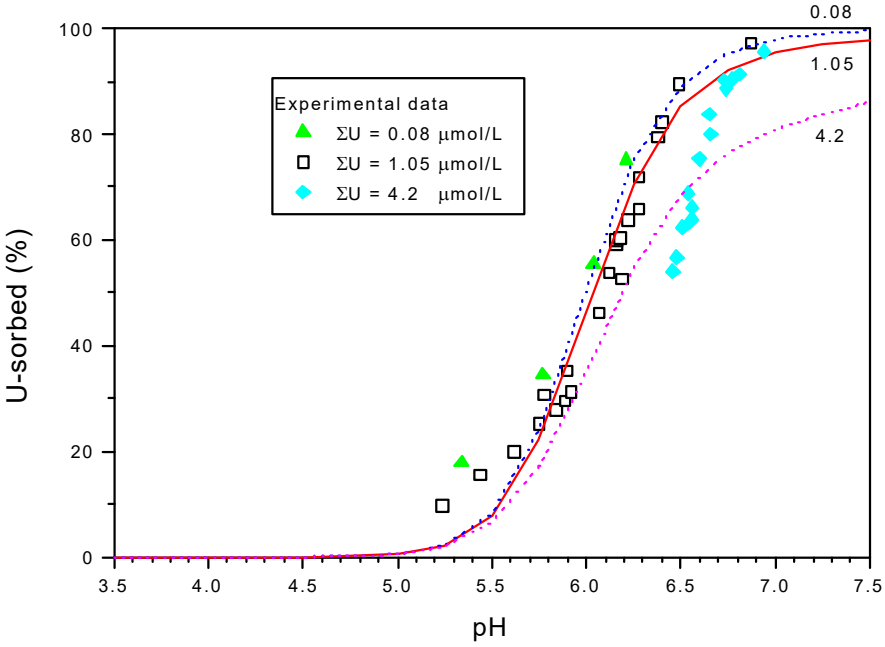


FIGURE 4.1 Experimental data for U sorption on goethite [Tripathi, 1983] and model curves calculated from data in Table 4.1. For each model curve, ΣU is indicated (µmol/L).

However, the differences in the models also stem from underlying differences in the 'philosophy' of the modelling approach. For example,

- Hsi and Langmuir considered that surface sorption of U involved the uptake of the predominant aqueous species in existence at the experimental pH (which, in their speciation model, were UO_2OH^+ and $(UO_2)_3(OH)_5^+$). In contrast, Tripathi modelled uptake of $UO_2(OH)_3^-$, which only forms in solution at a higher pH values.
- Tripathi only allowed sorption where it was favoured by electrostatic considerations (adsorption of cations on positively charged sites was excluded at the outset). On the other hand, Hsi and Langmuir could not even consider the adsorption of negatively charged species, because

their uranyl speciation scheme only included cationic species, regardless of pH (Table 4.1). Their model requires that cations approach a surface which is generally positively charged, since the experiments were carried out at pH values well below the pH_{zpc} of the Fe-oxide surface.

- The formation of ternary surface complexes (e.g. those involving carbonate) was excluded by Tripathi, although it has been proposed in several studies. Hsi and Langmuir did include ternary U-carbonate complexes to model carbonate-containing systems.

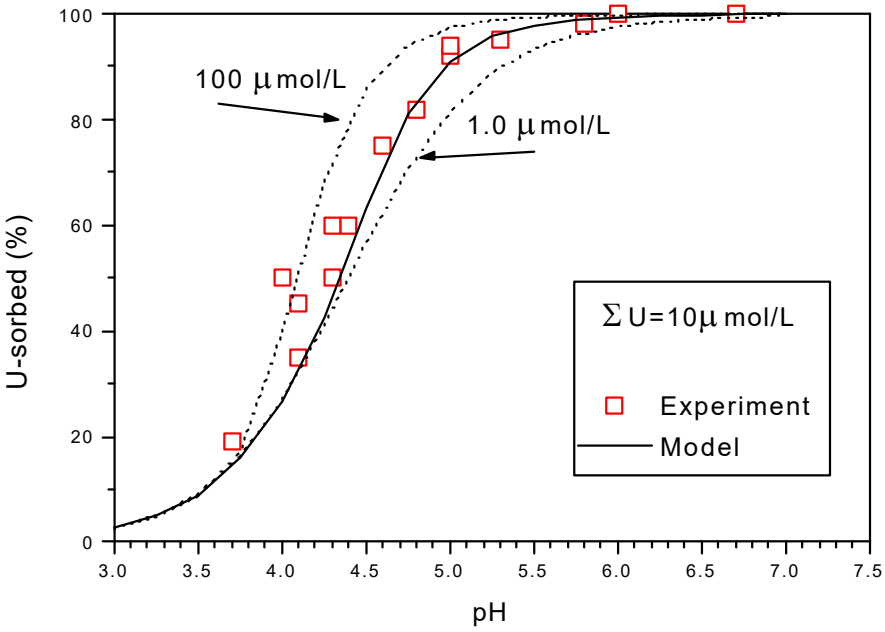


FIGURE 4.2 Implementation of the U sorption model of Hsi and Langmuir [1985]. The solid curve and data refer to ΣU of 10^{-5} mol/L. The two dashed curves are model predictions for ΣU of 1.0 µmol/L and 100 µmol/L. Note that this model predicts that the percentage of U adsorbed should *increase* with increasing ΣU.

One of the points of agreement in the two models was the use of the TLM for the electrical double layer. In this model, competition between uranyl and the background electrolyte can lead to reduced sorption at higher ionic strength. This can be demonstrated using the model of Tripathi, which indicates that U sorption should be dependent on ionic strength (Figure 4.3). This ionic strength dependence (together with the other parameters such as ΣU) could be useful in assessing models for U sorption, assuming adequate data are available.

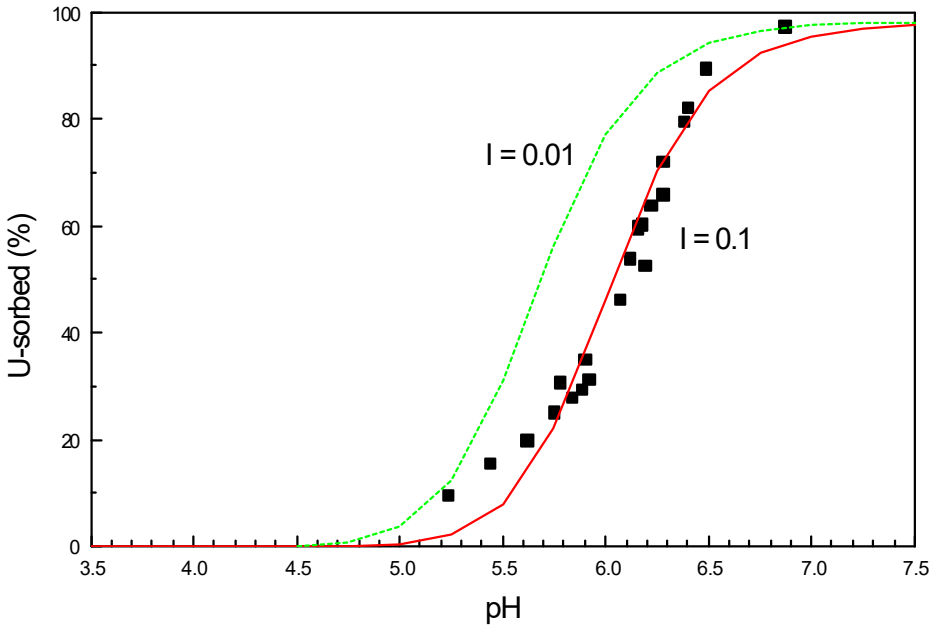


FIGURE 4.3 The model of Tripathi [1983] predicts a shift of the U sorption edge to lower pH values with a decrease in ionic strength. The experimental data are for U = 250 ppb, I = 0.1. Conclusive data about the ionic strength dependence were not obtained by Tripathi, although limited data at higher I indicated a small effect.

This review of two previous studies demonstrates an important feature of surface complexation models. That is, the models can be used to make predictions beyond the system for which they were developed. While these predictions may not prove to be correct, they provide an objective means of testing any proposed model. This aspect of SCM's promises to make a major contribution to improving future simulations of environmental phenomena.

4.3 U sorption on complex geologic substrates

In common with studies of U sorption by model minerals, U retention in natural systems has been studied spasmodically for several decades. Most studies have been qualitative, and modelling has rarely been attempted. Where modelling has been undertaken, it has mostly been limited to developing isotherms, which have very little predictive power.

Masuda and Yamamoto [1971] reported some studies of interactions of U with representative soils, described as alluvial soil, sandy soil and volcanic ash soil. The sorption data are difficult to interpret, as no experimental pH values were reported. The experiments were carried out with very high U concentrations of up to 4.2×10^{-2} mol/L. If the experiments were carried out in the absence of complexants in an environmental pH range, this high concentration should have ensured some precipitation (see Figure 3.8). In summarising their study, the authors cautioned that "these results may not be applied directly to environmental problems".

Approximately a decade later, Ames *et al.* [1982] reported the results of some experiments with basalt and associated secondary smectites (some work by Ames and co-workers with simple minerals was reviewed above). The natural materials were characterised for their chemical and mineralogical properties, and the surface area was measured (using ethylene glycol adsorption). The rocks were crushed before experiments, which apparently increased the surface area significantly. The aqueous phases were 'synthetic groundwaters' (i.e. having a composition similar to natural groundwaters). The authors mainly concentrated on the effect of ΣU and

modelled the data using sorption isotherms.

The first U sorption study with natural substrates which involved variation of several parameters such as pH, complexing ligands and ionic strength appears to have been that of Warnecke *et al.* [1984]. This study considered several radionuclides and 19 soil types. The experimental work extended to studies of sorption under conditions of elevated pCO_2. However, the report is rather brief, and is limited to reporting ranges of observed K_d values. In the case of U, the range of K_d values was from 0.5 to 5000 mL/g. The authors concluded that "many of the radionuclides had broad ranges of distribution" and that the influencing parameters should be identified. Given the results of this study, it is not surprising that the sorption behaviour of radionuclides such as U has become the subject of more detailed investigations.

Milton and Brown [1987] reported some laboratory studies on the uptake of U by secondary minerals retrieved from fracture surfaces in the Canadian shield. They reported that U uptake on ferric oxyhydroxide played a significant role in that system and also carried out some kinetic studies.

Payne and Waite [1991] reported on some work carried out at ANSTO prior to the commencement of the study described in this thesis. These authors studied U sorption by crushed natural materials from the Koongarra and Ranger U deposits. Although showing some scatter, the pH dependence of the data conformed to the general trend (found with model minerals) for systems equilibrated with CO_2, with increasing sorption up to pH about 7 and a subsequent decrease. These authors attempted to model the data using the surface complexation approach, applying the Fe-oxide model of Hsi and Langmuir [1985]. As such, it was assumed that Fe-oxides were the major phase adsorbing U in the system, which was in accord with the assertion of Jenne [1968], that Fe-oxides dominate sorption by many natural materials. The authors found that they needed to estimate several parameters in order to implement the model. The amount of Fe-oxide and the ΣU in the experimental systems was estimated from a chemical extraction (the estimate for ΣU was verified using an isotope exchange procedure). The model could only be made to fit the data

by adjusting the log K values for the surface complexes, and then including another surface reaction (adsorption of a uranyl monocarbonate complex). The final model fitted the data-sets for both the substrates quite well. However, the authors observed that “such an approach to sorption modelling is essentially a curve fitting exercise with enough variables added to ensure an adequate fit”. As such, they cautioned that the chosen suite of surface complexes and associated constants should not be assumed to represent reality.

4.4 Developments between 1993 and 1998

In recent years, the literature on U sorption has been growing rapidly, and there have been several papers reporting systematic experimental and modelling studies. In addition, some groups have attempted to obtain direct information about the structure of U(VI) surface complexes by spectroscopic techniques such as EXAFS or XAFS ((extended) X-ray absorption fine structure).

The work of Thompson *et al*. [1994] was mainly concerned with the structure of surface complexes, which was investigated using EXAFS in air and in N_2 at pH 6 to 8. The EXAFS was used to infer the proximity of adsorbed U to other atoms, particularly other U atoms. It was concluded that, in air-equilibrated systems, an inner sphere, mononuclear U surface complex formed on the kaolinite surface at pH values between 6 and 7. Between pH of 7 and 7.5, a multinuclear surface complex formed. In the absence of carbonate, the dominant U surface species contained at least three U atoms, although such multinuclear complexes did not exist in the aqueous phase under the conditions of their experiments. This was interpreted as indicating that U polymerisation is enhanced by proximity to the kaolinite surface. The formation of a precipitate was considered to be unlikely, and this would be consistent with the ΣU employed (2×10^{-5} mol/L). The authors concluded that U sorption on kaolinite was sufficiently strong to make it promising as a sorbent for removing U from contaminated waters.

Chisholm-Brause *et al.* [1994] reported on U sorption by montmorillonite at acidic pH values (3.0-3.5). Surface structures were determined using XAFS. They concluded that the sorption complexes are structurally distinct from those in solution. McKinley *et al.* [1995] also studied U sorption on montmorillonite, and found a strong ionic strength dependence, particularly in the low pH range. This suggested that fixed charge sites dominate adsorption at low pH values. McKinley *et al.* [1995] used the results of experiments with simpler substrates - gibbsite and silica (representing Al and Si sites, respectively) to help in modelling the montmorillonite data.

Bruno *et al.* [1995] reported on an experimental system comprising amorphous Fe-oxide and U(VI), which were precipitated together. They felt that the behaviour of this system could be equally well described by modelling the U uptake by surface complexation on the Fe-oxide surface, or alternatively as a co-precipitation process. They preferred the latter explanation, apparently because it was simpler to model. In addition, it would seem reasonable based on their experimental technique. It was suggested that the co-precipitation mechanism could apply in nature. The authors noted that very little was known about the effect of the aging of Fe(III) oxides on uranium sorption.

Duff and Amrhein [1996] reported a detailed studied of U(VI) adsorption on goethite. A number of key variables were studied, including pH, pCO_2 (and carbonate alkalinity), and the presence of Ca, Mg and P. Dissolved Ca and Mg decreased U(VI) adsorption, but only at high pH values. The study included an extensive discussion of surface complexation modelling with a diffuse double layer model. The modelling proceeded using the familiar assumption that predominant solution phase species adsorbed onto the surface (in this case the UO_2OH^+ and $(UO_2)_2CO_3(OH)_3^-$ species). Given the inclusion of the latter binuclear surface species in their model, it is perhaps unfortunate that experiments were only carried out with only one ΣU (8.4 μmol/L). The authors felt that other carbonate surface species (such as $Fe\text{-}UO_2CO_3$ or $Fe\text{-}UO_2(CO_3)_2^{2-}$) should not be included in their model because adsorption was lowest in solutions that contained uranyl-carbonato species. Thus, they reached exactly the opposite conclusion of Kohler *et al.* [1992], who used a similar U speciation scheme

but different reasoning.

It is clear that U sorption has continued to be an area of active research interest, and attention has increasingly focussed upon developing models based on the surface complexation approach. However, there continues to be a lack of consensus on many key questions surrounding the structure of surface complexes. These include issues such as whether the surface speciation resembles that in solution, and whether uranyl carbonate species adsorb to the surface. In conclusion, it can be stated that there have not been any comprehensive experimental studies on U sorption by complex substrates (such as soils) involving the systematic variation of key parameters, including pH, ΣU, ionic strength and pCO_2. Given the absence of such studies, it is not surprising that there have been no substantial attempts to model sorption on natural materials with a mechanistic model such as the SCM.

PART II.

Experimental studies of U sorption on model minerals and natural materials

5 EXPERIMENTAL METHODS FOR U SORPTION

5.1 Substrates for U sorption experiments

5.1.1 Model minerals

Ferrihydrite (also referred to as hydrous ferric oxide - HFO) is an amorphous iron oxide with a high specific surface area, and is thought to be an important U-sorbing phase in the near-surface environment. It has been widely used as a model sorbent for anions and cations [Dzombak and Morel, 1990]. When first precipitated, HFO is X-ray amorphous, however, when aged for about 2 weeks, goethite begins to appear in the suspension [Dzombak and Morel, 1990]. The pH of a freshly precipitated HFO suspension changes rapidly for several hours. Thus, stable solution conditions can only be achieved if the suspension is aged briefly before experimentation. However, it should not be stored for long periods at room temperature, because the transformation to more crystalline Fe-oxides may change its sorption properties. For this reason, fresh ferrihydrite was prepared for each experiment. The transformation of Fe-oxides has implications for U sorption and is discussed in detail in Chapter 9.

The ferrihydrite used for sorption experiments was precipitated by raising the pH of a Fe(III) / HNO_3 solution to 6.0, and then aged for 65 hours at 25°C in a stirred jacketed vessel. The resulting precipitate has a stoichiometry near $Fe_2O_3.H_2O$ (i.e. 89 g of solid HFO / mol Fe) and a surface area of 600 m^2/g. These values were recommended by Dzombak and Morel [1990] for the purposes of standardising modelling approaches on HFO.

Kaolinite standards KGa-1 and KGa-1B were obtained from the Clay Minerals Society (CMS) Source Clays Repository in Columbia, USA. KGa-1 has been extensively characterised [Van Olphen and Fripiat, 1979], and KGa-1B is a mineralogically similar sample which was selected to replace the exhausted stock of KGa-1 [Pruett and Webb, 1993]. KGa-1 and KGa-1B are well crystallised kaolins

from Washington County, Georgia, and both samples contain a trace abundance of anatase. The BET surface areas of KGa-1 and KGa-1B are 8.4 m^2/g and 11.7 m^2/g, respectively. Prior to sorption experiments it was established that leaching of natural U from these clay materials was insufficient to significantly increase the amount of U in any of the experiments.

Uranium sorption on mixed substrates containing both kaolinite and ferrihydrite was also studied. These substrates were prepared by raising the pH of an acidic solution of Fe(III) in the presence of a weighed amount of kaolinite (KGa-1). After an aging time of 65 hr, the mixed slurry was vigorously agitated and aliquots were transferred to centrifuge tubes for sorption experiments. The amounts of ferrihydrite and kaolinite were chosen so that the final suspension had the same mass loadings of these minerals as were present in most other experiments (89 mg/L and 4 g/L respectively).

5.1.2 Koongarra substrates
5.1.3

Cores were obtained from a number of locations (boreholes W1, W2, and W7) in the Koongarra weathered zone using a cable-tool rig, which produces intact samples (rather than the pulverised samples obtained with a percussion rig). The W1 core was a highly weathered schist from above the upstream edge of the orebody - a region considered to be the former upward extension of the primary ore. W2 is near the leading edge of the dispersion fan approximately 50 m down-gradient from the primary ore zone. W7 is about 100 m further down-gradient and the U content of this solid phase was only slightly elevated relative to background. This sample allowed the study of systems containing much lower total U (ΣU). The approximate locations of W1, W2 and W7 relative to the primary and secondary orezones are indicated on Figure 1.1. A detailed description of the geology of the Koongarra deposit and the location of boreholes is given by Snelling [1994].

A fine fraction for use in sorption experiments was obtained from the core materials, by sieving through a 1 mm mesh, then a 250 μm mesh, followed by

sedimentation. The sampled fraction had a particle size which was nominally below 10 μm (as defined by Stoke's Law). The mass loading in this slurry was determined by vigorously shaking to homogenize the slurry and then taking fixed volumes and evaporating them to dryness. The slurry was found to consist of a homogeneous suspension of fine particles, that could be reproducibly sub-sampled provided it was vigorously agitated beforehand. Repeat samplings showed that the sample removal technique was reproducible to within 3%.

The Koongarra samples were examined using electron microscopy and subjected to a sequential extraction procedure. These investigations are discussed in Chapter 8.

5.2 Procedure for sorption experiments

Experiments with model minerals

Batch experiments were carried out in polypropylene centrifuge tubes. Each tube had a 2 mm hole in the lid to permit air equilibration without loss of sample during agitation. An aliquot of the ferrihydrite slurry was suspended in $NaNO_3$ (usually 0.1 mol/L). For most experiments, the amount of solid corresponded to a total Fe content (ΣFe) of 1 mmol/L (89 mg/L as $Fe_2O_3.H_2O$). The procedures used for kaolinite were similar, except that a weighed amount of clay (usually with a mass loading of 4 g/L) was substituted for the HFO.

In experiments with added ligands, phosphate (as NaH_2PO_4), humic acid (a filtered solution of sodium humate), sodium citrate or sodium sulfate was added at this stage. For studies at pH > 7.0, sufficient $NaHCO_3$ was added to the system to achieve equilibrium with air at the desired pH. This ensured pH stability and fixed the carbonate content of the system. The required amount of $NaHCO_3$ was calculated using MINTEQA2. Continued equilibration of carbonate species in the system with air was ensured by the tubes being open to the air (as described above). This is

important because the equilibrium state of the system is determined by whether it is open or closed with respect to CO_2.

Uranium was added either as ^{236}U or as depleted natural uranium (predominantly ^{238}U) depending on the experimental requirements. ^{238}U was used for higher concentration ranges with subsequent analysis using the kinetic phosphorescence analyser (see below). ^{236}U was used for experiments with low ΣU. The U(VI) was added after 24 hr 'pre-equilibration' during which the system was allowed to come to equilibrium under the appropriate chemical conditions. The contact time for U was 48 hr, with the pH being checked and adjusted if necessary after 24 hr. The equilibration time was selected after carrying out preliminary experiments in which the uptake of U on ferrihydrite was studied as a function of time (Section 6.1). The experimental tubes were gently shaken in a waterbath at 25°C. Immediately prior to sampling, the pH was again determined and assessed for acceptable stability. The acceptability criteria was a pH change of less than 0.1 pH units in the final 24 hours of the experiment (also see Section 6.1). The aqueous phase was then separated by high speed centrifugation (RCF > 6500*g*) for 30 minutes. This centrifugation procedure was selected after assessing the relative merits of an alternative filtration technique (see Section 5.7).

While most U sorption experiments were undertaken under atmospheric conditions, some investigations were performed in a glove-box at an elevated partial pressure of carbon dioxide. A special gas mixture of 2% CO_2 and 98% N_2 was obtained for these experiments. The gas composition used in the glove-box was a 50:50 mixture of this gas with ordinary air. The gas composition was thus approximately 1% CO_2 : 10% O_2 : 89% N_2. The presence of oxygen derived from the air ensured the stability of the solid phases against reductive dissolution, and provided a convenient means to monitor the mixing ratio of the air and the special gas. This was done by measuring the oxygen concentration in the glove-box and maintaining the measured value at close to 10%, i.e. half the value in normal air[1].

[1]The assistance of D. Garton in setting up the glove-box is gratefully acknowledged.

Experiments with natural substrates

The experimental procedures with Koongarra materials were similar to those used for the sorption experiments with the model minerals. The stock slurry of fine particles was vigorously agitated to fully suspend the solid, and aliquots containing known amounts of particles were transferred to 25 mL polypropylene centrifuge tubes, and suspended in $NaNO_3$ (usually 0.1 mol/L). After 24 hours at the experimental pH, U was added to the systems either as ^{236}U or ^{238}U. The system was then equilibrated for 48 hours and the aqueous phase separated as described above. As in the experiments with the model minerals, experimental parameters such as pH, ΣU, ionic strength and pCO_2 were systematically varied to determine their effect on U sorption.

The artificial isotope, ^{236}U, was used in many experiments with natural substrates in order to distinguish between the natural uranium derived from the samples and ^{236}U added to the aqueous phase. The subsequent analysis in these cases was by α-spectrometry. The amount of ^{236}U spike added was either 10^{-8} mol/L or 10^{-7} mol/L. Except for experiments with the W7 sample, the amount of ^{236}U added to the aqueous phase was much lower than the concentration of ^{238}U derived from the accessible U content of the solid phase. Therefore the latter contribution must be estimated in order to determine the total amount of U (ΣU) in the experimental systems (see Section 8.3).

^{238}U was used for experiments with high total U concentrations when isotopic information was not required. In these experiments, the added U (typically 10^{-4} mol/L) provided the major part of the total U in the system. The subsequent analysis was by kinetic phosphorescence analysis or α-spectrometry. The analytical techniques are discussed in Section 5.3.

5.3 Analytical techniques for dissolved U

Uranium concentrations in the supernate were determined using the Kinetic Phosphorescence Analyser (model KPA-10) or by α-spectrometry. The latter technique provides isotopic measurements and was used for experiments where ^{236}U was added.

Uranium analysis using the KPA

In the KPA, a laser pulse is used to electronically excite uranyl-containing ions. The excited phosphor then returns to the ground state with the emission of a photon, following first-order kinetics [Chemchek, 1990]. The KPA measures the time-dependent decay of light intensity, and calculates the initial intensity by extrapolating to time zero (i.e. the end of the laser pulse). The initial intensity is proportional to the U concentration. For good precision, several hundred laser pulses are used in each measurement and the results averaged. The KPA enables rapid determination of U concentrations in aqueous samples with good sensitivity and accuracy, provided that interferences are not present.

The operation of the KPA is straightforward and is controlled through a personal computer. Several standards spanning the concentration range of interest are used to calibrate the instrument. In each case, 1.0 mL of sample (previously acidified with HNO_3 to pH ~1.5) and 1.5 mL of Uraplex (a proprietary complexing agent) are placed in a 1.0 cm cuvette and the emission intensity measured. A typical calibration curve is shown in Figure 5.1.

After calibration, samples were measured in a similar manner to the standards. Although the technique can be prone to interferences, no interfering substances were present in typical sorption experiments with model minerals and a background electrolyte of $NaNO_3$. In experiments with citrate or humic acid (HA), organic materials were destroyed by repeated digestion with HNO_3 prior to the KPA measurement.

Uranium analysis using alpha-spectrometry

As indicated above, α-spectrometry was used in many studies with natural substrates, as this allowed both the uptake of ^{236}U and the partial desorption of the natural ^{238}U in the samples to be monitored. The various U isotopes were simultaneously measured using α-spectrometry, after addition of ^{232}U as a yield tracer. The U was separated by anion exchange techniques and electrodeposited on a stainless steel disc for α-spectrometry [Payne *et al.*, 1994].

The uranium spectrum of the solution phase on completion of a U sorption experiment is shown in Figure 5.2. The ^{238}U peak results from the leaching of natural uranium into the aqueous phase, whereas the ^{236}U peak indicates the amount of the ^{236}U spike remaining in solution after adsorption. The amounts of ^{238}U and ^{236}U in the solution phase were calculated from their count rate relative to the ^{232}U peak after correction for the minor background counts.

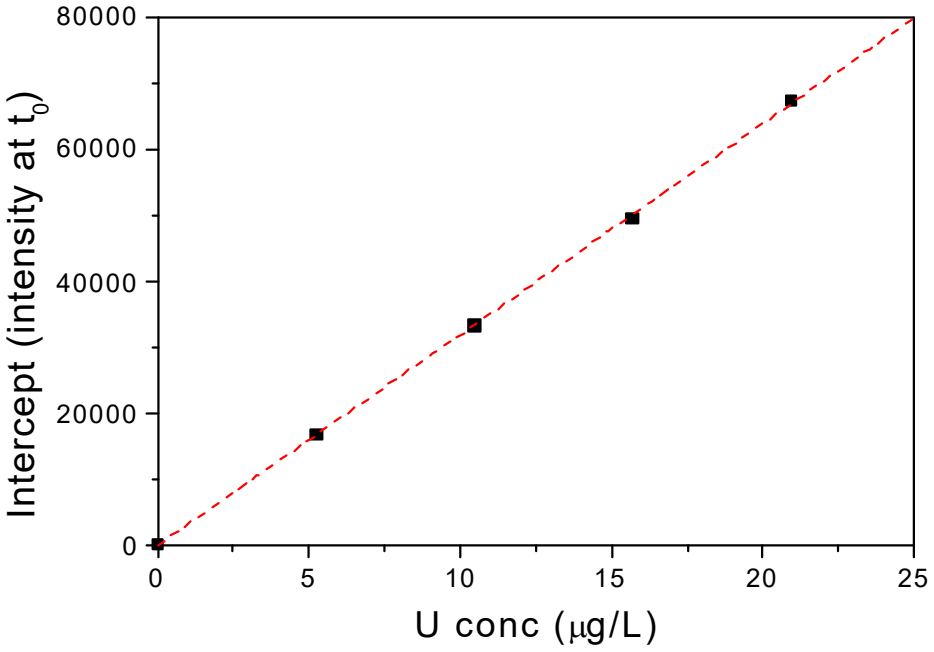


FIGURE 5.1 Calibration curve for KPA in the concentration range below 25 ppb.

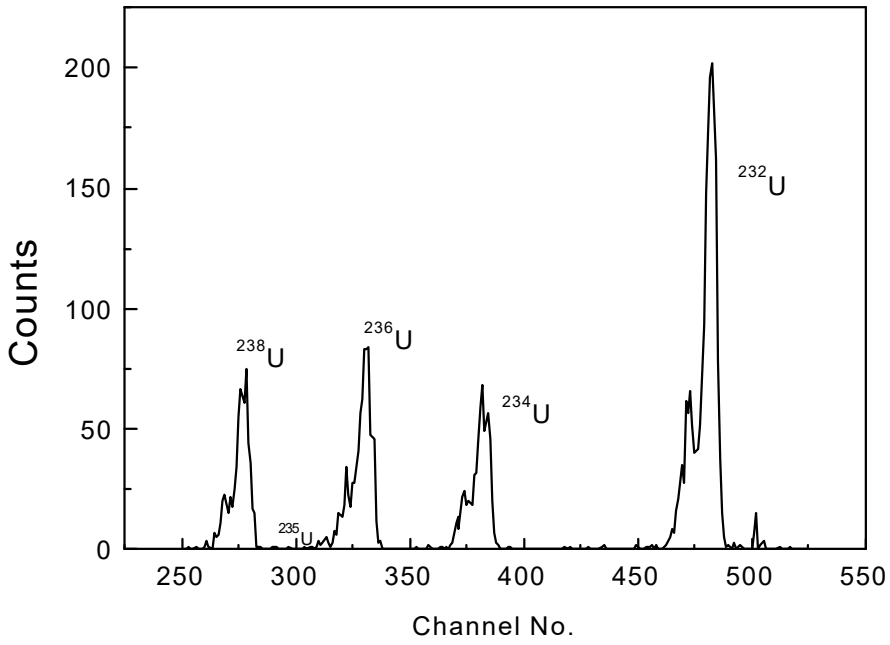


FIGURE 5.2 Uranium α-spectrum obtained after adsorption / desorption experiment.

5.4 Analytical electron microscopy (AEM)[1]

The association of adsorbed U with kaolinite surfaces was studied using a JEOL 2000FX transmission electron microscope (TEM) equipped with a Tracor-Northern Si(Li) energy dispersive X-ray (EDX) spectrometer and a Link Isis analyser (Oxford Instruments). These samples were prepared by evaporating a small droplet of clay suspension onto a holey carbon TEM grid. Samples which had been suspended in $NaNO_3$ were centrifuged and re-suspended in milli-Q water prior to the evaporation step, to reduce the amount of $NaNO_3$ on the grid.

AEM was carried out with an operating voltage of 200 kV and a beam current of 110 μA. Analyses were acquired for 400 - 600 seconds live time and reduced to

[1]The AEM instrument was operated by Dr G. Lumpkin (Advanced Materials Division, ANSTO).

elemental weight percentages using the Link Isis software package TEMQuant. Experimental k-factors for the data reduction were obtained from a large suite of silicate mineral standards.

5.5 Reproducibility and sources of error in U sorption experiments

The techniques used in deriving U(VI) adsorption data were tested by repeating a U(VI) adsorption experiment to determine the U sorption edge on ferrihydrite. (In this section, attention is restricted to the reproducibility of the sorption data. The features of the U-sorption edges are discussed in detail in Chapter 6). The results of the two sets of experiments (Figure 5.3) show that good reproducibility (in terms of the position of the pH edge) can be obtained using the experimental techniques employed in this project.

It is important when interpreting the experimental results to take into consideration that the amount of U adsorbed was determined from the measurement of *dissolved* uranium concentrations. The percentage of U adsorbed was then calculated by subtracting the measured U concentration in solution (which was generally assigned an error of $\pm$ 4%) from the U initially added to the experiment. In most cases, the error bars shown on the figures arise from this source. The principal advantages of the separation technique are that it is simple, reproducible, and provides suitable samples for direct U analysis (i.e. liquid of low acid strength). It also enables the position of the centre of the pH edge to be precisely determined. However, small uptakes of U cannot be precisely measured by this technique, and as a result, experimental scatter tends to be greatest at low (and high) pH values where U sorption is minimal.

Another source of error can be inadequate separation of solid and liquid phases, leading to the inclusion of particles in the ‘dissolved’ or supernate fraction. This always results in an over-estimate of dissolved U concentrations, and is more serious when U uptake on the solid is close to 100% (see Section 5.7 below for

further discussion of solid-liquid separation techniques). As shown by Hsi and Langmuir [1985] this can be a major problem if the U sorption data in the mid pH range are converted to K_d values. This source of error is less of a problem for the type of modelling described in this thesis, where the focus is on a model fit for the sorption 'edge' where U uptake increases rapidly from zero to above 90%. The adequacy of the experimental separation technique is assessed further in Section 5.7.

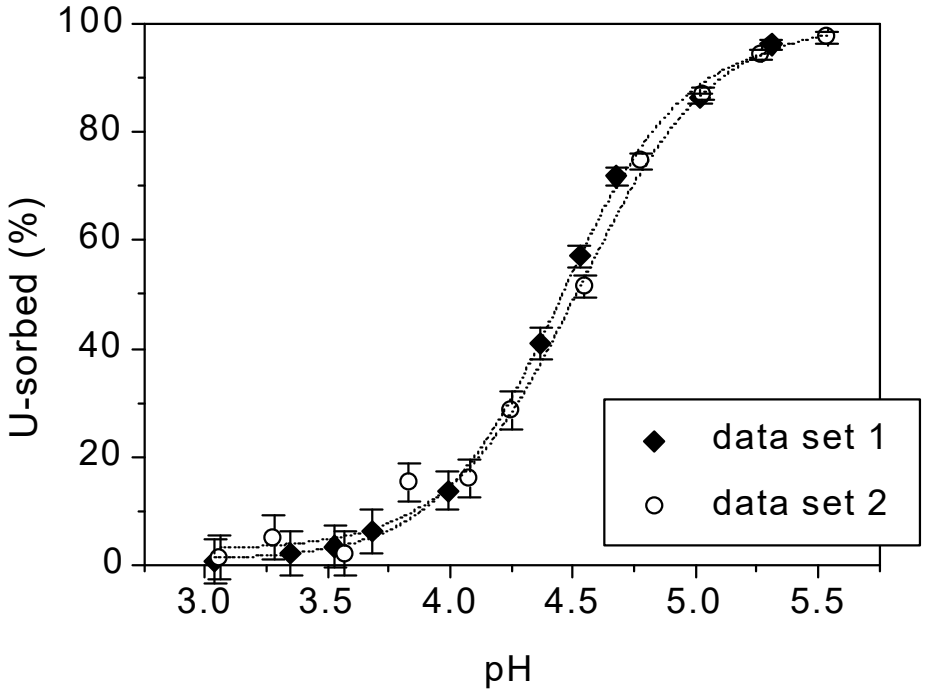


FIGURE 5.3 Reproducibility of data obtained for U sorption on ferrihydrite. (ΣU = 1 μmol/L, ΣFe = 1 mmol/L, 0.1 M $NaNO_3$)

5.6 Sorption on container materials

Trace metals and radionuclides tend to adsorb on any available surface. As a result, blank experiments carried out without a mineral sorbing phase present often indicate substantial uptake of metal on the container walls. Recent work with several plastic materials (polypropylene, teflon and polycarbonate) has shown that these materials can remove 50% or more of U(VI) from solution, particularly at low total U concentrations [Pabalan *et al.*, 1994]. Teflon vessels were not used in the experimental work, because fluoride has been detected in experimental solutions contained in Teflon, even in non-irradiated Teflon at low temperatures [Solomah, 1983; Crine, 1987]. This presumably results from leaching of F from the Teflon. If this occurred, complexation of U(VI) with F would influence experimental results. Polypropylene centrifuge tubes were used for the sorption experiments. Blank experiments with polypropylene tubes in the absence of a sorbing solid showed that uptake on the vessel walls reached almost 25% at pH values between approximately 5 and 7 (Figure 5.4). In comparison, U sorption on ferrihydrite (ΣFe of 1 mmol/L) was close to 100% across this pH range. In order to determine the quantity of U adsorbed by the vessel when ferrihydrite was present, some experiments were carried out in which the tube contents were vigorously shaken and then decanted, removing both the solid and liquid. The vessel walls were then leached with HNO_3 and the U content was determined. Iron was also measured in order to quantify the amount of U bound to ferrihydrite particles which were themselves attached to the vessel walls. It was concluded that direct uptake of U on the vessel walls was greatly reduced by the presence of ferrihydrite, and was probably less than 5% under the conditions of these experiments (Figure 5.4).

Wall sorption was also expected to be a potential problem in experiments with kaolinite, which has a smaller specific surface area, and is a weaker U adsorber than ferrihydrite. Experiments to precisely quantify tube sorption with kaolinite present were unsuccessful, because the kaolinite particles tended to aggregate and adhere

to the vessel walls. However, the results indicated that if sufficient solid was present, the mineral surfaces would dominate U sorption in the system. As a result of these investigations, much higher mass loadings (4 g/L) were used for kaolinite sorption experiments than were used with ferrihydrite (89 mg/L).

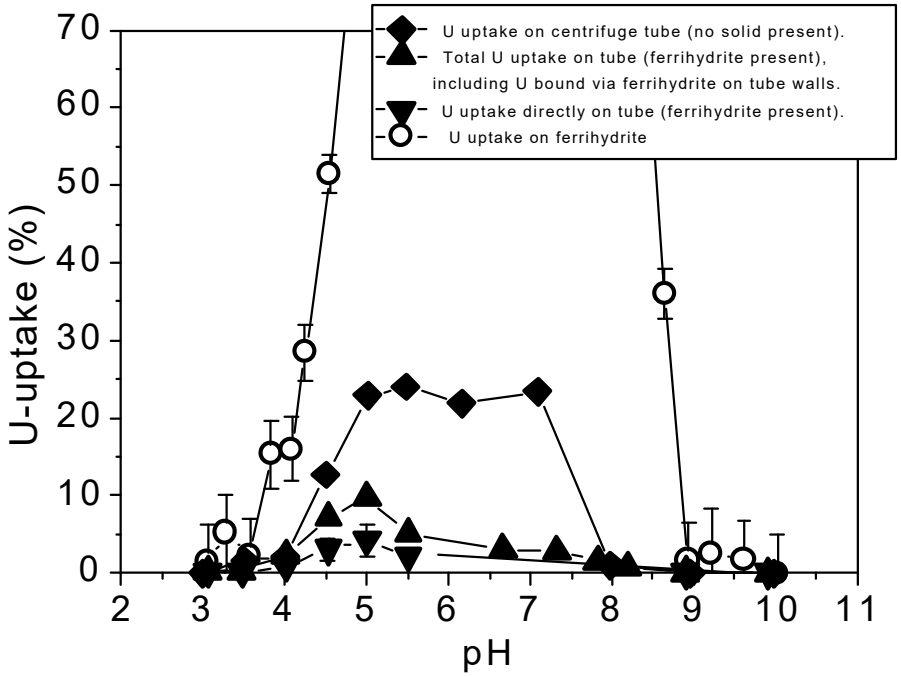


FIGURE 5.4 U (VI) uptake on polypropylene centrifuge tubes in presence and absence of ferrihydrite (ΣU = 1 µmol/L). Uptake curve of U on ferrihydrite is also shown. (ΣFe = 1 mmol/L, 0.1 M $NaNO_3$)

5.7 Assessment of separation technique

As noted above, high speed centrifugation was normally used for solid / liquid separation in the U sorption experiments. Compared to the alternative method of filtration, the main advantages of centrifugation are its greater simplicity, the lower probability of sample contamination, and the reduced

opportunity for sorption on the surfaces of filters and containers. These benefits arise because there is no transfer of sample into filtration equipment.

The main drawbacks of centrifugation include the loss of information relating to the particle size distribution of adsorbed U, and the possibility of inadequate separation of solid and liquid leading to over-estimation of aqueous U. In order to compare the results obtained by filtration and centrifugation, the position of the low-pH U adsorption edge was determined after separation using both procedures for some experiments. The filtration was carried out using various pore-sizes of 10,000 MW, 100,000 MW and 0.45 μm.

During the course of this work it was found that the U contents in filtrates obtained using new filters were lower than those obtained when the filters had been pre-conditioned with the sample solution. This indicated that adsorption of U occurred on unconditioned filter membranes, and is consistent with results obtained for other ions by Salbu *et al.* [1985]. It was concluded that pre-conditioning is necessary when filtration is used for solid / liquid separation.

The U sorption results obtained by filtration with pre-conditioned filters of various pore-sizes were not significantly different to those obtained using centrifugation (Figure 5.5). This is possibly surprising considering that freshly precipitated HFO particles are reported to be in the size range 1 – 10 nm [Dzombak and Morel, 1990]. It appears that during the preparation and aging of the ferrihydrite, some agglomeration of particles must occur. The particle sizes are such that no effects of filter pore-size and no differences between centrifugation and filtration were observed.

The data suggest that the use of centrifugation rather than filtration does not significantly affect data obtained in sorption edge type work, in which attention is primarily focussed on the position of the sorption edges (i.e. where sorption increases from negligible amounts to >90% sorption). However, centrifugation is less susceptible to problems of cross-contamination and is much simpler, particularly when the necessity of pre-conditioning filters is considered.

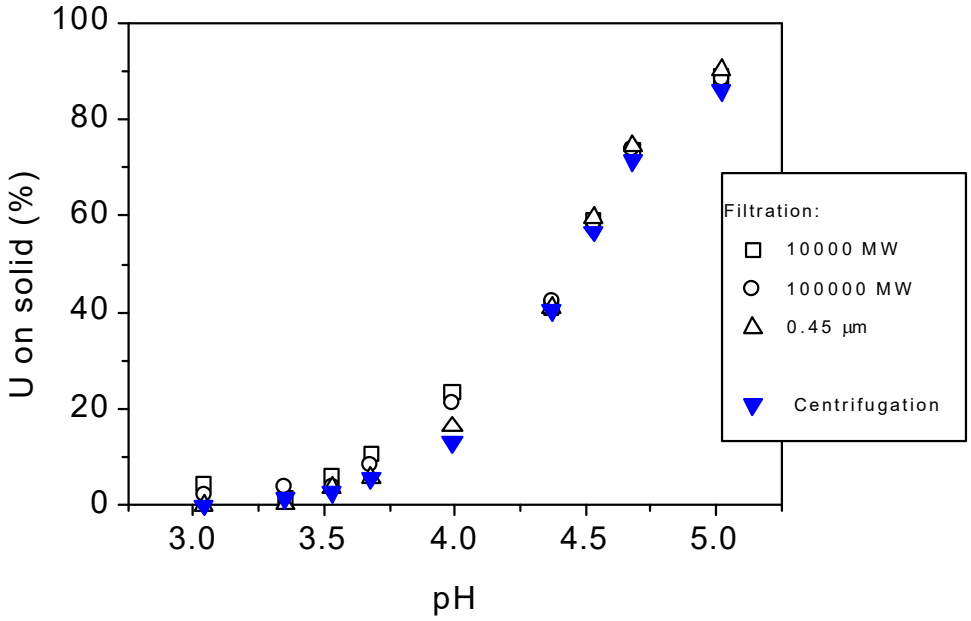


FIGURE 5.5 Uranium associated with solid determined by centrifugation or by membrane filtration using pre-conditioned membranes. (ΣU = 1 µmol/L, ΣFe = 1 mmol/L, 0.1 M $NaNO_3$)

Centrifugation may be susceptible to the inadvertent inclusion of particles when sorption is close to 100%. This could cause significant over-estimates of dissolved U concentrations. Hsi and Langmuir [1985] noted this as a likely cause of discrepancies in dissolved U under conditions of high U sorption on Fe-oxides.

5.8 Sample preparation for EXAFS

As mentioned in Section 4.4, spectroscopic techniques, including EXAFS, are now being used to derive information about the structure of surface complexes on mineral surfaces. The development of this technique means that the formulation of equations to describe the sorption of trace metals is less reliant on guesswork about the stoichiometry and structure of surface complexes.

Within this project, EXAFS was undertaken at the Center for Materials Research, Stanford University[1]. EXAFS analysis was performed on ferrihydrite containing U that had been adsorbed under similar conditions to those used for the batch adsorption experiments. However, the experimental procedure was modified because the EXAFS measurement required relatively high U contents. In order to achieve this with minimal possibility of precipitation, U was adsorbed onto the ferrihydrite from relatively dilute solutions of uranyl, and the resulting slurry was subsequently concentrated using centrifugation.

The adsorption solutions contained 1 mmol/L of ferrihydrite (as ΣFe) in a volume of 2000 mL. The ferrihydrite had been prepared in the usual way (i.e. precipitated at pH of 6.0 and aged for 65 hours at 25° C). The pH of the ferrihydrite slurries was then adjusted to the required pH values (5.0 and 5.5). Uranyl spike was then added to total of 2.5 μmol/L and 100 μmol/L. (Figure 3.8 shows that precipitation of amorphous uranyl hydroxide would not be expected under these conditions). After 48 hours at constant pH, during which the suspensions were agitated, the four samples were concentrated to wet pastes by centrifugation. The samples were shipped to California and analysed shortly thereafter. Most of the EXAFS analysis was carried out on samples denoted UF3 and UF4, containing U/Fe molar ratios of 0.044 and 0.077 respectively. Two samples with lower U contents (UF1 and UF2) provided insufficient signal strength for quantitative EXAFS analysis.

[1] The samples were prepared by the author, but the work at Stanford was undertaken by a group led by Drs G.A. Waychunas and N. Xu

6 URANIUM(VI) UPTAKE ON FERRIHYDRITE

This chapter presents experimental results for U sorption on ferrihydrite in systems containing $NaNO_3$ as the background electrolyte. These systems were equilibrated with air, or an atmosphere containing an elevated partial pressure of CO_2. Due to the presence of CO_2 in both types of experiments, complexation of U with carbonate species is of major importance, and such systems are referred to as 'simple $NaNO_3/CO_2$ systems'. The pH, ΣU, ionic strength, partial pressure of CO_2 (pCO_2) and mass loading were systematically varied in these experiments. In terms of surface complexation studies, this means varying the following aqueous components: H^+, UO_2^{2+}, Na^+, NO_3^- and CO_3^{2-}; and the quantity of sorbing minerals. In this chapter the effects on U sorption by ferrihydrite of complexing and competing ligands including phosphate, citrate, sulfate and humic acid are also discussed. Possible models for the experimental data are presented in Part III of this thesis.

The majority of the experimental data is presented as pH edges, in which pH is the independent variable and U uptake is the dependent variable. This format is particularly suitable for modelling the data with the SCM. However, because of the complexity of some of the experimental systems (particularly those containing both U and P), some experiments were carried out in which the pH was held constant and the amount of U was varied. These data are presented in section 6.5 in isotherm format (i.e. adsorbed U as function of dissolved U).

6.1 Kinetics of U sorption on ferrihydrite

As observed by Dzombak and Morel [1990], “appropriate reaction times in ion sorption experiments are critical to ensure the achievement of equilibrium”. In order to select an appropriate experimental duration for the batch experiments, a series of preliminary kinetic experiments were carried out. In these experiments, 250 mL of HFO suspension solution was prepared, aged and a U spike was added. A pH-stat was used to maintain the pH. Small sub-samples were periodically removed and centrifuged to determine the dissolved U content. The technique differed slightly from

the subsequent batch experiments, which consisted of separate smaller tubes (25 mL), which were only sampled once (see Section 5.2).

The uptake of dissolved U on the solid was very rapid in the first hour of the experiment (Figure 6.1), with a significant rate of uptake continuing for about one day. The data for time periods greater than 24 hours are ambiguous, and may reflect a continuing slow uptake.

In selecting a 'standard' equilibration time, several factors were considered. Clearly, equilibration times shorter than about 10 hours do not represent equilibrium for U sorption on ferrihydrite. Dzombak and Morel [1990], who reviewed the literature studies of cation and anion sorption on HFO, rejected numerous data-sets because of insufficient equilibration times.

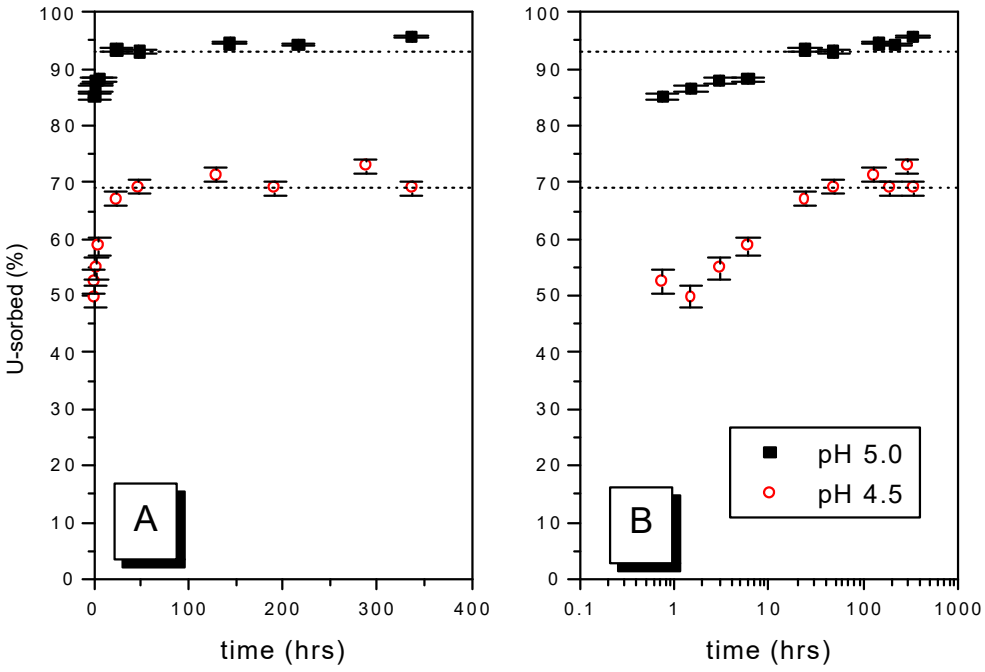


FIGURE 6.1 Kinetics of U sorption on ferrihydrite at pH 5.0 and 4.5. The horizontal lines indicate the amount of U sorbed after 48 hours equilibration time. Time axes are (A) linear and (B) logarithmic. ($\Sigma U = 10^{-7}$ mol/L, ΣFe = 1 mmol/L, 0.1 M $NaNO_3$)

During longer equilibration periods of several hundred hours, it would be expected that the sorption properties of ferrihydrite would change, due to its partial conversion to goethite. In addition, it would be difficult to maintain a stable pH in the subsequent batch adsorption experiments over long time-periods (experience showed that, in the absence of a pH-stat, pH values tended to gradually drift with time). The pH cannot be stabilised using a pH buffer in this type of experiment, because pH buffers would introduce additional ions with unknown effects in terms of complexing U and / or competing for surface adsorption sites. In addition, the complexities involved in running the apparatus for periods exceeding a few days would also limit the rate with which data could be collected.

After considering the data presented in Figure 6.1 and the experimental constraints, it was decided that an equilibration time of 48 hours was appropriate for the batch adsorption experiments. The experimental protocol described in Section 5.2 was then established. It should be noted that the pH was not adjusted during the 24 hours prior to sampling, and samples were rejected if an unacceptable pH drift (more than 0.005 pH units per hour) occurred in this period. Typically, data were obtained with a pH drift below 0.05 units in the final 24 hours of each experimental run.

6.2 Effect of experimental conditions on U sorption

6.2.1 pH and mass loading

In the initial set of batch adsorption experiments, the percentage of U adsorbed by ferrihydrite was measured across a wide pH range. The experimental data are shown in Figure 6.2. The data for the air-equilibrated system containing a total of 1.0 μmol/L of U and 1.0 mmol/L of Fe in a background electrolyte of 0.1 M $NaNO_3$ (shown as ■) comprise a standard data set with which much of the data obtained for U sorption on ferrihydrite will be compared.

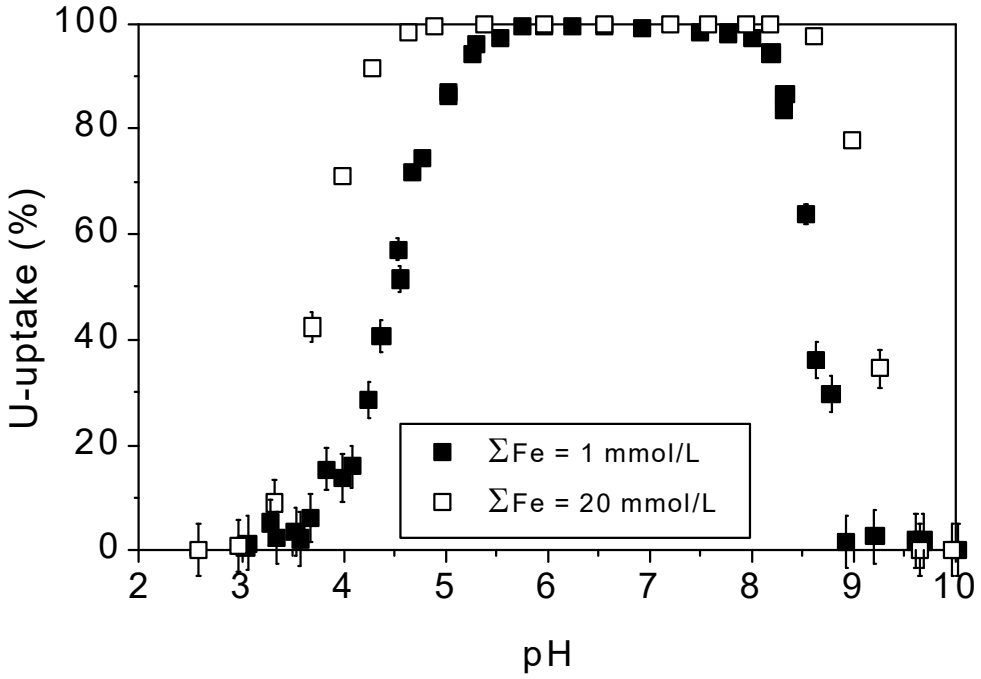


FIGURE 6.2 U(VI) sorption on ferrihydrite – effect of pH and mass loading of ferrihydrite. (ΣU = 1 μmol/L, 0.1 M $NaNO_3$)

Below pH 7, the sorption of UO_2^{2+} in air-equilibrated systems increased with increasing pH (the 'low pH sorption edge'), with a sharp decrease in sorption occurring above pH about 8 (the 'high pH edge'). The data confirm that the uptake of U in air-equilibrated systems is greatest at near-neutral pH values. The strong complexation of U(VI) with carbonate in the solution phase (Section 3.2) is responsible for the decrease in adsorption of U(VI) at pH values above 8. Tripathi [1983] showed that there is no decrease in the extent of U(VI) sorption at high pH values in systems which are free of CO_2.

As might be expected, the uptake of U on ferrihydrite is a function of the mass loading of the solid in the system (Figure 6.2). This is due to the greater number of surface sites available for U uptake.

6.2.2 Total U

Figure 6.3 shows sorption curves for U on ferrihydrite over a range of ΣU from 10^{-8} mol/L to 10^{-4} mol/L. The positions of the sorption edges in Figure 6.3 are dependent on ΣU. For a given pH, the percentage of U adsorbed decreases with increasing ΣU. This can be explained on the basis of the existence of a relatively small number of 'strong' surface sites, and a larger number of 'weak' sites. Such two-site models have been found to be applicable to the sorption of a range of metals on ferrihydrite [Dzombak and Morel, 1990].

The dependence of the position of the U sorption edges on ΣU (Figure 6.3) is a significant result, since it implies that U sorption can only be understood and modelled if data are obtained over a range of ΣU. As was discussed in Chapter 4, many previous studies of U sorption only included one value of ΣU. It will be observed that the data shown in Figure 6.3 are incompatible with the predictions based on the model of Hsi and Langmuir [1985] as depicted in Figure 4.2.

Uranium sorption isotherms

The adsorption of U on ferrihydrite (expressed as mol U adsorbed per mol Fe) can be plotted against the concentration of U in solution to yield a plot known as an adsorption 'isotherm'. The shape and slope (if linear) of the resulting curve may then be examined to determine if it conforms to one of various expressions including the Langmuir and Freundlich isotherms (Figure 2.2). In cases when sorption is strongly dependent on pH (such as U) the construction of such curves is only of value when the pH is held constant. In Figure 6.4, a series of isotherms for U sorption on ferrihydrite (at various pH values) is plotted. The data-points were obtained by re-plotting some of the data from 6.3 in an isotherm format. The results clearly show that U adsorption on ferrihydrite is non-linear. This indicates that sites of differing affinity for U sorption are present on the surface of the solid. It should be noted in interpreting Figure 6.4 that U-speciation is a function of U concentration as well as of pH (see Chapter 3).

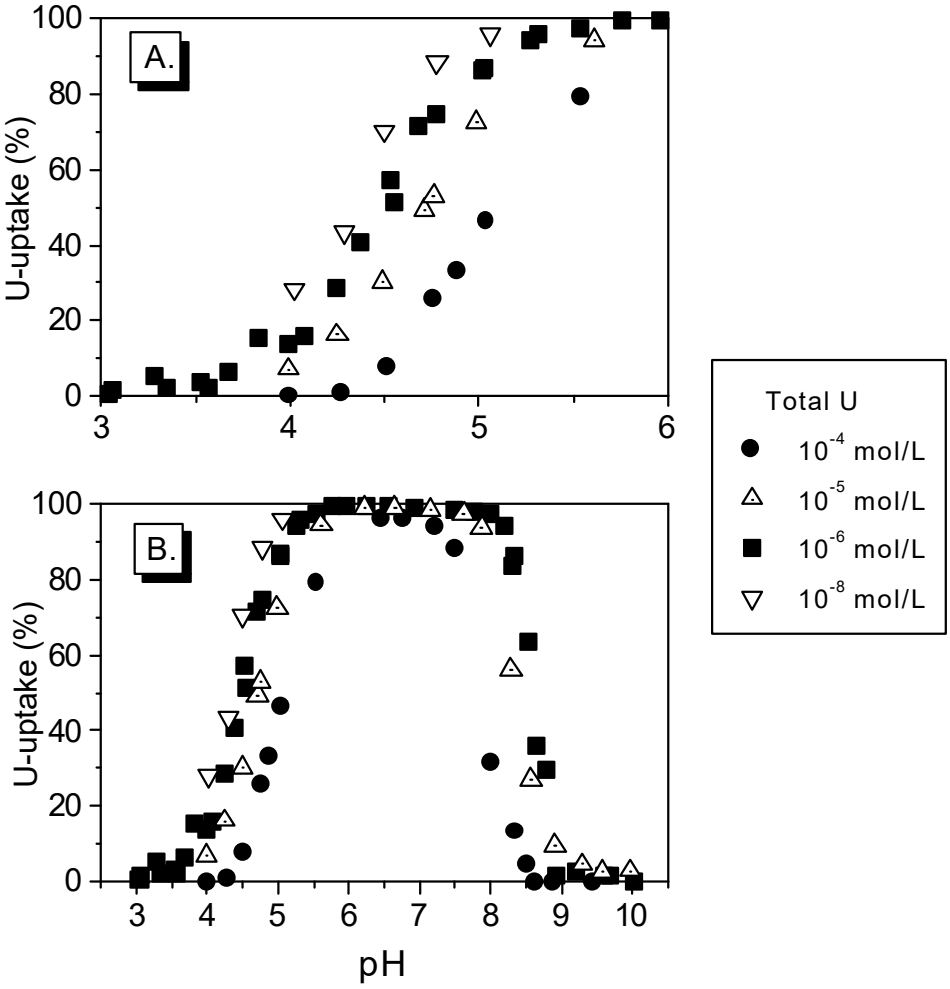


FIGURE 6.3 U(VI) sorption to ferrihydrite for a range of ΣU.

A. Low-pH edge B. Full pH range

(ΣFe = 1 mmol/L, 0.1 M $NaNO_3$)

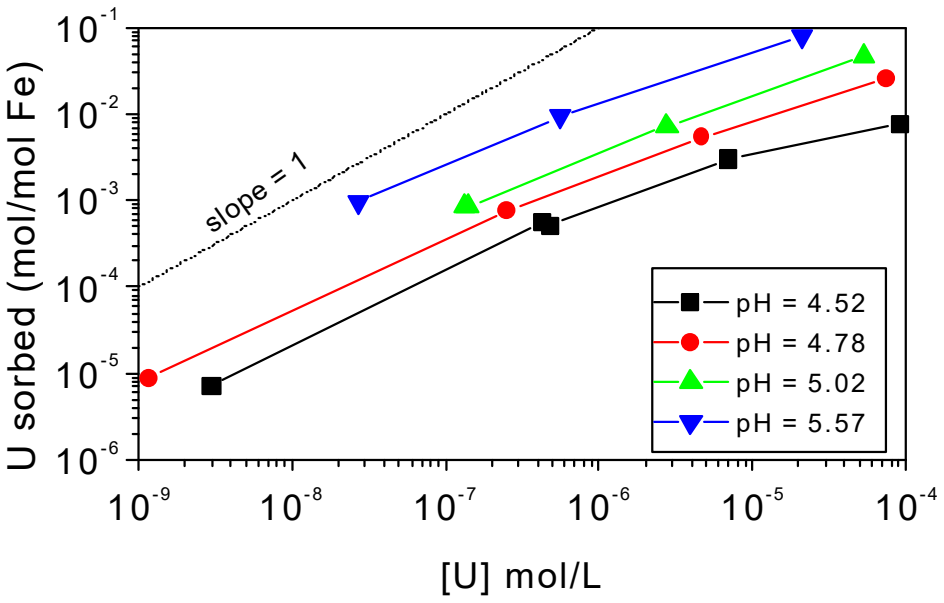


FIGURE 6.4 U sorption data on ferrihydrite presented as 'isotherms', obtained by re-calculating selected data points from Figure 6.3. Each of the curves was obtained at a fixed pH value, with an uncertainty in pH of approximately 0.05 units. A hypothetical isotherm with a slope of unity is shown for comparison.

Some additional experiments were carried out to study the sorption isotherms in detail, at fixed pH values of 4.5 and 5.25. The data showed a dramatic decrease in the percentage of U adsorbed with increasing ΣU, and corresponded to Freundlich isotherms with slopes significantly below 1.0, indicating multiple site adsorption (Figures 6.5 and 6.6). A significant implication of these data is the apparent absence of precipitation in the experiments summarised in Figure 6.6.This would be indicated by an upward deviation of the data-curve at high values of ΣU. However, the solubility calculations discussed in Chapter 3 indicate that the system at pH 5.25 is close to precipitation of $UO_2(OH)_2$ at the highest values of ΣU studied in these experiments.

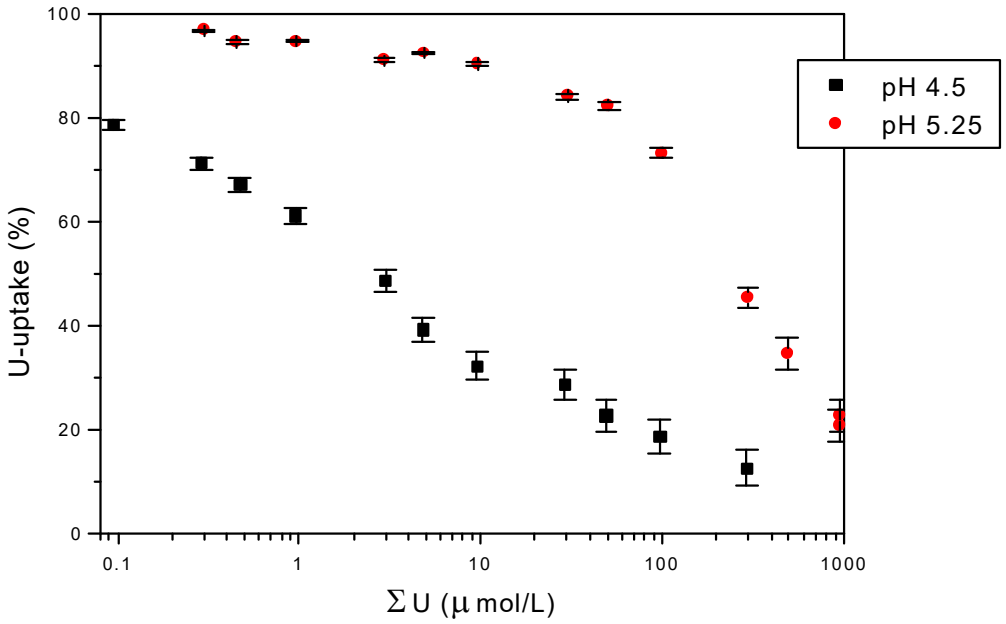


FIGURE 6.5 U uptake as a function of ΣU at fixed pH values of 4.5 and 5.25. Note the much lower percentage of U adsorbed in systems with higher ΣU. (ΣFe = 1 mmol/L, 0.02 mol/L $NaNO_3$)

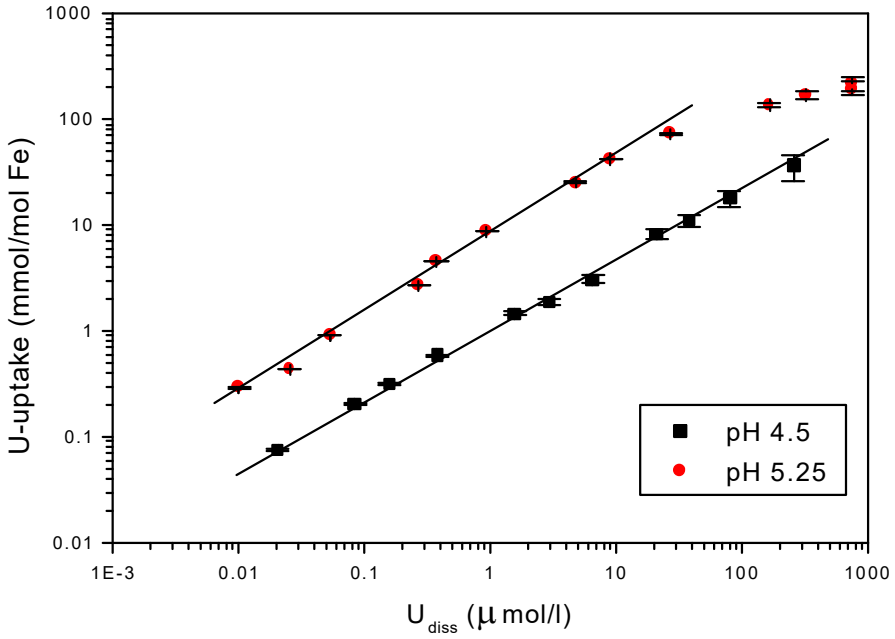


FIGURE 6.6 U sorption isotherms for systems shown in Figure 6.5. The isotherms are approximately linear (slope <1), but level off at high [U] indicating site saturation is being approached. In contrast to the analogous kaolinite experiments (see Chapter 7), there is no evidence for precipitation in these systems.

6.2.3 Partial pressure of CO_2 and ionic strength

As noted above, carbonate is important in uranyl speciation, so additional experiments were carried out in a glove-box, with an elevated pCO_2 of 10^{-2} atm. The sorption of U on ferrihydrite in the high pH range was significantly reduced at the higher partial pressure of CO_2, due to the dominance of weakly sorbing anionic uranyl carbonate species (Figure 6.7). The low pH adsorption edge was not significantly affected by pCO_2 although there may be a slight increase in sorption at higher pCO_2.

Another parameter which was considered likely to affect U sorption is the ionic strength, which in natural systems may vary over a wide range. The dependence of

metal uptake on ionic strength can sometimes indicate whether inner sphere or outer sphere surface complexes are present [Stumm, 1992]. As shown in Figure 4.3, the triple layer model for U sorption adopted by Tripathi [1983] predicts that the low pH edge for U sorption should be sensitive to ionic strength.

The results of U sorption experiments with ferrihydrite indicated that ionic strength had little or no measurable effect on the low pH edge, but at high pH values increasing ionic strength reduced U sorption on ferrihydrite (Figure 6.8). The reasons for the observed phenomena, as well as possible mechanisms and models, will be discussed in Part III of this thesis.

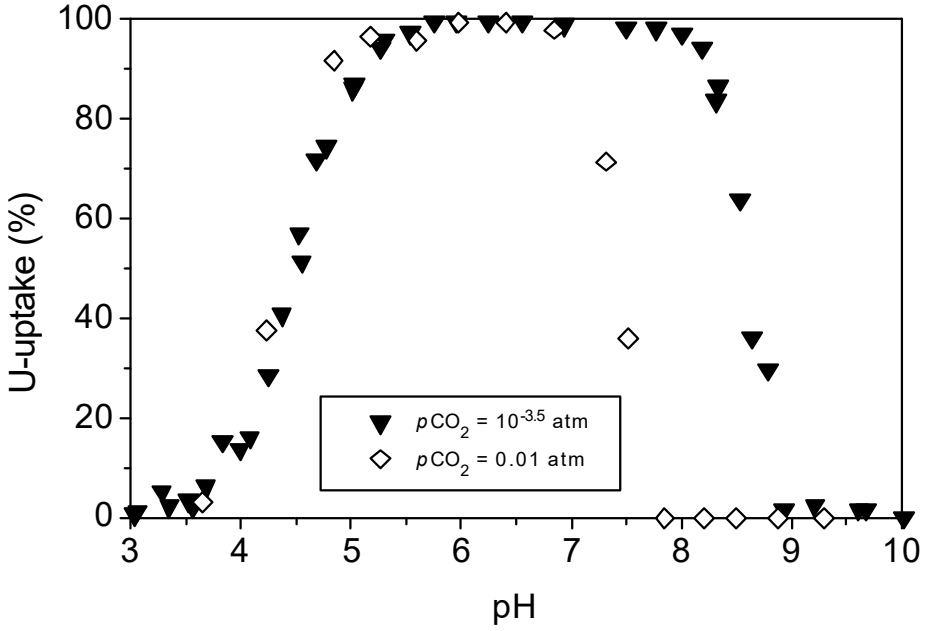


FIGURE 6.7 Effect of pCO_2 on sorption of U by ferrihydrite.
(ΣU = 1 μmol/L, ΣFe = 1 mmol/L, 0.1 M $NaNO_3$)

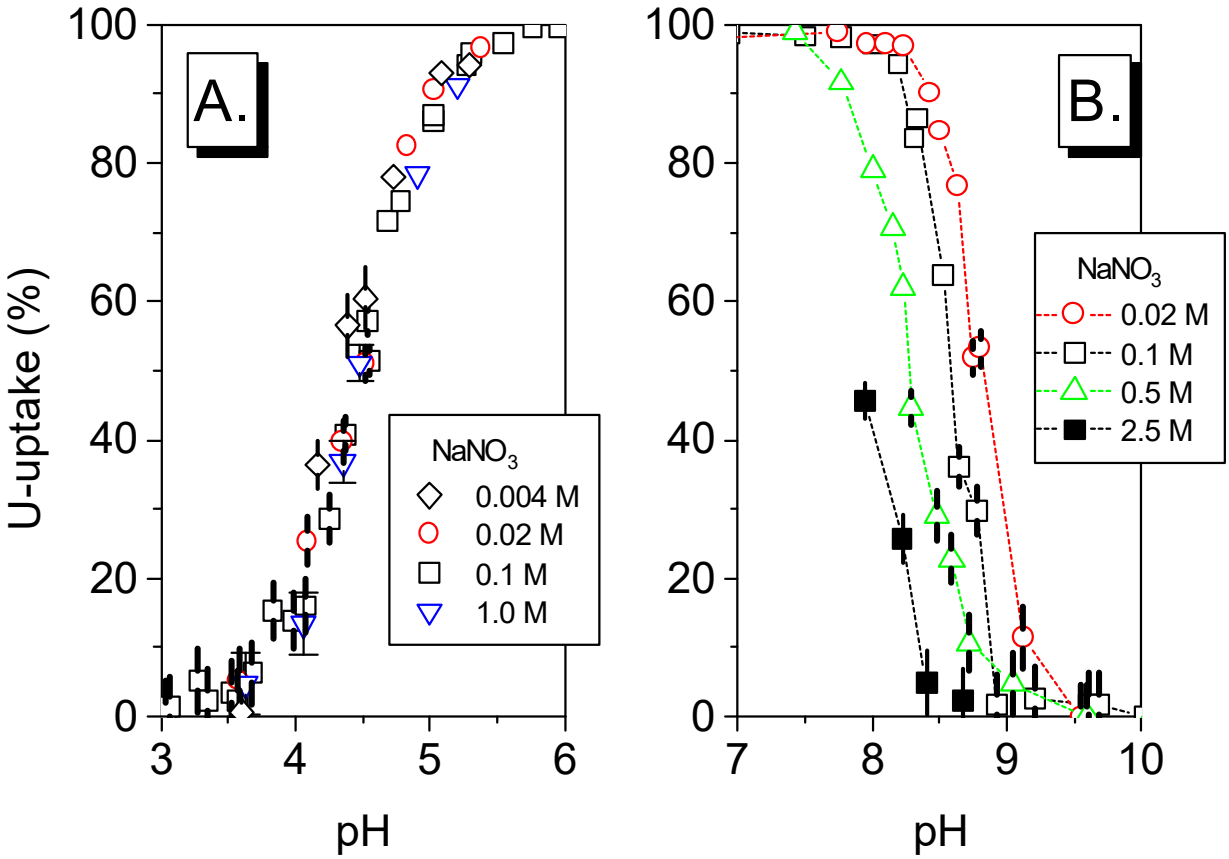


FIGURE 6.8 Effect of ionic strength on U sorption edges. A) Low pH sorption edge B) High pH edge. (ΣU = 1 μmol/L, ΣFe = 1 mmol/L)

6.3 Comparison of U sorption with co-precipitation

Iron oxides precipitate (and may re-dissolve) in aquatic environments due to redox cycling or pH changes. Therefore, the mechanism of trace metal or anion incorporation may involve co-precipitation as well as adsorption. This has led to some speculation about whether the equilibrium distribution of contaminants incorporated by these two distinct mechanisms is significantly different. A key study was reported by Fuller *et al.* [1993], who investigated the kinetics of arsenate adsorption on ferrihydrite and also co-precipitation of arsenate with ferrihydrite. They concluded that arsenate concentrations were controlled by an adsorption process, but that diffusion processes within ferrihydrite aggregates controlled the rate of attainment of equilibrium. Bruno *et al.* [1995], who studied equilibria involving U(VI) and $Fe(OH)_3$ reached the conclusion that the behaviour of the system could be modelled either by surface complexation (sorption) or by solubility approaches. In order to address some of these issues, some experiments involving co-precipitation of U(VI) with ferrihydrite were carried out.

For these experiments, a slightly modified protocol was used. A stock solution containing uranyl ion, Fe^{3+}, and $NaNO_3$ was prepared, at a pH of 2.6. A sample of this solution was removed, and the pH of the remaining solution was raised to 3.0. This process was repeated, each time removing a sample and then raising the pH, until samples had been collected across the pH range from 2.6 to 6.5. This process was carried out as quickly as practicable (within 1 hour), and the samples were allowed to equilibrate for 2 days (as in the sorption experiments). The final pH was determined, and the sample was centrifuged. The supernate was analysed for U using the KPA. The main difference with this experimental procedure was that the U was present during the formation of the ferrihydrite, rather than contacting pre-formed ferrihydrite.

The obtained data are compared with the sorption of U on ferrihydrite in Figure 6.9. The differences are quite small, which suggests that the two mechanisms may be difficult to distinguish experimentally. Indeed it is possible that they may occur together, both in experimental systems and in nature. These issues are considered further in Part III of this thesis.

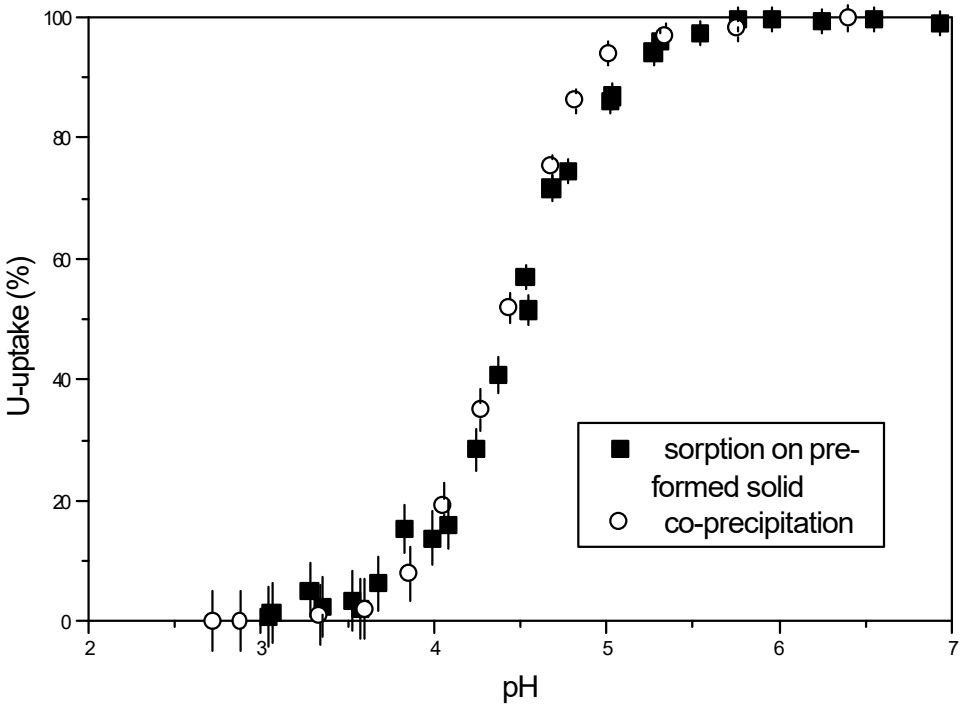


FIGURE 6.9 Comparison of the percentage of U bound by ferrihydrite in sorption and co-precipitation experiments. (ΣU= 1 μmol/L, ΣFe = 1 mmol/L, 0.1 mol/L $NaNO_3$)

6.4 Effect of complexing ligands on U sorption by ferrihydrite

The experimental work described above shows that the sorption of U(VI) in simple laboratory systems is influenced by a number of experimental parameters, including pH, ionic strength, ΣU, mass loading and pCO_2. Considering the complexity of natural systems, it would be expected that U adsorption in the environment would be influenced by additional factors, including the presence of inorganic and organic ligands in the aqueous phase.

In the initial studies of the role of complexing ligands, the effect of phosphate and humic acid (HA) on U uptake by ferrihydrite were investigated. These ligands were chosen because they may be important in the migration of U at the Koongarra uranium deposit [Yanase *et al.*, 1995]. Both ferrihydrite and uranyl phosphate minerals (e.g. saleeite - $Mg(UO_2)_2(PO_4)_2.8H_2O$) are present at Koongarra, and significant

levels of PO_4^{3-} (up to 700 μg/L) have been measured in contacting groundwaters [Payne *et al.*, 1994]. The presence of natural organic matter has also been reported in Koongarra groundwaters, however the behaviour and distribution of humic materials in this system has not been studied in detail. Nonetheless, the reported levels of natural organic matter at Koongarra may well be sufficient to influence the migration of uranium [Yanase *et al.*, 1995].

The studies of complexing ligands also included the effects of SO_4^{2-} and citrate. These ligands may affect U-speciation in both surface and sub-surface environments. For example, SO_4^{2-} may be present in waste-water from uranium milling operations or in acid mine drainage, and citrate is a component of some mixed wastes from the nuclear industry.

6.4.1 Phosphate

The addition of phosphate to the U / ferrihydrite system might be expected to have several possible effects.

- competition with PO_4^{3-} for surface sites could decrease UO_2^{2+} sorption.
- non-adsorbing aqueous UO_2^{2+}/PO_4^{3-} complexes might compete with the surface for co-ordination of UO_2^{2+}, which would also tend to reduce U uptake. As shown by the speciation diagram for U(VI) in the presence of phosphate (Figure 3.6), the $UO_2HPO_4^0$ and $UO_2PO_4^-$ complexes are predicted to have an important role in U speciation under some experimental conditions.
- precipitation of a uranyl phosphate phase could decrease the amount of U in solution.
- interactions between Fe^{3+} and PO_4^{3-} may lead to the formation of a new surface with a greater or lesser affinity for aqueous uranyl.
- U sorption may be enhanced by the formation of ternary surface complexes involving both UO_2^{2+} and PO_4^{3-}. The formation of ternary surface complexes has been considered in modelling trace metal sorption [Davis and Kent, 1990; Davis and Leckie, 1978].

Experimental studies of the effect of phosphate on U sorption were initially undertaken in a system containing ΣU of 1 μmol/L, ΣFe of 1 mmol/L and with 100 μmol/L of P added as NaH_2PO_4. The amount of phosphate adsorbed was routinely measured in the U sorption experiments, and a significant amount of data regarding the adsorption of PO_4^{3-} on ferrihydrite was obtained. Phosphate in solution at equilibrium was measured using the ascorbic acid spectrophotometric method [APHA, 1985].

The presence of phosphate in the U / ferrihydrite system substantially increased U uptake at low pH values (Figure 6.10). The adsorption of PO_4^{3-} was almost 100% for pH values up to about 6, with a gradual decrease above this pH. The fact that U uptake increased in the presence of phosphate immediately enabled the first two possibilities listed above (decreased sorption due to competition or aqueous complexation) to be ruled out. However, several further experiments were then undertaken in order to unravel the remaining phenomena potentially occurring in the phosphate containing systems, as will be described below.

The experiments with added phosphate (100 μmol/L) were repeated with a higher ΣU of 100 μmol/L and the results were compared with those obtained with ΣU of 1 μmol/L. At both U concentrations studied, the low-pH sorption edge was moved to the left by about 0.8 pH units by the addition of PO_4^{3-} (Figure 6.11). The uptake of PO_4^{3-} by the ferrihydrite was almost complete in this pH range (Figure 6.10), which suggests that the increased sorption of U is due to a surface process, such as the formation of a ternary complex, rather than a change in aqueous speciation. Increasing ΣU from 1 μmol/L to 100 μmol/L moved the high pH edge to the left (decreased the proportion of U sorbed - Figure 6.11), both in the presence and absence of phosphate.

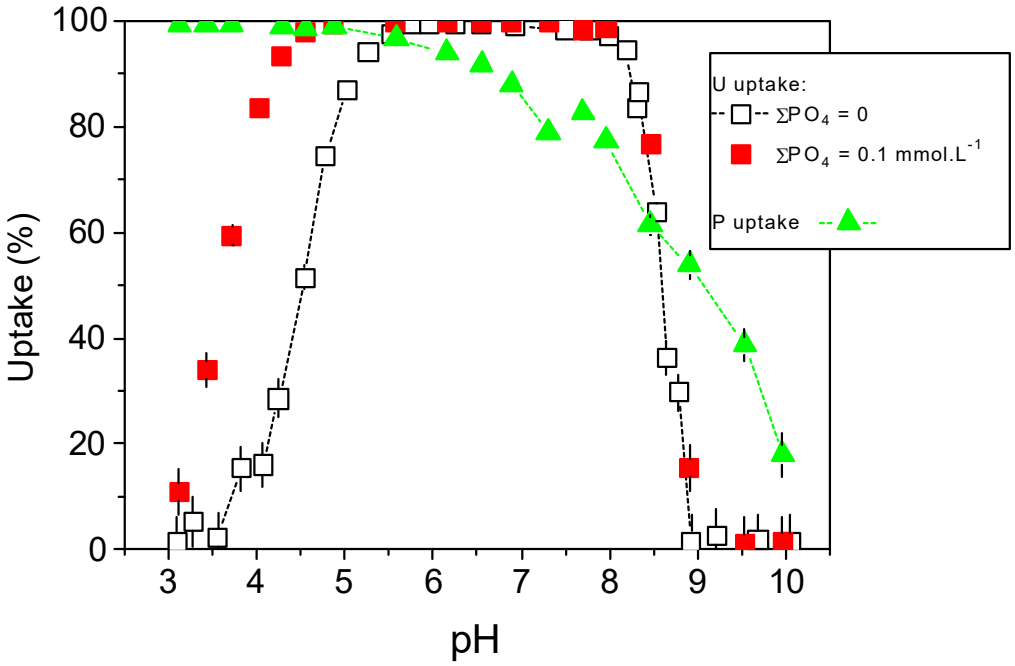


FIGURE 6.10 Effect of phosphate on the sorption of uranium by ferrihydrite (0.1 M $NaNO_3$ in equilibrium with air, ΣU = 1 μmol/L, ΣFe = 1mmol/L)

For experiments with ΣU of 100 μmol/L, the addition of phosphate moved the high pH edge for U-sorption to the right (increased uptake), whereas PO_4^{3-} had little or no effect on the high pH edge for ΣU of 1 μmol/L (Figure 6.11). It may at first seem surprising that the effect of PO_4^{3-} is much smaller in the latter case, where it is present in a large excess relative to UO_2^{2+}. However, it has been suggested that PO_4^{3-} is more important than carbonate in U speciation when the ratio of ΣPO_4^{3-} to ΣCO_3^{2-} exceeds 0.1 [Sandino and Bruno, 1992]. In these experiments, ΣPO_4^{3-} is fixed, and $\Sigma PO_4^{3-}/\ \Sigma CO_3^{2-}$ decreases from about 0.15 at pH 8 to 0.015 at pH 9 (due to the increase of ΣCO_3^{2-} with increasing pH). Therefore, the value of this ratio suggests that phosphate may have a greater effect on the high pH edge for ΣU of 100 μmol/l (which, in the absence of PO_4^{3-}, occurs in the pH range 7 to 8) than on the edge for ΣU of 1 μmol/L.

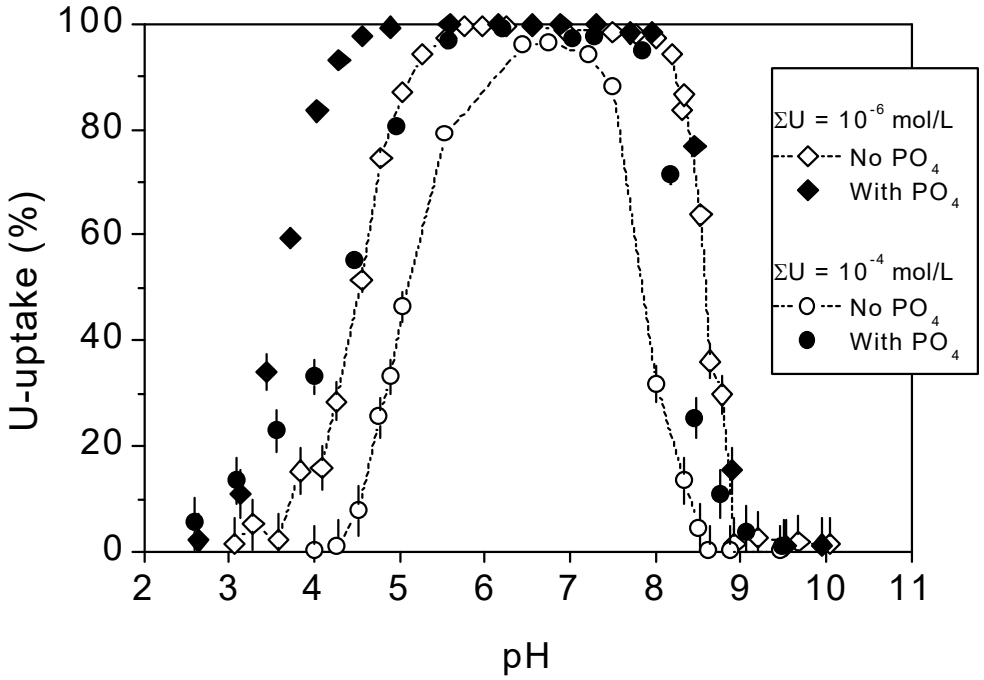


FIGURE 6.11 Effect of phosphate and ΣU on U(VI) adsorption by ferrihydrite. (ΣFe = 1 mmol/L, ΣPO_4 = 0 or 100 μmol/L, ΣU = 1 μmol/L or 100 μmol/L, 0.1 M $NaNO_3$ in equilibrium with air)

Ionic strength effect on U sorption with phosphate present

The effect of ionic strength on U sorption in the presence of phosphate was studied by varying the concentration of the background electrolyte ($NaNO_3$). As with the phosphate-free systems, total ionic strength did not affect the low pH U-sorption edge (Figure 6.12), but it had a significant effect on the high pH U adsorption edge. The high pH region is shown in expanded form in Figure 6.13, with data obtained both in the presence and absence of phosphate at various ionic strengths. Phosphate has no effect on U sorption above pH 8.2, although the ionic strength has a significant effect. The presence of phosphate appears to increase in U sorption in the pH range from 7.5 to 8.2 with I = 0.5 mol/L.

The absence of a significant ionic strength effect on the low-pH edge suggests that outer sphere surface complexes do not play a role in this pH range, either in the absence or presence of phosphate. The absence of a sensitivity to sodium concentration also suggests that the precipitation of $NaUO_2PO_4$ is not a significant mechanism of U removal from solution. This observation has important implications for the modelling of the system, and will be discussed further in Chapter 13.

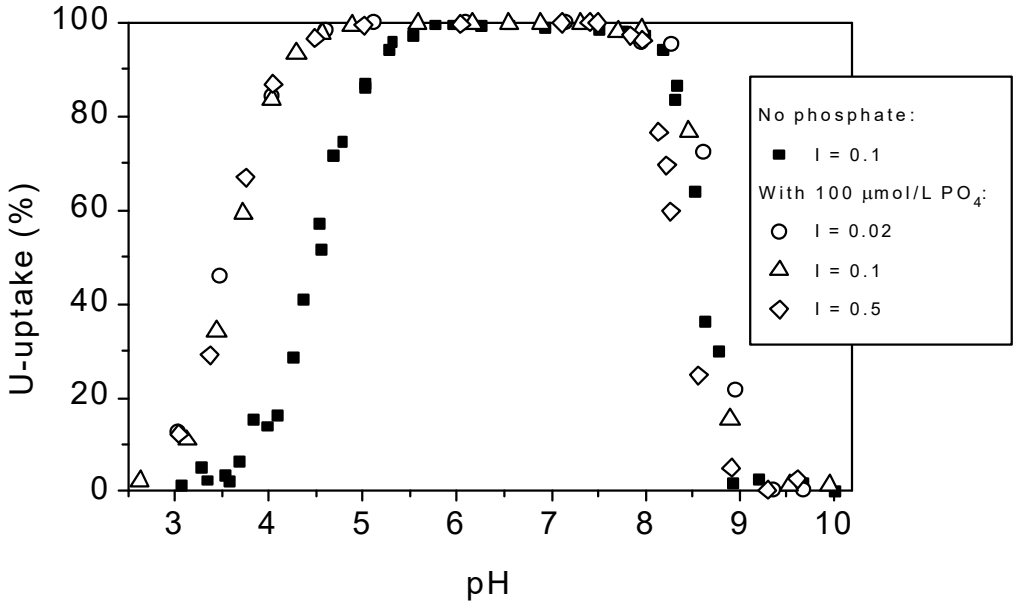


FIGURE 6.12 Effect of phosphate and ionic strength on U(VI) adsorption by ferrihydrite. Data with added phosphate were obtained in 0.02 M, 0.1 M, and 0.5 M $NaNO_3$ (ΣFe = 1 mmol/L, ΣU = 1 µmol/L).
See also Figure 6.13.

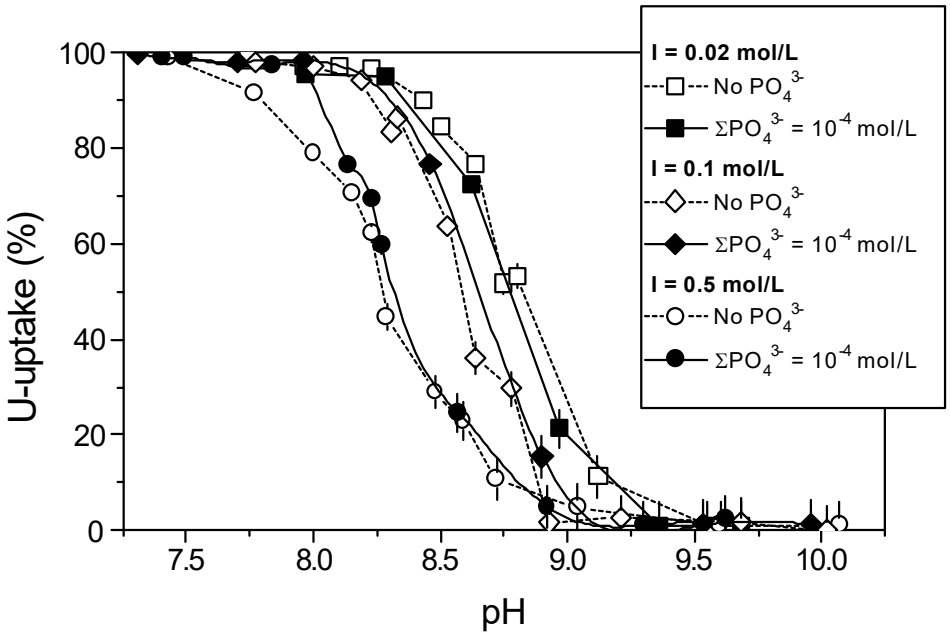


FIGURE 6.13 U(VI) adsorption by ferrihydrite: effect of ionic strength on the high-pH edge in the presence and absence of phosphate. (ΣU = 1 μmol/L, ΣFe = 1 mmol/L)

Uptake of P on ferrihydrite in presence and absence of U

As noted above, the adsorption of PO_4^{3-} was measured in the U sorption experiments with ΣU of both 1 μmol/L and 100 μmol/L. For comparative purposes, a set of PO_4^{3-} sorption data was also obtained when U was absent was obtained (Figure 6.14).

The adsorption of PO_4^{3-} was almost 100% for pH values up to about 6, with a gradual decrease above this pH (Figure 6.14). This trend of decreasing phosphate uptake with increasing pH was also found in a previous study of PO_4^{3-} sorption [Hawke *et al*., 1989]. The sorption of phosphate does not seem to be affected by the presence of ΣU of 10^{-6} mol/L, which is not surprising because the PO_4^{3-} is present at 100 times greater levels. Although the data are somewhat scattered, particularly above pH 8, Figure 6.14 suggests that the presence of ΣU of 10^{-4} mol/L increases

PO_4^{3-} sorption in the pH range between about 6 and 8. The uptake of U is strong at these pH values (Figure 6.10) and this again suggests the formation of a ternary surface complex between PO_4^{3-} and UO_2^{2+}. Similar results have been found in studies of zinc and phosphate adsorption on goethite [Bolland *et al.,* 1977]. These authors reported that "the presence of phosphate or zinc on the goethite surface was found to increase slightly the adsorption of zinc and phosphate respectively", and suggested the formation of a surface complex involving both Zn and phosphate ions.

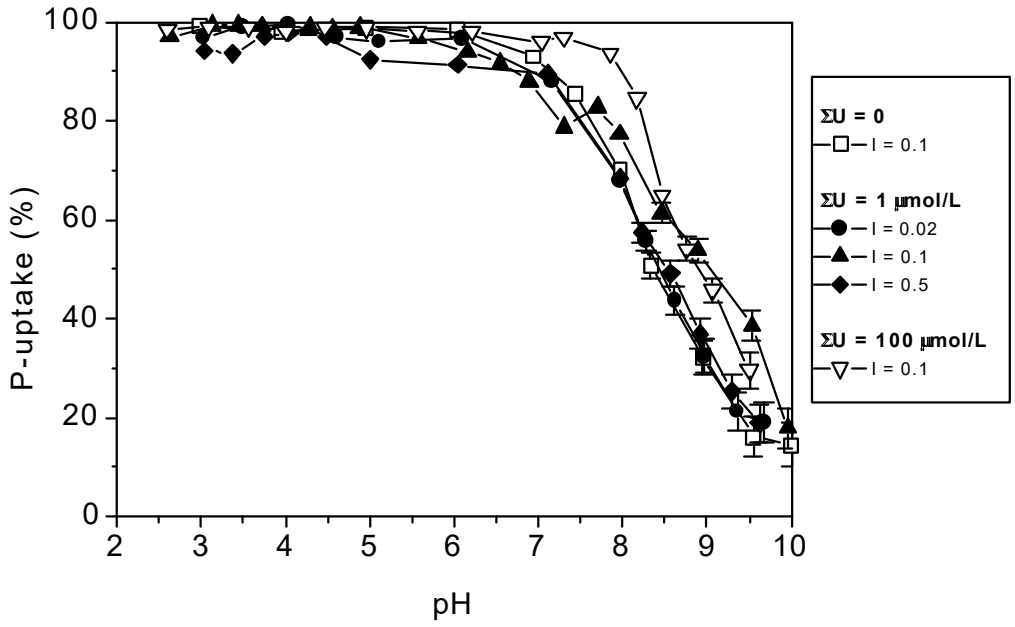


FIGURE 6.14 Uptake of phosphate (100 µmol/L) on ferrihydrite in the presence of various ΣU. The experiments with 1 µmol/L of U were carried out at 3 ionic strengths and are the same experiments for which U uptake data are shown in Figure 6.11.

There is no discernible effect of ionic strength on the uptake of P, although (as mentioned previously) the high pH sorption edge for U in both the presence and absence of phosphate is affected by ionic strength (compare Figures 6.13 and 6.14). It may be tentatively concluded that if a ternary uranyl phosphate surface complex is formed, it involves surface binding via the uranyl ion, rather than phosphate being the bridging ligand.

Experiments in which ΣU and ΣP were varied

In Figure 6.6, data obtained in experiments carried out at fixed pH, but with variable ΣU were presented as sorption isotherms. Similar experiments with variable ΣU were also carried out at pH 4.5 in systems which contained fixed added phosphate (ΣP = 100 μmol/L). Figure 6.15 shows the experimental results plotted as the percentage of U adsorbed against ΣU. Figure 6.16 presents the same data in a standard isotherm format. It is clear that the presence of phosphate in the system enhances the uptake of U across a wide concentration range. The data plot as typical adsorption curves, very similar in shape to the phosphate free systems. At very low values of ΣU, the concentration of U is insufficient for the solubility limits of any U minerals to be exceeded (see Chapter 13 for a detailed discussion). This means that for at least part of the range of experimental conditions which was studied, precipitation of a uranyl phosphate mineral cannot be invoked as an explanation for the data.

Although this thesis is primarily concerned with the adsorption of U, some data for the adsorption of phosphate was obtained under standard experimental conditions. Experimental results for phosphate adsorption in uranyl-free systems at pH of 5.25 and 8.25 are presented in Figure 6.17. The data show that phosphate, like uranyl, is much more weakly adsorbed at higher concentrations, possibly indicating a multiple site adsorption or surface saturation effect.

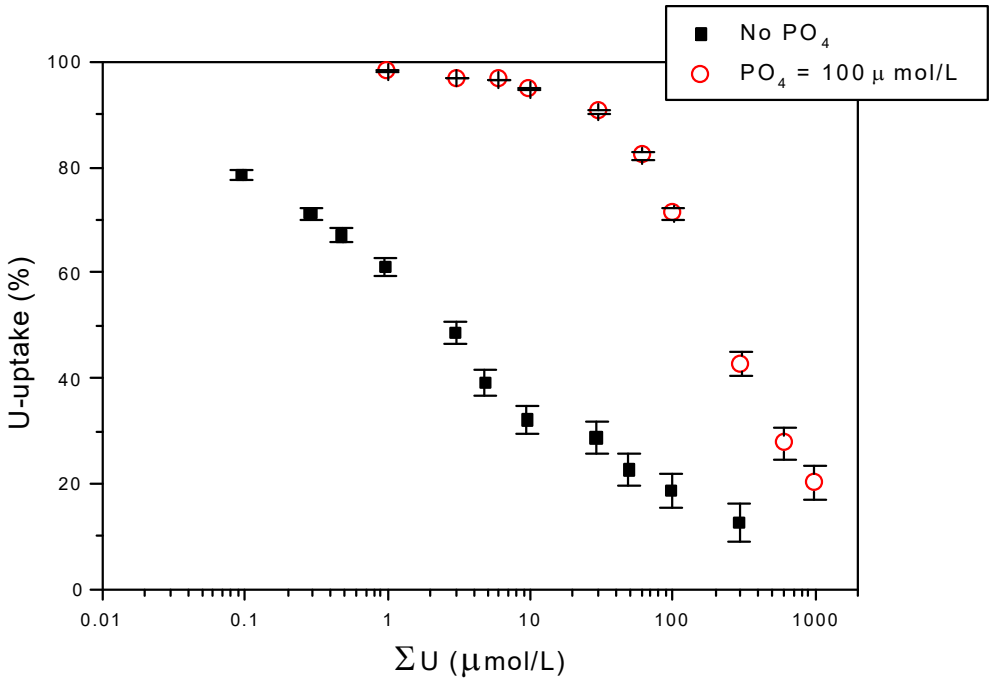


FIGURE 6.15 Percentage of U adsorbed by ferrihydrite (ΣFe = 1 mmol/L) as a function of ΣU - effect of added total phosphate of 100 µmol/L. Background electrolyte 0.02 mol/L $NaNO_3$, pH 4.5.

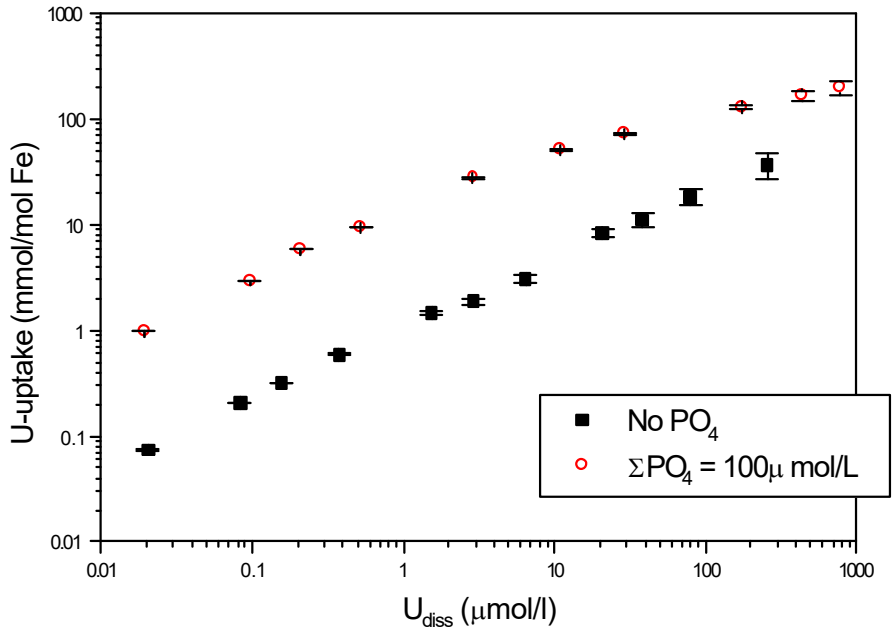


FIGURE 6.16 Adsorption isotherm for U in phosphate-free systems, and in systems containing fixed total phosphate of 100 μmol/L. Background electrolyte 0.02 mol/L $NaNO_3$, pH 4.5, ΣFe = 1 mmol/L.

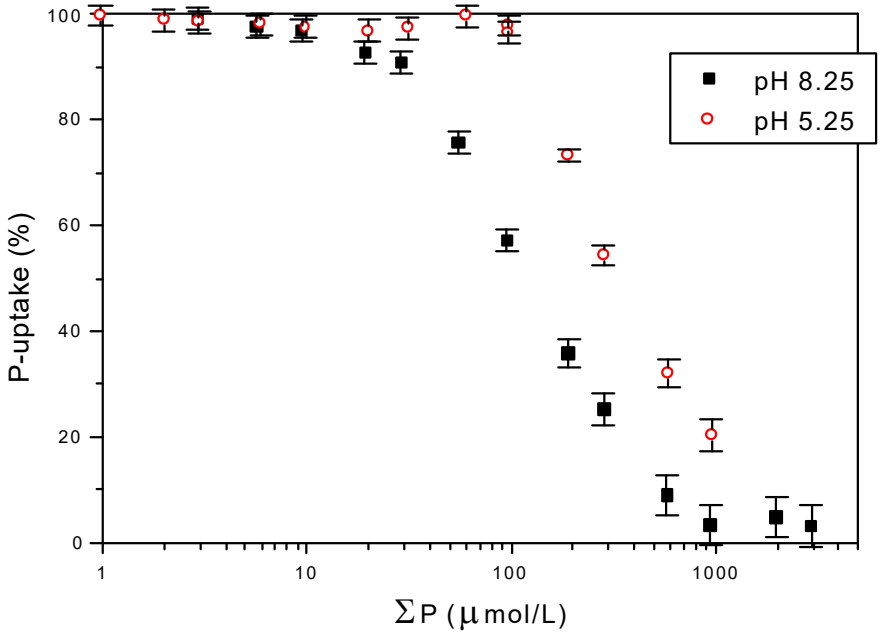


FIGURE 6.17 Percentage of P adsorbed as a function of ΣP in uranyl free systems at pH 5.25 and 8.25. 0.02 mol/L $NaNO_3$, ΣFe = 1mmol/L.

6.4.2 Humic acid

The effect of natural organic materials on the mobility of various pollutants has been studied by several workers. It has been suggested that the sorption behaviour of oxide surfaces is modified when adsorption sites for trace metal ions become dominated by the functional groups of adsorbed humic compounds [Davis and Leckie, 1978].

There have been several studies of the importance of humic substances in actinide speciation [e.g. Tipping, 1993], and some previous work has focussed on the impact of these substances on actinide sorption [Ho and Miller, 1985; Moulin and Ouzounian, 1992]. Uranium uptake on hematite was increased by the presence of HA [Ho and Miller, 1985], whereas the presence of model organic materials did not alter the sorption of Np on Fe- and Al- oxides, or tuff material [Kung and Triay, 1994].

For the experiments with HA, a stock solution of HA was prepared by dissolving 50 mg of Aldrich sodium humate in 500 mL of milli-Q water, and filtered through a glass fibre filter. The proportion of solid retained by the filter was determined (by weighing) to be 10 ± 2%. The amount of HA in the sorption experiments was a 1:10 dilution of the filtered stock solution, corresponding to a HA content of approximately 9 mg/L. The amount of HA adsorbed was determined using spectrophotometry at 350 nm [Nomizu *et al*., 1989]. Shorter wavelengths could not be used due to absorption by the background electrolyte ($NaNO_3$). Although the absorbance at 350 nm followed a Beer's law relationship, the technique is non-specific and gave only a semi-quantitative indication of HA uptake by the solid.

The addition of HA (9 mg/L) moved the low pH U-sorption edge on ferrihydrite to the left (increased sorption), and had little effect on the high pH edge (Figure 6.18). The uptake of HA by the ferrihydrite was generally strong, but decreased at high pH values, which is a similar trend to that previously reported for adsorption of HA on Al_2O_3 [Stumm, 1992] and hematite [Ho and Miller, 1985].

Moulin and Ouzounian [1992] reported that the formation of an organic coating increased the adsorption of Am at low pH values, whereas at higher pH values, humic substances were predominantly in solution and prevented Am sorption through

aqueous complex formation. The present results for U sorption are consistent with the reported behaviour of Am. Humic acid was strongly adsorbed across a wide pH range, and there were no conditions under which U sorption was prevented by the formation of aqueous complexes involving HA. However, as was observed for Am, the presence of HA increased U uptake in the low pH range, thereby moving the low pH U-sorption edge to the left.

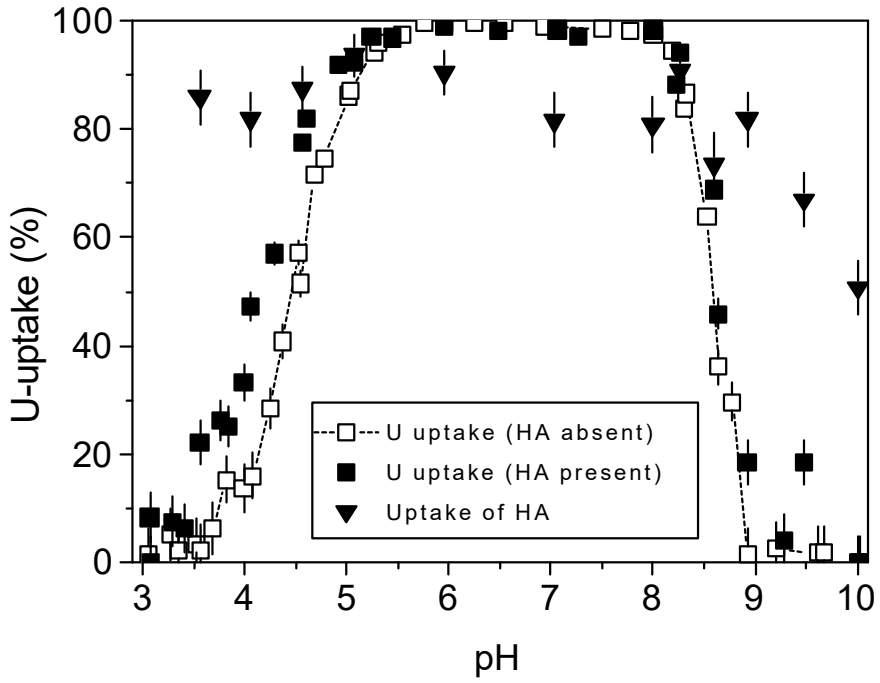


FIGURE 6.18 Effect of humic acid on the sorption of uranyl by ferrihydrite (ΣFe = 1 mmol/L, ΣU = 1 µmol/L, 0.1 M $NaNO_3$ in equilibrium with air).

During the sorption experiments, over 80% of the HA was adsorbed to the ferrihydrite, and the final concentrations of HA in solution (1 - 2 mg/L) were comparable to the amount of total organic carbon (TOC) reported for Koongarra groundwaters by Yanase *et al.* [1995]. Therefore, it seems probable that organic matter has a significant affect on U sorption at the Koongarra field site, although only present at low concentrations in the groundwater. However, natural humic materials are dissimilar in many respects to commercial humic substances, such as the Aldrich humic acid used in this work [Malcolm and MacCarthy, 1986], and the natural organic materials present in Koongarra groundwaters have not been characterised in detail. Consequently, the effect of natural organic matter on U sorption in the Koongarra system is yet to be fully understood.

6.4.3 Sulfate

The presence of SO_4^{2-} has a significant influence on U speciation at pH values up to about pH 6 (see Figure 3.5). Both increases and decreases in U sorption have been observed when SO_4^{2-} was present [Venkataramani and Gupta, 1991]. Sulfate is a component of many groundwaters, but is of particular importance in the vicinity of some uranium milling operations, where sulfuric acid may be used in the leaching process. Sulfate is also a component of acid mine drainage. Consequently the effect of sulfate on U sorption is of both theoretical and practical interest.

Experimental data for U sorption on ferrihydrite in the presence and absence of SO_4^{2-} (0.01 mol/L) are given on Figure 6.19. Sulfate has a small effect on the low pH edge, generally causing a slight decrease in U sorption at pH values below approximately 6 at both total U concentrations. The data are a marked contrast to phosphate, which when present in small amounts dramatically increased U uptake on ferrihydrite. The decrease in sorption could be attributed to the formation of complexes in the solution phase between U and sulfate (Figure 3.5), or competition between uranyl and sulfate ions for surface sites. These possibilities are considered in Section 11.5.

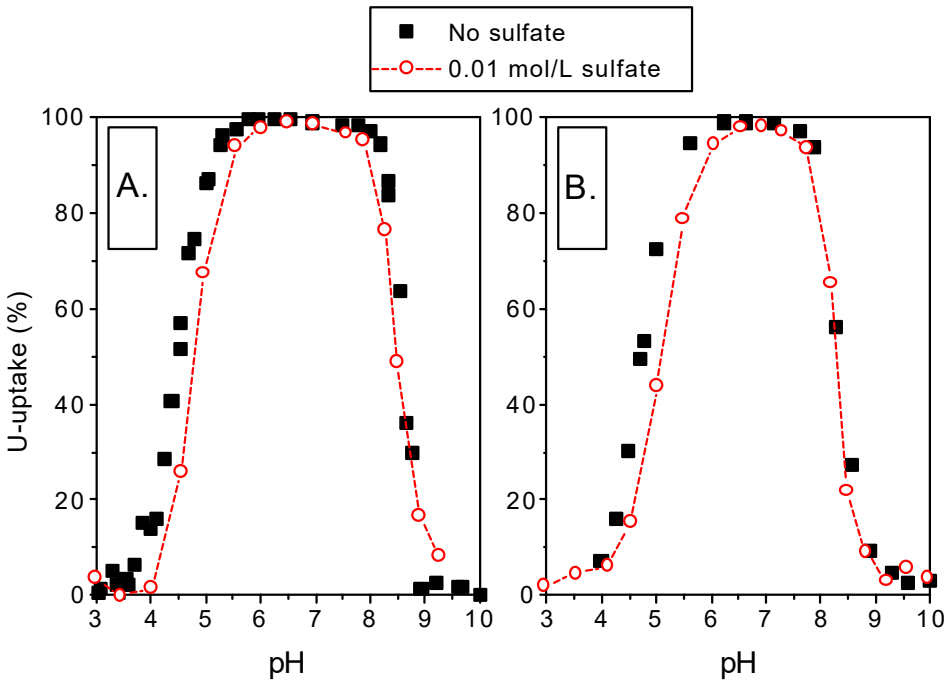


FIGURE 6.19 Effect of sulfate on U adsorption by ferrihydrite (ΣFe = 1 mmol/L, I = 0.1, system in equilibrium with air). A. ΣU = 1 µmol/L. B. ΣU = 10 µmol/L.

6.4.4 Citrate

The citrate anion is another ligand which is of relevance to U migration studies, and is present at low levels in natural soil solutions [Sposito, 1989]. It is also present in domestic and industrial wastes [Francis *et al.*, 1992], and is expected to be present in radioactive wastes which may be emplaced in repositories [Choppin *et al.*, 1996]. Citrate complexation may be important in the migration of these hazardous wastes, as several radionuclide-citrate complexes are not readily degraded by bacteria [Francis *et al.*, 1992]. Citrate also serves as a model ligand representing the functional groups found in natural organic materials. For these reasons, some experiments were undertaken in systems in which citrate was present.

The presence of citrate of 0.01 mol/L had a major effect on the adsorption of UO_2^{2+} by ferrihydrite (Figure 6.20). At total U concentrations of 1 μmol/L and 10 μmol/L, the adsorption of U was entirely suppressed across the complete experimental pH range from 3 to 10. In the ligand-free system, U uptake was close to 100% at pH values from 5 to 8. This large decrease in U sorption was not observed in any experimental system which had been previously studied. Based on visual observations, the ferrihydrite apparently dissolved during the course of many of the experiments, particularly in the low pH range.

To further investigate this phenomena, both the solid and aqueous phases (after centrifugation) were analysed for Fe, by the standard phenanthroline technique. This involves the formation of an intense red Fe-phenanthroline complex which was analysed spectrophotometrically at 510 nm [APHA, 1985]. The Fe results are shown on Figure 6.21, together with corresponding data for systems in which no citrate was present. When citrate was absent, the ferrihydrite was stable across a wide pH range, with significant amounts of Fe only coming into solution below a pH of about 3.5. However, when citrate was present, the ferrihydrite was entirely dissolved at all pH values below about 6.5. Thus, the reduced uptake of U can be attributed to both complexation of U in the aqueous phase by citrate, and to the dissolution of the ferrihydrite sorbing phase. This is discussed further and modelled in Chapter 11.

It has recently been reported that uranyl sorption on goethite, gibbsite and phyllosilicate minerals is unaffected, or dramatically *increased* by the presence of citrate [Redden *et al*., 1996], with a stable bridging structure between uranyl and citrate being suggested. This report is in marked contrast with the above results for ferrihydrite, and it seems likely that the observed phenomena may be sensitive to the ratio of citrate to ΣFe. In the preceding experiments, the amount of citrate (0.01 mol/L) was an order of magnitude higher than the total amount of Fe (ΣFe was 1 mmol/L). Therefore, it was not surprising that the ferrihydrite completely dissolved and there was no adsorption of U. Consequently, a series of experiments were carried out with a much lower amount of citrate, 100 μmol/L, with the experimental conditions being otherwise standard. The U-sorption results are shown in Figure 6.22.

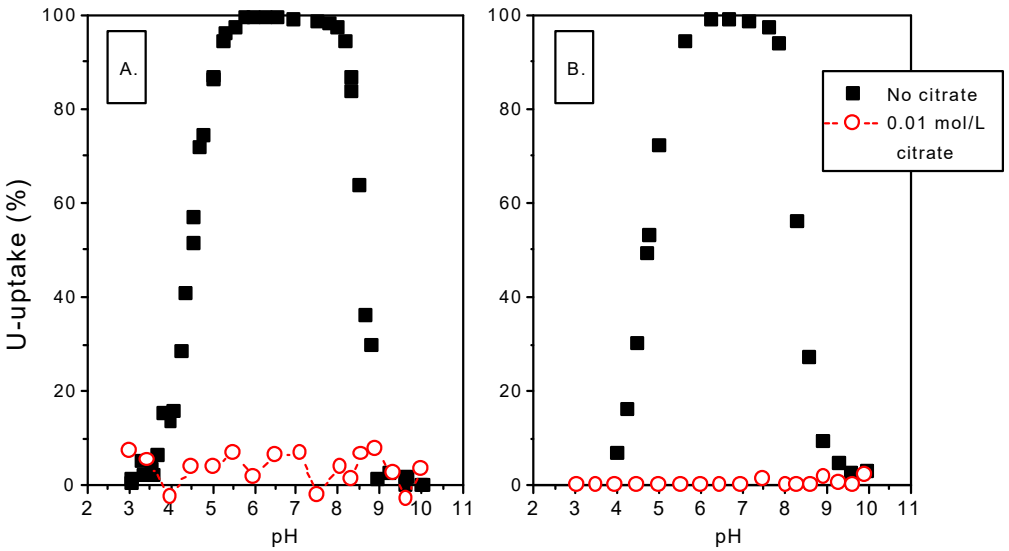


FIGURE 6.20 Effect of 0.01 mol/L citrate on U sorption by ferrihydrite. (ΣFe = 1 mmol/L, background electrolyte 0.1 M $NaNO_3$, system in equilibrium with air). A. ΣU = 1 µmol/L B. ΣU = 10 µmol/L

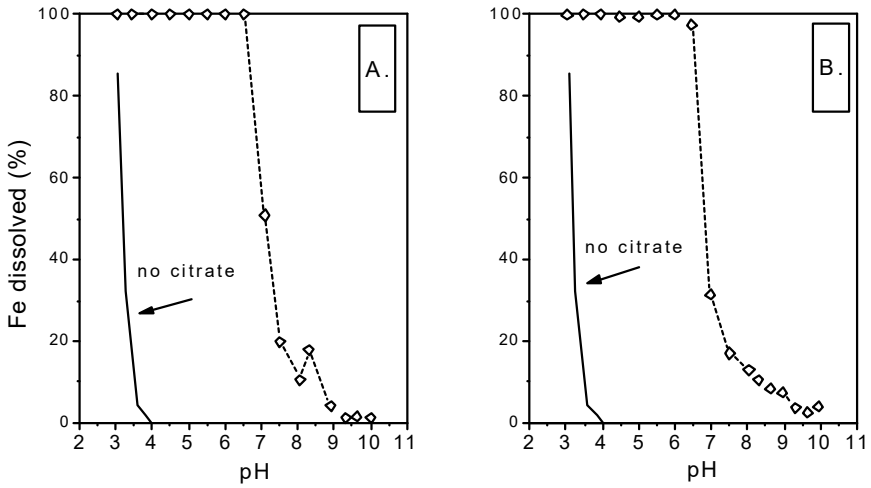


FIGURE 6.21 Dissolved Fe in the U sorption experiments shown in Figure 6.20. (ΣFe = 1 mmol/L, ΣCIT = 10 mmol/L). The presence of citrate causes the complete dissolution of 1 mmol/L ferrihydrite at pH values below 7.

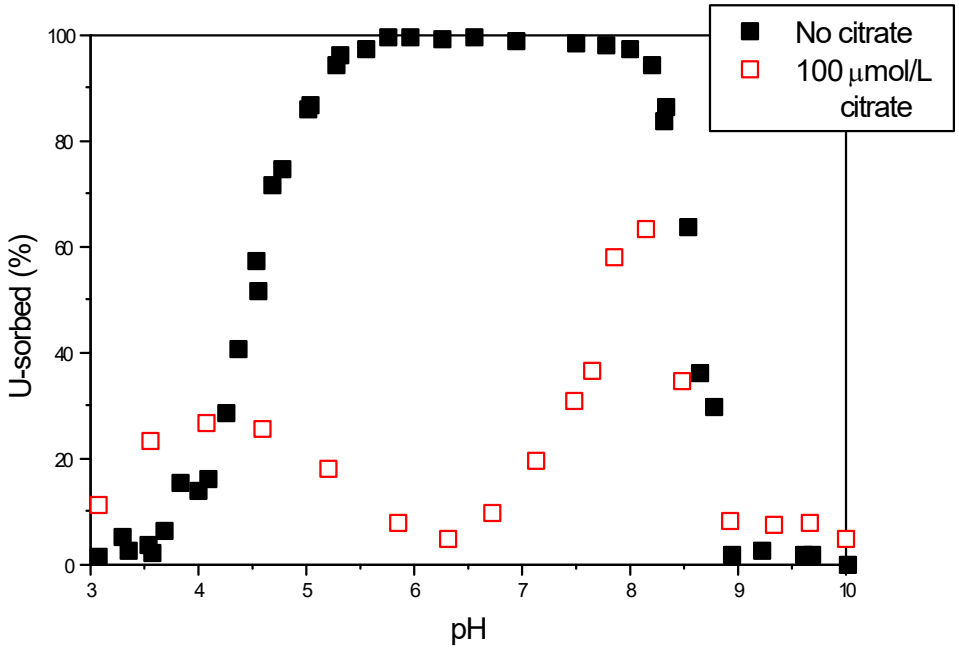


FIGURE 6.22 Adsorption of U in systems containing insufficient citrate to entirely dissolve the ferrihydrite. The resulting sorption curve exhibits an unusual 'double-hump' (ΣU = 1 μmol/L, ΣFe = 1 mmol/L, Σcitrate = 100 μmol/L, 0.1 M $NaNO_3$ in equilibrium with air).

The U-sorption data for this system (Figure 6.22) were unlike any U sorption curve previously obtained, since there were two separate regions of U uptake, resulting in a curious 'double-humped curve'. There also seems to be a slightly enhanced uptake of U at low pH values (<4) relative to the ligand free system. This latter feature is similar to the behaviour reported by Redden *et al.* [1996].

The corresponding Fe data (Figure 6.23) show that there was partial dissolution of the ferrihydrite across the pH range up to about 8. However, the decreased sorption of U in the neutral pH range (pH 5-8) cannot be explained by the absence of a ferrihydrite sorbing phase in this case, since 90% of the ferrihydrite remains undissolved in the system. Consequently, the interactions of U in this system are also probably affected by complexation between U and citrate in the aqueous

phase. This would explain the reduced adsorption of U under conditions in which the sorbing substrate is still present. The interactions in this experimental system are quite complex and are discussed and modelled in Section 11.7.

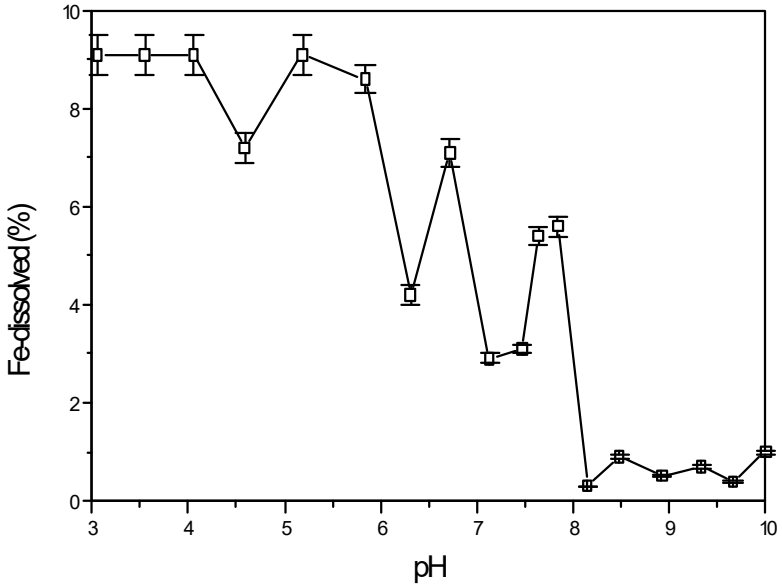


FIGURE 6.23 Amount of dissolved Fe in the U sorption experiments shown in Figure 6.22. The presence of citrate results in the partial dissolution of 1 mmol/L ferrihydrite at pH values below 7. However, approximately 90% of the ferrihydrite remains undissolved.

As with the other ferrihydrite-U systems discussed in this chapter, the experimental data for the U –citrate-kaolinite systems (Chapter 7) provide some useful further insights into the likely phenomena controlling U partitioning in the U-ferrihydrite-citrate systems. The experimental data for the ferrihydrite-U systems will be discussed further and an attempt made to model them in Part III of this thesis.

7 URANIUM(VI) UPTAKE ON KAOLINITE

Iron oxides and clay minerals occur throughout the Koongarra weathered zone and are a product of the weathering of chlorite which is a major component of the host chlorite schists [Murakami *et al.*, 1994]. During weathering, the iron-rich chlorite is converted to vermiculite, then kaolinite, in a sequence of reactions which also leads to the precipitation of iron minerals including goethite, hematite and ferrihydrite. Ferrihydrite is believed to play a major role in adsorbing U in the weathered part of the Koongarra system, and a detailed study of the sorption of U on ferrihydrite was presented in Chapter 6. However, the relative importance of various other minerals in sorbing U in the Koongarra system has not yet been conclusively demonstrated. Giblin [1980] considered that U sorption on kaolinite was an important concentration mechanism for U in the Alligator Rivers Region deposits. Thompson *et al.* [1994] have also reported strong adsorption of U on kaolinite, making it promising for reducing the U content of waste waters.

In this chapter, the results of an experimental study of U sorption on kaolinite in systems containing $NaNO_3$ as the background electrolyte are presented. As with the analogous experiments with ferrihydrite (discussed in Chapter 6), these systems were equilibrated with air and are referred to as 'simple $NaNO_3/CO_2$ systems'. Several variables including pH, ΣU, ionic strength, and mass loading were systematically varied. The effects of complexing and competing ligands including phosphate, citrate, sulfate and humic acid were also investigated.

7.1 Effect of pH and mass loading

The main features of U sorption on the KGa-1B kaolinite are shown in Figures 7.1 and 7.2. The total U in these Figures is 1 μmol/L and 10 μmol/L respectively. The experimental curve for a mass loading of 4 g/L and a ΣU of 1 μmol/L was obtained with a higher density of data and serves as a reference curve for other experiments under variable conditions with this substrate.

In qualitative terms, the U sorption data on kaolinite are similar to those of ferrihydrite. In particular, sorption is greatest in the near-neutral pH range, with a 'low pH edge' of increasing uptake from pH of about 3.5 to 6.5, and a much steeper 'high pH edge' between pH 8 and 9. Compared to ferrihydrite, the amount of sorption (expressed as amount of U adsorbed per gram of sorbing substrate) is much lower. This reflects the much higher specific surface area of ferrihydrite. The comparison with ferrihydrite is discussed in further detail below. As was the case with ferrihydrite, the amount of U sorbed on kaolinite is increased at higher mass loadings (Figures 7.1 and 7.2).

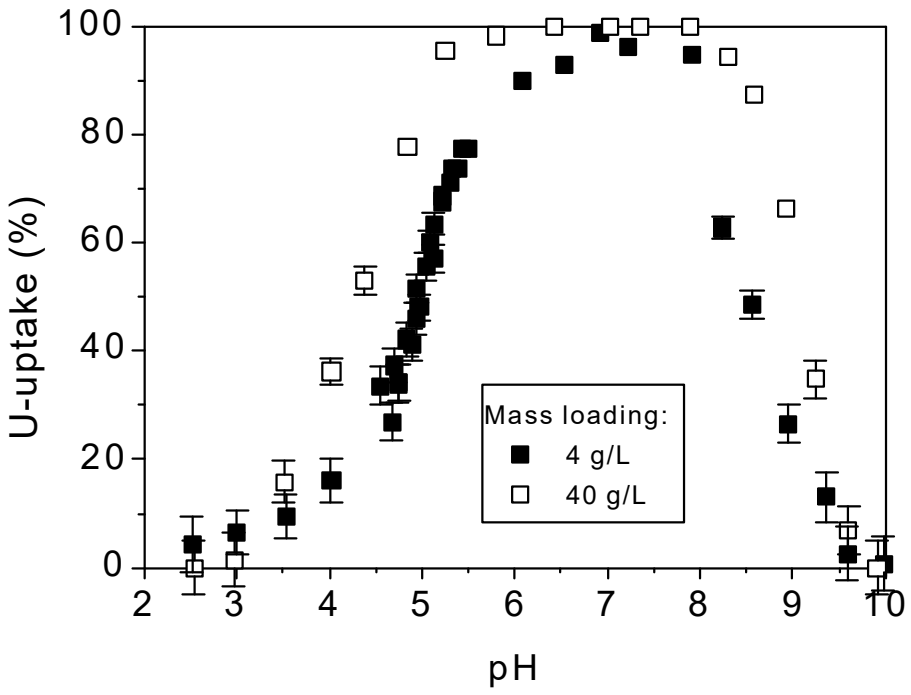


FIGURE 7.1 Uranium sorption on kaolinite (KGa-1B) – pH dependence and effect of solid mass loading. (ΣU = 1 μmol/L, 0.1 M $NaNO_3$ equilibrated with air)

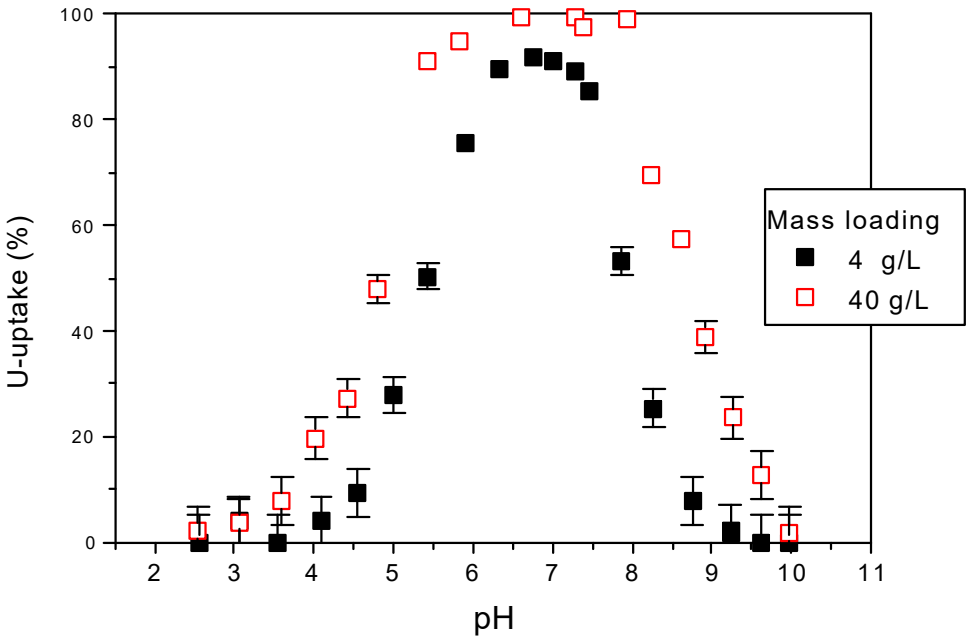


FIGURE 7.2 Uranium sorption on kaolinite (KGa-1B) – pH dependence and effect of solid mass loading for ΣU of 10 μmol/L.

7.2 Effect of total U – evidence for precipitation

The effect of increased ΣU in the experimental systems with kaolinite KGa-1B was studied at a mass loading of 4 g/L. As with ferrihydrite, there is a decreasing percentage of U sorbed with increased ΣU in the system (Figure 7.3), which suggests that there are at least two types of binding sites with different affinities for U sorption on the KGa-1B kaolinite.

Similar data for the KGa-1 kaolinite across a wide range of ΣU (mass loading of 4 g/L), indicate a substantial shift in the position of the low pH-edge between ΣU of 1 μmol/L and 10 μmol/L (Figure 7.4). These two uptake curves were similar to those of the KGa-1B sample (Figure 7.3). Uptake curves for 10^{-4} and 10^{-3} mol/L ΣU had an entirely different pH dependence, with the pH edge being much steeper and

moving to the left with increasing ΣU. These distinctive curves obtained at high U concentrations suggest that another process (apart from sorption), such as precipitation, may be important.

As was discussed in Section 3.3, the precipitating solid in this type of experiment is unlikely to be a crystalline phase such as β-$UO_2(OH)_2$ or schoepite, and has previously been modelled as being an unspecified 'uranyl hydroxide' [Tripathi, 1983]. Tripathi defined a solubility product for this phase as $\{UO_2^{2+}\}.\{OH^-\}^2$, with a value of log K_{SO} = -22.43. When the experimental results are plotted as U in solution as a function of pH, it appears that the data are consistent with the solubility of this phase placing an upper limit on dissolved U (Figure 7.5). Data for the higher ΣU tends to lie below (rather than on) the calculated solubility curve, suggesting that U concentrations are further reduced by adsorption.

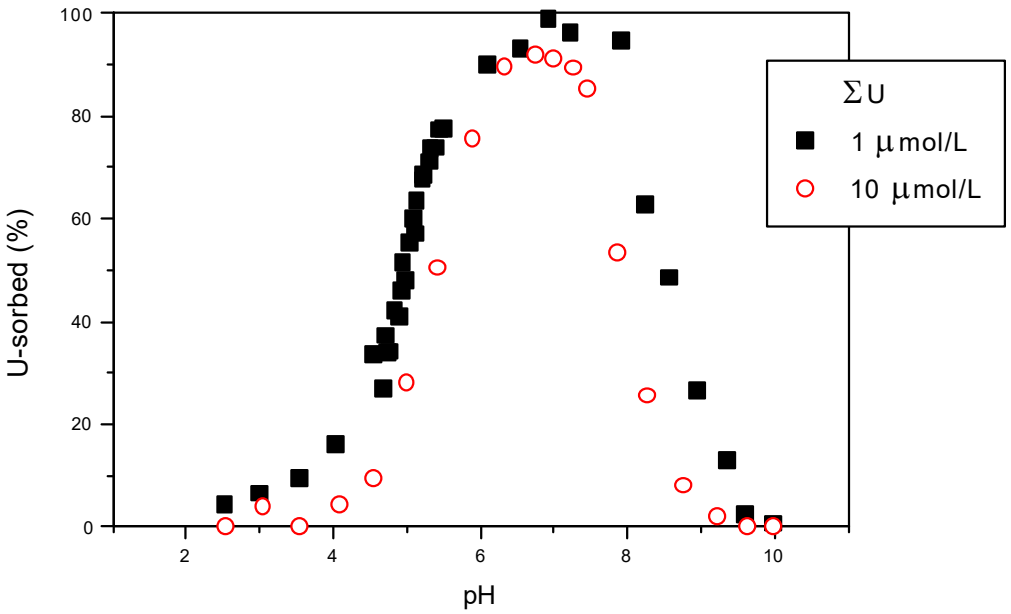


FIGURE 7.3 Effect of ΣU on U sorption by kaolinite KGa-1B. Mass loading of 4 g /L, 0.1 M $NaNO_3$, equilibrated with air.

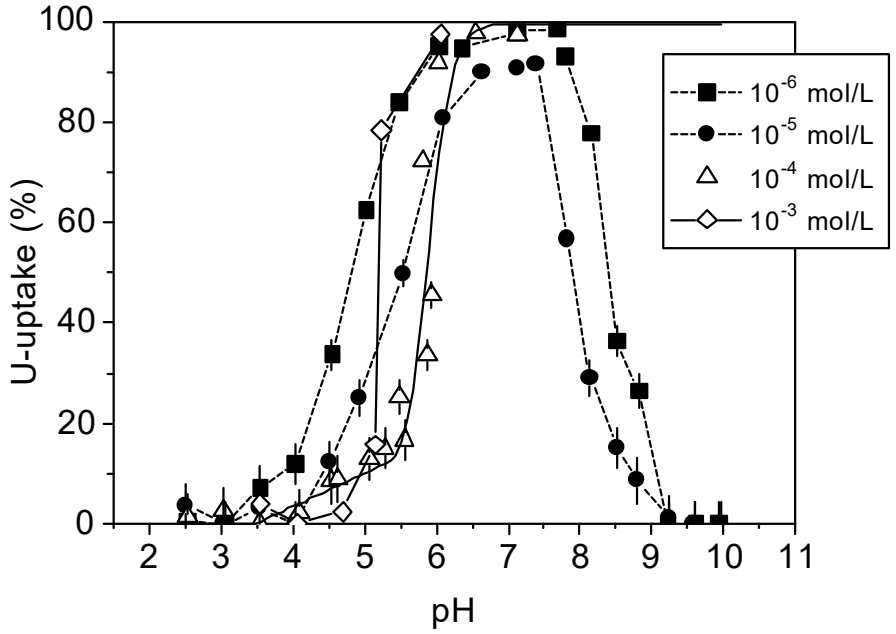


FIGURE 7.4 Uranium uptake on KGa-1 (mass loading 4 g/L) - effect of ΣU.

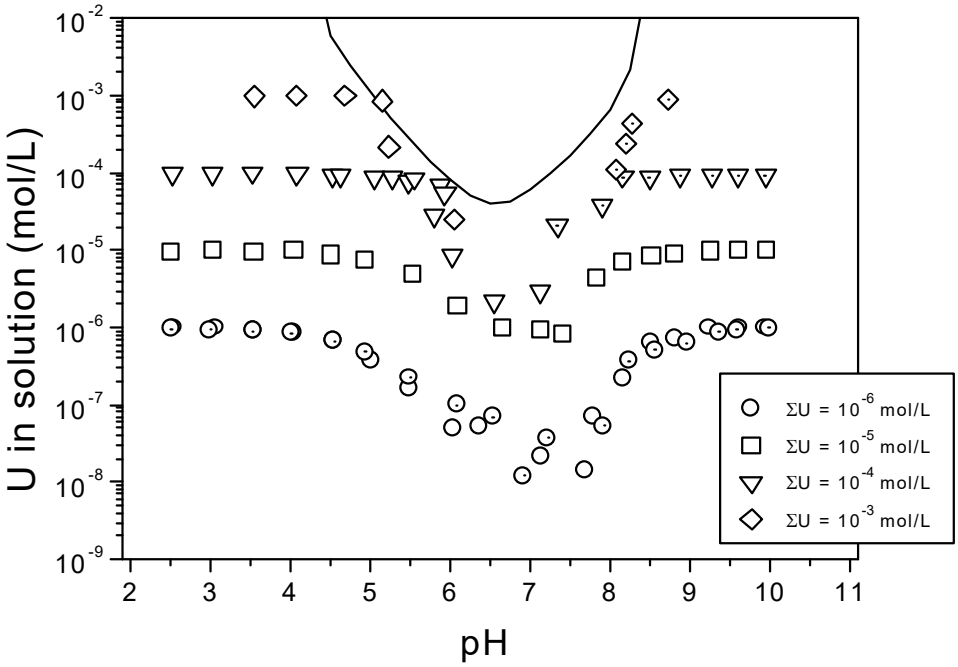


FIGURE 7.5 Total dissolved U in experiments with kaolinite for ΣU from 10^{-6} mol/L to 10^{-3} mol/L. The curve was calculated from the solubility of uranyl hydroxide with log K_{SO} for $UO_2(OH)_2$ of -22.43 [Tripathi, 1983]. Data are for experiments with kaolinite KGa-1 (open symbols) and with KGa-1B (dot centre). Mass loading 4 g/L, 0.1M $NaNO_3$.

It is instructive to compare the set of experimental data obtained with ΣU of 10^{-3} mol/L with model predictions based on the precipitation of the above uranyl hydroxide phase. In this case, the experimental data are plotted as 'U associated with the solid' rather than 'U-sorbed' to emphasise that sorption is not the major process involved. (This distinction is not always made in interpreting 'sorption' experiments, because it can be difficult to separate the effects of sorption and precipitation).

The resulting data are presented in Figure 7.6. It can be seen that the agreement between the model predictions and experimental data is quite satisfactory. While the fit is not perfect, particularly at high pH values, it should be borne in mind that the published K_{SO} values for $UO_2(OH)_2$ cover a vast range of many orders of magnitude. This is largely due to errors introduced by incomplete hydrolysis schemes and poor solid characterisation (as discussed by Tripathi [1983]). Thus the agreement between model and experiment can be considered to be surprisingly good, even though precipitation was the only process considered in this instance. The experimental evidence therefore indicates that precipitation was probably occurring at high ΣU in these experiments, and the solid suggested by Tripathi provides a reasonable explanation of the data.

An important feature of the model curve shown in Figure 7.6 is the very steep (almost vertical) initial slope of the 'low pH edge' (the experimental data also climb very steeply near pH 5). This contrasts with the distinctive 'S' curve of the low pH edge that was observed in numerous experiments in which sorption appeared to be the major process.

The shapes of these different types of uptake curves may be compared in Figure 7.4. Based on the precipitation calculations, the data-sets for ΣU of 1 and 10 μmol/L (Figure 7.4) were below solubility limitations. It will be observed that, whereas the sorption curves for ΣU of 10^{-5} and 10^{-6} mol/L move to the right with increasing ΣU, the vertical edge for ΣU of 10^{-3} mol/L is to the left of that for ΣU of 10^{-4} mol/L (Figure 7.4). Thus, constraints imposed by solubility affect the data curves in a different way to those due to sorption phenomena. This suggests that

families of curves such as those in Figure 7.4 can be used to identify when

precipitation is occurring (rather than sorption), as well as providing information about binding sites of different affinity.

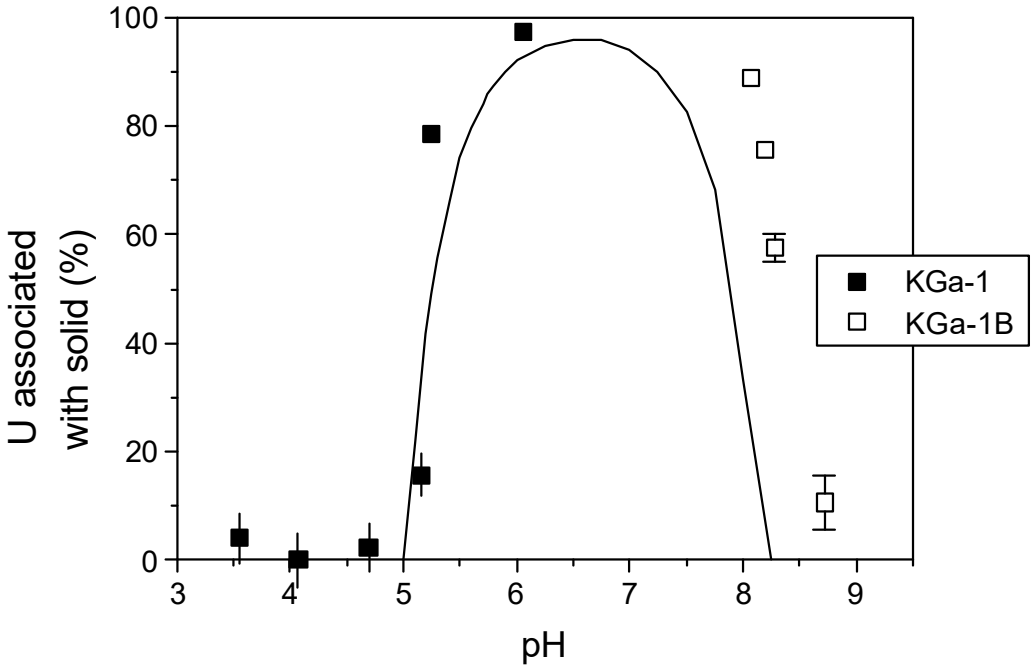


FIGURE 7.6 Uranium associated with solid phases in experiments with kaolinite (4g/L) and with ΣU of 10^{-3} mol/L. The line is calculated for the precipitation of amorphous $UO_2(OH)_2$ with log K_{SO} = -22.43 [Tripathi, 1983]. The curve shows a good fit to the data, considering the range of published log K_{SO} values and the sensitivity of the calculations to a small change in this parameter.

7.3 Effect of ionic strength

A limited amount of data for the ionic strength dependence of U sorption on kaolinite KGa-1B was obtained (Figure 7.7). The data indicate that the high pH edge is displaced to the left (i.e. sorption is reduced) with an increase in ionic strength. This is consistent with the behaviour of ferrihydrite. The effect of ionic strength at low to neutral pH values is less clear. Taken at face value, the data may indicate an increase of sorption at *higher* ionic strength (Figure 7.7). In contrast, some data obtained with KGa-1 in U sorption studies performed by workers from the Japan Atomic Energy Research Institute suggested an increase with *lower* ionic strength, although the data were again inconclusive [Sekine *et al.,* 1990]. After reviewing all the available data-sets, it appears that the differences between the two uptake curves on Figure 7.7 (at pH values below 7) may be explained by experimental variation. Although greater than the analytical uncertainty (shown by the error bars), there may be additional sources of experimental error which could lead to slight variations in measured sorption. The most important of these (in this case) may be differences in the solid / liquid separation with the ionic strength affecting the aggregation and settling of the particles during centrifugation. This would particularly affect data obtained under conditions of high sorption (pH 5.5 - 7.5). Another possibility may be sampling variation in the source clay materials.

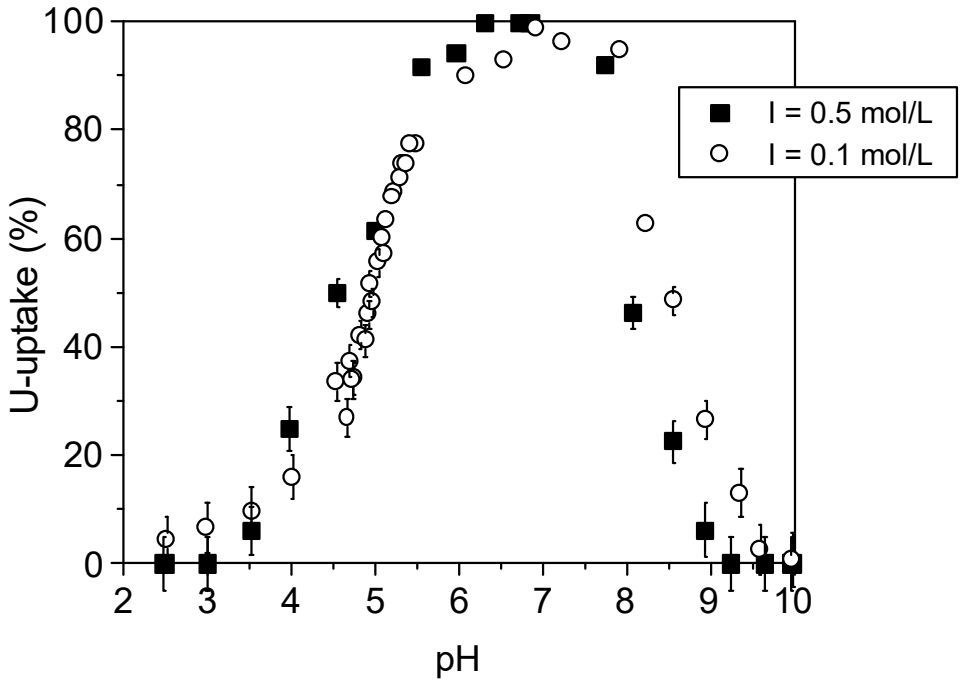


FIGURE 7.7 U-uptake by kaolinite KGa-1B - effect of ionic strength. ΣU = 1 μmol/L, mass loading 4g/L.

7.4 Comparison of U-sorption behaviour of KGa-1, KGa-1B and ferrihydrite

As noted above, supplies of the standard KGa-1 kaolinite, which was used in the early part of the experimental program, became exhausted, and the Clay Mineral Society substituted the similar material denoted KGa-1B. A description of the latter material and a comparison with KGa-1 has been published [Pruett and Webb, 1993]. The elemental compositions of the two kaolinites are given in Table 7.1. The comparison of U sorption data on KGa-1 and KGa-1B is shown in Figure 7.8. In general the data are quite similar. It will be observed that in Figure 7.8B ($\Sigma U = 10^{-5}$ mol/L) both samples appear to be near to saturation with U, since the maximum U uptake does not reach 100%.

TABLE 7.1 Chemical composition of KGa-1 and KGa-1B kaolinite samples. (weight %, not including H_2O)

	KGa-1 [a]	KGa-1B [b]
SiO_2	44.2	45.2
TiO_2	1.39	1.64
Al_2O_3	39.7	39.1
Fe_2O_3	0.13	0.21
FeO	0.08	-
MnO	0.002	-
MgO	0.03	0.05
CaO	n.d	0.02
Na_2O	0.013	0.04
K_2O	0.05	0.02
P_2O_5	0.034	-

[a] Van Olphen and Fripiat [1979]
[b] Pruett and Webb [1993]

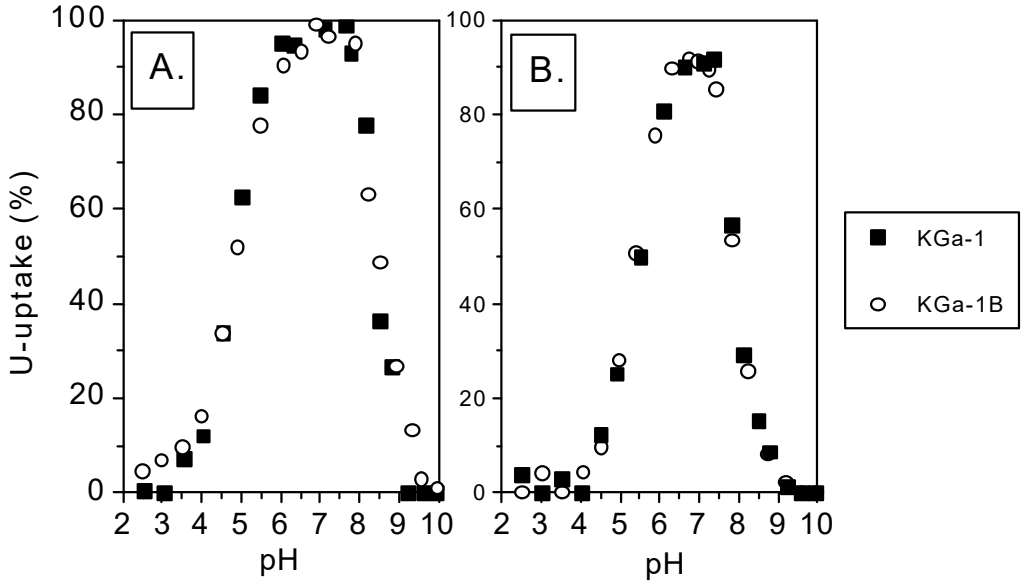


FIGURE 7.8 U-uptake by kaolinites KGa-1 and KGa-1B (mass loading 4 g/L). A) ΣU = 1 μmol/L B) ΣU = 10 μmol/L

The experimental data for experiments with ferrihydrite and kaolinite are compared directly in Figure 7.9. Here attention is restricted to U concentrations that are below solubility limitations. The sets of curves are distinctive both in the steepness of the curves and in their spacing. Compared to the corresponding experimental data for ferrihydrite, the pH dependence (steepness of the edges) is smaller for kaolinite, possibly indicating a different proton stoichiometry of adsorption (see Chapter 12). The displacement between the curves at different ΣU is much greater for kaolinite than those of ferrihydrite, which are quite closely spaced.

As might be expected, the data clearly indicate that, on a mass basis, ferrihydrite is a much stronger adsorber of U than kaolinite. This can be expressed by the experimental K_d (this parameter was discussed in Section 2.2). For example, at pH of 4.5 and ΣU of 1 μmol/L the K_d values for U sorption for ferrihydrite and kaolinite are about 10^4 mL/g and 10^2 mL/g, respectively. To some extent, this reflects their surface areas of approximately 600 and 8.4 m^2/g. While the K_d for U-sorption on ferrihydrite is inevitably greater than on kaolinite under similar conditions, the ratio between the two values is variable and dependent on factors such as pH and ΣU.

7.5 Effect of complexing ligands on U sorption by kaolinite

7.5.1 Phosphate

Experiments with added phosphate (ΣPO_4 of 10^{-4} mol/L) showed that the presence of phosphate substantially increased U uptake on kaolinite at low pH values (Figure 7.10) and had little effect at higher pH values. In contrast to the data for ferrihydrite, the adsorption of PO_4^{3-} was minor, less than 20% at all pH values. However, because the total amount of P in the system is greater than that of U, the sorption density of P is probably greater than that of U.

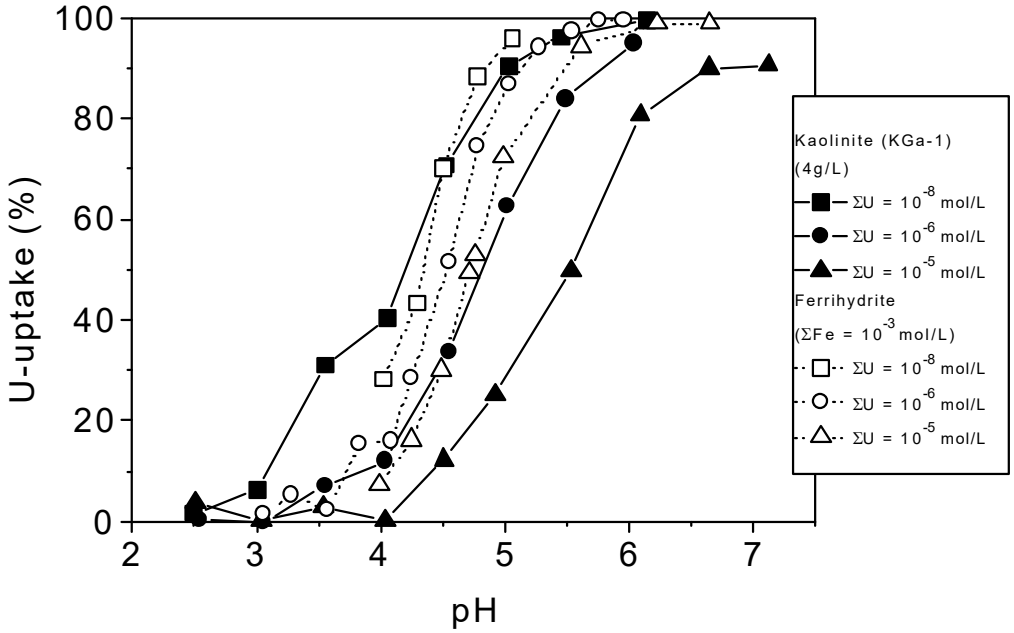


FIGURE 7.9 pH-edges for U uptake on kaolinite and ferrihydrite for various ΣU. Note that the curves for ferrihydrite are more closely spaced and have a steeper slope.

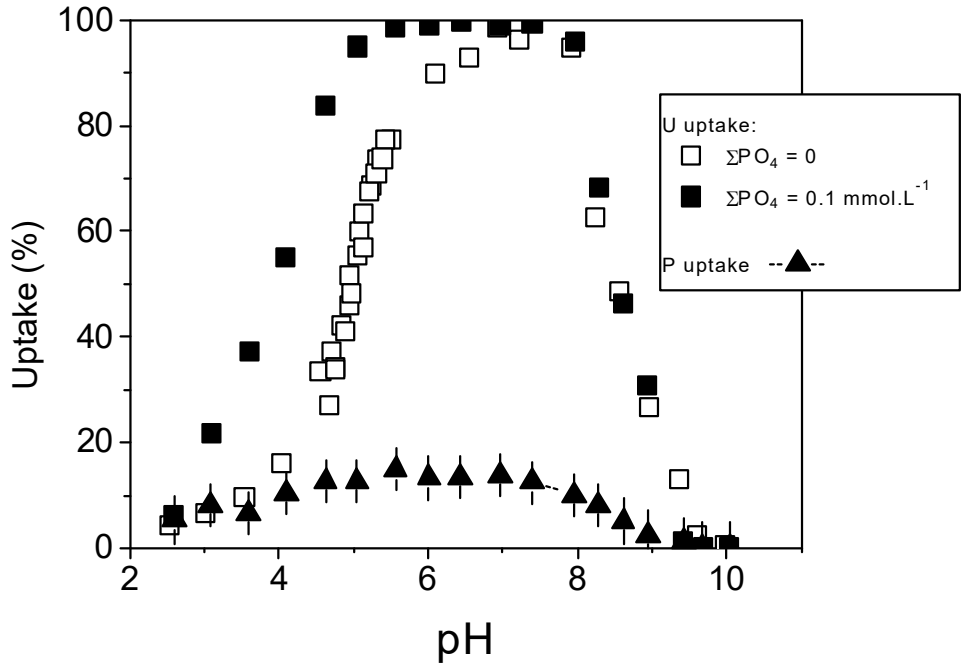


FIGURE 7.10 Effect of phosphate on U uptake by kaolinite (KGa-1B). ΣU = 1 μmol/L. Kaolinite loading 4 g/L.

The low-pH U sorption edge on kaolinite was displaced to more acidic pH values when phosphate was present, although only a relatively small proportion of phosphate was adsorbed (Figure 7.10). The presence of phosphate increased U sorption across a wide pH range from 3 to 7.5. The increase in U uptake occurred across a pH range in which U-phosphate complexes are important in the aqueous phase (Figure 3.6). In the experiments with ferrihydrite, it was considered possible that the formation of a new $FePO_4$ phase on the ferrihydrite surface could provide an explanation for the increased sorption of U in the presence of phosphate. In the kaolinite case, a surface precipitate of Fe and PO_4^{3-} appears unlikely, and the increased U sorption may be attributable to the formation of a ternary surface complex. This reasoning shows an important benefit of studying more than one solid substrate, in that possible U uptake mechanisms can be subjected to more rigorous testing when results for a variety of experimental systems are available.

In addition to providing insights about the possible formation of ferric phosphate solids, the results of these experiments suggest that precipitation of U(VI)-phosphate phases was not responsible for removing U from solution in the experiments with ferrihydrite. A comparison of the data for the kaolinite and the ferrihydrite solids in the critical pH range of the low pH U sorption edge clearly indicates that higher equilibrium dissolved concentrations of both U and phosphate were measured with kaolinite for pH values between 3.5 and 6 (Figure 7.11). This would not be expected if precipitation was occurring in the experiments with ferrihydrite.

It is also worth noting that in the presence of phosphate, the slopes of the U sorption edge on kaolinite and ferrihydrite are similar to those obtained in the phosphate-free systems (compare Figure 7.11 with Figure 7.9). Although not conclusive evidence, this would suggest that similar processes remove U from the aqueous phase in both the presence and absence of phosphate in these systems.

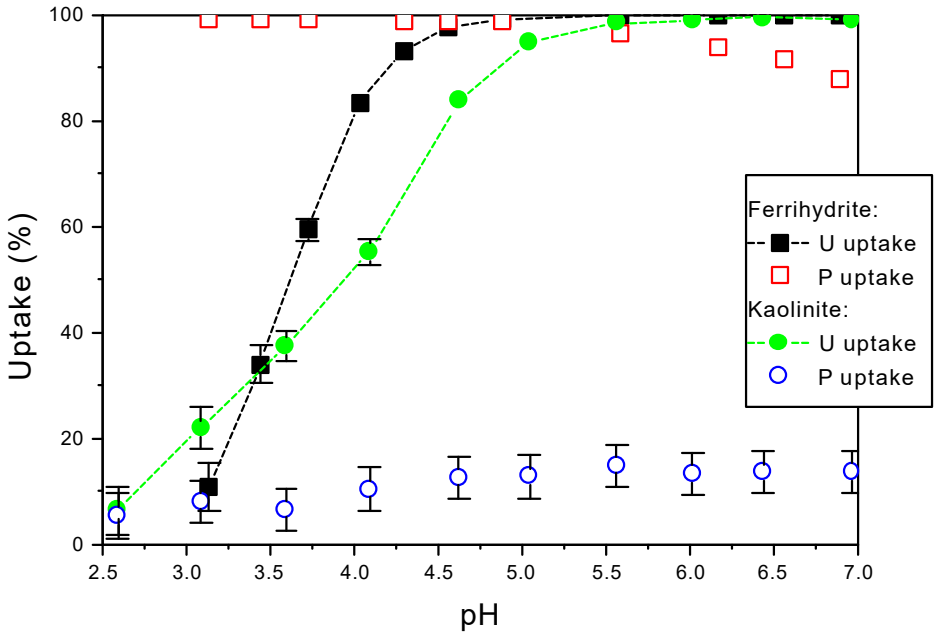


FIGURE 7.11 Comparison of U sorption on ferrihydrite (ΣFe = 1 mmol/L) and kaolinite (KGa-1B, 4 g/L) in the presence of 100 µmol/L of added PO_4^{3-}. ΣU = 1 µmol/L.

In order to further understand the phosphate-containing systems, further experiments were carried out with a higher mass loading of kaolinite, of 40 g / L (Figure 7.12). The sorption of both U and phosphate was greater than with the lower mass loading (4 g/L). As was the case with the lower mass loading, the presence of phosphate increased U adsorption. The data again suggest sorption rather than precipitation occurs, since the amount of surface sites should not affect a solubility-controlled equilibrium.

To allow better comparison of the effect of mass loading, the data for systems containing both P and U, with differing mass loadings of kaolinite, are compared directly in Figure 7.13. Clearly the uptake of both P and U are related to the solid mass loading. In the case of U this leads to a displacement of the pH edge to the left, and the upper edge to the right (i.e. increases sorption) whereas the uptake of phosphate is fairly uniformly increased across the entire pH range.

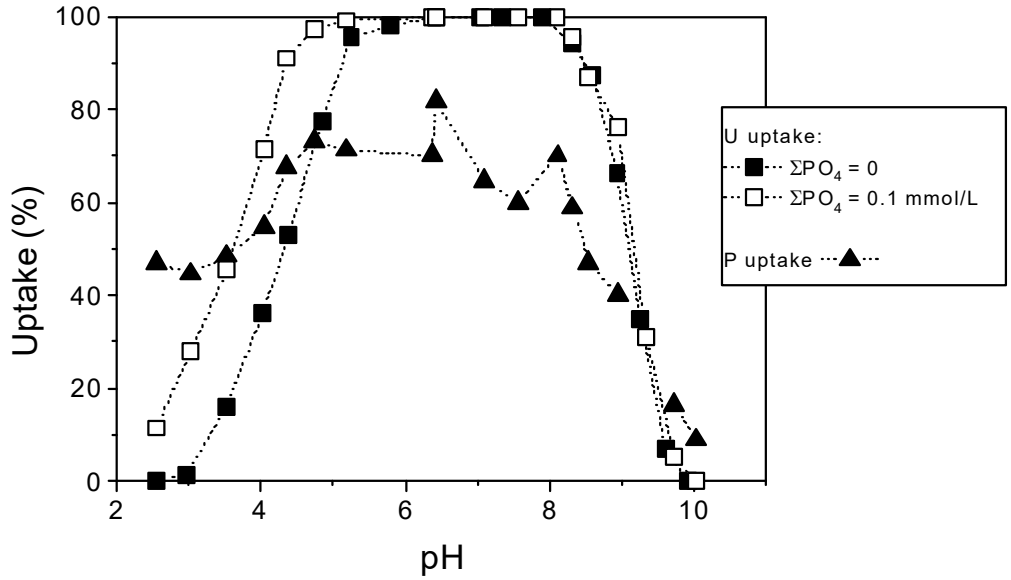


FIGURE 7.12 Effect of phosphate on U uptake by kaolinite (KGa-1B). ΣU = 1 μmol/L. Kaolinite loading 40 g / L.

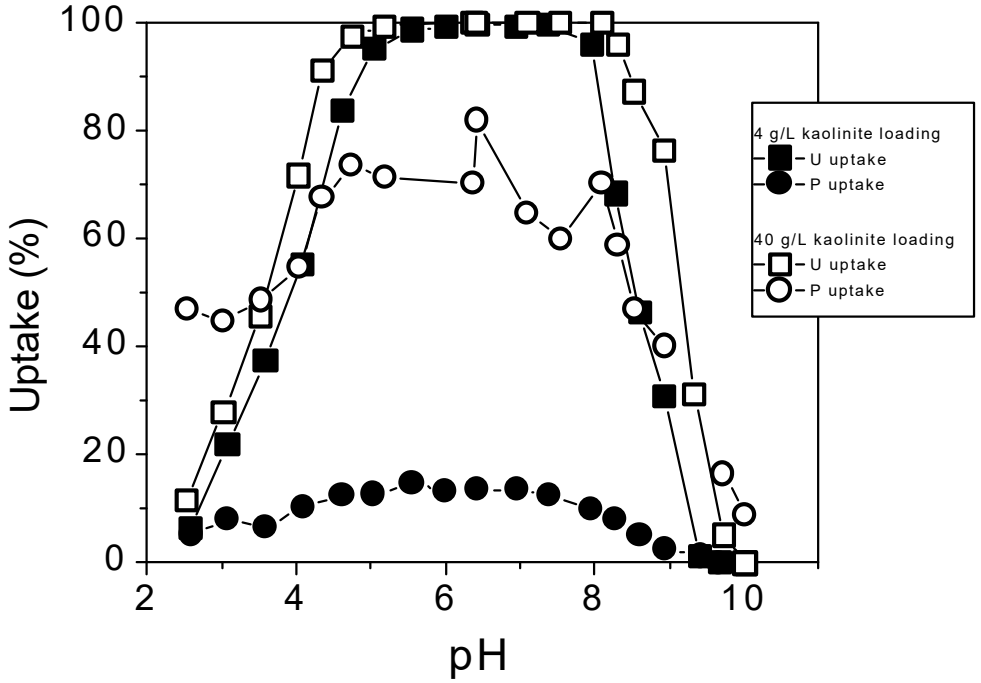


FIGURE 7.13 Uranium and P uptake by kaolinite at mass loadings of 4 g/L and 40 g/L. ΣU = 1 μmol/L, ΣP = 100 μmol/L.

7.5.2 Humic acid, sulfate and citrate

The rationale for studying the effect of humic acid (HA) on actinide sorption was discussed in Section 6.4.2. Uranyl sorption experiments with kaolinite showed that the addition of HA (9 mg/L) moved the low pH U-sorption edge to the left (increased sorption), and had little effect on the high pH edge (Figure 7.14). These results are similar to the U / ferrihydrite / HA system (Section 6.4.2).

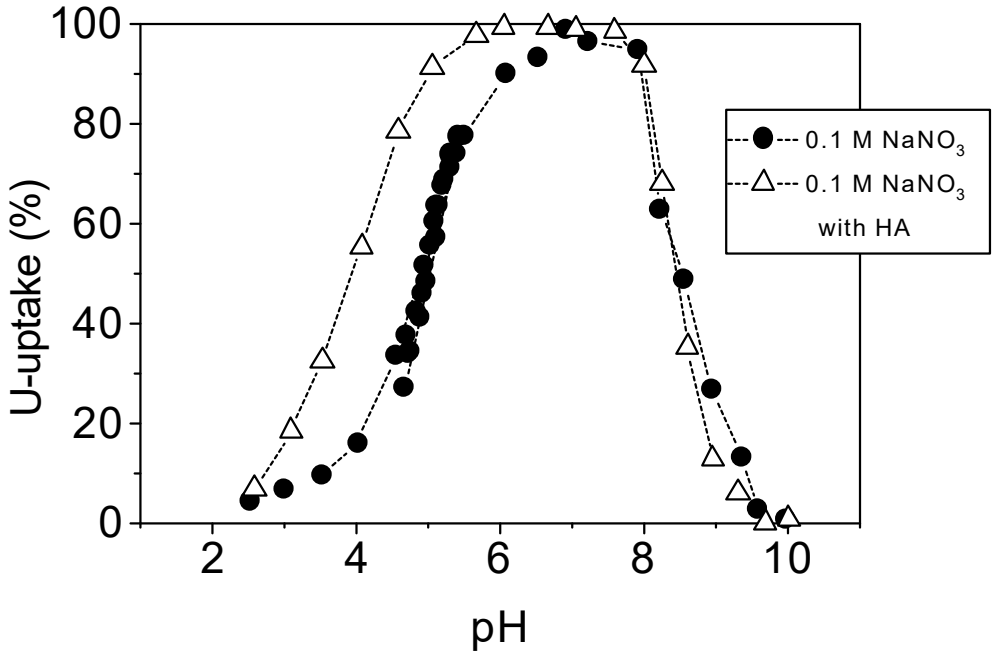


FIGURE 7.14 Effect of humic acid (HA) on U uptake by kaolinite (KGa-1B). ΣU = 1 μmol/L, clay = 4 g/L, HA = 9 mg/L.

Results of experiments exploring the effect of sulfate and citrate on U sorption by kaolinite are presented in Figure 7.15. In all experiments the kaolinite was KGa-1B. The effect of 0.01 mol/L sulfate on U sorption by kaolinite was relatively small. The data possibly suggest a small decrease in U uptake, however the effect is minor compared to the effects of changes in other experimental conditions.

As was found with the ferrihydrite, the presence of citrate caused a dramatic decrease in U uptake on kaolinite across the entire pH range (Figure 7.15). It is possible that some dissolution of the kaolinite solid phase (particularly of any iron-rich impurity phases which may be present) may occur, which may contribute to the reduced sorption in the presence of citrate. However, it appears that the most likely explanation of the kaolinite data is that complexation of U(VI) by citrate in the aqueous phase greatly reduces U uptake.

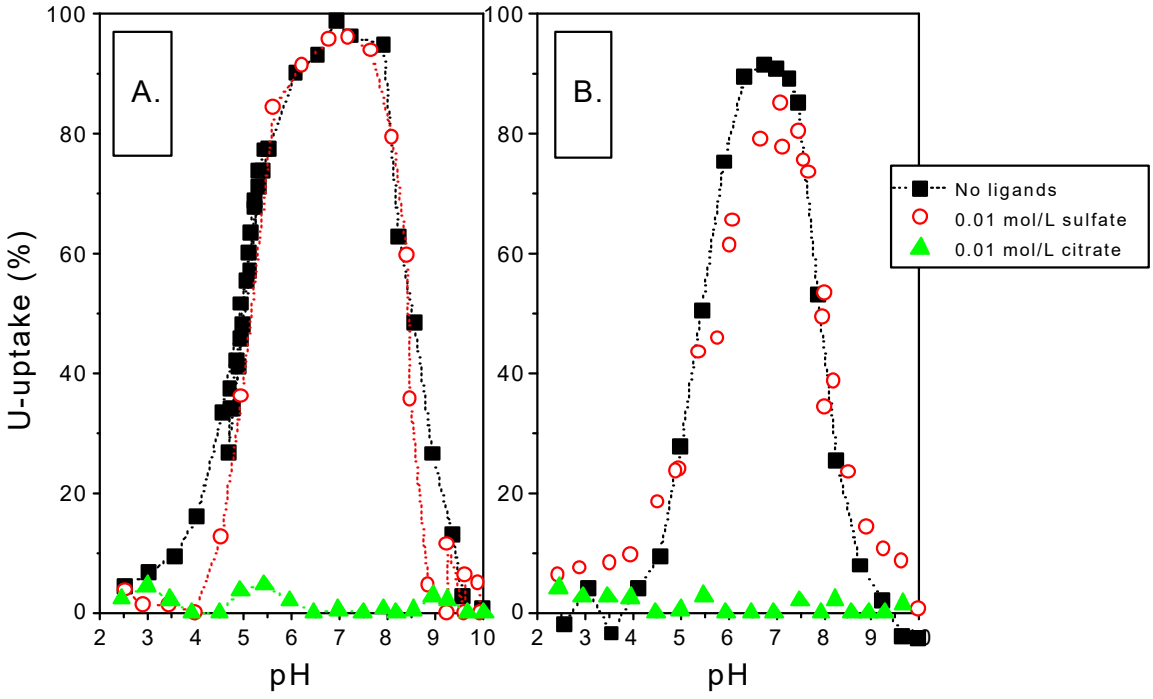


FIGURE 7.15 Effect of sulfate and citrate ligands on U sorption by KGa-1B kaolinite. A) ΣU = 1 μmol/L B) ΣU = 10 μmol/L Mass loading 4 g/L of kaolinite. 0.1M $NaNO_3$, equilibrium with air.

As was mentioned in Chapter 6, the systems with ΣCIT of 0.01 mol/L contain a large excess of citrate relative to ΣU. Therefore, U sorption was also studied in experimental systems to which 100 μmol/L of citrate had been added. The results (Figure 7.16) showed that in this case U sorption was again substantially reduced relative to the ligand-free case. However, there was a small pH range (around pH 8 - 9) in which some of the uranyl was adsorbed. The data somewhat resemble the analogous results for ferrihydrite (shown in Figure 6.22.). There is a slight indication of U uptake in the low pH range between 3 and 4, however it is not possible to be sure that the data follow the unusual double-humped U sorption curve found with ferrihydrite.

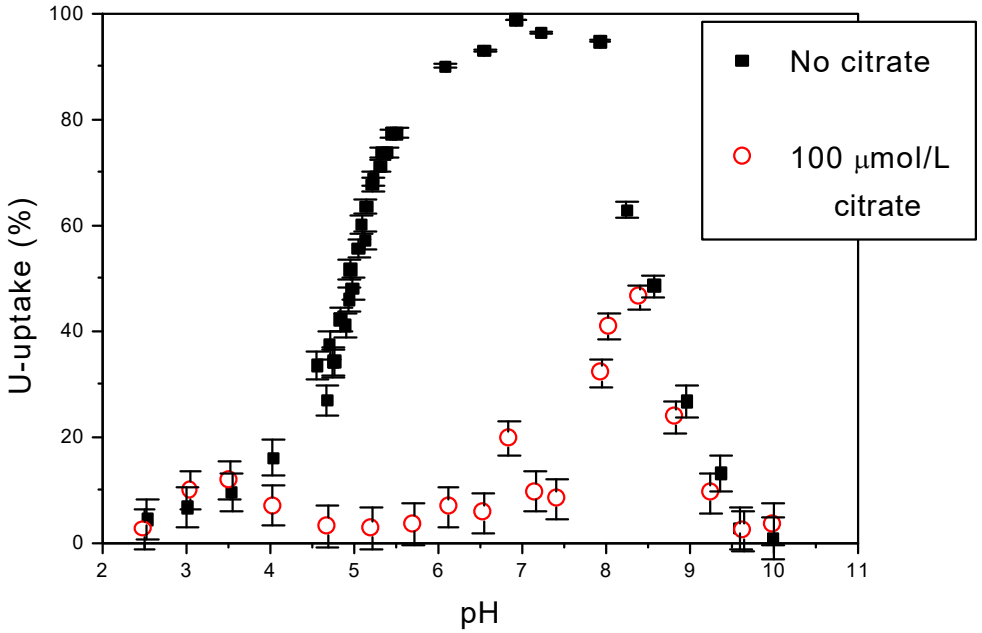


FIGURE 7.16 Effect of the addition of 100 μmol/L citrate on U sorption by kaolinite. (KGa-1B, loading 4 g/L, ΣU = 1 μmol/L, 0.1 mol/L $NaNO_3$)

7.6 Effect of trace impurities on uranium sorption by kaolinite

7.6.1 U sorption in mixed ferrihydrite / kaolinite systems

Uranium sorption was studied on a mixed substrate containing kaolinite and ferrihydrite, with mass loadings of 4 g/L and 89 mg/L respectively. This was prepared following the procedure described in Section 5.1.1. Under the experimental conditions, the ferrihydrite probably coats the surface of kaolinite, as has been observed in nature. The resulting solid had a slight pink tinge, whereas pure kaolinite is off-white in colour.

The sorption results (Figure 7.17) showed that the sorption properties of the mixed system were very similar to ferrihydrite, although it was the minor phase on a mass basis (about 2.2 wt%). This supports the hypothesis that strongly sorbing trace phases may dominate U-sorption in the natural environment.

7.6.2 Analytical electron microscopy

The association of sorbed U with the various mineral surfaces in the model kaolinite was studied using AEM[1]. A sample of kaolinite KGa-1, which had been used in an experiment with ΣU of 10^{-4} mol/L, was found to consist of abundant kaolinite particles and a smaller proportion of Ti-rich particles. Although the presence of the latter phase had been reported previously, it was more readily visible than had been expected, given its low abundance.

Electron microscope images and corresponding point analytical data for the kaolinite and Ti-rich particles are shown in Figure 7.18 and 7.19 respectively. The particles are entirely different both in their appearance and chemical composition.

The AEM data for 25 kaolinite grains in this sample are summarised in Table 7.2. The elemental results for Al and Si are similar to that expected for a pure kaolinite, and are close to reported values for the bulk composition of KGa-1. The

[1] The AEM analyses were carried out by Dr G. Lumpkin, Materials Division, ANSTO

average U content of the kaolinite particles examined was only 0.06%, which was much less than was expected on the basis of the amount of U taken up by the solid in this experiment. Therefore, the kaolinite particles in this sample were only responsible for a small proportion of the U uptake.

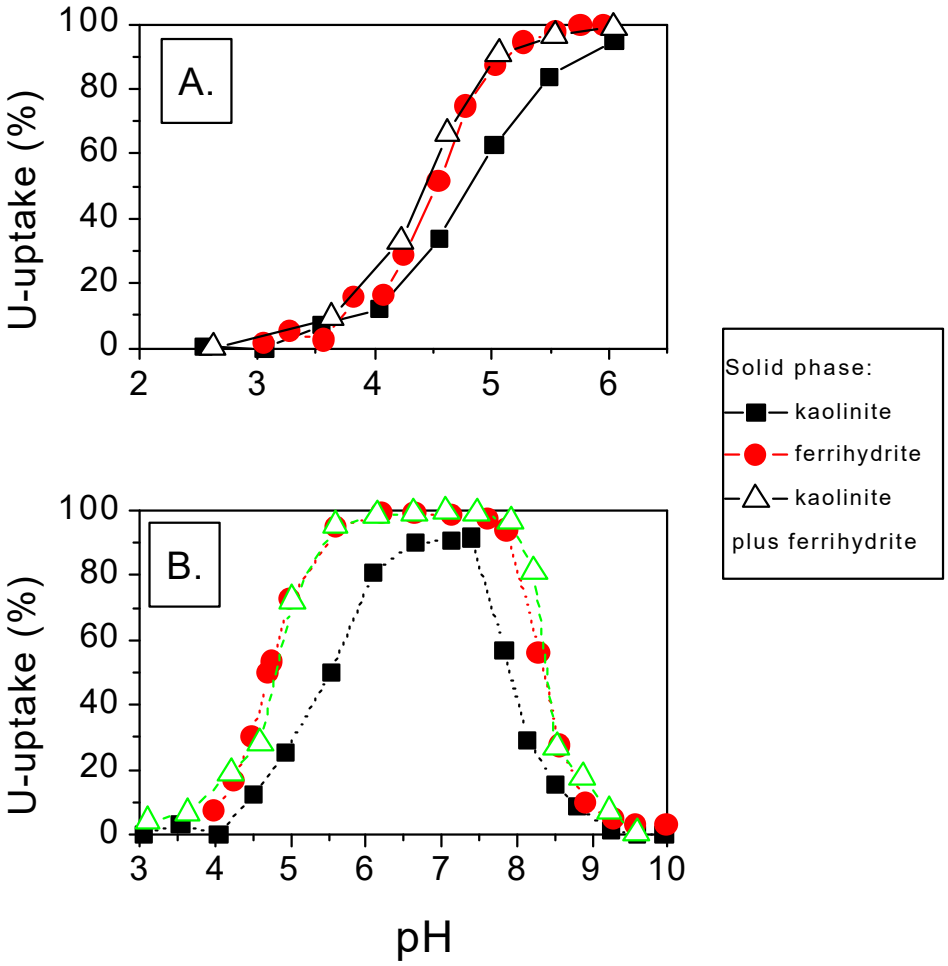


FIGURE 7.17 Adsorption of U on ferrihydrite (ΣFe = 1 mmol/L), kaolinite (KGa-1, 4g/L) and a mixed substrate comprising both minerals

(ΣFe of 1mmol/L and 4 g/L kaolinite).

A) ΣU = 1 µmol/L B) ΣU = 10 µmol/L

The separate Ti-rich particles were identified by electron diffraction as being anatase and rutile. Anatase is the more abundant TiO_2 polymorph, and occurs as clusters consisting of grains generally less than 0.2 - 0.3 μm in size, and also as single crystals up to 0.5 μm in size. Rutile is less common, but several single crystals up to approximately 1 μm in length were observed. The presence of these phases is consistent with previous work on Georgia kaolinite [Weaver, 1976]. The amount of U associated with Ti-rich particles was about 0.7%, more than ten times higher than the kaolinite particles (Table 7.2). Therefore, the Ti-rich particles, despite being less abundant than the kaolinite particles, were responsible for a substantial proportion of the total U adsorbed by the KGa-1 sample. There was a significant negative correlation between the amount of U present and the grain size of the Ti-rich particles, indicating that U is preferentially adsorbed by the fine-grained anatase clusters.

Mass balance calculations showed that the anatase and kaolinite particles could not be responsible for all the loss of U from solution. This discrepancy was resolved when a grain containing predominantly U in the EDX spectrum was observed in the sample (Figure 7.20, Table 7.2). This indicated that some precipitation had occurred in experiments with high ΣU on the KGa-1 sample, and was consistent with the solubility calculations described above. Based on the presence of diffuse rings in its diffraction pattern, the U-rich particle was predominantly amorphous. However, it had some crystallinity which may have been acquired by evaporation during the sample preparation, or by electron beam heating while under observation in the TEM. Crystalline spots in the diffraction pattern were consistent with a partially dehydrated form of schoepite.

Mixed KGa-1 / ferrihydrite samples with adsorbed U were also studied. Kaolinite and anatase particles were both examined, and the results showed that Fe was fairly uniformly distributed over the clay and anatase particles (Table 7.2). The Fe content of the kaolinite grains averaged 0.76% compared to 0.15% in pure KGa-1. The Fe associated with the anatase increased slightly from 0.62% to 0.94%. Presumably the U was adsorbed on Fe coatings, since separate particles rich in Fe or U (or both) were not observed.

TABLE 7.2. Summary of AEM data for samples from U-sorption experiments

(all data expressed as wt %).

	KGa-1 bulk compo-sition[a]	Kaolinite (KGa-1) with added U of 0.6 wt %			KGa-1 + ferrihydrite (Fe of 1.4 wt %, added U of 0.06 wt%)	
		Kaolinite grains (n = 25)	Ti-rich grains (n = 12)	U-rich grain (n = 1)	Kaolinite grains (n = 25)	Ti-rich grains (n = 6)
Al	21.0	20.7	1.23	1.35	20.6	0.85
Si	20.7	21.6	0.75	0.69	21.4	0.36
Ti	0.83	0.14	56.0	0.00	0.12	56.9
U	-	0.06	0.71	76.4	0.05	0.08
Fe	0.15	0.15	0.62	0.15	0.76	0.94

[a]From Van Olphen and Fripiat (1979).

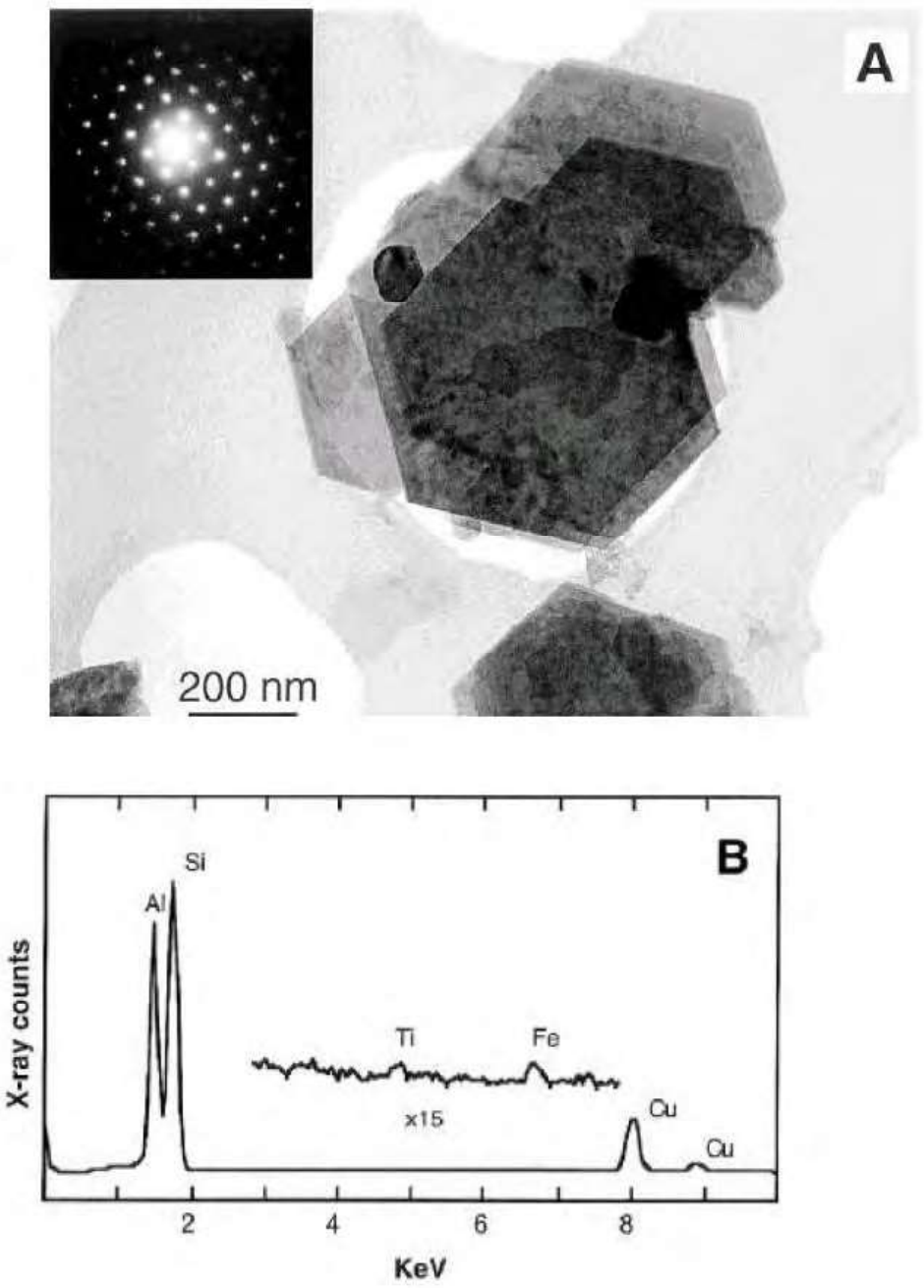


FIGURE 7.18 Electron microscopy results for U sorption experiments with KGa-1 kaolinite.

A) TEM bright field image and electron diffraction pattern (inset). Note two small anatase single crystals on the kaolinite in the bright field mage.

B) EDS spectrum of kaolinite. The expanded scale shows little evidence of adsorbed U.

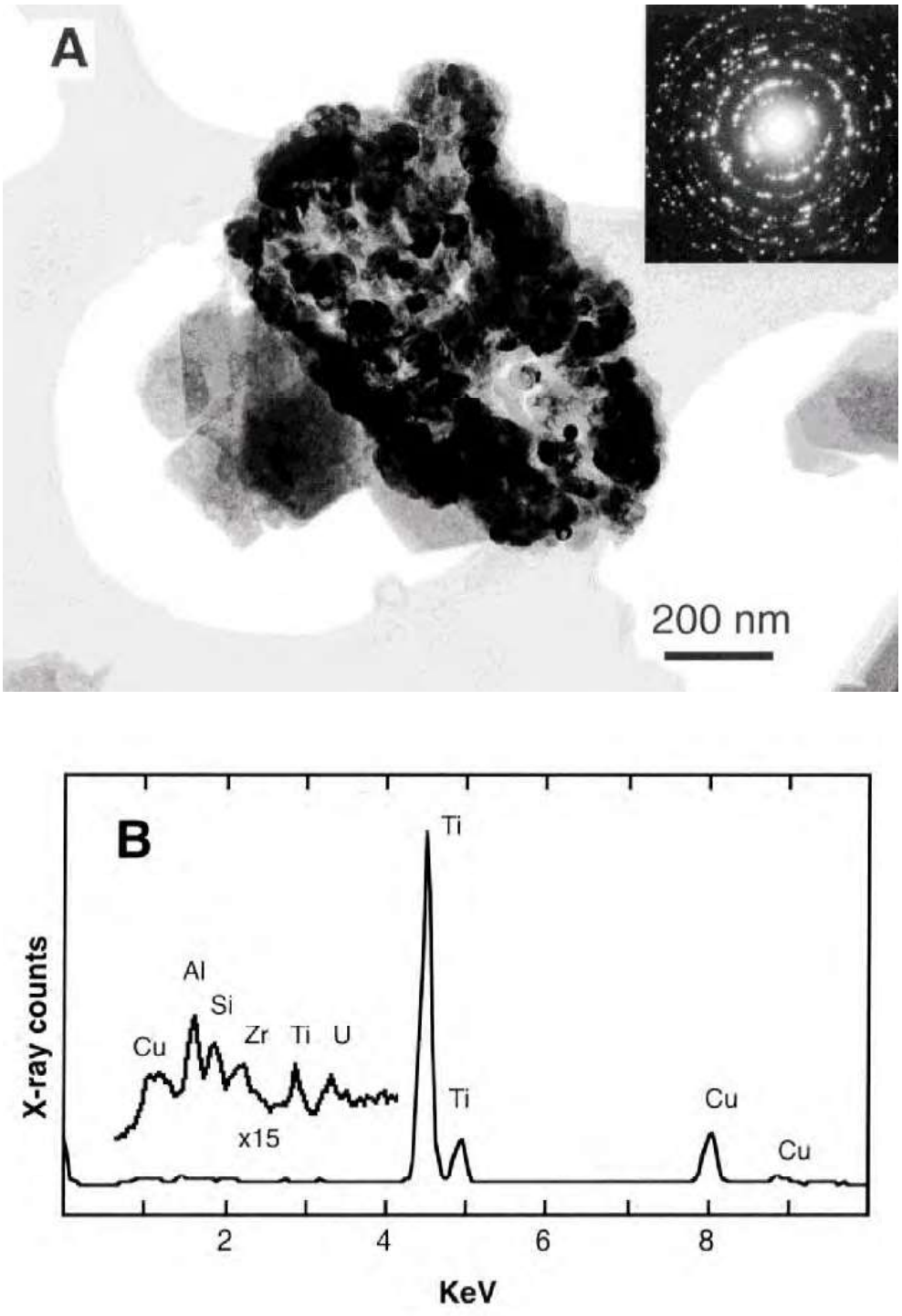
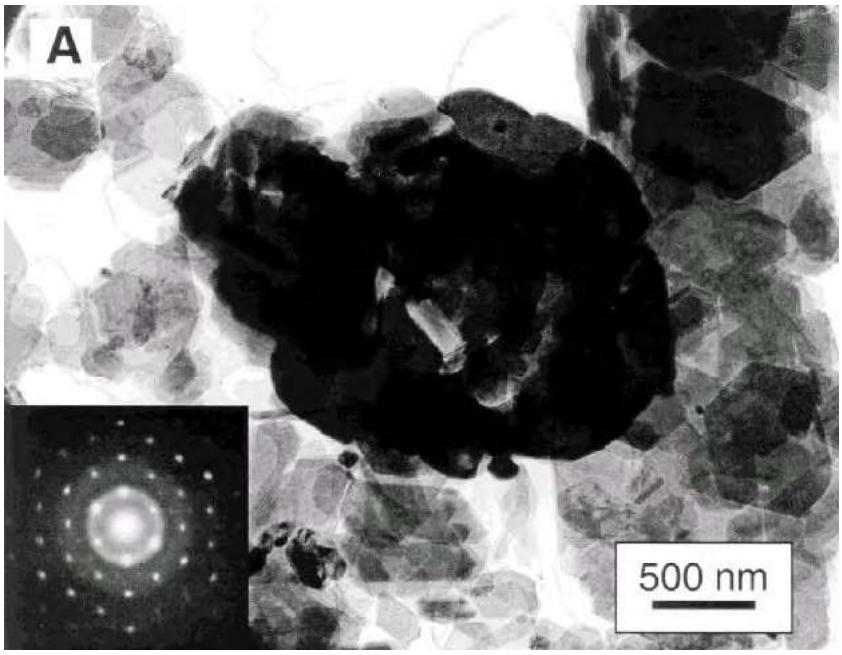


FIGURE 7.19 Electron microscopy results for anatase.

A) TEM bright field image and electron diffraction pattern (inset). In this example, the anatase occurs as a cluster of many small crystals.

B) EDS spectrum of anatase. Expanded scale shows positive evidence of adsorbed U.



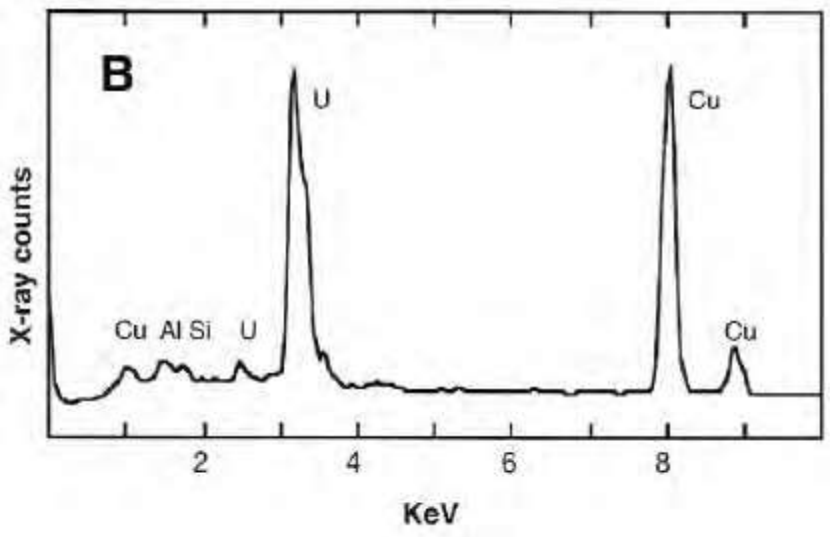


FIGURE 7.20 Electron microscopy results for U-rich precipitate.
a) TEM bright field image and electron diffraction pattern (inset). Note diffuse rings in the diffraction pattern.

b) EDS spectrum. Combined data indicate that the phase is a partially dehydrated form of schoepite.

7.6.3 Implications of the presence of anatase in Georgia kaolinites

The influence of Ti-rich particles on the U-sorption behaviour of KGa-1 may be important in any study in which KGa-1 or a similar kaolinite is used, and suggests that the uptake of U (and possibly other species) by KGa-1 should not be modelled on the basis of surface coordination by Al or Si surface sites alone. The much higher sorption on anatase should be taken into account. Although the AEM work in the present study was carried out at relatively high sorption densities of U, it is likely that the preferential uptake of U on anatase will be even greater at lower concentrations. The greater Fe content of the anatase particles (relative to the kaolinite particles) may also be of significance (Table 7.2). Clearly, minor phases such as anatase or ferrihydrite potentially play a major role in systems where much greater amounts of kaolinite are present.

In Chapter 8 it will be shown that extractions of weathered natural samples with the CDB (citrate / dithionite / bicarbonate) reagent, which dissolves amorphous and crystalline iron minerals, removed less than 2% of the contained titanium. Therefore, extraction techniques which aim to dissolve trace iron impurities may well be ineffective in dissolving anatase. The minerals used in the present study were not pre-treated to remove amorphous or trace mineral phases. The presence of chemically resistant anatase in the KGa-1 sample (and possibly other kaolinites) may well influence the results of sorption experiments, even after prior chemical extraction.

7.7 Summary of experiments with kaolinite

For a given set of experimental conditions, U uptake by kaolinite (expressed as U sorbed per gram of sorbent, or as an experimental K_d value) is much less than for ferrihydrite. However, the amount of U adsorbed by kaolinite shows a similar dependence on experimental variables such as pH, total U, mass loading and the presence of complexing ligands. The low-pH sorption edge is less steep for kaolinite than for ferrihydrite.

Uranium sorption on model kaolinites appears to be strongly influenced by the presence of Ti-rich impurity phases (predominantly anatase), which occur in many natural kaolinites. Due to the weak sorption on kaolinite, precipitation of a U-rich phase occurred in some experiments. The removal of impurities from model kaolinites by chemical extractions is not straightforward, as the anatase is chemically resistant. A small amount of a ferrihydrite phase added to the model kaolinite completely modified its behaviour, further demonstrating the importance of trace impurity phases in the natural environment.

The presence, and the significant role in U sorption, of the anatase phase in the model kaolinites casts some doubts on previous trace-metal sorption studies with Georgia kaolinite, where the role of the anatase has not been taken into consideration in interpreting experimental results. It also complicates the modelling approaches which can be taken to describe U sorption on this material. This issue will returned to in Chapter 12.

When considered in parallel with the results of the experiments with ferrihydrite, the experiments with kaolinite provide useful additional information that can be used to constrain the mechanisms of U retention in both systems. For example, some experimental systems with kaolinite contain higher amounts of dissolved U than the analogous systems with ferrihydrite. This provides evidence that U removal from the aqueous phase in the ferrihydrite experiments is not a consequence of direct precipitation of a uranyl phosphate mineral, and may instead be ascribed to sorption processes. Further evidence that sorption is the dominant process in the experimental systems with lower ΣU (<100 μmol/L) is provided by the sensitivity to kaolinite mass loadings of several of the U uptake curves, including those with phosphate present. This would be expected when sorption is the dominant process, since site populations will have a major influence on the observed phenomena. These aspects of the study are considered in Part III of the thesis where possible U retention mechanisms are discussed and modelled.

8 URANIUM(VI) SORPTION ON SUB-SURFACE MATERIAL FROM THE KOONGARRA WEATHERED ZONE

This chapter presents the results of the experimental study of U sorption by weathered rock material from the Koongarra uranium ore deposit. The experimental systems contained $NaNO_3$ as the background electrolyte. As with the analogous experiments with ferrihydrite and kaolinite (discussed in Chapters 6 and 7), these systems were equilibrated with air (or a mixture of air and CO_2) and are referred to as 'simple $NaNO_3/CO_2$ systems'.

The experiments with the natural substrates required prior separation of a fine particle fraction (described in Chapter 5). Various sample characterisations are described in this chapter. These included measuring the total and 'accessible' U content, and carrying out a sequential extraction to study the association of U and other key elements with chemically separated phases. The sequential extraction also provided data on $^{234}U/^{238}U$ ratios in chemically extracted phases, which are relevant to modelling U migration in the Koongarra system [Airey, 1986].

As in the experiments with the model minerals, the effects on U sorption by these Koongarra materials of pH, ΣU, pCO_2, ionic strength, and mass loading were studied. Some additional sorption investigations were carried out with the natural substrates. These included the effect on U sorption of removal of Fe-oxides (using the CDB reagent), and isotope exchange studies. These involved exchange between ^{236}U in the aqueous phase and ^{238}U from the solid phase. In addition, some systems also included Mg^{2+}, which was added to the aqueous phase. These experiments were undertaken because Mg^{2+} is the dominant cation in Koongarra groundwaters (resulting from weathering of the host-rock chlorite).

The samples discussed here are from Koongarra boreholes W1, W2 (2 samples) and W7 (see Figure 1.1 and Table 8.1). A second sample of the W2 material was separated towards the end of the experimental program. To distinguish it from the previous W2 sample, the more recent composite sample is referred to as W2c (with the original sample referred to as W2).

8.1 Sample characterisation by SEM[1]

The fine particle samples from boreholes W1, W2 and W7 were examined using SEM / EDX. All EDX spectra exhibited peaks of Si and Al. Where only Si and Al were present, the particles were assumed to be kaolinite. Where K was observed in the EDX, it was attributed to the presence of mica. A peak of Mg was assumed to indicate chlorite, or more probably altered chlorite (this may include vermiculite or smectite).

All samples were predominantly kaolinite, however the W1 sample had greater amounts of hematite as evidenced by its brick-red colour. In contrast, the W2 and W7 samples were yellow / brown.

The main features of the samples can be generalised as follows:

- The mineralogy of the samples is quite uniform being dominated by kaolinite.
- Mica is a minor component of all samples.
- Altered chlorite was found in W2 and W7, but was almost absent from W1. This may be attributed to the greater depth of weathering (leading to alteration of chlorite) near to the Koongarra fault (see Figure 1.1).
- Iron was found as coatings on clay particles and as abundant fine particles of around 1 μm in size .
- The Fe-dominated particles appeared to consist of aggregates of smaller particles.
- The minor components P, Ti and Mn were only observed in particles rich in Fe, indicating a possible association of these elements.

The BET surface area of the fine fraction of the W2 and W7 materials were significantly higher (per unit mass) than W1 (Table 8.1).

[1] This section is based on SEM analysis undertaken by ANSTO Materials Division.

TABLE 8.1 Summary of Koongarra samples used in sorption experiments (data for separated fine fractions).

Sample name[a]	Depth (m)	Total U content (μg/g)	TAO extractable U content (μg/g)[b]	BET surface area[c] (m^2/g)
W1	13.0 – 13.2	356	42.6	24.6
W2	14.0 – 14.2	426	225.0	52.3
W2c	12.0 – 12.2	213.5	97.3	20.3
W7	13.0 – 13.2	10.4	1.0	51.9

[a] Sample name is the same as the borehole except for the second sample from W2 which is denoted W2c.

[b] See text.

[c] Provided by ANSTO Materials Division (Particle Characterisation Laboratory)

The samples were analysed using X-ray diffraction (XRD). The main peaks observed in the XRD spectrum of the W1 sample corresponded to muscovite, kaolinite and quartz, with a small peak of goethite. Chlorite, kaolinite, goethite and mica were present in the W2 sample.

8.2 Sequential extraction study

A detailed characterisation of the fine fractions used in the sorption studies was undertaken using a selective extraction technique. This involved treating the sample with a sequence of chemical reagents, with the objective of partitioning the contained elements amongst a series of phases (adsorbed metals, carbonate minerals, iron oxides, etc). It is generally agreed that the resulting information is of greater use in environmental studies than merely determining total metal concentration [Tessier *et al*., 1979]. Although in some cases considerable information

about the extracted phases can be obtained, it should be remembered that these phases are operationally defined by the extractants used to remove them.

Tessier *et al.* [1979] used a five step chemical extraction procedure to separate exchangeable, carbonate, Fe / Mn oxide, organic and residual phases of river sediments. Similar techniques have been applied in studies of radionuclides. A sequential extraction procedure was used in a study of U and Th isotopic distributions in deep soil profiles from the Ranger No.1 ore body [Lowson *et al.*, 1986]. In this case the extraction scheme separated the following phases:

1) soluble salts and exchangeable ions,
2) amorphous oxide minerals,
3) crystalline iron minerals,
4) amorphous alumina and silica compounds, and
5) resistate material.

Sequential extraction techniques were successfully applied to samples from the Koongarra deposit [Yanase *et al.*, 1991], and were extensively used within the ARAP project, during which the work described in this thesis was commenced.

The samples used in the sorption studies were subjected to a five-stage sequential extraction scheme (Table 8.2). This extraction scheme was developed from the one employed by Lowson *et al.* [1986]. The selection of chemical reagents and extraction conditions has been previously discussed [Yanase *et al.*, 1991]. Extraction solutions obtained from each extraction step were analysed for their radionuclide content using alpha spectrometry. The W2c sample was subjected to duplicate extractions and the data for the two extractions were compared.

TABLE 8.2 Extraction scheme used for Koongarra samples.

Reagent	Main phases dissolved	Extraction conditions
1) Morgan's solution	Carbonate minerals, adsorbed trace elements	40 mL / g sample, shaken for 4 hours
2) Tamms acid oxalate (TAO)	Amorphous minerals of Fe, Al and Si; secondary U minerals	40 mL / g sample, shaken in dark for 4 hours
3) Citrate / dithionite / bicarbonate (CDB) reagent	Crystalline iron oxides, hydroxides and oxyhydroxides	60 mL / g sample, stirred for 30 minutes at 85°C (repeated)
4) 6 M HCl	Clay minerals, uranium oxides	Stirred for 2 hours at 85°C
5) Digestion and fusion	Remaining resistant minerals (quartz, muscovite)	HF / $HClO_4$ digestion followed by Na_2CO_3/ borax fusion

Reagent composition:
Morgan's solution: 1M NaOAc adjusted to pH 5.0 with acetic acid
TAO: 10.9 g / L oxalic acid + 16.1 g /L ammonium oxalate.
CDB: 0.3 M tri-sodium citrate, 0.2 M $NaHCO_3$, 1 g / g sample sodium dithionite

Elemental distributions in chemically separated phases

The chemical extraction data (Table 8.3) indicated that Al, Ti and K were predominantly associated with residual phases, such as anatase and clay minerals. The Fe tended to be associated to a large extent with the fractions extracted by the CDB reagent or the 6M HCl extraction. About 1% of the Fe in the samples was in the amorphous phases extracted with the TAO reagent. Manganese was much less abundant than Fe in these samples. Magnesium was associated with a readily extractable phase, presumably adsorbed or as carbonate minerals (dissolved by the Morgan's reagent). Mg was also found in residual phases, possibly primary or altered

chlorite, but was not associated with the Fe-minerals. The data in Table 8.3 are particularly useful for estimating the amount of sorbing mineral phases (such as ferrihydrite or crystalline Fe-oxides) in the samples.

The reproducibility of the technique was also studied. Table 8.3 shows results obtained from repeated extractions of the W2c sample. Typically the extraction data for a particular sample are highly consistent. However, in common with many other types of geological analyses, sampling variability can lead to significant differences between samples, even those in close proximity to one another.

Uranium-series data

For these analyses, a known amount of ^{232}U was added to the solution obtained from the chemical extraction. Following standard radiochemical separation procedures (Section 5.3) the uranium isotopes were counted in an ORTEC ALPHA-KING α-spectrometer, and the amounts of ^{234}U and ^{238}U were determined from their count rates relative to ^{232}U.

Data on the distribution of uranium amongst the chemically separated phases in the samples from the Koongarra weathered zone are shown in Table 8.4. Relatively large amounts of the uranium were removed by Morgan's reagent. This reagent appears to remove adsorbed uranium, since there is only minor dissolution of other mineral phases (Table 8.3). When carried out after an extraction with Morgan's reagent, the TAO extraction removed only a small increment of U. This indicates that U is more likely to be bound to the surface of amorphous Fe-oxides, rather than incorporated within them.

TABLE 8.3 Elemental distribution in Koongarra samples as determined by a sequential extraction.

W1 (13-13.2 m) Elemental distribution (mg extracted/g of solid)

Extractant	Fe	Al	Mn	Mg	Ca	Ti	K
Morgans	0.12	0.18	0.00	0.52	0.08	0.00	0.22
TAO	0.88	0.58	0.00	0.06	0.01	0.00	0.25
CDB	35.10	1.08	0.00	0.03	0.07	0.05	0.60
HCl	35.30	6.37	0.00	0.28	0.01	0.16	1.42
Fusion	9.14	166.0	0.03	4.30	0.01	2.76	9.82
Sum(mg/g)	80.6	173.8	0.04	5.2	0.2	3.0	12.3

W2 (14-14.2 m) Elemental distribution (mg extracted/g of solid)

Extractant	Fe	Al	Mn	Mg	Ca	Ti	K
Morgans	0.52	0.61	0.01	3.93	0.20	0.00	0.37
TAO	1.17	1.21	0.15	0.25	0.01	0.01	0.04
CDB	6.77	0.89	0.03	0.13	0.11	0.00	0.54
HCl	79.20	35.00	0.13	9.67	0.01	0.05	0.28
Fusion	20.80	90.30	0.04	3.48	0.03	0.84	7.84
Sum(mg/g)	108.4	128.1	0.3	17.5	0.4	0.9	9.1

W2c (12-12.2 m) Elemental distribution (mg extracted/g of solid)
Data for duplicate extractions (1 and 2) are shown.

Extractant		Fe	Al	Mn	Mg	Ca	Ti	K
Morgans	1	0.00	0.00	0.00	4.72	0.12	0.0	0.0
	2	0.00	0.00	0.00	4.93	0.12	0.0	0.0
TAO	1	0.26	0.41	0.11	0.42	0.48	0.0	0.0
	2	0.27	0.42	0.12	0.46	0.50	0.0	0.0
CDB	1	0.33	0.49	0.00	0.08	0.37	0.0	0.27
	2	0.41	0.46	0.00	0.07	0.31	0.0	0.34
HCl	1	75.50	64.5	0.08	12.60	0.03	0.20	2.00
	2	78.50	53.0	0.08	12.45	0.06	0.16	1.25
Fusion	1	4.83	32.8	0.01	1.51	0.23	4.46	2.76
	2	8.40	54.0	0.02	2.66	0.20	5.3	3.88
Sum	1	80.9	98.2	0.20	19.3	1.23	4.66	5.03
(mg/g)	2	87.6	107.5	0.22	20.6	1.19	5.46	5.47

W7 (13-13.2 m) Elemental distribution (mg extracted/g of solid)

Extractant	Fe	Al	Mn	Mg	Ca	Ti	K
TAO[a]	0.41	0.41	0.18	2.04	<0.04	<0.06	0.07
CDB	6.83	1.01	0.02	0.46	<0.10	<0.01	0.27
HCl	38.20	23.60	0.10	3.51	<0.01	0.18	0.98
Fusion	7.68	60.9	0.04	1.27	<0.01	1.26	4.95
Sum(mg/g)	53.1	85.9	0.3	7.3	<0.15	1.50	6.30

[a]There was no extraction with Morgan's solution for the W7 sample.

TABLE 8.4 Uranium distribution and $^{234}U/^{238}U$ in Koongarra samples as determined by a sequential extraction.

U content of extracted phases (μg/g)

	W1	W2	W2c	W7
Morgan's	30 ± 1	182 ± 8	69.3 ± 2.4 71.1 ± 1.5	-
TAO	12.6 ± .4	43 ± 2	26.0 ± 0.9 28.2 ± 0.9	1.00 ± 0.06
CDB	131 ± 4	65 ± 3	15.1 ± 0.7 16.1 ± 1.0	4.6 ± 0.6
HCl	177 ± 8	130 ± 3	98.1 ± 2.6 97.1 ± 2.6	3.9 ± 0.4
Fusion	5.2 ± .1	6.4 ± 0.2	5.0 ± 0.3 6.3 ± 0.4	0.9 ± 0.1
Total	356 ± 14	426 ± 16	213.5 ± 3.8 218.8 ± 3.4	10.4 ± 0.8

$^{234}U/^{238}U$ in extracted phases

	W1	W2	W2c	W7
Morgan's	0.82 ± 0.03	0.61 ± 0.03	0.64 ± 0.03 0.66 ± 0.02	-
TAO	0.85 ± 0.03	0.64 ± 0.05	0.66 ± 0.03 0.63 ± 0.03	0.97 ± 0.06
CDB	0.93 ± 0.03	0.9 ± 0.1	0.67 ± 0.04 0.75 ± 0.06	0.80 ± 0.10
HCl	1.02 ± 0.03	1.20 ± 0.04	1.16 ± 0.04 1.17 ± 0.03	1.00 ± 0.10
Fusion	1.71 ± 0.06	1.83 ± 0.07	1.85 ± 0.11 1.96 ± 0.14	1.60 ± 0.15

The $^{234}U/^{238}U$ ratio for each phase is also indicated in Table 8.4. The readily leachable uranium in the Morgan's and TAO phases has a much lower $^{234}U/^{238}U$ isotope ratio than the chemically resistant phases. In samples from the Koongarra weathered zone this ratio is generally significantly below 1.0. This is very similar to the $^{234}U/^{238}U$ isotope ratio in groundwater samples from the weathered zone [Payne *et al.,* 1994]. Thus, it may be inferred that uranium present in the TAO and Morgan's fraction is accessible to the groundwater over relatively short geological timescales.

These fractions are therefore of most interest in interpreting the results of adsorption experiments, which necessarily have a short duration.

The $^{234}U/^{238}U$ ratios in the Koongarra samples tend to increase from the more readily extracted phases (Morgan's, TAO) through the more resistant phases (CDB, 6M HCl, and resistate fractions). This suggests that the U in these latter phases does not rapidly exchange with the groundwater, and may therefore be regarded as immobile over short timescales. The data show that a large proportion of U is associated with crystalline iron minerals.

The isotopic fractionation between ^{234}U and ^{238}U has been attributed to alpha-recoil emplacement of ^{234}U in resistate phases. These phases have a low uranium content and make up the majority of the sample mass. When the decay of a ^{238}U nucleus occurs in an adjacent U-rich mineral phase, the daughter ^{234}U may lodge in the U-poor resistate phase. Indeed, this is likely since the resistate phase comprises such a large proportion of the sample. This process causes an input of ^{234}U to the resistate, resulting in an excess of ^{234}U developing in this phase [see Edis *et al*., 1994].

8.3 Total and added U in experimental systems

It is important in interpreting the experimental results to distinguish between 'added' and 'total' U in the experiments, and to be able to estimate the total labile U (ΣU). As indicated above, there are two sources of U in the experimental systems. One source of U is natural U contained in the Koongarra substrate (Table 8.1), and the other is the added U spike.

It will be shown that some of the natural U in the solid phase is 'inaccessible' or unavailable for leaching. For the purposes of the present study, this is not part of the 'accessible' or 'labile' U pool and plays no role in adsorption / desorption experiments. The amount of the natural U in the samples which participates in sorption reactions (accessible U) may be estimated by the TAO extraction (see Table 8.1). These amounts may then be combined with the added U (either ^{236}U or ^{238}U) to

give the total U in the experimental systems (Table 8.5).

The purpose of Table 8.5 is to demonstrate the method of estimating ΣU in typical sorption experiments with the natural substrate, and to emphasise that the different sources of U must be considered in order to understand and model the system. The exact amount of U participating in sorption interactions and the method used to estimate 'accessible' U (in this case using the TAO extraction) are discussed further below. However, it will be demonstrated that there is a fair correspondence between the accessible U determined by the TAO extraction and the estimate obtained by isotope exchange.

TABLE 8.5 Representative calculations of total U in experimental systems, with ΣU estimated by TAO –extraction.

Solid	TAO extractable U	Mass loading	Natural U in experiments*		Added U	Total U (ΣU)
	(µg/g)	(g/L)	(µg/L)	(µmol/L)	(µmol/L)	(µmol/L)
W1	42.6	20	852	3.6	0.1	3.7
W1	42.6	4	170.4	0.72	0.01	0.73
W2	225	4	900	3.8	0.1	3.9
W2	225	4	900	3.8	100 (as ^{238}U)	103.8
W2c	97.3	4	389	1.6	0.01	1.6
W7	1.0	4	4	0.017	0.01	0.03
W7	1.0	4	4	0.017	100 (as ^{238}U)	100.02

*Assumed to comprise the U extracted by the TAO reagent, and estimated by multiplying the TAO-extractable U by the mass loading.

8.4 Results of U-sorption experiments with Koongarra substrates

Effect of pH

The main features of U sorption on the Koongarra natural materials (W1, W2, W2c and W7) are shown in Figure 8.1. These data are for experiments in which a trace of ^{236}U was added to the system as a spike. The mass loading of Koongarra solids was 4 g/L.

In qualitative terms, the data are similar to those for U sorption by ferrihydrite. In particular, sorption is greatest in the near-neutral pH range, with a 'low pH edge' of increasing uptake from pH of about 2.5 to 6.5, and a much steeper 'high pH edge' (desorption edge) between pH 8 and 9. This is due to the effect of complexation between UO_2^{2+} and carbonate in the aqueous phase at high pH values (see Chapter 3).

The sorption data for the W7 sample are significantly different to the other samples. These could reflect a difference in mineralogy or surface area. However, the mineralogy of W7 is similar to the W2 sample, and its surface area is not significantly higher than the W1 and W2 samples (Table 8.1). The stronger sorption on the W7 sample is more probably a result of the much lower ΣU in the experiments with the W7 sample (see Table 8.5). This is because the ΣU in the experiments is dominated by the U naturally present in the samples (rather than the U spike), and W7 has a low intrinsic U content. The stronger sorption in experiments with lower ΣU is attributed to the presence of a small number of strong binding sites on the surfaces of the natural substrates. These would dominate sorption phenomena when ΣU is small. Further experiments in which ΣU was manipulated by adding larger increments of U (as ^{238}U) are discussed below.

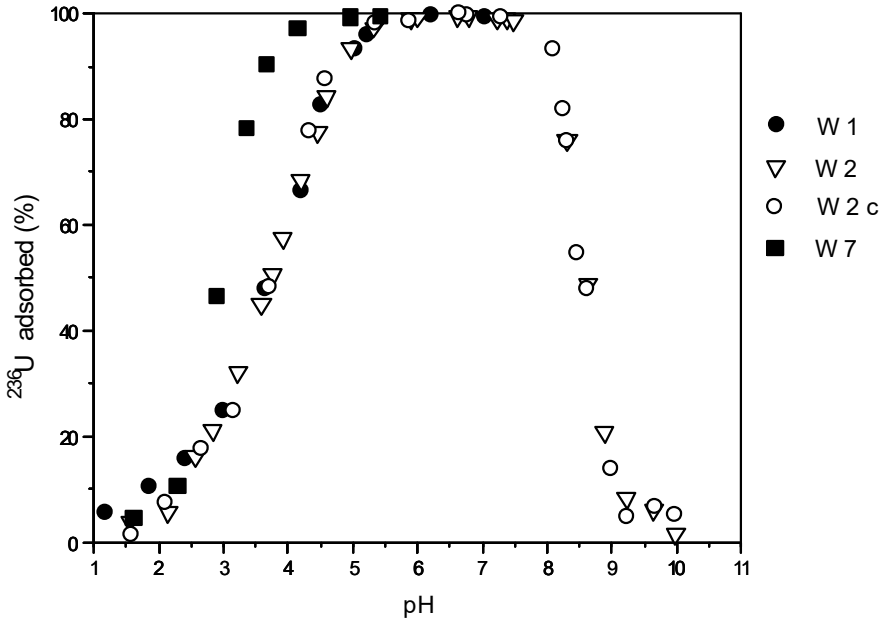


FIGURE 8.1 Uptake of ^{236}U spike as a function of pH in experiments with Koongarra natural substrates. Mass loading 4 g/L. The total U (ΣU) in each experiment is dominated by the natural U in the samples, and is much lower in the experiment with the W7 sample (see Table 8.5).

Effect of mass loading

Results of experiments with different mass loadings of solid are shown in Figure 8.2. This figure shows that sorption is greater with a higher mass loading, as is typically found in experimental systems (see also Figures 6.2 and 7.1).

In considering the data in Figure 8.2, the different ΣU in the two experimental systems must be taken into account. In the experiments with the higher mass loading, ΣU is also greater, because most of the U in the system is derived from the natural U content of the solid phase. Thus, the experimental data obtained with these natural substrates may be less strongly dependent on mass loading than is typically found with model substrates (which contain negligible U). In the latter case, ΣU remains the

same when loading is increased.

To summarise, there is usually much stronger sorption when the mass loading is increased in experiments with a model substrate (e.g. kaolinite or ferrihydrite). This is because more unoccupied sorption sites, including those with high affinity for U sorption, are added. However, a similar increase in the mass loading with the U-rich natural substrates may have a lesser effect, because the sorption sites on the added solid are already occupied, and more U is added to the system when the mass loading is increased.

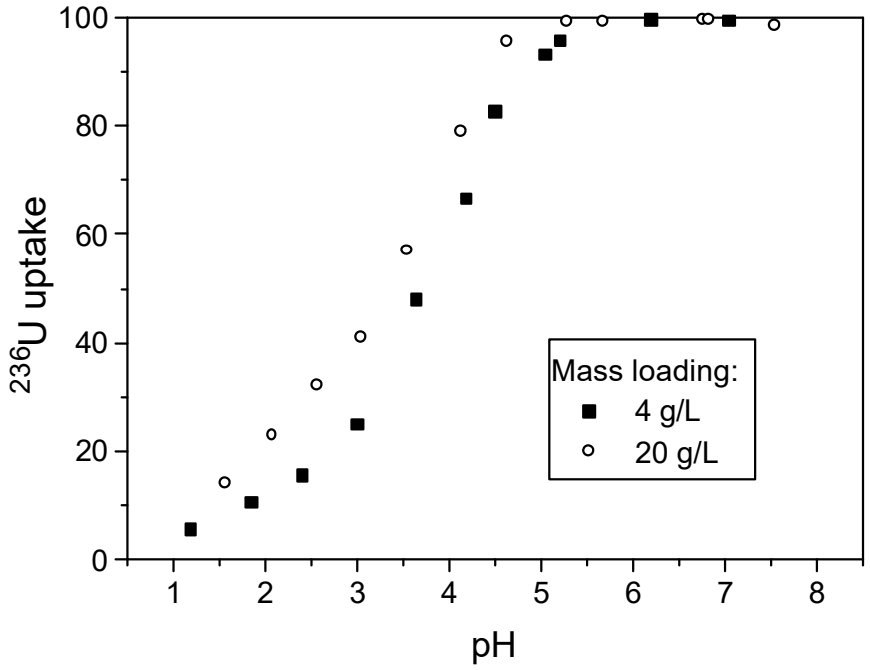


FIGURE 8.2 Uptake of ^{236}U on the W1 sample at two mass loadings. Note that as most of the U in the system comes from the solid, ΣU differs between the 2 data sets (see Table 8.5).

Effect of total U

As with ferrihydrite, there was a decreasing percentage of U sorbed with increased ΣU in the system (Figure 8.3). This suggests that there are at least two types of binding sites with different affinities for U sorption, and is similar to the trends obtained with the model minerals.

It is instructive to compare the W2 and W7 data-sets, obtained with 100 μmol/L of added U (mass loading 4 g/L). The curves are very similar, with the pH_{50} (the pH where 50% of the added U is adsorbed) being close to 5.3 (Figure 8.3). This contrasts with the data obtained when a trace amount of U was added as a spike (Figure 8.1), where the W2 and W7 results were quite dissimilar. The reason for this is that when 100 μmol/L of ^{238}U was added, the natural U content of the samples was greatly exceeded in both cases and the ΣU was almost the same (as shown in Table 8.5). This confirms the conclusion reached above that the most reasonable explanation for the different behaviour of the W2 and W7 samples in the experiments with the added ^{236}U spike (Figure 8.1) was the intrinsic low U content of the W7 sample.

The data for the W7 sample were obtained across a wide range of ΣU, because of its lower natural U content. These results indicate a substantial shift in the position of the low pH-edge between ΣU of 3×10^{-8} mol/L and 10^{-4} mol/L. The stronger sorption of U at lower ΣU was also encountered in the experiments with ferrihydrite and clays. It is of significance that it also occurs in the experiments with the natural samples, and by implication, the Koongarra system. This would imply that a linear K_d model is inapplicable in the natural environment.

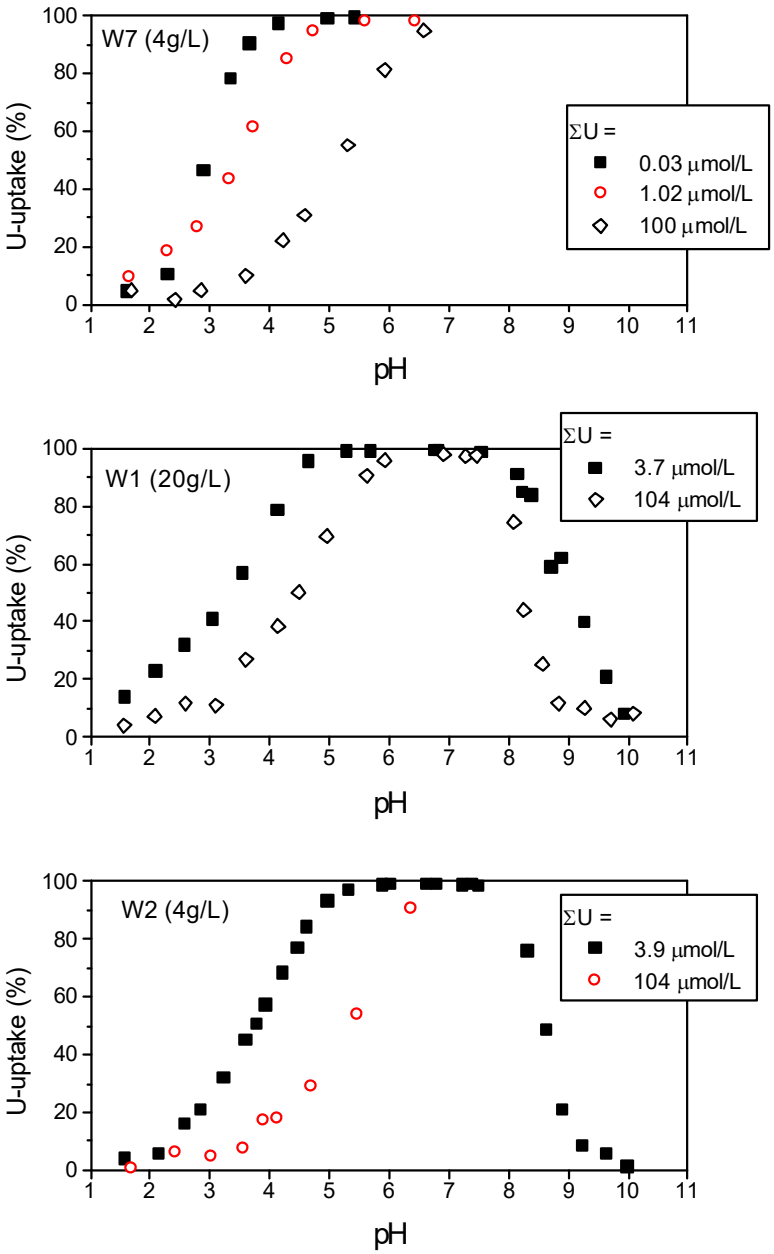


FIGURE 8.3 Effect of increased total U (ΣU) on the results of U sorption experiments with the natural substrates. The data indicated with the closed symbols (■) were obtained after the addition of a ^{236}U spike. The ΣU in these experiments reflects the U of the solid phase (see Table 8.5). In the experiments denoted with ✧ or ❍, data were obtained after addition of ^{238}U.

Effect of increased pCO_2

The pCO_2 in Koongarra groundwaters is higher than that found in ordinary air. In experiments carried out with 1% CO_2, U sorption was greatly reduced for pH values above 6.0, relative to experiments carried out in air (Figure 8.4). This is due to the greater dominance of non-sorbing uranyl carbonate complexes [Waite *et al.,* 1994]. The low pH U-sorption edge was not significantly affected by the higher pCO_2.

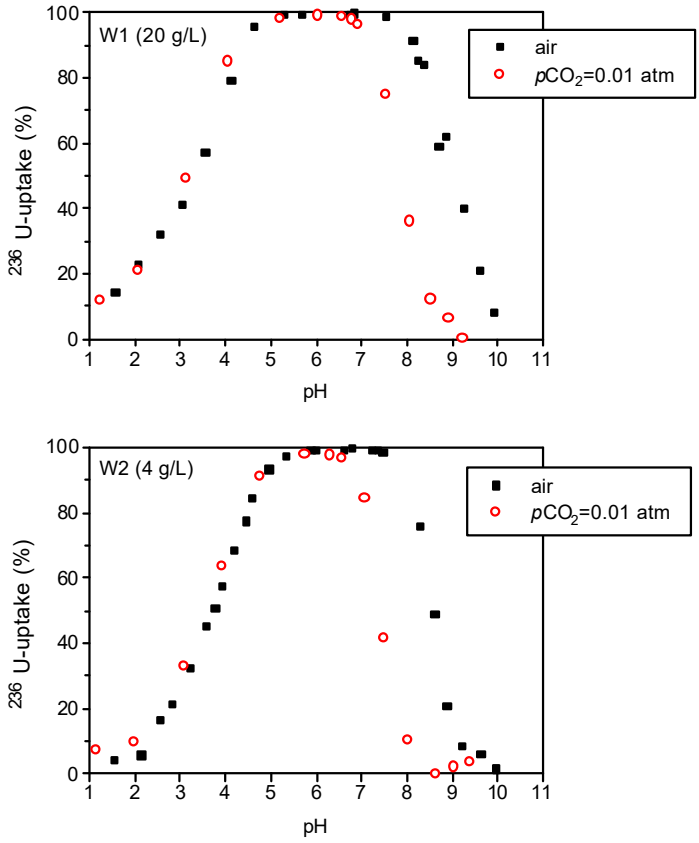


FIGURE 8.4 Effect of elevated pCO_2 on sorption experiments with the Koongarra natural substrates.

Effect of ionic strength

A limited amount of data for the ionic strength dependence of U sorption on natural substrates was obtained. The data indicate that the high pH edge is displaced to the left (i.e. sorption is reduced) with an increase in ionic strength (Figure 8.5). This is consistent with the behaviour of ferrihydrite. The effect of ionic strength at low to neutral pH values is less clear. However, it appears that there are no systematic trends in the data obtained in the region of the low pH edge.

Although an ionic strength dependence can be attributed to outer sphere surface complexes, the diffuse double layer model, which was used to model the ferrihydrite U sorption data [Waite *et al.*, 1994, see Chapter 11], does not accommodate outer sphere surface complex formation. However, even with only inner-sphere complexes included, the model would predict a decrease in sorption with increasing ionic strength. This is because the activity of the highly charged carbonate species, which prevail in the high pH range, is significantly affected by ionic strength. This influences the distribution of aqueous species and in turn, the uptake of U. It appears likely that a similar explanation may be applicable to the data obtained for the natural substrates.

Effect of presence of Mg^{2+}

The effect of elevated concentrations of Mg^{2+} on the sorption of U by the W2c natural substrate was investigated. This is of interest because Mg is present in Koongarra groundwaters [Payne *et al.,* 1994] as a result of weathering reactions involving chlorite. Typical Mg concentrations are about 1 mmol/L. The presence of Mg might be expected to reduce U sorption as a result of competition for surface sites, as has been reported for montmorillonite [Borovec, 1981]. The amount of Mg added in these experiments was 243 mg/L (10 mmol/L), which exceeds the amount of Mg in Koongarra groundwaters. In addition, it is about an order of magnitude greater than

the amount of readily leachable Mg in these experiments (Table 8.3).

The addition of this relatively large amount of Mg^{2+} had no apparent effect on U sorption (Figure 8.6). In addition, there was no significant uptake of added Mg from the aqueous phase. It would appear that Mg plays very little role in affecting U sorption in the Koongarra system.

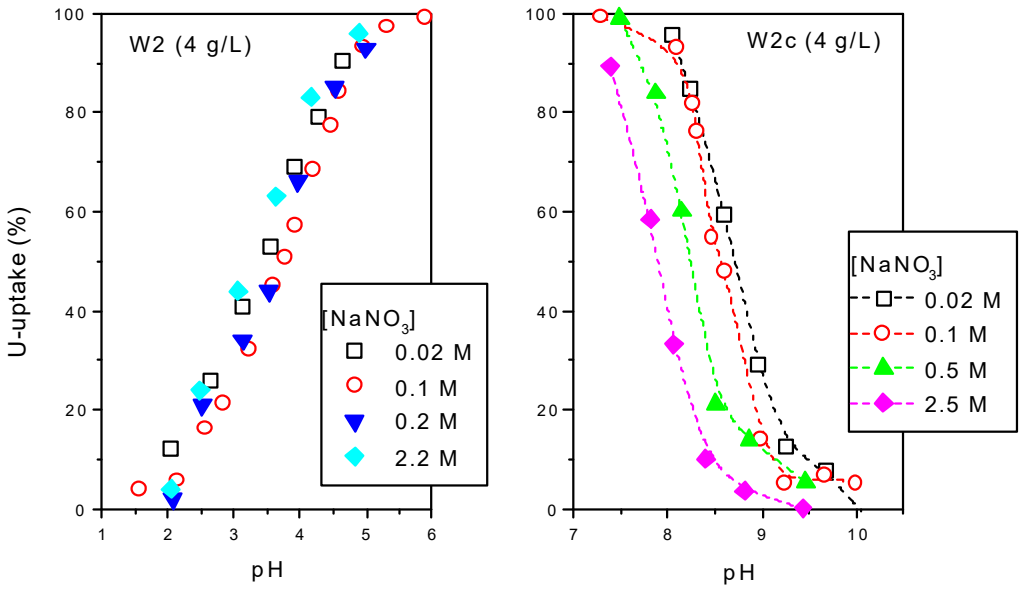


FIGURE 8.5 Effect of ionic strength on U sorption by Koongarra natural substrates. At high pH values, U uptake is significantly reduced by higher ionic strength.

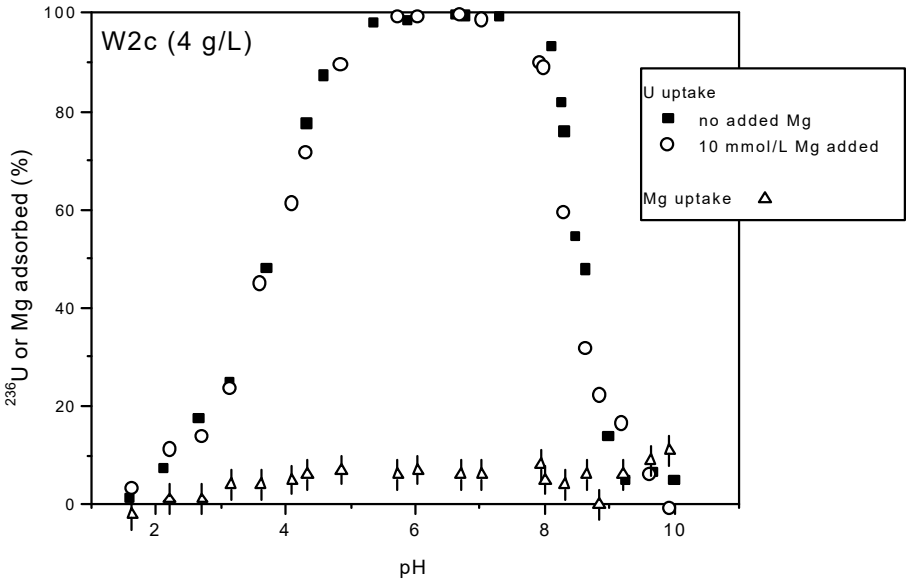


FIGURE 8.6 Results of sorption experiments with Koongarra W2c substrate in systems with and without added Mg^{2+} (243 mg/L). The uptake of Mg is also shown.

8.5 Effect of the CDB extraction on U sorption by Koongarra materials

Additional substrates for sorption experiments were prepared by treating the W1 and W2 fine-particle slurries with the CDB reagent to remove iron oxides (see Table 8.2). The samples were then repeatedly washed with de-ionised water until the conductivity of the aqueous phase was unchanged by contact with the solid. The solid residue was tested for the presence of organic material using the Walkley-Black method [Allison, 1965]. This analysis was performed because of the potential impact of any trace of reagent on subsequent sorption experiments. The amount of organic matter was below the detection limit, from which it was concluded that the CDB reagent had been eliminated from the samples.

The samples were analysed using X-ray diffraction (XRD). The main peaks observed in the XRD spectrum of the untreated W1 sample corresponded to muscovite, kaolinite and quartz, with a small peak of goethite. The goethite reflection was absent after the CDB extraction, whilst all other peaks were unaffected. Chlorite, kaolinite, goethite and mica were present in the XRD pattern of the untreated W2 sample, and all of these peaks except for the goethite were present in the CDB-treated sample. These results confirmed that crystalline iron minerals were selectively removed by the CDB reagent.

Sorption experiments were then carried out using a ^{236}U spike (10^{-7} mol/L) with mass loadings of 4 g/L on CDB-treated W1 and W2 samples, and the data were compared with the results obtained with untreated samples (Figure 8.7).

The effect of the CDB extraction was to move the pH of the sorption edges upwards by approximately 0.5 pH units (i.e. reduce U sorption). The lower sorption on the CDB-treated Koongarra samples was attributed to the removal of Fe oxides, which generally make up a substantial proportion of the total surface area of a soil [Borgaard, 1982]. Iron oxide removal does not always result in decreased sorption of heavy metals, and may increase uptake by unblocking surface sites [Elliott *et al.,* 1986]. However, the effect of the CDB treatment on U uptake by the W1 and W2 samples suggests that, in these samples, Fe-oxides are important in U-sorption.

The surface areas of the samples used in these experiments were determined using the BET technique. The W1 sample had a surface area of 19.0 m^2/g, with this value reduced to 13.3 m^2/g by the CDB treatment. The corresponding figures for the W2 sample were 53.3 m^2/g (untreated) and 29.5 m^2/g (treated). Therefore, the lower sorption on the samples after the CDB treatment corresponded with a reduction in surface area of 30-40%. However, factors other than surface area must also play a role, because the curves for the untreated W1 and W2 samples were similar, although the surface area of the W2 sample was much greater. The same is true of the CDB-treated samples.

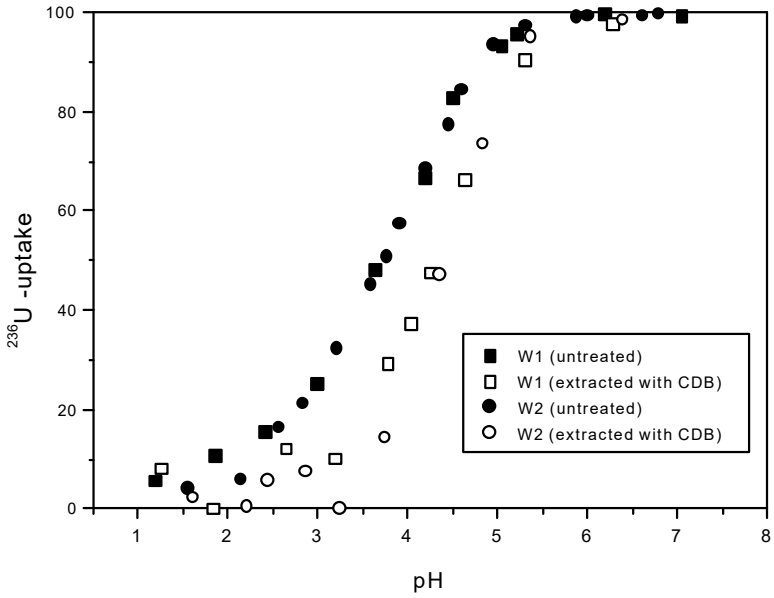


FIGURE 8.7 Effect of the CDB treatment on the adsorption of U by the Koongarra W1 and W2 samples (mass loading of 4 g/L).

It should be taken into account that, as well as removing crystalline iron minerals, the CDB treatment reduced the ΣU in the experimental systems. This is because labile U would have been removed together with the Fe-oxides, leaving only the inaccessible U, which plays no role in U sorption experiments (as discussed above). The experiments with the CDB-extracted samples would therefore have been carried out with a lower ΣU than the corresponding experiments with the untreated samples. On the basis of the α-spectrometry data for the aqueous phases, this ΣU was estimated as being below 0.2 μmol/L, compared to about 3.7 – 3.9 μmol/L in the experiments with the untreated samples (Table 8.5). Thus, the reduced sorption found with the CDB treated samples occurred *despite* the fact that the ΣU in the experimental systems was lower. As discussed above, the effect of decreasing ΣU would normally be to increase the proportion of ^{236}U spike adsorbed, if all other parameters remained the same. Thus, in this case, the effect of Fe-oxides on U-sorption appears to be substantial.

8.6 Isotope exchange and leaching results

As has been previously reported [Payne and Waite, 1991], the adsorption experiments in which ^{236}U is added to the aqueous phase allow measurement of both ^{238}U and ^{236}U in the aqueous phase by α-spectrometry. Consequently, information can be derived about the amount of natural ^{238}U in the samples that participates in adsorption / desorption reactions. This provides a method of estimating accessible ^{238}U, which can be used to assess the accuracy of estimating accessible U using a chemical extraction (e.g. with the TAO reagent).

The basis of the method is to construct a plot of the amount of ^{238}U leached from the solid into the aqueous phase, as a function of the percentage of ^{236}U in solution at equilibrium. In Figure 8.8, the results of sorption experiments in air-equilibrated systems are shown in this form. The corresponding plots derived from the experiments in the elevated CO_2 experiments are shown in Figure 8.9.

The linear nature of these graphs suggests that isotope exchange occurs between ^{236}U in solution and accessible ^{238}U on the surface of the solid phase [Payne and Waite, 1991]. The position of each data-point depends on the experimental pH, which determines the amount of both ^{236}U and ^{238}U in the aqueous phase. The intercept on the y-axis on the right hand-side indicates how much of the ^{238}U participates in the sorption reactions. This corresponds to the amount of aqueous ^{238}U when 100% of the ^{236}U is in solution (this occurs at high and low pH values where little U is sorbed). The resulting estimates of the amounts of accessible ^{238}U in the samples may then be compared with estimates from the chemical extraction method (Table 8.6).

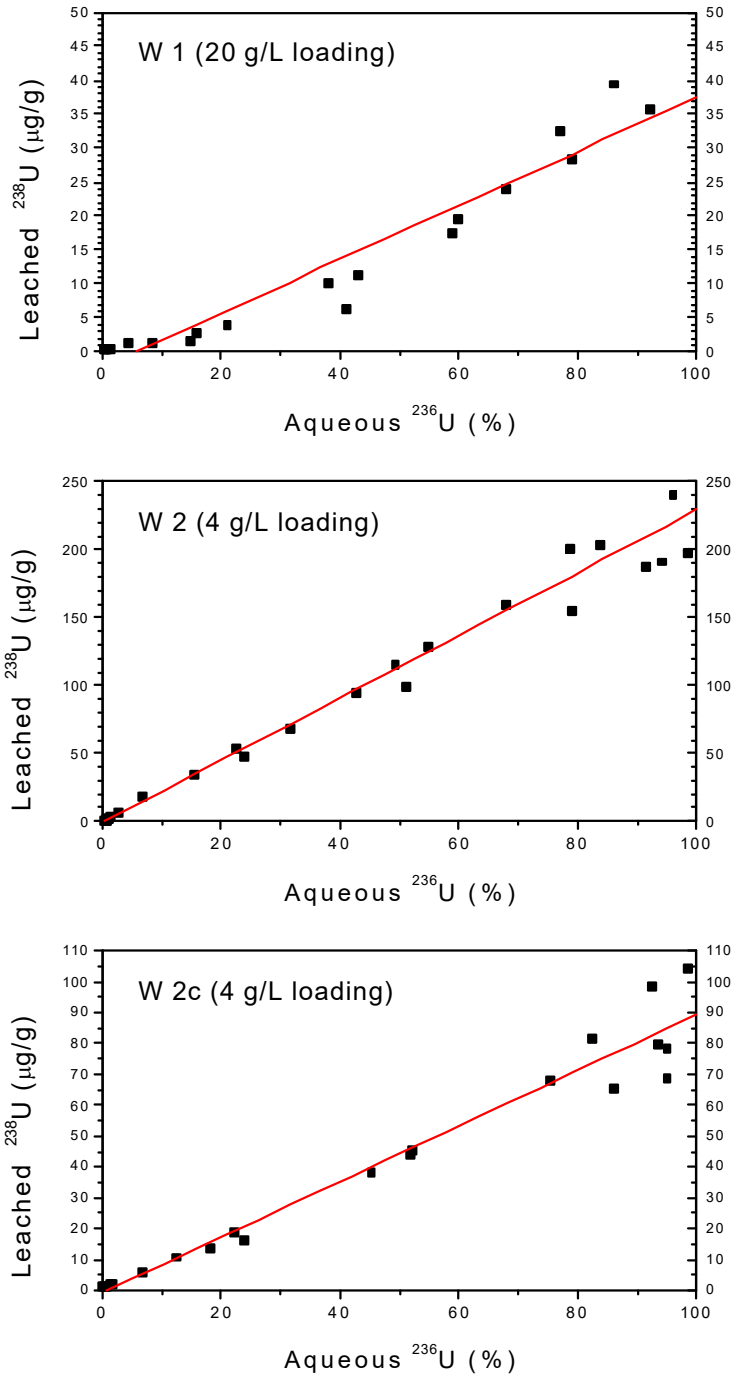


FIGURE 8.8 Summary isotope exchange plots for adsorption / desorption experiments with Koongarra natural substrates in air-equilibrated systems.

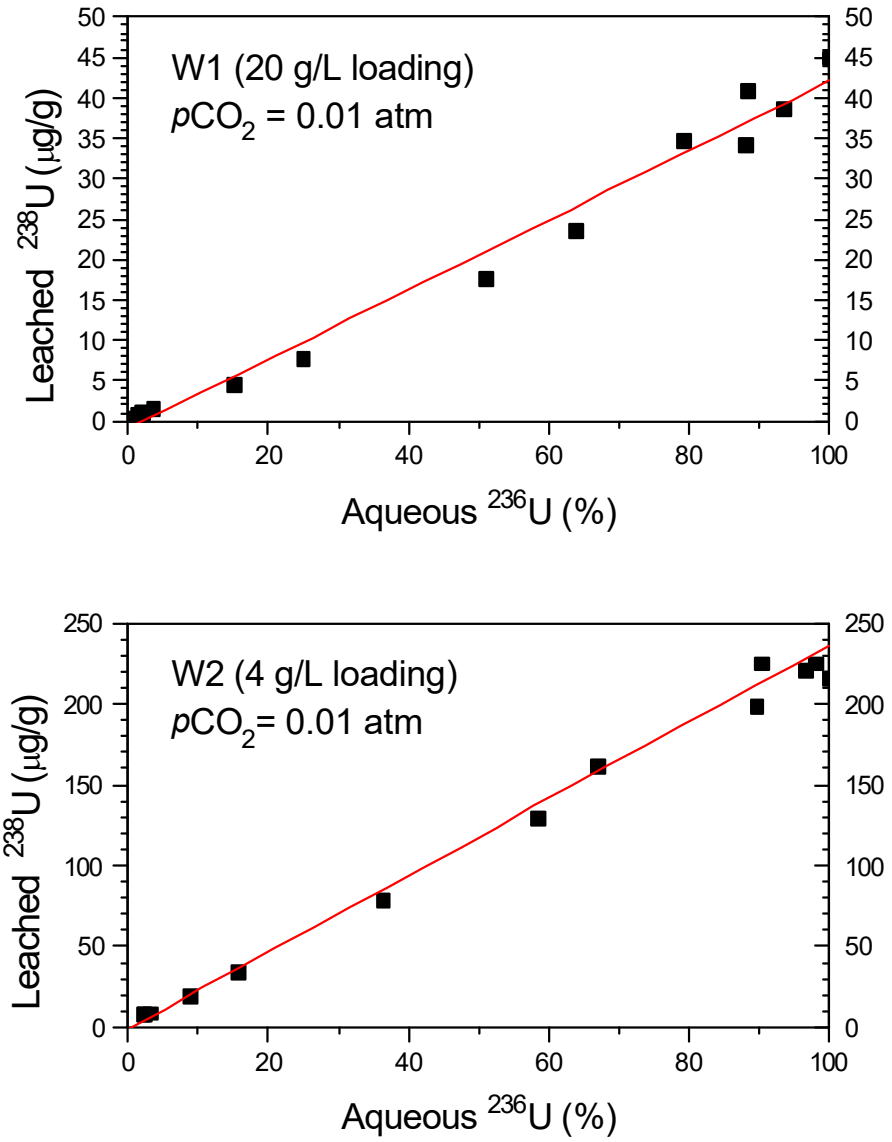


FIGURE 8.9 Summary isotope exchange plots for adsorption / desorption experiments for Koongarra natural substrates in systems equilibrated with 1% CO_2.

TABLE 8.6 Estimates of accessible natural ^{238}U in Koongarra substrates by isotope exchange compared with estimates from TAO-extraction. Isotope exchange data were obtained in both air-equilibrated and elevated CO_2 systems.

	Accessible ^{238}U (μg/g)		
Sample	Isotope exchange in air [a]	Isotope exchange in 1% CO_2 [b]	TAO extraction[c]
W1	37	42	42.6
W2	230	235	225
W2c	89	-	97.3

[a] from Figure 8.8 [b] from Figure 8.9 [c] from Table 8.1

The correspondence between the data obtained by isotope exchange and by TAO extraction (Table 8.6) provides support for using both methods to estimate accessible U in the Koongarra samples. As noted above, this quantity is critical in modelling sorption, where the ΣU in experimental systems is required. It should be pointed out that a linear relationship between ^{236}U and ^{238}U in solution (as shown in Figures 8.8 and 8.9) can only be expected when the solution conditions are mild; i.e. the amount of accessible uranium is constant. Under extreme leaching conditions, the amount of ^{238}U available to the solution phase would be increased by the dissolution of stable mineral phases, and the release of the uranium contained within these phases.

The linear exchange between ^{236}U and accessible ^{238}U in these experiments implies that the adsorption / desorption reaction involving aqueous and adsorbed U must be reversible. However, there is no isotopic exchange with the remainder of the intrinsic U content of the samples, which is irreversibly bound.

8.7 Comparison of natural substrates with ferrihydrite and kaolinite

As noted above, the experimental results obtained for the natural substrates are qualitatively similar to those obtained for model substrates. Data for the Koongarra W2 substrate are compared with data for ferrihydrite and kaolinite in Figure 8.10. The data sets have been chosen so that ΣU and the surface area are within a factor of 5 for all experiments compared. The experimental conditions are summarised in Table 8.7.

This comparison shows that although the results from the different systems are similar, there are some differences between the natural substrate and the model minerals. For example, the low pH edge on the natural materials commences at a lower pH value, and also has a different slope from some of the model systems. The causes of these differences may be attributed to the effects of complexing ligands (e.g. phosphate or humic acid) which were shown in Chapters 6 and 7 to have a significant effect on the pH edge, as well as the mineralogy and surface chemistry of the sorbing solids.

TABLE 8.7 Summary of experimental conditions for the data sets compared in Figure 8.10.

Sample	Loading	Surface area		ΣU
W2	4 g/L	52.3 m^2/g	209.2 m^2/L	3.9 μmol/L (Table 8.5)
Kaolinite (KGa-1b)	4 g/L 40 g/L	11.7 m^2/g	46.8 m^2/L 468 m^2/L	1.0 μmol/L 1.0 μmol/L
Ferrihydrite	89 mg/L	600 m^2/g	53.4 m^2/L	1.0 μmol/L

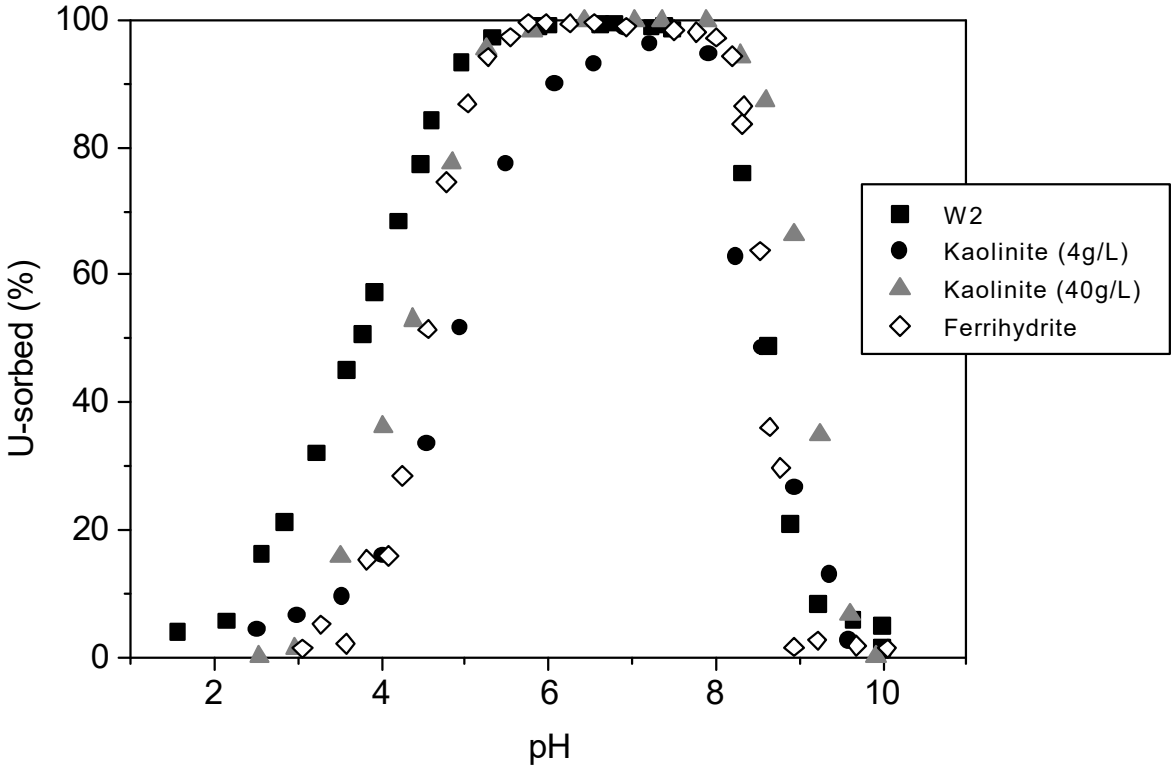


FIGURE 8.10 Comparison of U-sorption data on natural substrates with data for model minerals (kaolinite and ferrihydrite). The experimental conditions of the various experimental systems are summarised in Table 8.7.

8.8 Discussion

The experimental studies undertaken in this project have provided a large amount of U sorption data on the Koongarra natural substrates. The mineralogy of the samples is broadly similar, and this is reflected in their similar adsorption of the uranyl species. The differences in sorption behaviour observed with the W7 sample in experiments with tracer ^{236}U are attributable to its lower accessible U content. In addition, other species contained in the samples (humic acid, phosphate, Mg) may

affect the outcome of the experiments.

The intrinsic accessible U content, which contributes to the total U (ΣU) in experiments with the natural substrates, must be taken into account when interpreting the sorption data. Two methods of estimating this quantity were considered. The sequential extraction and associated $^{234}U/^{238}U$ ratios provided valuable insights into the amount of accessible U in the Koongarra samples. The isotope exchange results obtained in sorption experiments were consistent with the extraction results, and indicated the proportion of the natural U content which participated in adsorption / desorption reactions. The isotope exchange results have the advantage that they do not involve chemical extractions and assumptions about their effects.

When compared with the model substrates, U sorption on the natural materials was broadly similar, including the effects of

- pH
- mass loading
- ionic strength
- pCO_2, and
- ΣU.

Magnesium had no effect on U sorption, and was itself only weakly adsorbed. The effect of the CDB extraction was to decrease sorption. This may be attributed to the removal of strongly sorbing Fe-oxides (and other oxides) with an associated reduction in surface area.

The overall similarity between the model minerals and the natural substrates implies that the chemistry of the aqueous phase must be well understood in order to model U sorption in environmental systems. A successful model for U sorption on the model minerals will be a major step forward towards a quantitative understanding of U sorption on the natural materials.

9 TRANSFORMATION PROCESSES OF IRON MINERALS

9.1 Aim of the transformation study

Iron oxides are widespread throughout the near-surface environment and play an important role in regulating the migration of pollutants. Thirteen members of this group of minerals (which includes the oxyhydroxides and hydroxides [Taylor, 1990]) have been identified and characterised [Schwertmann and Cornell, 1991]. Ferrihydrite (HFO) is the only major iron mineral that cannot be obtained in a well crystallized form, and is therefore referred to as 'amorphous'. It is considered to be a 'young' Fe oxide [Schwertmann and Cornell, 1991], in that it readily precipitates from solution in accordance with changes in pH or redox conditions, but given time, will transform to more crystalline forms, primarily goethite (α-FeOOH) or hematite (α-Fe_2O_3). As demonstrated in Chapter 6, ferrihydrite may play a significant role in the adsorption of radionuclides from solution. This can be ascribed to its high surface area and tendency to occur as coatings on fracture surfaces or mineral grains in natural environments. However, several other Fe-oxides may influence the environmental transport of contaminants.

Ferrihydrite transformation processes have been the subject of a number of laboratory studies [e.g. Schwertmann and Murad, 1983; Johnston and Lewis, 1983]. As was discussed in Section 3.3, transformation processes have the potential to alter the sorption behaviour of Fe-oxides, both in laboratory and natural systems [Shuman, 1977; Gadde and Laitinen, 1974]. One of the key questions is whether adsorbed radionuclides are retained or released during the transformation of amorphous Fe oxides.

Chemical extractions on core samples from Koongarra have shown that U is predominantly associated with ferrihydrite and crystalline iron minerals [Yanase *et al.,* 1991]. To some extent, this conclusion was supported by the extraction studies reported in Chapter 8 of this thesis. A previous experimental study demonstrated that U sorption on Koongarra substrates could be modelled with some success based on

the assumption that amorphous Fe-oxide was the mineral phase controlling U adsorption [Payne and Waite, 1991]. In addition, the experiments described in Chapter 6 have conclusively shown that ferrihydrite is a very strong U adsorber over a range of experimental conditions. Therefore, possible transformation processes of ferrihydrite have a significant potential to affect U mobility in the environment.

The objective of the work described in this chapter was to undertake detailed experiments to determine

- whether the sorption behaviour of Fe-oxides for U was significantly altered by transformation, and
- whether adsorbed U was incorporated or released during Fe-mineral transformation.

The experiments involved U sorption on three synthetic iron oxide samples with varying degrees of crystallinity: a fresh ferrihydrite, an 'aged ferrihydrite' showing some crystallinity, and a recrystallised sample containing goethite and hematite. In this study, the isotopic techniques which were described in Chapter 8 were applied to study the fate of adsorbed U during the recrystallisation of ferrihydrite.

9.2 Experimental study of transformation of Fe-oxides and effects on adsorbed U

The objective of this part of the work was to produce synthetic iron oxides by aging ferrihydrite in systems containing added ^{238}U. Therefore, the general procedure was firstly to precipitate ferrihydrite, secondly to adsorb ^{238}U onto it, and finally, to age the sample to produce crystalline iron minerals. These substrates were then used for uranium adsorption / desorption experiments, with a spike of ^{236}U added to the aqueous phase. These experiments were similar to those with natural substrates (Section 8.4).

A major consideration was selecting the appropriate transformation procedure to produce the solid substrates. Various preparative techniques for obtaining various iron minerals by the transformation of ferrihydrite have been described [Schwertmann and Cornell, 1991]. However, many of the procedures involve the addition of foreign ions, which would have had the potential to affect subsequent sorption experiments. Thus, transformation techniques were selected which only involved manipulation of pH and temperature. Many of these transformations are carried out at low or high pH values, where U tends to be desorbed from iron oxide surfaces (as has been demonstrated by the experimental work described in Chapters 6 - 8). Therefore, one aging experiment was undertaken at a neutral pH where U is strongly adsorbed.

Three samples, anticipated to exhibit various degrees of crystallinity were prepared, using the following procedures:

- *Sample A.* 0.404 g of $Fe(NO_3)_3.9H_2O$ was dissolved in 10 mL of de-ionised water in a 25 mL Teflon tube (Teflon was chosen because of its stability when heated). The sample was neutralised to pH 7.0 by dropwise addition of NaOH, and the ferrihydrite precipitated immediately. Uranium (2380 μg) in dilute HNO_3 was then added to the sample, the pH was readjusted to 7.0, and the volume was made up to 20 mL. The slurry was equilibrated for one hour before being used in sorption experiments. This sample was a fluffy red precipitate of ferrihydrite.
- *Sample B.* In a second Teflon tube, ferrihydrite was precipitated and U was adsorbed following the same procedure. However, after the U was added, the sample (at pH 7.0) was placed in a heated water bath and aged at 70°C for one week in the sealed tube. The precipitate appeared similar to sample A, but was slightly darker in colour.
- *Sample C.* The third sample was aged under conditions selected to produce crystalline iron-minerals. The initial precipitation of ferrihydrite and adsorption of ^{238}U proceeded as before, after which the pH of the sample was raised to 12. The sample was then aged at 70°C for one week in a sealed Teflon tube.

The appearance of this sample was markedly different to the others, being a compact pink-coloured solid.

The synthetic iron oxides containing ^{238}U were transferred to 25 mL polyethylene centrifuge tubes and contacted with an aqueous phase spiked with ^{236}U (10^{-7} M). For the iron oxides, the mass loading of Fe (ΣFe) was 1 mmol/L. The tubes had small holes in their lids, which leads to more reproducible results due to the free access to the system of atmospheric CO_2 (described in Chapter 6). The aqueous phase was 0.1 M $NaNO_3$, and the experiments covered the pH range from 3 to 7. After a contact time of 2 days, during which time the tubes were gently agitated in a shaking water bath at 25°C, the solid and liquid phases were separated by high-speed centrifugation. The levels of ^{236}U and ^{238}U in solution were then determined by α-spectrometry (as described in Chapter 5). The amounts of ^{236}U and ^{238}U chosen for these experiments enabled both adsorption (of ^{236}U) and desorption (of ^{238}U) to be readily quantified.

9.3 Change in sorption behaviour of iron minerals of increasing crystallinity

The XRD spectra for the transformed ferrihydrite samples A, B, and C are given in Figure 9.1. Sample A shows no crystallinity, whereas sample B exhibits minor peaks of hematite. Sample C contains substantial amounts of both hematite and goethite. These results are broadly in accord with results of previous experiments, which indicated that goethite formation is favoured at elevated temperatures and high pH values, whereas transformation at near-neutral pH is slower and produces a relatively greater amount of hematite [Schwertmann and Cornell, 1991; Schwertmann and Murad, 1983]. The transformation products are affected by the presence of foreign ions [Cornell, 1987], and the presence of U in the experimental system may be partly responsible for the amount of hematite in sample C.

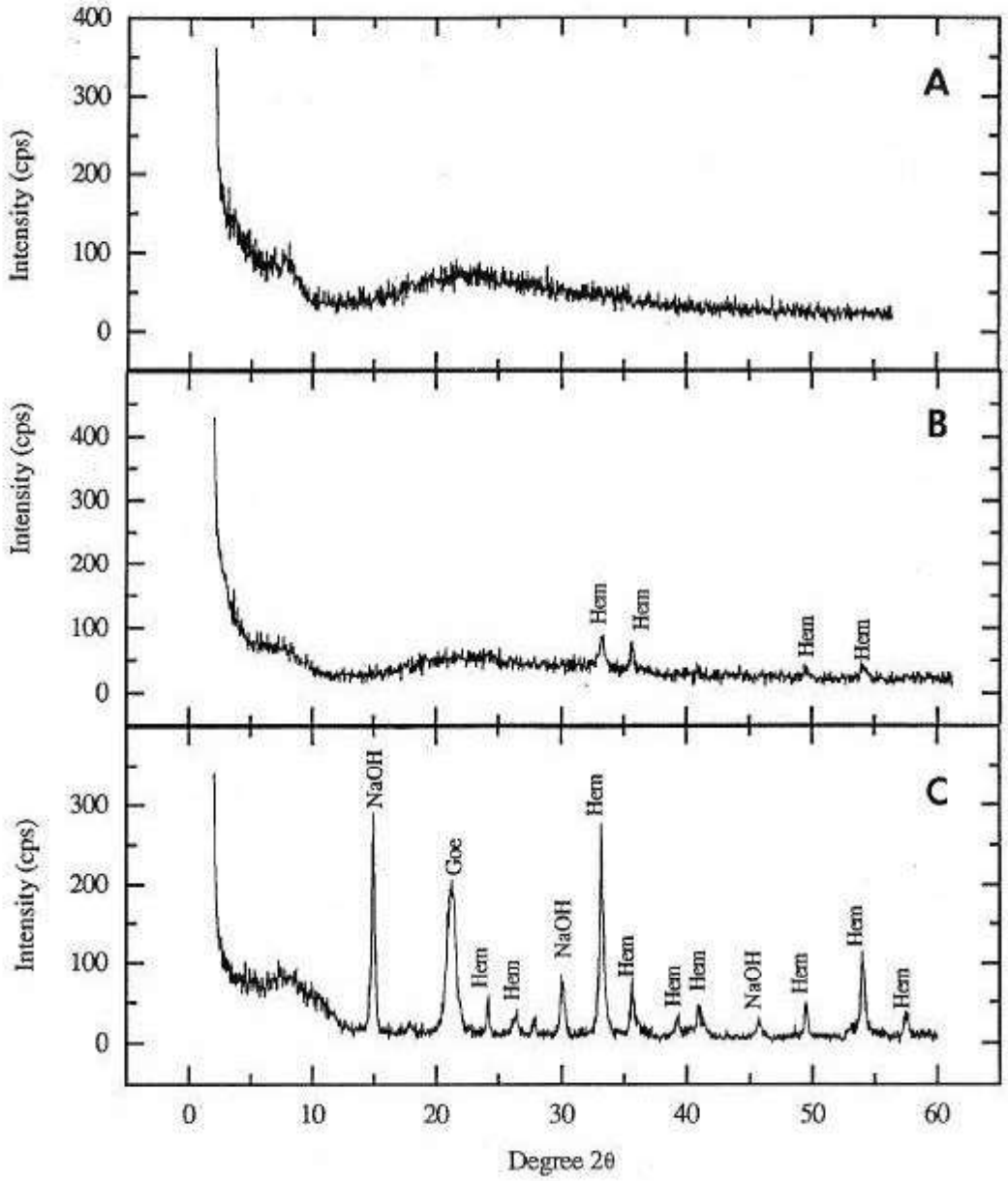


FIGURE 9.1 X-ray diffraction patterns (Cu *K*α radiation) for samples A, B and C. Details of sample preparation are given in the text.

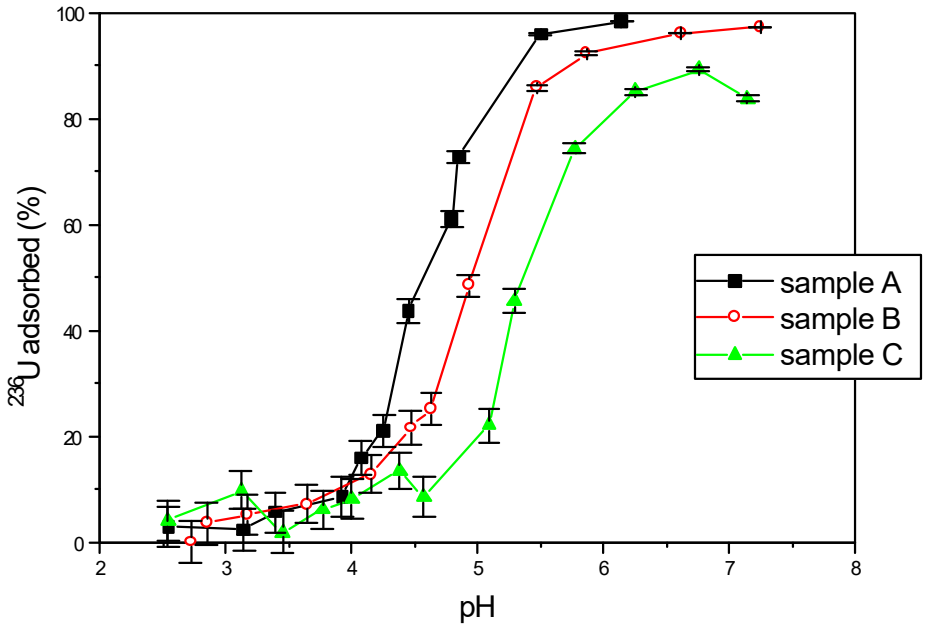


FIGURE 9.2 Adsorption of ^{236}U on Fe-oxide samples A, B and C. Sample A is ferrihydrite, and sample C consists of crystalline transformation products. Sample B has intermediate crystallinity. (ΣFe = 1mmol/L, ΣU = 10 µmol/L)

The ^{236}U-sorption edges for samples A, B and C moved progressively towards higher pH values (Figure 9.2), with the greatest U sorption on sample A, which was predominantly ferrihydrite. Therefore, these experiments with a common ferrihydrite starting material, confirm that as Fe oxide crystallinity increases, U-sorption is reduced. The surface area appears to play a role, with the BET surface areas of samples produced by techniques A, B, and C being 48, 29 and <6 m^2/g respectively.

The amount of dissolved Fe in the supernate was determined for sorption experiments with the Fe oxides. These analyses showed that sample A was partially dissolved during the course of the sorption experiments below pH 4, with over 85%

of the Fe content of this sample in solution at pH 3. In the case of Sample B, dissolution occurred below pH of 3.5 with 31% of the solid dissolved in the experiments at the lowest pH of 2.72. In contrast, sample C was unaffected by pH with no dissolution even at the lowest pH value (2.5). Thus, for sample C, in the pH range between 2.5 and about 4.5, the solid was stable but did not adsorb significant amounts of ^{236}U, whereas sample A adsorbed ^{236}U for the full pH range within which the solid was stable.

9.4 Evidence for incorporation of ^{238}U in the transformed Fe-oxides

As was noted above, analysis of the aqueous phase by α-spectrometry allowed measurement of both adsorption (of ^{236}U) and desorption (of ^{238}U) from the synthetic Fe oxides during the sorption experiments. For each set of sorption experiments, the percentage of both ^{236}U and ^{238}U in solution at equilibrium are shown in Figure 9.3.

The data for sample A show that the percentages of ^{238}U and ^{236}U in solution at each pH were approximately the same. This is because the ^{238}U was adsorbed immediately before the adsorption experiment, and there was no intervening transformation step. Therefore, there was no opportunity for the ^{238}U to be incorporated in the Fe-oxide, and the ^{238}U and ^{236}U in the system exchanged freely in the sorption experiments. The data in Figure 9.3A therefore provide a control experiment showing the data obtained when neither isotope of U is incorporated in the Fe oxide.

In the case of sample B, there was a divergence between the results for ^{238}U and ^{236}U, although the shapes of the curves were similar (Figure 9.3B). The data suggest that some portion (about 20-30%) of the ^{238}U was trapped and was not released by the Fe oxide during the experiments. This ^{238}U remained bound by the solid even at the lowest experimental pH values.

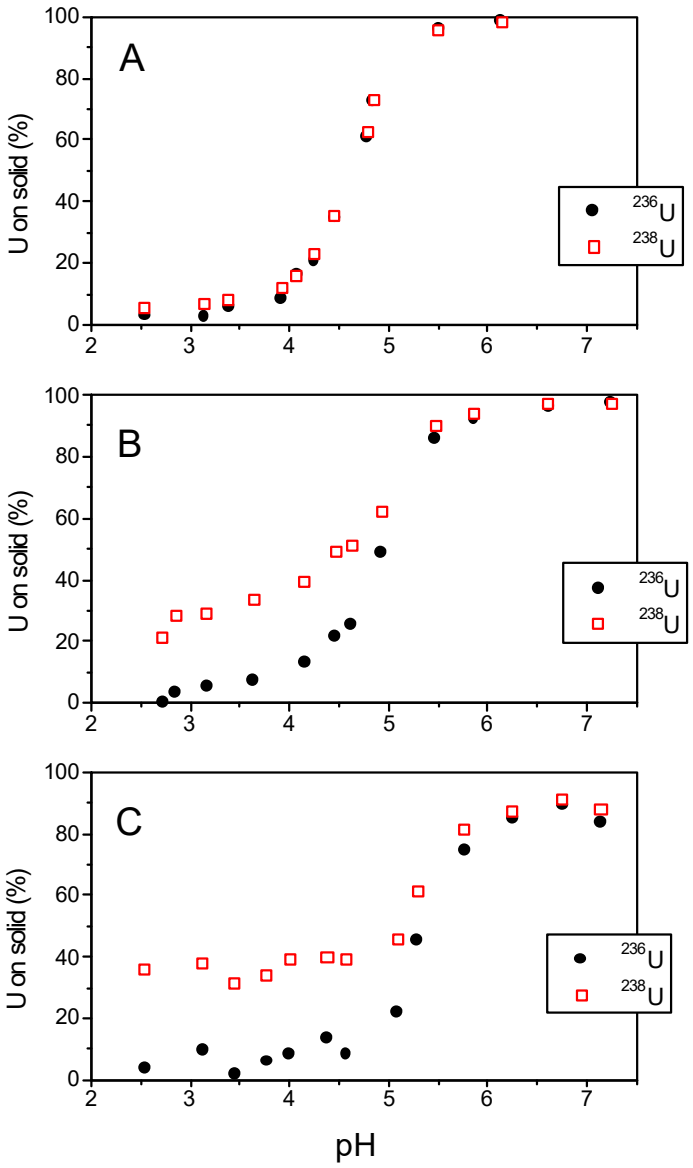


FIGURE 9.3 Adsorption of ^{236}U and desorption of ^{238}U on Fe-oxide samples A, B and C.

Finally, for sample C, there was a substantial pH range (2.5 to 4.5) within which the ^{236}U was almost entirely in solution but approximately 30-35% of the ^{238}U was bound by the solid. This result suggests that during the transformation process in which crystalline iron oxides were formed from ferrihydrite, about 30-35% of the ^{238}U was incorporated into the solid in a way that prevented release during the subsequent adsorption / desorption experiment.

In Figure 9.4 the results of sorption experiments with sample C are shown in a different form, by plotting the percentage of ^{236}U in solution against the percentage of ^{238}U in solution. As was shown previously [Payne and Waite, 1991], the linear nature of this graph suggests isotope exchange between ^{236}U in solution and accessible ^{238}U on the surface of the solid phase (see Section 8.6). The intercept on the y-axis on the right hand-side (corresponding to 100% of ^{236}U in solution) is about 70%. Therefore the exchange only involved about 70% of the ^{238}U in the system. The remainder is assumed to be incorporated into the solid in a way that makes it resistant to leaching.

A similar graph for sample B was constructed, with an intercept corresponding to about 80% of the ^{238}U in solution. However, the plotted data were slightly curved, possibly because the solid partially dissolved in the experiments at pH values below 3.5, and released some of the incorporated ^{238}U to solution. In the case of sample A this curve was linear, indicating free exchange between the isotopes, with an intercept at 100% indicating that all of the ^{238}U was available to desorb into solution from the solid.

The isotope data provide strong evidence for the incorporation of adsorbed uranium into the structure of Fe-oxides during the transformation (aging) of ferrihydrite. These results may be compared with those of a recent study in which arsenate adsorption on ferrihydrite was contrasted with the co-precipitation of As(V) with ferrihydrite [Fuller *et al.,* 1993]. The amount of As bound by the solid in the latter case was much greater. Therefore, it appears that species which are present during mineral transformation *or* co-precipitation processes may be incorporated within the mineral structure of the resulting solid phase.

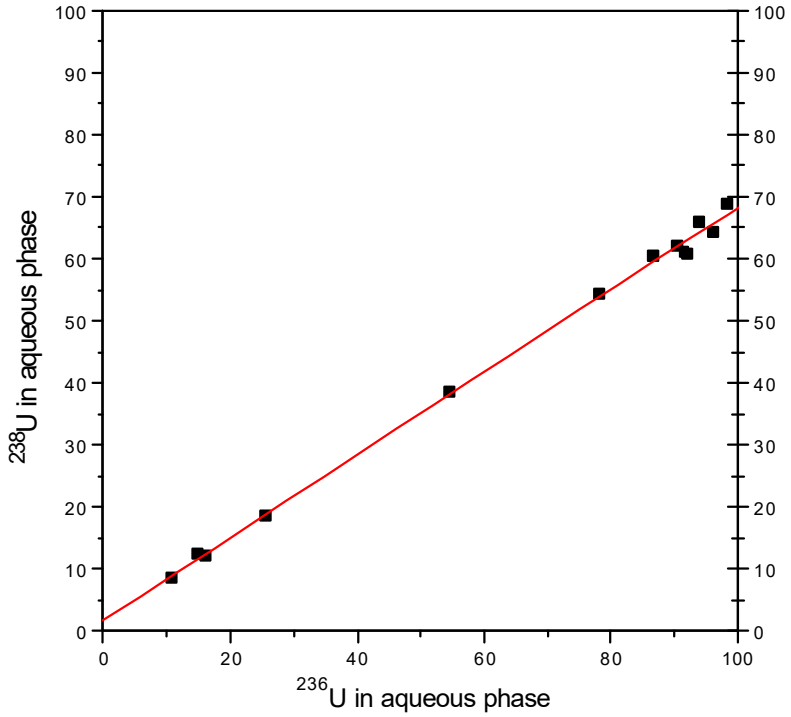


FIGURE 9.4 Isotope exchange between ^{238}U and ^{236}U in experiments with Fe-oxide sample C.

9.5 Amount of ^{238}U and Fe released from synthetic iron oxides by the TAO reagent

The synthetic iron oxides obtained after the transformation step were treated with TAO to dissolve ferrihydrite. The objective was to determine chemically the extent to which the ferrihydrite had transformed to crystalline iron oxides, and to assess how much of the uranium was trapped in these phases. After the TAO treatment, the samples were fully dissolved in 6 M HCl. The amounts of ^{238}U and Fe in both fractions were determined. The percentage of total Fe and ^{238}U dissolved by the TAO are given in Table 9.1. The untransformed ferrihydrite (sample A), was fully soluble in TAO, whereas less than 2% of the Fe-content of sample C was dissolved by TAO, indicating that the conversion of ferrihydrite to TAO-resistant crystalline forms was almost complete. The TAO treatment released all of the ^{238}U from sample A, whereas, it was only able to remove about 70% of the ^{238}U from sample C. This showed that about 30% of ^{238}U was incorporated into sample C during the transformation process, and confirmed the data obtained by isotope exchange. The data for sample B suggested an intermediate degree of crystallinity and less ^{238}U incorporated in the solid. However, a significant amount of ^{238}U was incorporated into sample B even though the transformation process was incomplete.

TABLE 9.1 Percentages of Fe and ^{238}U dissolved by TAO from iron mineral samples

	Fe	^{238}U
Sample A	100	100
Sample B	49.3	78.4
Sample C	1.7	69.9

The total amount of Fe and ^{238}U recovered after dissolving the residue in HCl exceeded 95% for both Fe and ^{238}U.

9.6 Conclusions and implications of the transformation study

In this chapter, the potential importance of iron mineral transformations in influencing U mobility has been demonstrated. These transformations have two important effects. Firstly, they produce a more stable solid substrate which has a lower tendency to sorb U than fresh ferrihydrite. Secondly, some uranium can be incorporated into the solid during the transformation (aging) process, and thereby isolated from interactions with the aqueous phase. The desorption data for ^{238}U showed that some of the ^{238}U which was adsorbed to samples B and C prior to the transformation step was irreversibly incorporated within the mineral structure during the transformation process. However, in these experiments, over half of the adsorbed uranium remained available for desorption after the transformation. Given the reduced ability of the transformed solids to remove U from solution, this U could be leached and would be relatively mobile in a system containing a greater proportion of crystalline transformation products. Thus, Fe oxide transformations have a complex effect on U mobility. Whilst transformations provide a mechanism for U immobilisation by incorporation in the solid, the transformed solid has less ability to sorb U directly from solution.

These experiments highlight the potential importance of iron minerals both in the initial sorption of radionuclides and in isolating them from interactions with the aqueous phase. Transformation of iron minerals from amorphous to crystalline forms provides a possible mechanism for uranium immobilisation. In considering the overall effect on U migration, this must be balanced against the reduced ability of the transformed iron oxide to adsorb U from solution.

PART III.

Uranium (VI) sorption on model minerals - controlling factors and surface complexation modelling

10 FACTORS INFLUENCING U UPTAKE ON MINERAL SURFACES

The experimental study of U sorption presented in Part II enables many of the major characteristics of U sorption on ferrihydrite, kaolinite and natural substrates to be elucidated. This chapter summarises the main aqueous phase parameters that have been found to influence the sorption of U on these diverse mineral surfaces. This includes experimental parameters such as pH, ionic strength and the presence of complexing ligands, which appear to influence U uptake regardless of the identity of the mineral substrate.

10.1 Parameters having a major influence on U-sorption

Some of the main factors that influence U sorption on ferrihydrite and the model kaolinites are summarised in Tables 10.1 and 10.2. Uranium sorption is influenced by a large number of factors, including pH, ionic strength, partial pressure of CO_2, sorbent loading, the total amount of U present and the presence of complexing ligands.

The effects of various ligands on U sorption are diverse (Table 10.2). Phosphate appears to generally increase U sorption, possibly by the formation of a ternary surface complex, and may affect U solubility. Phosphate affects sorption on both kaolinite and ferrihydrite. The effects of phosphate are quite complex and the results are discussed and modelled in Chapter 13.

Humic acid is adsorbed strongly at low pH and increases sorption of U. At higher pH values, humic material may be predominantly dissolved and could decrease U sorption by keeping U in solution. Sulfate decreases U sorption, and this appears to be partly due to formation of aqueous U complexes. If a large excess of citrate was present, U sorption decreased to essentially zero, probably due to complexation of uranyl in solution. In experiments with ferrihydrite, citrate induced the dissolution of the ferrihydrite that forms the sorbing substrate. However, in some experiments citrate slightly enhanced U sorption in part of the pH range.

TABLE 10.1 Factors which have been shown to influence U-sorption on ferrihydrite and kaolinite ($NaNO_3/CO_2$ systems).

Factor	Range studied	Effect
pH	3 to 10	In air-equilibrated systems, there is an increase in sorption up to about pH 7, with a sharp decrease at high pH values
Ionic strength [$NaNO_3$]	0.02 - 2.5 mol/L	An increase in ionic strength reduces U uptake at high pH values, but does not significantly affect sorption at pH < 7.0.
pCO_2	$10^{-3.5}$ atm and 10^{-2} atm	Increasing pCO_2 decreases U sorption at high pH values.
ΣU	10^{-8}, 10^{-6}, 10^{-5} and 10^{-4} mol/L	The proportion of U adsorbed tends to decrease with increasing ΣU. That is, the low pH edge moves to the right and the high pH edge to the left.
Amount of solid	*ferrihydrite* - 1 and 20 mmol/L as ΣFe *kaolinite* – 4 g/L or 40 g/L	Increasing total Fe or kaolinite increases U sorption.

TABLE 10.2 Ligand effects on U sorption

Factor	Range studied	Effect
Carbonate	As determined by equilibration with $pCO_2 = 10^{-3.5}$ atm or 0.01 atm.	At high pH values, carbonate decreases U sorption. This is evidenced by the decrease in sorption with increasing pH (at fixed pCO_2) and with increasing pCO_2 (at a given pH). At pH<6, carbonate species are minor in solution (Figure 3.1) and there is little effect on U uptake.
Humic acid	HA = 0 or 9 mg/L	HA increases U uptake at pH < 7, and has little effect at high pH values
Phosphate	ΣPO_4 = 0 or 0.1 mmol/L	The presence of PO_4 appears to increase U uptake at pH values up to about 8, but has little effect on the high pH 'desorption' edge.
Sulfate	0 or 10 mmol/L	Sulfate slightly decreases U sorption at pH values below about 7.0. This appears to be partly due to formation of aqueous $UO_2SO_4^0$ and $UO_2(SO_4)_2^{2-}$ (Figure 3.5). The effect on U sorption is much less than that of phosphate.
Citrate	0, 0.1, 10 mmol/L	10 mmol/L citrate completely suppressed U sorption on ferrihydrite and kaolinite. At pH values up to about 6.5 it also dissolved the ferrihydrite. When lesser amounts of citrate were present and some ferrihydrite was undissolved, there was a slight increase in U sorption in part of the pH range. A curious double-humped U sorption curve was observed for this system (Figure 6.22).

The experimental results show that carbonate, phosphate, sulfate, citrate and dissolved humic material may influence U migration in natural environments. Phosphate and humic substances had a strong effect on U sorption even when they were strongly adsorbed (and therefore present at very low levels in the solution phase). Consequently, the possible role of surface-bound PO_4^{3-} and humic materials in U migration may need to be considered, even when analysis of the groundwater indicates that only small amounts of these substances are present in the aqueous phase.

The study highlights the complex nature of U sorption, and indicates that it is worthwhile to understand the sorption behaviour of ligands as well as U in order to model the system. The observations provide a rational basis for subsequent geochemical modelling. A large number of parameters affect U sorption, and large multi-dimensional data sets will be required to apply the SCM to natural systems.

10.2 Comparison with previous studies

The effects on U sorption of several of the parameters listed in Tables 10.1 and 10.2 have been previously investigated to some extent. However, the various ligands such as citrate, sulfate and phosphate have been the subject of very little study. As pointed out by Venkatarami and Gupta [1991], "except for carbonate ions, the effect of anions on the sorption of uranyl ions on hydrous oxides has not been reported in the literature". Few previous studies of U sorption have included more than a few variables, or more than one substrate.

Although HFO has been widely used as a model sorbent for various cations and anions, Dzombak and Morel [1990] did not find any acceptable data for uranyl sorption in their comprehensive survey of ion sorption by HFO. Consequently, there is limited existing information with which to compare the present U sorption results, although there are some data for other trace metals. The following discussion aims to highlight similarities and differences with previous U sorption studies on various substrates.

Effect of pH and carbonate

The general pH dependence of U sorption on ferrihydrite, kaolinite and the natural substrates is in agreement with most previous studies cited in Chapter 4, commencing with the early work of Starik *et al.* [1958]. Although a few previous workers omitted studies of pH dependence (in some cases the pH was neither measured nor controlled), most authors have reported that U uptake increases with increasing pH in the pH range below about 7 (the low pH 'adsorption' edge) on a range of substrates. With the exception of some studies which were carried out in glove-boxes with CO_2 exclusion, most authors also reported the desorption of U(VI) at high pH values, and attributed this to carbonate complexation. The work of Hsi and Langmuir [1985] showed that the amount of U in the solution phase in contact with various iron minerals was increased by about 3 orders of magnitude when total carbonate of 10 mmol/L was present.

Ionic strength

Ionic strength was conclusively shown to have a substantial effect on U sorption above a pH of about 7, on ferrihydrite, kaolinite and natural materials (Figures 6.8, 7.7 and 8.5). Surprisingly, there have been few previous studies of the effect of ionic strength on U sorption. As shown by Figure 4.3, the model proposed by Tripathi [1983] for U sorption on goethite predicts a decrease of U sorption with increasing ionic strength at low pH values. This was not observed in the experiments with ferrihydrite, or the other substrates.

Borovec [1981] suggested that U sorption on clays was reduced at increasing ionic strength. This seems to agree with the results of the present study, at least for carbonate containing systems at pH > 7.0. However, the experiments of Borovec [1981] were only carried out at pH of 6.0, and there was no indication whether the systems contained CO_2. Indeed, the speciation scheme used by Borovec omitted carbonate entirely, which makes the results difficult to assess. As noted in Chapter

4, the U concentrations used by Borovec were very high and precipitation was likely in some experiments.

In general it can be stated that previous studies of U sorption omitted adequate study of the effect of ionic strength. In some of the rare cases where models were proposed, these could have been tested by varying the ionic strength.

U concentration

In common with the dependence on ionic strength, the effect of increasing U concentration has hardly been studied, with the work of Tripathi [1983] being a notable exception. The general lack of data in this area is of concern, because sorption density is generally not proportional to dissolved concentration for cation sorption isotherms [Dzombak and Morel, 1990]. Therefore attempts to model cation sorption with only one experimental value of total metal (ΣU in the present case) are expected to produce incomplete models.

Tripathi's data and model both indicated that the proportion of U adsorbed would decrease with increasing ΣU (Figure 4.1), although the model imperfectly fitted the data. As shown on Figure 4.2, the model of Hsi and Langmuir [1985] predicts an increase in U sorbed (%) with increasing ΣU. The data of Hsi and Langmuir [1985] were insufficient to test this aspect of their proposed model, and their predicted trend was not observed with any of the materials used in the present work. With all substrates in this thesis (including the natural Koongarra materials), the effect of increasing ΣU was to decrease the percentage of U uptake (Figures 6.3, 7.3 and 8.3). The position of the sorption edge for both kaolinite and the Koongarra substrates was very sensitive to the amount of U in the system. It would be desirable for the metal concentration to be varied over a wide range in future studies. This parameter is critically important in developing and testing proposed models, even if only understood qualitatively.

As mentioned previously, an apparent shortcoming in some previous studies has been supersaturation of possible U containing solids. However, if parameters are varied in a systematic fashion, the occurrence of precipitation can be 'flagged', as

was done in Section 7.2. This would also assist in modelling the experimental systems.

Sulfate

The effect of sulfate on the experimental results was relatively small. This tends to support the results of Venkataramani and Gupta [1991], who concluded that the effect of sulfate was a slight increase or slight decrease on U sorption, dependent on the experimental conditions. It would appear that the present results can be explained, at least in part, by complexation between sulfate and uranyl in the aqueous phase. In addition, the modelling study indicates some competition between SO_4^{2-} and UO_2^{2+} for surface sites (further discussed in Section 11.5).

Citrate

No previous study of the effect of citrate on U sorption was available when the work in this thesis was commenced. However, Redden *et al.* [1996] have reported that citrate can increase adsorption of uranyl rather than decrease it, as would generally be expected (due to aqueous complexation between UO_2^{2+} and citrate). The results in the present thesis show a general decrease in sorption when citrate is present, but some instances where U sorption was increased by the presence of citrate. Redden *et al.* [1996] observed that the presence of soluble chelators may increase rather than decrease sorption of uranyl, and this may well be the case.

Humic acid

As with the citrate, few previous studies about the effect of humic acid on uranyl sorption existed in the early 1990's, with the exception of the study by Ho and Miller [1985]. These authors had reported that the presence of humic acid increased U uptake on hematite at low pH. This result has now been confirmed in both the case

of kaolinite and ferrihydrite. A recent paper [Benes *et al.,* 1998] reported that the adsorption of uranyl on a Czechoslovakian clay was increased at low pH values by the presence of humate. They noted that this confirmed previous results reported by Ho and Miller [1985] and by Payne *et al*. [1996]. (The latter paper1 reported on some of the data for the U / ferrihydrite / humic system contained in Section 6.4.2.). Thus, the role of humic materials in U retention is becoming more clear.

Phosphate

The key paper of Langmuir [1978] clearly implicated phosphate as a major complexant for uranyl in natural waters, with the postulated $UO_2(HPO_4)_2^{2-}$ species suggested as being dominant in natural waters in the pH range from 4 to 7.5. As such, the presence of phosphate could be expected to have a mobilising effect on uranium. However, as discussed by Tripathi [1983] and Grenthe *et al.* [1992], the complexation constants of Langmuir [1978] were incorrect, and the importance of U phosphate complexes was consequently over-estimated.

The experimental results of Tripathi [1983] indicated that small amounts of phosphate slightly decreased U uptake on goethite. However, Tripathi questioned his own data on the basis that his experimental design had been flawed. In the design stage of his work, he had assumed the thermodynamic data of Langmuir [1978] to be correct. Having reassessed the work of Langmuir, Tripathi stated that “the newly selected thermodynamic data**…..**render the solutions used in adsorption studies highly supersaturated with respect to sodium uranyl phosphate”. While he noted that precipitation may not ensue at equilibrium, he questioned the appropriateness of his own experimental design.

It may be that the concerns of Tripathi [1983] about the precipitation of sodium uranyl phosphate were unwarranted. As the present study shows, increasing the ionic strength in systems containing 100 μmol/L of phosphate (by raising the amount of $NaNO_3$ present) resulted in either no effect on U sorption (at low pH) or a decrease

1 see Appendix 3.

at high pH (Figures 6.12 and 6.13). This appears to rule out the precipitation of sodium uranyl phosphate over the timescale of these experiments, and presumably the same would apply to the experimental systems of Tripathi [1983]. However, this is a matter for conjecture.

The present results for both ferrihydrite and kaolinite clearly show that the presence of 100 μmol/L phosphate increased U uptake. Therefore, the presence of phosphate is unlikely to mobilise U, particularly when the possible precipitation of U-phosphate minerals is considered. Consequently the results of the present study are not in accordance with expectations based on either Tripathi [1983] or Langmuir [1978].

The current results are more in agreement with those observed for the adsorption of Zn on ferrihydrite by Benjamin and Bloom [1981]. These authors reported that Zn uptake dramatically increased in the presence of 1 mmol/L of phosphate (with the pH edge moving by about 1.5 units to lower pH values). Similar results have been found in studies of zinc and phosphate adsorption on goethite [Bolland *et al.,* 1977]. These authors reported that "the presence of phosphate or zinc on the goethite surface was found to increase slightly the adsorption of zinc and phosphate respectively", and suggested the formation of a surface complex involving both Zn and phosphate ions.

The formation of a ternary surface complex involving both U and phosphate on the ferrihydrite surface provides a possible explanation for the present experimental results on ferrihydrite and kaolinite. In the case of kaolinite, a surface precipitate of Fe^{3+} and PO_4^{3-} appears unlikely. In both cases, it appears that phosphate strongly increases U retention by the solids. However it could be considered problematical whether the mechanism is by sorption or by some other process such as co-precipitation. This issue is discussed in Chapter 13.

11 A SURFACE COMPLEXATION MODEL FOR U(VI) SORPTION BY FERRIHYDRITE

11.1 Structure of U surface complexes on ferrihydrite

The first step in developing a surface complexation model for U sorption is to postulate a reasonable set of adsorption reactions for uranyl at the surface. In order to achieve this, one needs to take into account existing knowledge about the structure of uranyl solids and aqueous complexes.

Evans [1963] described general features of the structure of uranyl compounds and complexes. The structural moiety is always characterised by the uranyl group (UO_2^{2+}), which consists of a central U atom bonded to two O atoms by relatively short, collinear axial bonds. Based on consideration of likely bond lengths, he showed that some bidentate oxyanion groups would favour a flat hexagon arrangement in the equatorial plane (perpendicular to the axial bond axis). In this co-ordination, two oxygen atoms from one ligand would be drawn very close together by the strong polarising effect of the anion nucleus group, forming a hexagon edge. Such short oxygen-oxygen distances are present in ligands such as CO_3^{2-} (2.25 Å) and NO_3^- (2.10 Å). Evans [1963] showed that pentagonal co-ordination was as prevalent as the previously accepted plane-square or plane-hexagon, and enunciated several principles regarding uranyl structures:

- the uranyl group will coordinate 4, 5, or 6 oxygen atoms around its equator, with a strong tendency to make these atoms coplanar
- four-fold and five-fold configurations are geometrically stable, allowing oxygen atoms to approach at optimum distance in a plane without overcrowding
- stable six-fold coordination can occur when the oxygen atoms are donated by highly polarised bidentate anionic groups which can draw them very close together
- when isolated oxygen atoms (or hydroxyl groups) are brought into six-coordination with uranyl, they are forced out of the plane in a puckered configuration

- bridges between two uranyl groups can be formed by one or two hydroxyl groups, fluoride or oxide ions, but not water molecules. Two or three uranyl groups may be linked by one bridging atom.

A more recent summary of the structural chemistry of U(VI) solids appears in Thompson *et al.* [1994]. The U-O_{ax} bond length is between 1.75 and 1.83 Å, and the equatorial plane typically contains 4 to 6 equatorial ligands. With a greater number of ligands, the equatorial bond lengths increase in the range from 2.17 Å to 2.58 Å, with the length also depending on the types of functional groups.

Some examples of the structure of U(VI) salts and complexes are given in Figure 11.1. Bonding to form an extended U(VI) structure always involves equatorial, rather than axial ligands. The solids tend to be layered, with the layer thickness approximately equal to the distance between the axial O atoms. Multiple layers are held together by hydrogen bonding between axial O atoms and interlayer water molecules. As observed by Thompson *et al.* [1994], the structure of different U(VI) solids is fairly consistent, and this gives some indication of the likely structures occurring at the solid-water interface.

At the time the present project commenced, little direct information was available about uranyl coordination at the solid / liquid interface. The proposed complexes put forward by authors such as Tripathi [1983] and Hsi and Langmuir [1985] were entirely hypothetical. Tripathi himself observed that his model was not ‘structurally valid’ in the sense that it necessarily had any relationship to real surface complexes, a limitation that was applicable to other existing metal adsorption studies. This situation has begun to change in recent years, due to the development of EXAFS, but at the time of writing the application of EXAFS has not been sufficiently extensive to allow comparison with a large data-base of existing results.

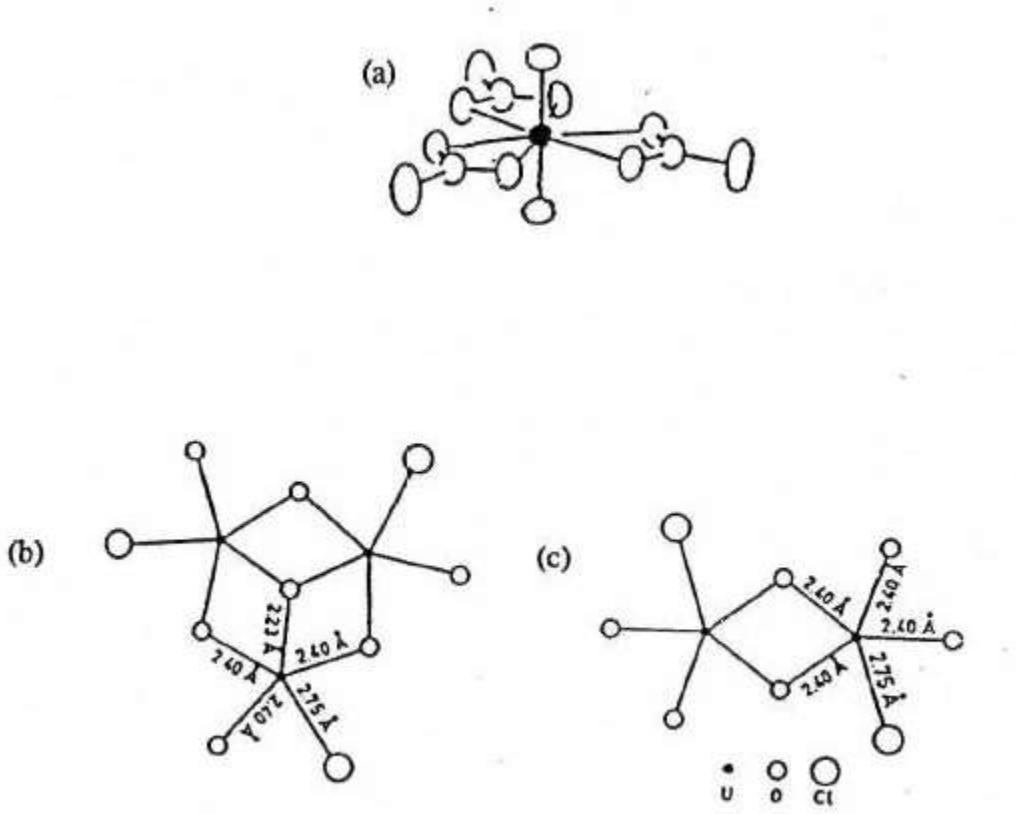


FIGURE 11.1 Structure of uranyl salts and complexes (from Thompson *et al.* [1994]). (a) Rubidium uranyl trinitrate solid, not showing Rb atoms. The linear axis of the UO_2^{2+} ion is vertical. (b) Trinuclear uranyl hydroxo complex, $[(UO_2)_3(OH)_4Cl_3(H_2O)_3]$ (aq) (c) Uranyl dimer solid or aqueous complex $[(UO_2)_2(OH)_2Cl_2(H_2O)_4]$. In (b) and (c), uranyl bonds are perpendicular to the plane of the page.

The samples prepared at ANSTO for EXAFS (Section 5.8) were analysed at Stanford University, Center for Materials Research[1]. The following discussion is based on results for two samples with higher U concentrations (UF3 and UF4). The samples with lower U contents (UF1 and UF2) gave spectra that were qualitatively similar, indicating the presence of the same types of surface complexes. However, the EXAFS spectra from these samples were too poor for a quantitative fitting of the spectrum. The EXAFS work was reported in detail in Waite *et al.* [1994] and only the conclusions are reported here.

The main results of the EXAFS work can be summarised as follows:

1. The uranyl surface complex is mononuclear rather than polynuclear (i.e. the surface species contains only a single U).
2. The surface complex is an inner-sphere complex, coordinated in bidentate fashion, involving two surface hydroxyls of an Fe octahedron edge and the uranyl cation.
3. The coordination environment at the surface limits the complexity of U(VI) surface speciation in comparison to the complex aqueous speciation (e.g. Figure 3.3).

The model structure for the bidentate surface complex of UO_2^{2+} on ferrihydrite is shown in Figure 11.2. The coordination environment of the U atom in the surface complex involves seven U-O bonds. These consist of the inevitable two axial oxygen atoms (1.79 Å), three equatorial oxygens not involved in the surface complex (2.35 Å), and two equatorial oxygen atoms shared with the iron octahedron (2.52 Å). These are the two bonds attaching the uranyl ion to the surface. In addition, the U-Fe distance is about 3.4 Å. The absence of any evidence for a U-U backscattering contribution to the EXAFS yielded the significant conclusion that no multinuclear uranyl complexes are adsorbed.

[1] The author was not directly involved in the EXAFS measurements (a full account appears in Waite *et al.* [1994]).

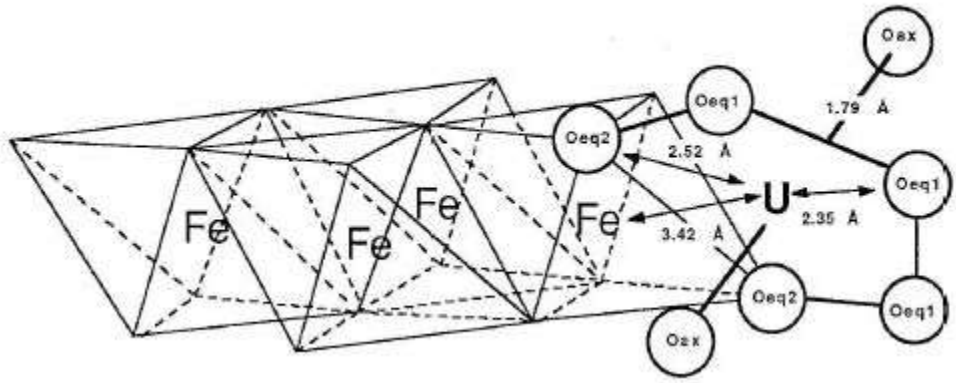


FIGURE 11.2 Model structure for the surface complex of UO_2^{2+} on ferrihydrite, showing the edge sharing bond of U with an iron octahedron that is part of a dioctahedral chain. O_{ax} denotes axial oxygen in uranyl, O_{eq1} represents equatorial oxygen atoms not involved in the complex, and O_{eq2} represents oxygen atoms shared with the iron octahedron.

Almost at the same time as the publication of the above results, Thompson *et al.* [1994] reported EXAFS work on U sorption by kaolinite. These authors reached quite similar conclusions, again finding that the equatorial environment consisted of five oxygen atoms, although in this case involving three long (2.48Å) and two short (2.28 Å) bonds. A slight difference with the results for ferrihydrite was that a few samples at pH above 7 gave evidence of U neighbours at 3.9 Å (i.e. polynuclear surface complexes).

Dent *et al.* [1992] reported that U(VI) sorption on silica and montmorillonite proceeded by different mechanisms. The EXAFS of uranyl species adsorbed on clay resembled the EXAFS of uranyl in a hydrolysed solution, suggesting an outer sphere, ion exchange mechanism of sorption. In contrast, EXAFS of uranyl species adsorbed on silica was more like a hydrous oxide, and suggested an inner sphere surface complex. This work clearly indicated that the surface coordination of U on different surfaces varies significantly, although a structure for the surface complexes was not proposed. The few existing studies of uranyl EXAFS therefore indicate that the structure of

U bound at the surface depends on the type of mineral surface, and on the chemistry of the aqueous phase, including U concentration and pH.

The outcome of the present EXAFS study can be summarised as follows:

- In air-equilibrated systems at pH values below 7, U uptake on ferrihydrite appears to consist of uptake of UO_2^{2+} on surface sites, with the surface species being of the form $(>FeO_2)UO_2$, an inner sphere, bidentate complex with the structure indicated in Figure 11.1.

11.2 Surface complexation model of U sorption

In addition to the EXAFS surface analysis discussed above, the other main source of information about the likely nature of the uranyl surface complex consists of the large amount of sorption data for U on ferrihydrite assembled for the current thesis. An earlier (incomplete) version of this set of set of data was available at the time of the EXAFS work described in Waite *et al.* [1994].

The key variables that influence U sorption on ferrihydrite and are relevant to surface complexation modelling can be summarised as follows:

- The U uptake is strongly dependent on pH.
- The upward shift of the low-pH edge with increasing ΣU indicates the presence of more than one type of surface site.
- The sorption of U is dependent on the ionic strength at high pH values.
- The partial pressure of CO_2 strongly affects U sorption.

The pH dependence and effect of pCO_2 on U-sorption have been reported by numerous authors (Section 10.2), and previous models of U sorption have been able to reproduce these features in at least a qualitative sense. However, the dependence of U sorption on these parameters does not provide a basis for choosing one model over another. The two models for U sorption on goethite which were examined in Section 4.2 both adequately predicted these aspects of U sorption. However, the response of experimental systems to ionic strength changes, and to increased ΣU, appear to provide much more exacting constraints on these models (see Figures 4.1 and 4.2).

The prediction of the model of Hsi and Langmuir [1985] that an increasing percentage of U would be adsorbed with increasing ΣU (Figure 4.2) is extremely unusual. It differs from the results for numerous trace metals summarised by Dzombak and Morel [1990], and also from the behaviour found in the systems studied in this thesis (e.g. Figures 6.3, 7.2 and 8.3). Hsi and Langmuir [1985] did not experimentally test this aspect of their model. The model of Tripathi [1983] does predict a decrease in sorption with increasing U (Figure 4.1), but examination of the model shows that this is a result of surface site saturation being approached. Consequently the model-generated curves (Figure 4.2) remain in the same pH range (with different slopes), whereas a better simulation might have been achieved if the position of the edges moved to higher pH with increasing ΣU. This would require a second sorption site to be added to the model.

In order to produce a set of model curves resembling the experimental data for ferrihydrite (Figure 6.3), it is necessary to have at least two site types of different strength. As reported by Dzombak and Morel [1990] "two sites are required to model cation sorption because sorption density is not proportional to dissolved concentration in cation sorption isotherms. However, usually only one kind of surface complex stoichiometry is needed for both site types". This comment suggests that the simplest approach to modelling cation sorption is to have different types of sites comprising 'strong' (type 1, high-affinity sites) and 'weak' (type 2, low-affinity sites).

It must be emphasised that the EXAFS measurement was only quantitative at the higher sorption density of samples UF3 and UF4. In other words, it yielded information about the surface complex stoichiometry and structure on the weak sites. However, in the absence of any other information it is reasonable to assume that the strong site stoichiometry is the same (as suggested by Dzombak and Morel [1990]). This is an assumption inherent in the model rather than being derived from the EXAFS measurement. In most cases it would appear that EXAFS does not yield information about the strong sites.

As noted previously, the effect of ionic strength on U sorption has not been subjected to much previous detailed examination. The data-sets obtained in this study show that there is no significant ionic strength dependence of U sorption on ferrihydrite at low pH values, whereas the sorption is sensitive to

ionic strength at high pH values (this is also true of the natural substrates and kaolinite). The dependence of metal uptake on ionic strength can sometimes indicate whether inner sphere or outer sphere surface complexes are present [Stumm, 1992]. In the present case, a possible explanation of the data is that inner sphere complexes form at low pH values, and outer sphere complexes at high pH values. The implementation of this concept (if valid) would inevitably result in a complex model with a large number of fitting parameters. As observed by Turner and Sassman [1996], it is preferable to use the simplest sorption model capable of reproducing the observed data (these authors refer to this as the 'principle of parsimony'). The possibility that both inner and outer sphere complexes are required to model U sorption phenomena will be held in reserve unless simpler explanations for the observed phenomena prove to be inadequate.

Therefore, another explanation for the ionic strength dependence of the high pH edge is proposed. The ionic strength dependence of U-sorption in the pH range from about 8 to 9.5 could be attributed to a change in the activity of aqueous species of U(VI) when the ionic strength is varied. In this pH range, the dominant aqueous U species are highly charged carbonate complexes such as $UO_2(CO_3)_3^{4-}$. The activity of these species is significantly affected by ionic strength. This could influence the distribution of aqueous species and in turn, the uptake of U. This prediction will be tested by ascertaining the extent to which a model which excludes outer sphere complexes is able to simulate the experimental data in the region of the high pH edge.

If one accepts this possibility, we are free to implement the diffuse double layer model (DDLM) rather than the more complex triple layer model for the electrostatic contribution to the free energy of adsorption. The DDLM has been championed by Dzombak and Morel [1990] who observe that "it is the simplest model that can account qualitatively and quantitatively for all available model-constraining experimental data". Davis and Kent [1990] also advocated the DDLM, and suggested that the selection of a uniform site-density for strongly binding sorbing surfaces would enable a more standard approach and 'encourage unanimity within the field'. As such, it seems reasonable to adopt a modelling approach with standard parameter values, and use the DDLM for electrical double-layer corrections. This approach is also supported by EXAFS

results, which clearly imply that over at least part of the pH range, the uranyl ion is bound to the ferrihydrite surface in an inner sphere fashion, which can be handled with the DDLM.

The preceding line of reasoning gives an indication of the factors that were considered during the development of the U-sorption model proposed in Waite *et al.* [1994]. This model is summarised in Table 11.1. Uranyl uptake on ferrihydrite was modelled as the uptake of UO_2^{2+} on weak and strong bidentate surface sites (denoted as Fe_w and Fe_s respectively), with the surface species being $(>FeO_2)UO_2$, an inner sphere, bidentate complex (reactions 5 and 6 in Table 11.1).

As well as the U surface complexation reactions, one needs to consider other reactions occurring on the surface involving protons, hydroxyl or carbonate species. These were obtained from various sources, as indicated in the footnote to Table 11.1. The complete set of reactions (Table 11.1) includes protonation and deprotonation of surface sites (reactions 1 and 2) together with adsorption of carbonate ions (reactions 3 and 4). For these reactions, strong and weak surface sites are assumed to have the same reaction constants.

The log K values in Table 11.1 were derived using the fitting program FITEQL with the assistance of the author of this code, Dr John Westall. This was a relatively complex undertaking due to the requirement for different stoichiometry in mass action and mass balance equations, and a full account was published by Waite *et al.* [1994].

A key aspect of the modelling was that the site density was treated as an adjustable (fitted) parameter, and was optimised (together with the log K values) using FITEQL. The best fit to the then-existing (circa. 1994) suite of experimental data was obtained with a total site density of 0.875 mol sites / mol Fe. The strong site density was optimised at 1.8 mmol / mol Fe. The total site density thus obtained considerably exceeds the median value of 0.2 mol /mol Fe advocated by Dzombak and Morel [1990].

TABLE 11.1 Ferrihydrite surface reactions and correction of log K values to I = 0.

	Reaction	log K I = 0.1	log K I = 0
1.	$>FeOH + H^+ = >FeOH_2^+$	6.51	6.62
2.	$>FeOH = >FeO^- + H^+$	-9.13	-9.24
3.	$>FeOH + H_2CO_3^0 = >FeCO_3H^0 + H_2O$	2.90	2.90
4.	$>FeOH + H_2CO_3^0 = >FeCO_3^- + H_2O + H^+$	-5.09	-5.20
5.	$(>Fe_s(OH)_2) + UO_2^{2+} = (>Fe_sO_2)UO_2^0 + 2H^+$	-2.57	-2.35
6.	$(>Fe_w(OH)_2) + UO_2^{2+} = (>Fe_wO_2)UO_2^0 + 2H^+$	-6.28	-6.06
7.	$(>Fe_s(OH)_2) + UO_2^{2+} + CO_3^{2-} = (>Fe_sO_2)UO_2CO_3^{2-} + 2H^+$	3.67	4.33
8.	$(>Fe_w(OH)_2) + UO_2^{2+} + CO_3^{2-} = (>Fe_wO_2)UO_2CO_3^{2-} + 2H^+$	-0.42	0.24

Notes:

a) $>Fe_s$ and $>Fe_w$ denote strong and weak sites respectively.

b) Total site density is 0.875 moles sites / mole Fe.

c) Strong site (Fe_s) density is 0.0018 moles sites / mole Fe.

d) Surface area of ferrihydrite taken to be 600 m^2 / g.

e) For reactions 1-4, reactions constants for strong and weak surface sites are assumed to be equal, and were derived from a FITEQL analysis of literature data as described in Waite *et al.* [1994].

f) log K values for I = 0.1 are as given in Waite *et al.* [1994]. Values for I = 0 were recalculated using the Davies equation (see text).

The higher site-density adopted for the U-sorption model means that adsorption constants for subsidiary reactions (such as reactions 1 - 4 in Table 11.1) cannot be taken directly from the literature. The choice of a different site density requires that *all* surface complexation constants must be re-derived. Consequently the Waite *et al.* [1994] paper included a re-calculation of the acidity constants and other sorption constants in Table 11.1 (this matter is considered further in considering the effect of sulfate in Section 11.5).

A ternary uranyl-carbonate surface complex was included in the suite of surface reactions on both site types (reactions 7 and 8), in order to provide a satisfactory fit to the experimental sorption data under conditions of elevated pCO_2 and high pH values [Waite *et al.,* 1994]. Similar uranyl-carbonate surface complexes have also been postulated in order to model the adsorption of U(VI) on goethite [Hsi and Langmuir, 1985; Kohler *et al.,* 1992].

As implied by the above discussion, this U sorption model was derived by a team of several researchers including the present author. To develop the model, a large data-base of U-sorption data obtained by the author was merged with information obtained by EXAFS and modelled using FITEQL. The remainder of this chapter will be concerned with the implementation of this model using the geochemical code, MINTEQA2. In particular, the ability of the model containing the full suite of surface reactions in Table 11.1 to describe uranyl adsorption under a wide range of conditions will be tested and various aspects of the model will be discussed in more detail. In addition, the model will be extended to simulate U sorption in the presence of sulfate and citrate.

11.3 Implementation of the model using MINTEQA2

The original derivation and optimisation of the model for U sorption on ferrihydrite was carried out using the FITEQL computer code. In this section, the geochemical code MINTEQA2 is applied to modelling the entire data-set described in Chapter 6. This popular speciation code was also used for the calculations described in Section 3.2.

MINTEQA2 is very widely used, and has a user-friendly pre-processor known as PRODEFA2 (PROblem DEFinition). However, the program needs to be carefully and systematically implemented to ensure that the input files are

correctly constructed. This requirement may appear obvious, however, even the thermodynamic database distributed with MINTEQA2 contains errors [Serkiz *et al.,* 1996] which derive from incorrectly expressing the reactions in terms of MINTEQA2 components, and also from the failure to correct the log K values to zero ionic strength. Consequently, the formulation of the U sorption model as a MINTEQ input file will be discussed in some detail in this section.

It should also be noted that to model bidentate surface complexes (of the type proposed for UO_2^{2+}) requires that the code must be able to accommodate reactions with differing mass balance and mass action stoichiometries. This is not possible with some speciation codes, but was incorporated into MINTEQA2 during the development of one of its component sub-models [J.A. Davis, personal communication, 1998]. However, the documentation accompanying the MINTEQA2 program [Allison *et al*., 1990] does not mention this feature or how to activate it.

This section describes the implementation of the model for U sorption on ferrihydrite using MINTEQA2. In the subsequent section, the results of the modelling are described. In this chapter, the model is used to simulate data under a wide range of conditions, including numerous experiments undertaken since the publication of the model in the 1994 paper.

Ionic strength corrections

The log K values for the reactions in Table 11.1 are referenced to an ionic strength of 0.1 M. However, the MINTEQA2 database requires that constants must be corrected to zero ionic strength (μ=0). During execution, activity coefficients (γ) are computed to correct the database log K for aqueous solutions having $\mu > 0$. The estimation of activity coefficients in MINTEQA2 is with the Davies equation:

$$\log \gamma_i = -0.51 z_i^2 \left[\frac{\sqrt{\mu'}}{1+\sqrt{\mu'}} - 0.3\mu' \right] \qquad (11.1)$$

where the subscript i refers to each of the reactants and products in the reactions, z_i is the ionic charge of each reactant or product, and μ' is the ionic strength reported for the experimental data. In order to correct the equilibrium constant to μ=0, activity coefficients derived at μ = 0.1 must be adjusted using the following relationship [Serkiz *et al.,* 1996]:

$$K_{\mu=0} = K_{\mu'} \frac{\prod_i \gamma_{i\ \text{products}}^{\nu}}{\prod_i \gamma_{i\ \text{reactants}}^{\nu}} \qquad (11.2)$$

where ν represents the reactant or product stoichiometric coefficient. The treatment of activity coefficients in the generalised two layer (DDLM) model of Dzombak and Morel [1990] involves the assumption that activity coefficients for all surface species are the same. However the activity coefficients for the reactions in Table 11.1 still need to be adjusted, because the activity coefficients for dissolved ionic species depend on ionic strength. To carry out this correction, the following version of equation 11.3 is useful:

$$\log K_{\mu=0} = \log K_{\mu=0.1} + \sum_i \nu_i \log \gamma_{i\ \text{products}} - \sum_i \nu_i \log \gamma_{i\ \text{reactants}} \qquad (11.3)$$

For all the reactions in Table 11.1, ν = 1 or 2 and z = 1 or 2. The values of log γ_z are -0.11 and –0.44 for z=1 and z=2 respectively, if the Davies equation is applied [Dzombak and Morel, 1990]. By using equation 11.3, it is now straightforward to correct the log K values to μ = 0. The resulting constants are shown in Table 11.1.

Re-formulation of surface reactions in terms of MINTEQA2 components

The MINTEQA2 code requires that all reactions be written in terms of MINTEQ components (see Section 2.3). Most of the reactions in Table 11.1 are already in this form, with the exception of reactions 3 and 4. The species $H_2CO_3^0$ is not a MINTEQA2 component, but can be readily formulated in terms of the MINTEQA2 components H^+ and CO_3^{2-}. The final equilibrium constant differs by a factor that reflects the equilibrium constant for the reaction:

$$2H^+ + CO_3^{2-} = H_2CO_3^0 \qquad \text{Log K} = 16.68 \qquad (11.4)$$

The final suite of surface reactions expressed as MINTEQA2 components with all log K values corrected to I = 0 is given in Table 11.2.

Mass action and mass balance stoichiometry for bidentate surface complexes

Mass balance equations with bidentate surface complexes require a stoichiometric coefficient of two for >FeOH, although the corresponding mass action (log K) equation has a coefficient of one [Davis and Leckie, 1980]. MINTEQA2 allows different stoichiometric coefficients in mass balance and mass action equations for surface complexes.

This feature of MINTEQ is poorly documented but can be activated by the following dialogue in PRODEFA2. (It will be assumed that the reader is familiar with the operation of MINTEQA2 and PRODEFA2). In order to do this, one enters all the surface complexation reactions into the input file as added species, with correct stoichiometry for the mass action expressions. The user should then return to the added species section of PRODEFA2, by choosing Edit Level 3 (“Check, edit all entries”). At the prompt requesting any changes, the user should choose to alter the stoichiometry. At this point, the program brings up the following query: “Do you want to alter stoichiometry or *stoichiometry”. The ‘stoichiometry’ is the mass action stoichiometry whereas the ‘*stoichiometry’ is the mass balance stoichiometry. For bidentate surface complexes, the value of *stoichiometry is two, since two surface hydroxyl sites are taken up by the adsorption reaction. An alternative to the above procedure would be to directly edit the input file using a text editor, however care must be taken to position all items in the input file correctly.

TABLE 11.2 Surface reactions expressed in terms of MINTEQ components and with log K adjusted to I = 0. Note that to simplify entry of formulae into the computer the notation >Fe_w and >Fe_s have been replaced by W and S respectively. The log K values are applicable for total site density of 0.875 mol / mol Fe and a weak site density of 0.0018 mol / mol Fe.

Reaction	log K $\mu = 0$
Weak sites (W)	
$WOH + H^+ = WOH_2^+$	6.62
$WOH = WO^- + H^+$	-9.24
$WOH + 2H^+ + CO_3^{2-} = WOCO_2H^0 + H_2O$	19.58
$WOH + H^+ + CO_3^{2-} = WOCO_2^- + H_2O$	11.48
$W(OH)_2 + UO_2^{2+} = WO_2UO_2^0 + 2H^+$	-6.06
$W(OH)_2 + UO_2^{2+} + CO_3^{2-} = WO_2UO_2CO_3^{2-} + 2H^+$	0.24
Strong sites (S)	
$SOH + H^+ = SOH_2^+$	6.62
$SOH = SO^- + H^+$	-9.24
$SOH + 2H^+ + CO_3^{2-} = SOCO_2H^0 + H_2O$	19.58
$SOH + H^+ + CO_3^{2-} = SOCO_2^- + H_2O$	11.48
$S(OH)_2 + UO_2^{2+} = SO_2UO_2^0 + 2H^+$	-2.35
$S(OH)_2 + UO_2^{2+} + CO_3^{2-} = SO_2UO_2CO_3^{2-} + 2H^+$	4.33

11.4 Comparison of model computations with experimental data

In this section, the sorption equations that were summarised in Table 11.2 are used to model the effects of pH, ΣU, ionic strength, pCO_2, and mass loading on U sorption by ferrihydrite. The model predictions are then compared with experimental results. In terms of surface complexation studies, the experimental data sets involved systematic variation of the aqueous components H^+, UO_2^{2+}, Na^+, NO_3^- and CO_3^{2-}, and the quantity of ferrihydrite.

Effect of pH and total U

Figure 11.3 shows sorption curves for U on ferrihydrite at a range of ΣU from 1 μmol/L to 100 μmol/L. As discussed in Chapter 6, these data were obtained in a background electrolyte of 0.1 M $NaNO_3$, in equilibrium with air. The pH dependence of U sorption shows increasing uptake to about pH of 6, and a strong decrease in sorption, (referred to as the 'high-pH' or 'desorption' edge) at pH values above 7. The positions of the edges are dependent on ΣU, with the percentage of U adsorbed at a given pH decreasing with increasing ΣU.

The model curves shown in Figure 11.3 were calculated using MINTEQA2 and the surface reactions in Table 11.2, as well as the full suite of thermodynamic constants summarised in Table 3.1. There is generally good agreement between the model predictions and the experimental data, which cover a wide range of ΣU and pH. The strong complexation of UO_2^{2+} with carbonate in the solution phase greatly reduces the adsorption of U(VI) at pH values above 8. Tripathi [1983] showed that there is no decrease in the extent of U sorption at high pH values in systems that are free of CO_2.

A significant achievement of the model is an extremely good simulation of the pH edges obtained with different ΣU. This cannot be adequately achieved with a single site model (see Figure 4.1), and also presents significant problems for models involving multinuclear surface complexes (see Figure 4.2 and accompanying discussion).

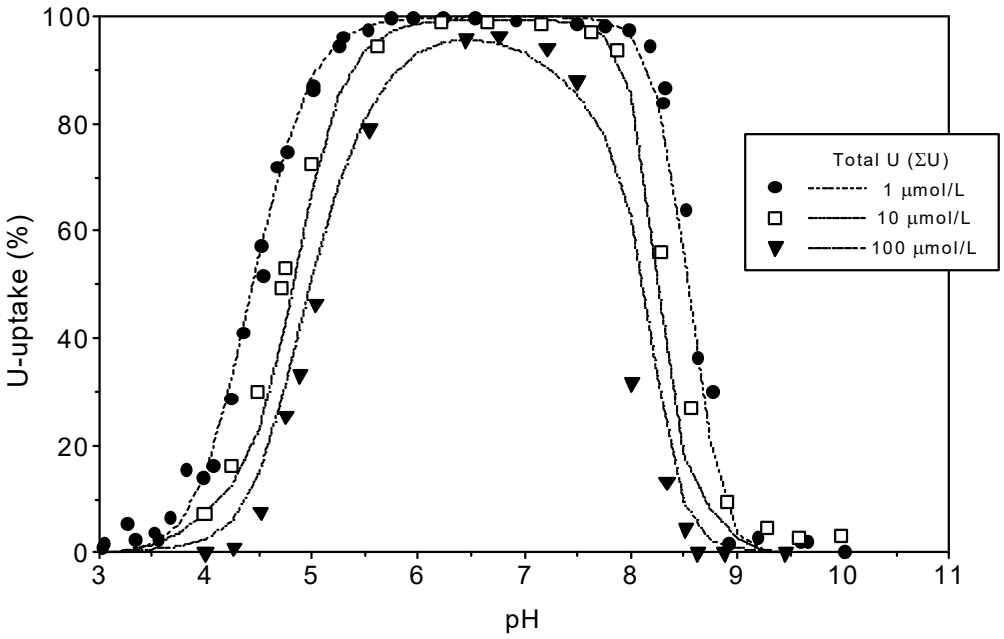


FIGURE 11.3 U(VI) sorption on ferrihydrite for a range of ΣU. Curves were calculated using MINTEQA2 with the suite of surface reactions in Table 11.2. (Experimental conditions: 0.1 mol/L $NaNO_3$, in equilibrium with air, ΣFe = 1 mmol/L)

Effect of mass loading, pCO_2 and ionic strength

The uptake of U on ferrihydrite is a function of the mass loading of the solid in the system (Figure 11.4). The model curves provide a reasonable fit to the data for U adsorption on ferrihydrite, although slightly under-predicting adsorption at high pH values with the higher mass loading. There is an excellent fit to the data obtained with the higher mass loading at pH values below 5.

The high loading data in Figure 11.4 were not used in the model optimisation discussed above, thus, the extent to which the model curve fits the data points reflects a true prediction. In this respect Figure 11.4 differs from Figure 11.3, which shows model fits to data sets which were considered in the model optimisation process.

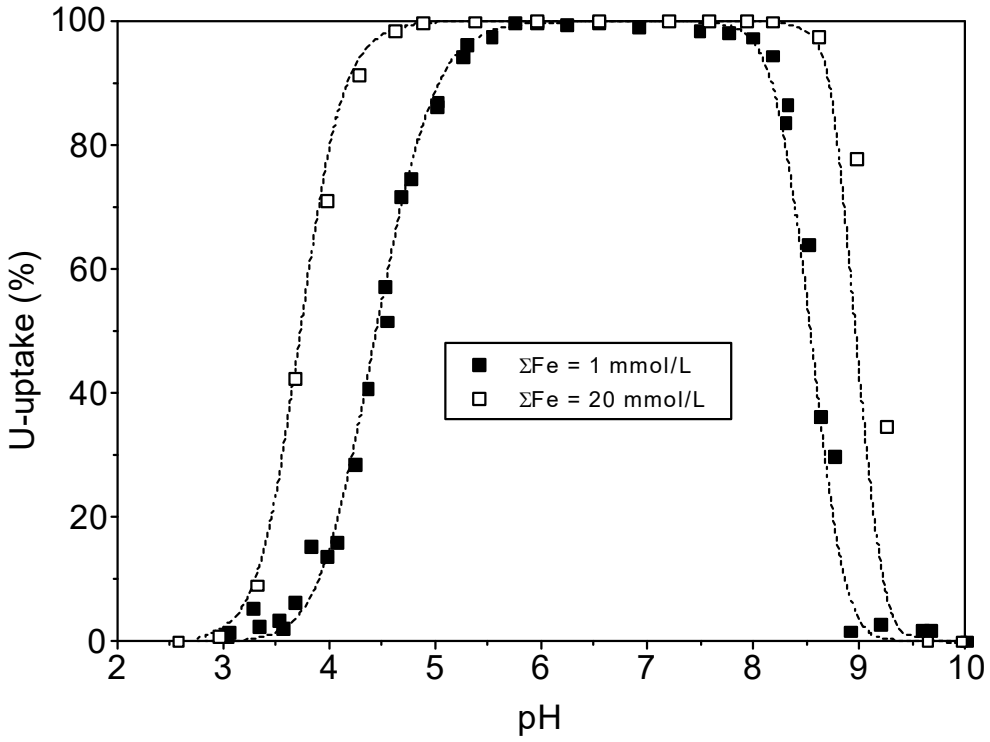


FIGURE 11.4 Effect of solid mass loading on U sorption by ferrihydrite. Model curves were calculated using the reactions in Table 11.2. (Experimental conditions: 0.1 mol/L $NaNO_3$, in equilibrium with air, ΣU = 1 μmol/L)

As was noted in Section 3.2, carbonate is important in uranyl speciation, so additional experiments were carried out in glove-box, with an elevated pCO_2 of 0.01 atm. This is approximately 30 times higher than in air, but reflects the higher pCO_2 measured in typical groundwater environments, including Koongarra [Payne *et al.*, 1994].

The sorption of U on ferrihydrite in the high pH range was significantly lower at the higher partial pressure of CO_2, due to the dominance of weakly sorbing anionic uranyl carbonate species in solution. The model provides an excellent fit to the high pCO_2 data (Figure 11.5). An interesting aspect of the model is that it suggests a slight increase in U uptake on the low pH edge at the elevated pCO_2. This is due to the inclusion of ternary uranyl-carbonate surface complexes in the model, and is consistent with the experimental results. However, more data points would be required to verify this aspect of the model.

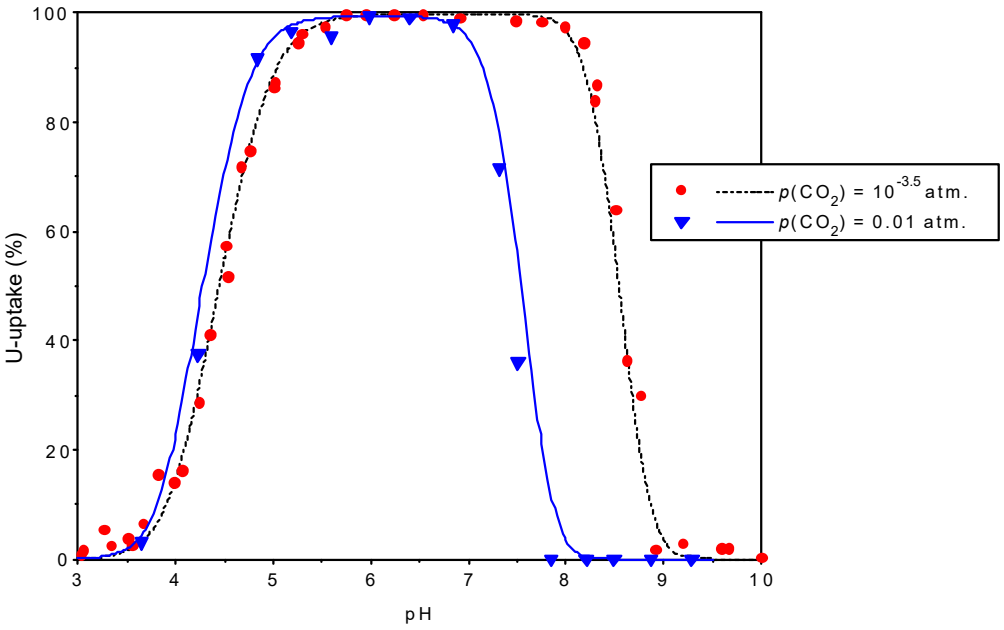


FIGURE 11.5 Uranium adsorption by ferrihydrite at two partial pressures of CO_2. Curves were calculated using MINTEQA2 and the reactions in Table 11.2. Experiments were carried out in 0.1 mol/L $NaNO_3$, ΣU = 1 μmol/L, ΣFe = 1 mmol/L.

At high pH values, increasing the ionic strength reduced U sorption on ferrihydrite (Figure 11.6A). Although an ionic strength dependence can be attributed to the presence of outer sphere surface complexes, the diffuse double layer model does not accommodate outer sphere surface complex formation. However, even with only inner-sphere complexes included, the model correctly predicts a decrease in sorption with increasing ionic strength. This is because the activity of the highly charged carbonate species, which prevail in the high pH range, is significantly affected by ionic strength. The model curves provide an adequate fit to the experimental data (Figure 11.6A).

In the case of the low pH edge, the model predicts a slight shift to lower pH values with decreasing ionic strength (Figure 11.6B). Although there is some scatter in the experimental data, this trend is not readily apparent in the measurements (in contrast to the high pH edge). This may reflect an inadequacy of the model.

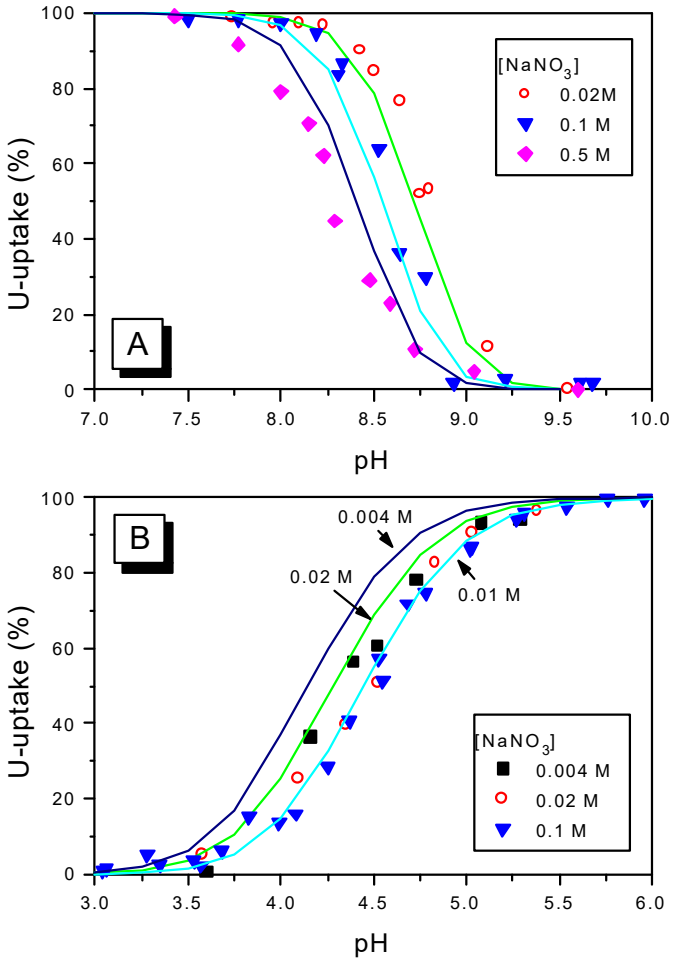


FIGURE 11.6 Effect of ionic strength on U sorption.

A) high pH 'desorption' edge, B) low pH adsorption edge. Experimental conditions: ΣU = 1 μmol/L, ΣFe = 1 mmol/L, air equilibration. Curves calculated using the reactions in Table 11.2. Note that range of ionic strength is limited because of limitations on the validity of the Davies equation (used for ionic strength corrections). *cf* Figure 6.8.

Modelling of U sorption isotherms at pH 4.5 and 5.25

As previously discussed, isotherms are obtained by carrying out experiments with a range of total U (ΣU) while keeping other experimental conditions (in particular the pH) constant. The experimental work on U sorption isotherms (shown in Figures 6.5 and 6.6) had not been carried out at the time of the derivation of the U sorption parameters using FITEQL [Waite *et al.,* 1994]. The FITEQL optimisation was based on the pH dependence of the U sorption edges. As such, the isotherm data provide a good opportunity to test the predictions of the model.

The fit of the model to the raw experimental sorption data is shown in Figure 11.7. As can be seen there is a remarkably good correspondence, with the points of inflexion of the data curve clearly reproduced by the model.

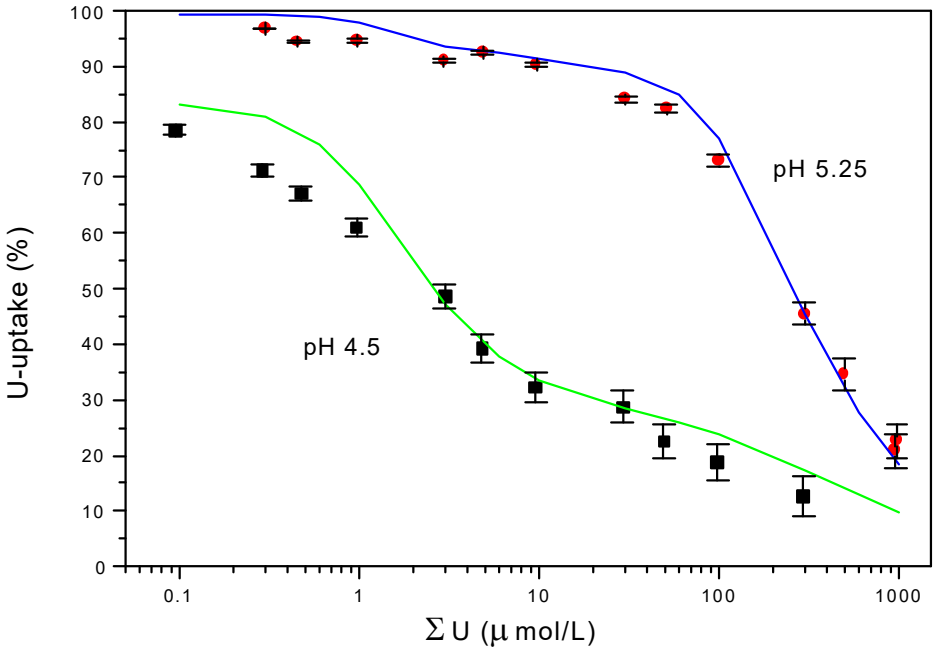


FIGURE 11.7 U sorption as a function of ΣU at pH values of 4.5 and 5.25 and corresponding model curves. Background electrolyte 0.02 mol/L $NaNO_3$ in equilibrium with air. ΣFe = 1 mmol/L.

The model curve also provides a satisfactory simulation of the experimental results when the data are converted to the isotherm format (Figure 11.8). It is noteworthy to compare the model curve in Figure 11.8 with the Freundlich isotherms shown in Figure 6.6, which model the same sets of data. The Freundlich isotherm requires arbitrarily fitting a line to the data points, whereas the SCM curve is a prediction obtained from the mechanistic model without any further parameter adjustment. The comparison of these figures graphically illustrates the advantages of the surface complexation sorption models.

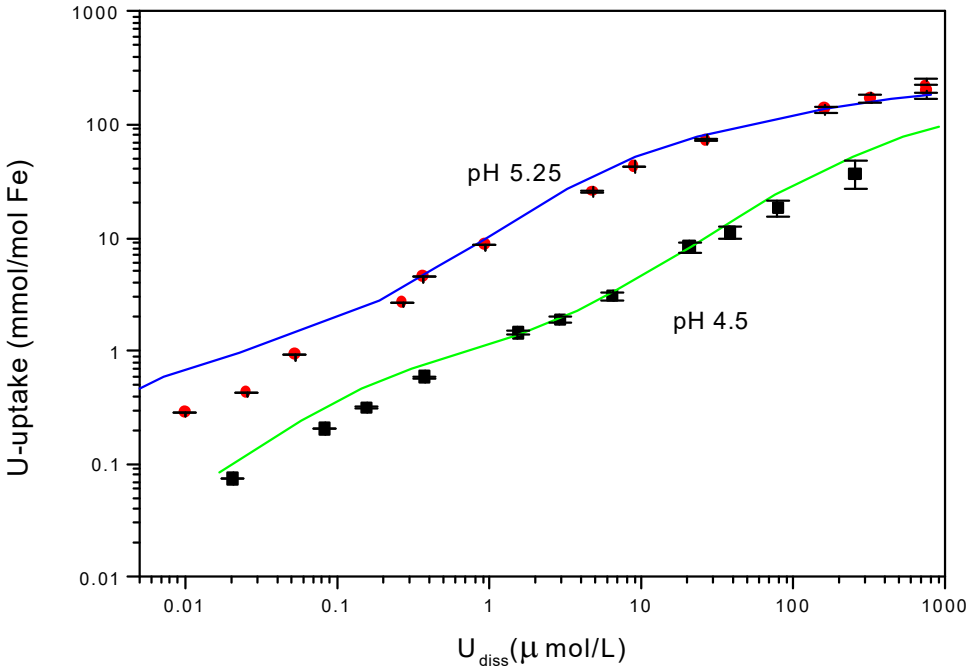


FIGURE 11.8 U sorption isotherms – comparison of experimental data and model calculations (I = 0.02)

Assessment of model adequacy

As has been discussed, some of the data for which model fits were shown (particularly the data shown in Figures 11.3 and 11.5) were used in the model optimisation. As such, one would expect a reasonable fit to the experimental data. Nonetheless, the ability of the model to adequately predict the effects of such a number of variables over fairly wide ranges is clearly superior to other models advanced for U sorption on iron-oxides.

However, the additional data-sets (shown in Figures 11.4, 11.6, 11.7 and 11.8) were not used to constrain the model. Thus, it appears that the proposed surface complexation model for U sorption has the ability to make predictions for systems beyond those which were used to derive it, correctly simulating the effect of mass loading, ionic strength (at high pH) and U concentration isotherms. In addition, the isotherms were obtained at a different ionic strength (I = 0.02) to the pH sorption edges used to derive the adsorption constants (I = 0.1).

The one puzzling aspect of the model is the prediction of a slight ionic strength dependence of the low pH edge. At this stage it is unclear whether this agrees with the slightly scattered data. Overall, the model described in Table 11.2 and implemented by MINTEQA2 has the ability to simulate U sorption on ferrihydrite over a very large range of experimental conditions:

In particular, these included:

- pH 2-12
- ionic strength (0.02 to 0.5 mol/L)
- mass loading of ferrihydrite (1 mmol/L and 20 mmol/L as ΣFe)
- total U (isotherms from 0.01 μmol/L to 1 mmol/L, pH edges from ΣU of 1 μmol - 100μmol/L)
- pCO$_2$ ($10^{-3.5}$ atm and 0.01 atm)

11.5 Surface speciation of adsorbed U

The speciation of U on the surface of ferrihydrite provides an insight into the relative importance of the four postulated surface species under different experimental conditions, and provides information that can be used to constrain models of the effects of various ligands on U sorption. The computed surface speciation for ΣU of 1 μmol/L and 100 μmol/L is shown in Figure 11.9. It will be observed that the importance of the carbonate containing surface species increases with increasing pH, whereas the relative importance of the strong sites rapidly decreases at higher U concentrations. These effects are in accord with expectations based on the chemistry of the system.

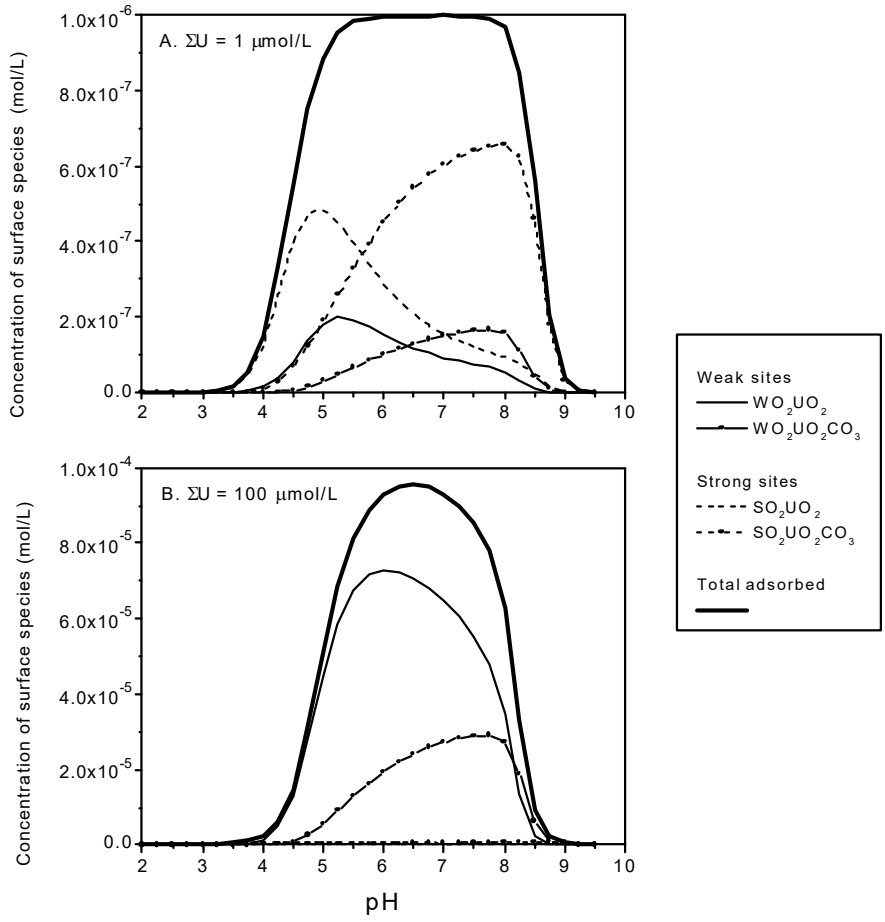


FIGURE 11.9 Surface speciation of adsorbed U(VI) for total U of : A) 1 μmol/L and B) 100 μmol/L. Systems are equilibrated with air.

The surface species are as designated in Table 11.2.

The speciation shown in Figure 11.9 suggests that ternary uranyl-carbonate complexes play a significant role in U(VI) adsorption across a wide pH range, particularly in systems with lower ΣU. As was discussed above, the existence of these complexes was not inferred from the EXAFS results. Rather, they were added to improve the fit of the model to the sorption data. Based on similar reasoning, the existence of ternary uranyl-carbonate surface complexes on the surface of goethite was previously postulated by Hsi and Langmuir [1985] and Kohler *et al.* [1992]. While some other workers have argued against this possibility (see Chapter 4), a recent spectroscopic study of uranyl on the hematite surface has indicated that uranyl-carbonate ternary complexes are present at all pH values between 4.5 and 8.5 [Reitmeyer *et al.*, 1999]. The speciation computed by the present model is therefore in concordance with the results of several other studies.

11.6 Modelling U sorption on ferrihydrite in the presence of sulfate

The experimental data for U sorption on ferrihydrite that have been discussed thus far relate to experimental systems that contain the aqueous components Na^+, NO_3^-, UO_2^{2+}, H^+, and CO_3^{2-}. As was shown in Chapter 6, the presence of complexing ligands affects U sorption. Sulfate is considered in this section, and the following section is concerned with citrate. Phosphate is discussed in Chapter 13.

It was shown in section 6.4.3 that the presence of sulfate decreases U adsorption. This effect was only observed in the region of the low pH U-sorption edge (i.e. pH values below 7). The simplest explanation of the observed effect is that there is complexation between SO_4^{2-} and UO_2^{2+} in the aqueous phase (as shown in Figure 3.5). The resulting competition for uranyl between the SO_4^{2-} ligand and surface sites would then reduce U sorption. This effect is straightforward to implement in MINTEQA2, by adding (to the suite of aqueous reactions) the complexation reactions:

$$UO_2^{2+} + SO_4^{2-} \Leftrightarrow UO_2SO_4^0 \qquad (11.5)$$

$$UO_2^{2+} + 2SO_4^{2-} \Leftrightarrow UO_2(SO_4)_2^{2-} \quad (11.6)$$

The log K values for reactions 11.5 and 11.6 are given in Table 3.1. In this simple model, the surface adsorption reactions for UO_2^{2+} (Table 11.2) are included without any modifications or adjustments of log K values.

When the U uptake curve (for ΣU of 1 μmol/L) was computed (with total SO_4^{2-} of 0.01 mol/L), there was only a very small displacement of the model curve compared to the curve obtained in the absence of sulfate (Figure 11.10A). The model pH edge moved to the right (towards higher pH values) by about 0.1 of a pH unit in the system containing sulfate. This is inadequate to explain the experimental data, in which the displacement between the two curves is approximately 0.4 pH units.

A similar situation exists for the experiments with ΣU of 10 μmol/L. Again the effect of sulfate is under-predicted by this simple approach. In this case, the model of the ligand-free system shows a slight systematic deviation from the experimental data. (This is a consequence of the fact that the model was optimised to simulate a number of data sets, of which the data on this curve is only a small part). However, the key issue here is that the effect of sulfate is clearly under-predicted. This is shown by the fact that the two model curves in Figure 11.10B are too close together, as is also the case for Figure 11.10A.

Therefore, we need to consider another explanation for the lower U uptake in the presence of 0.01 M sulfate. It seems reasonable that there could be competition between SO_4^{2-} and UO_2^{2+} for surface sites. In order to implement this mechanism, it is necessary to have a model for the uptake of SO_4^{2-} on the ferrihydrite surface. Data for sulfate uptake on ferrihydrite are sparse, but one data-set (that of Davis and Leckie [1980]) exists. This data set is shown in Figure 11.11. As can be seen, the uptake of sulfate is strong below pH 6, and it therefore seems possible that competition between SO_4^{2-} and UO_2^{2+} could occur in this pH range. (This would be analogous to the carbonate adsorption reactions in Table 11.2).

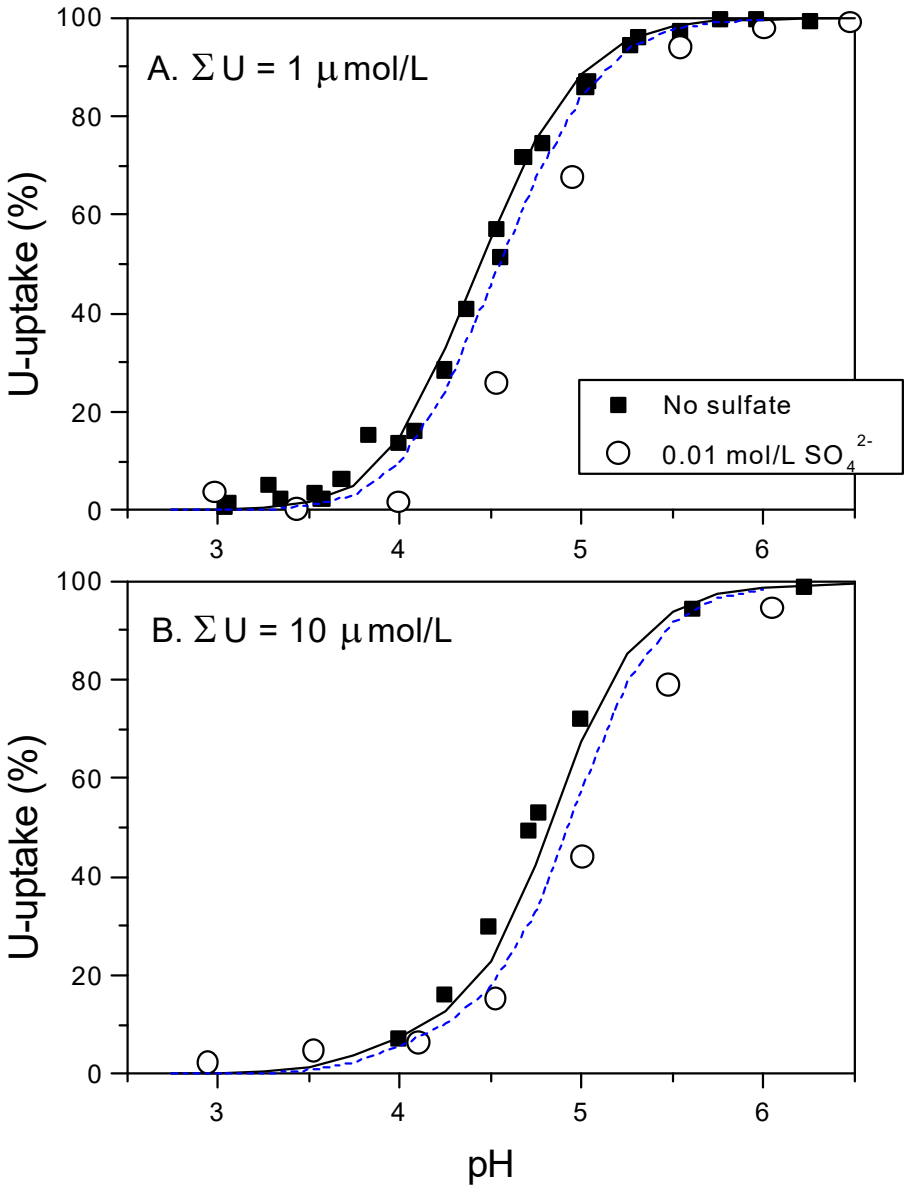


FIGURE 11.10 Modelling the effect of sulfate (0.01 mol/L) on U sorption by ferrihydrite. The solid curves represent the fit of the model in Table 11.2 to the data for the sulfate–free systems. The dotted curve is a similar model in which aqueous phase complexation between sulfate and uranyl is considered. A) ΣU = 1 μmol/L B) ΣU = 10 μmol/L

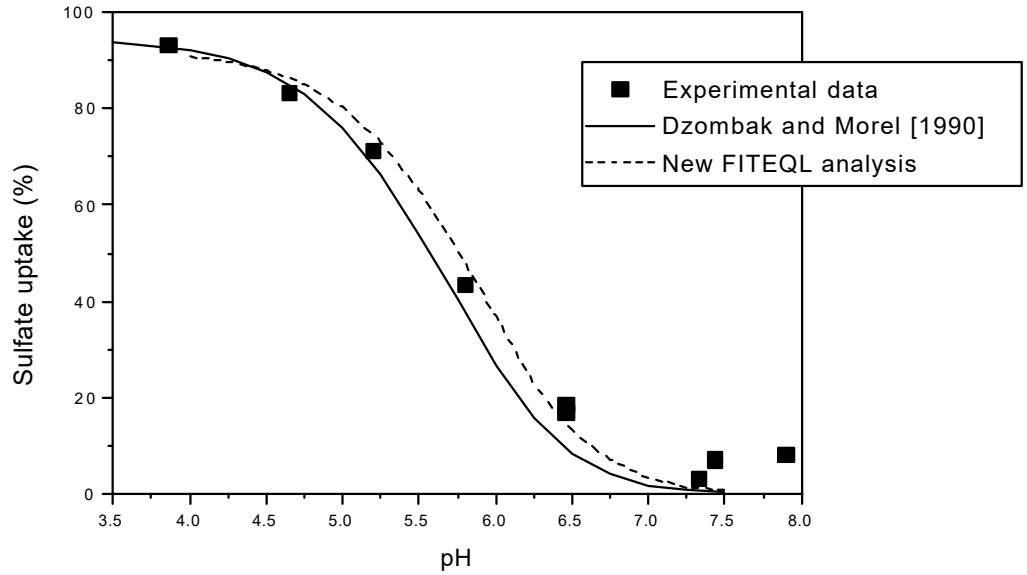


FIGURE 11.11 Data for sulfate adsorption on ferrihydrite (from Davis and Leckie [1980]). The two model curves are a) obtained by Dzombak and Morel [1990] and b) derived in this chapter using FITEQL, both with a site density of 0.2 mol sites / mol Fe and the surface reactions in equations 11.7 and 11.8 (see text).

FITEQL modelling of sulfate sorption with a site density of 0.2 mol sites / mol Fe

In the work described in this part of the study, the aim was to progressively achieve the following objectives:

1. To model the sulfate adsorption data in Figure 11.11 using FITEQL, with the same site density advocated by Dzombak and Morel (0.2 mol sites / mol Fe). This preliminary parameter optimisation exercise will establish the basic validity of the FITEQL parameter estimation procedure.
2. To re-derive the relevant sorption constants to make them consistent with the higher site density (0.875 mol/mol Fe) used in the U sorption model (Table 11.2).

3. To examine whether the resulting model can help to explain the observed change in U sorption in the sulfate-containing experimental systems, by invoking competition between uranyl and sulfate at ferrihydrite surface sites.

As discussed previously, FITEQL is a computer code for estimating chemical equilibrium constants from experimental data. As detailed by Herbelin and Westall [1994], the key to optimising log K values for proposed surface complexation reactions is to include a 'dummy' component for the sorbed species in the FITEQL input file. In this case SO_4^{2-} (ads) was added as a Type II 'dummy' component (see pp 6-20 and 6-21 in Herbelin and Westall [1994] for a discussion of a similar problem).

Dzombak and Morel [1990] recommended the following two surface reactions to describe sulfate adsorption:

$$>FeOH + SO_4^{2-} + H^+ \Leftrightarrow >FeSO_4^- + H_2O \quad (11.7)$$

$$>FeOH + SO_4^{2-} \Leftrightarrow >FeOHSO_4^{2-} \quad (11.8)$$

The first part of this exercise therefore involves determining the log K for these two reactions, using the experimental data in Figure 11.11 to constrain the model. Only one sorption site will be considered for sulfate adsorption. This is typically adequate for anion adsorption [Dzombak and Morel, 1990]. Also, the data-set is insufficient for a two site model, given that two surface reactions are already included.

The key parts of the FITEQL input file for this model are given in Table 11.3. The component data set includes the electrostatic component X(psi), the sorption site (Y), and the aqueous components H^+, SO_4^{2-} and Na^+. Sodium is required (although it plays no direct part in the sorption reactions) to account for complexation between SO_4^{2-} and Na^+ according to the reaction:

$$Na^+ + SO_4^{2-} = NaSO_4^- \quad (11.9)$$

TABLE 11.3 FITEQL input for modelling sulfate sorption on ferrihydrite (experimental data of Davis and Leckie [1980], site density of 0.2 mol sites / mol Fe)

A. FITEQL components and input values

ID	Name	log X	T	Type
160	X(Psi)	-1.0	0.00E+00	T(I)
2	SO4[2-]	-5.0	1.00E-05	T(I)
3	YOH	-4.0	2.00E-04	T(I)
4	Na[+]	-1.0	1.00E-01	T(I)
5	SO4(ads)	0.0	0.00E+00	X&T(II)
6	H[+]	0.0	0.00E+00	X(III)

X – free concentration

T – total concentration

Type I - components for which only T is known

Type II – components for which both X and T are known

Type III – components for which only X is known

B. FITEQL species and stoichiometry matrix

ID	Name	log K	X(Psi)	SO4[2-]	YOH	Na[+]	SO4[ads]	H[+]
1	H[+]	0.00	0	0	0	0	0	1
2	OH[-]	-13.78	0	0	0	0	0	-1
3	SO4[2-]	0.00	0	1	0	0	0	0
4	HSO4[-]	1.44	0	1	0	0	0	1
5	YOH2[+]	7.18	1	0	1	0	0	1
6	YOH	0.00	0	0	1	0	0	0
7	YO[-]	-8.82	-1	0	1	0	0	-1
8	YSO4[-]	5.00*	-1	1	1	0	1	1
9	YOHSO4[2-]	2.00*	-2	1	1	0	1	0
10	NaSO4[-]	0.48	0	1	0	1	0	0
11	Na[+]	0.00	0	0	0	1	0	0

* value to be optimised

This reaction was not mentioned in Dzombak and Morel [1990] and it may have been overlooked in their calculations. However, the output of their model for this data-set (discussed below) appears reasonable. This suggests that this reaction was considered in their computations (but was omitted from the report of their activities).

The matrix in Table 11.3 contains all the reactions that are likely to play a role in the system. Note that the log K values in the FITEQL input stoichiometry matrix (Table 11.3) have been adjusted to an ionic strength of 0.1 (μ = 0.1). This is because the aim is to model experimental data that were obtained in 0.1 M $NaNO_3$. As will by now be clear, the object of the exercise is to estimate log K values for the reactions forming the surface species YSO_4^- and $YOHSO_4^{2-}$.

The remaining information for the FITEQL input is the diffuse double layer model and the solid parameters. These are as follows:

- solid concentration of 0.089 g/L
- surface area of 600 m^2/g
- 0.1 M concentration of a 1:1 electrolyte.

In addition, the data points shown in Figure 11.11 were also added as 'serial' data (ie %adsorbed vs pH). These form the experimental data to which the computed curve is to be fitted. The original data were not available to me and I estimated the serial data from the figure in Dzombak and Morel [1990].

FITEQL was then executed and log K values were obtained for reactions 11.7 and 11.8. These log K values were 7.56 and 1.10, respectively (after correction to μ=0). These were similar to those obtained by Dzombak and Morel (i.e. 7.78 and 0.79). The slight differences may be due to errors in my estimation of the position of data points from the figure in Dzombak and Morel [1990], or may possibly be related to the inclusion of the $NaSO_4^-$ complex.

The model curve derived by FITEQL was compared with that derived by Dzombak and Morel [1990] and with the experimental data of Davis and Leckie [1980] (Figure 11.11). Both model curves provide a reasonable description of the data set. This exercise suggested that the FITEQL approach was successful in estimating formation constants for surface complexes in the experimental system.

FITEQL modelling of sulfate and U sorption data with a site density of 0.875 mol sites / mol Fe

Although the modelling exercise described above resulted in a fair simulation of the sulfate sorption data of Davis and Leckie [1980], the computed complexation constants are not suitable for direct inclusion in the sorption model for UO_2^{2+} proposed in Table 11.2. This is because the site density in the latter case was optimised at 0.875 mol sites / mol Fe in order to model the adsorption of U. However, the optimisation of the sulfate sorption data was carried out at the lower (more usual) site density of 0.2 mol / mol Fe.

To provide a sulfate sorption model that is compatible with the U sorption model, it is necessary for the adsorption constants for sulfate to be re-calculated at the higher site density. In order to achieve this, the FITEQL modelling was repeated, but with the input matrices modified as follows:

1. The total concentration for YOH surface sites was changed to 0.875 mmol/L.
2. The log K values for surface protonation and deprotonation reactions were changed to values which are appropriate for the higher site density and I = 0.1 (shown in Table 11.1).

When these small changes were made, the FITEQL program was again executed. Unfortunately, there was no convergence when both sorption reactions (11.7 and 11.8) were included. During the iteration procedure, the log K for reaction 11.7 became increasingly more negative, indicating that this reaction played no role in the optimum model of the experimental data. This may reflect the fact that the site density could not be optimised in this approach (as was done in modelling the U data). While FITEQL would not converge with both surface species included, it would converge when either of the two species (YSO_4^- or $YOHSO_4^{2-}$) was included alone.

FITEQL was then run individually for each of the two reactions, with the resulting log K values being:

$$YOH + SO_4^{2-} + H^+ \Leftrightarrow YSO_4^- + H_2O \qquad \log K_{\mu=0} = 7.75 \quad (11.10)$$

$$YOH + SO_4^{2-} \Leftrightarrow YOHSO_4^{2-} \qquad \log K_{\mu=0} = 0.24 \quad (11.11)$$

Because the reactions were computed separately, they cannot both be used in the sorption model. One or the other must be selected.

The two single-site, single-reaction models (Equations 11.10 and 11.11) are compared in Figure 11.12. The model involving only the species $YOHSO_4^{2-}$ was considered to be preferable to the model involving only YSO_4^{2-}, because it provided a slightly better fit to these data (as also indicated by the goodness-of-fit estimation (WSOS/DOF) in the FITEQL output). In addition, the non-converging iteration results for the model with the higher site density and both species included (mentioned above) suggested that the YSO_4^{2-} species did not assist in simulating the experimental data.

Thus, the final outcome of this investigation was the addition of reaction 11.11 to the U surface complexation model shown in Table 11.2. As with other reactions not involving uranyl in Table 11.2, the same sulfate sorption reaction was assumed to occur at both strong and weak sites.

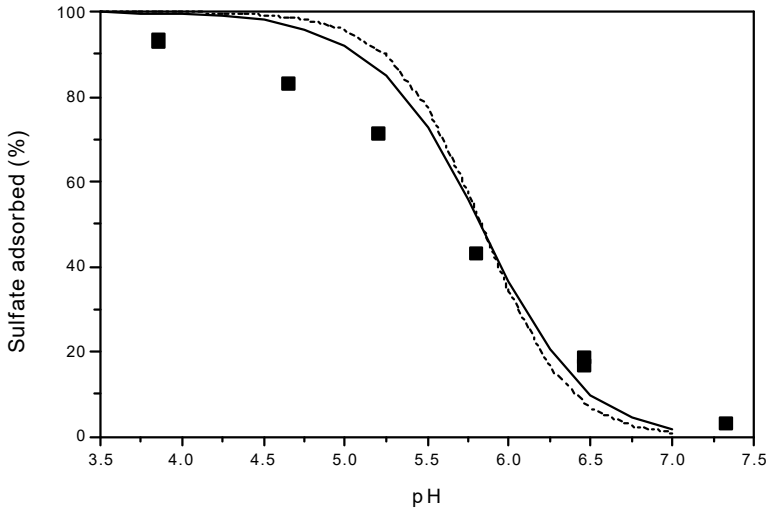


FIGURE 11.12 Modelling of sulfate adsorption on ferrihydrite assuming a high surface site density of 0.875 mol site/ mol Fe. The solid curve assumes the formation of $YOHSO_4^{2-}$ (reaction 11.11) whereas the dashed curve includes the YSO_4^- surface complex (reaction 11.10)

It was then a simple matter to compute the effect of sulfate on the adsorption of uranyl. MINTEQA2 was executed as before, with an input file that included:

- complexation between aqueous uranyl and sulfate (reactions 11.5 and 11.6) and
- competition for surface sites between uranyl and sulfate (reaction 11.11)

The resulting model curves (Figure 11.13) provided a good simulation of the effect of sulfate on the experimental data for U sorption on ferrihydrite.

As noted above, the object of this exercise was to provide a description of the effect of sulfate on U sorption, which is mathematically consistent with the model already advanced for U sorption in the absence of sulfate. While the modelling of the sulfate adsorption could not be fully optimised due to the constraint imposed by the high site density used in the U sorption model, the model fit to the sulfate sorption data was acceptable. The main objective, namely to model the effect of sulfate on U sorption has been achieved.

The experimental and modelling study of the effect of sulfate on U sorption by ferrihydrite is summarised as follows:

- The presence of sulfate results in a decrease in U adsorption in the pH region of the low pH edge (i.e. pH values < 7).
- The decrease in U sorption cannot be fully explained by the complexation between sulfate and uranyl. The UO_2^{2+} - sulfate aqueous complexes are relatively weak and the inclusion of these complexes in the model only causes a marginal decrease in predicted U sorption.
- The change in U sorption can be adequately explained by competition between uranyl and sulfate at surface sites.
- When reaction 11.11 for sulfate adsorption is included at both weak and strong sites, *with log K calculated at the appropriate site density,* then an adequate model of U sorption in the presence of sulfate can be obtained.
- No changes to the suite of sorption reactions for UO_2^{2+} are required.

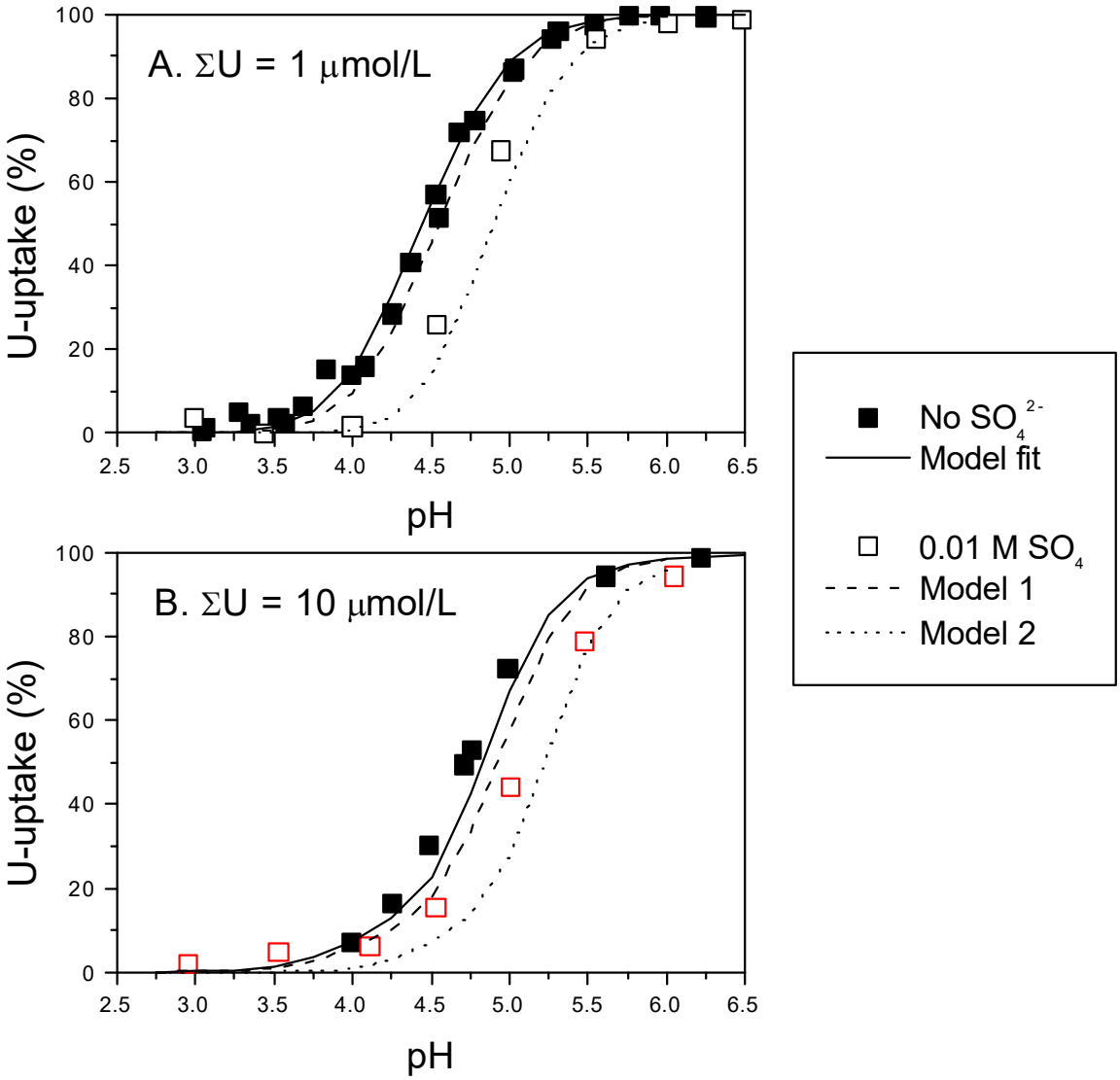


FIGURE 11.13 Experimental data and models for U sorption on ferrihydrite in absence and presence of sulfate. Model 1 only includes aqueous complexation between UO_2^{2+} and SO_4^{2-} (Equations 11.5 and 11.6). Model 2 also includes the adsorption of SO_4^{2-} on ferrihydrite surface sites (Reaction 11.11). This competitive adsorption explains the displacement of the U sorption edge in the presence of sulfate.

11.7 Modelling U sorption on ferrihydrite in the presence of citrate

The objective of this section is to model the experimental results for the U / ferrihydrite / citrate system. The experimental data (Section 6.4.4) showed that, in some cases, the ferrihydrite dissolved in the presence of citrate. In addition, aqueous complexes between citrate and uranyl could reduce the uptake of U on the surface. These mechanisms clearly contribute to the reduced sorption of U (compared to citrate-free systems) in at least some of the experimental systems considered.

Citric acid is a hydroxytricarboxylic acid with the structure shown in Figure 11.14a. It is usually regarded as a triprotic acid, and in aqueous modelling is conventionally referred to as H_3CIT, comprising the components H^+ and CIT^{3-}. Thus, CIT^{3-} is the ligand $HOC(COO^-)(CH_2COO^-)_2^{3-}$. Some authors have stated that citric acid can act as a tetraprotic ligand, with the fourth proton originating from the hydroxy group of the hydroxytricarboxylic acid [Smith, 1965; Manzurola *et al.,* 1989].

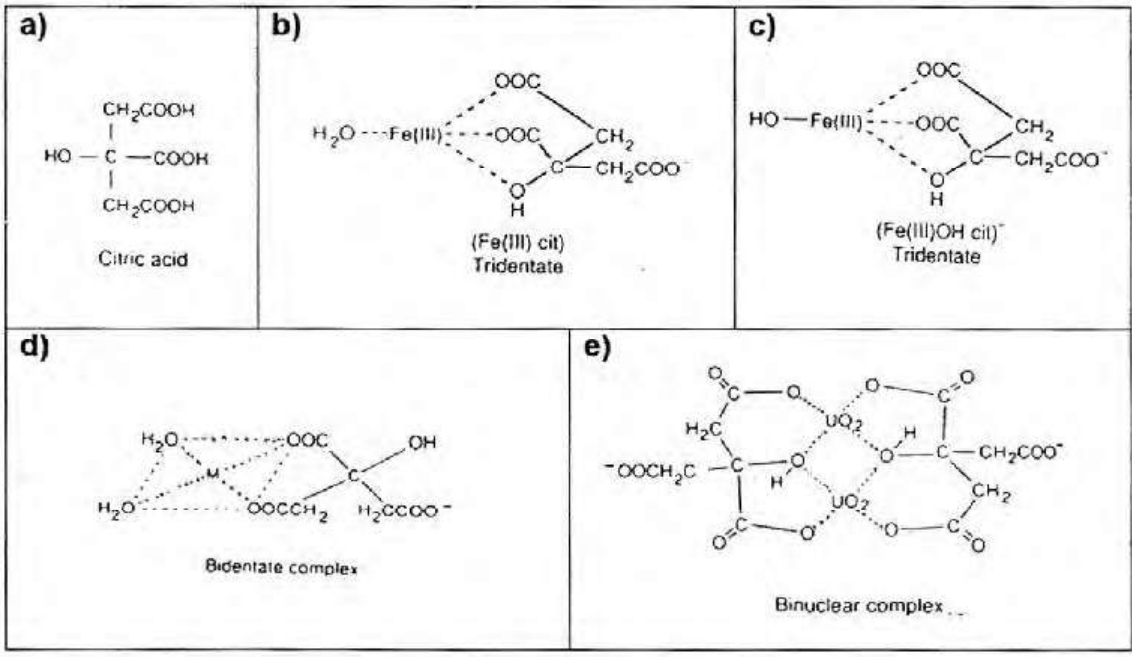


FIGURE 11.14 Structure of complexes in the UO_2^{2+} / Fe^{3+} / citrate system.

a) citric acid b) FeCIT c) $FeOHCIT^-$ d) UO_2CIT^- e) $(UO_2)_2(CIT)_2^{2-}$

Sources: (a,d,e) Francis *et al.,* 1992 (b,c) Francis and Dodge, 1993.

The dissolution of ferrihydrite by citrate

Modelling the dissolution of ferrihydrite in the presence and absence of citrate is straightforward. The applicable reactions of ferrihydrite and Fe-citrate complexes are reactions 1 to 5 in Table 11.4. The dissolution of ferrihydrite in the presence and absence of 10 mmol/L added citrate (experimental data in Figure 6.21) was modelled with MINTEQA2, and the computational results are shown in Figure 11.15A.

The curves in Figure 11.15A provide a reasonable description of the experimental data, although the ferrihydrite was slightly less soluble than predicted. This is possibly because the ferrihydrite was aged for 65 hours before the U-adsorption experiment, which then took a further three days to complete. Thus, the ferrihydrite was about 6 days old at the time of solid-liquid separation. During this time, it would be expected that its solubility would decrease. Ferrihydrite is a poorly defined solid, and it is likely that the equilibrium constant for reaction 1 (Table 11.4) was obtained under slightly different experimental conditions.

It would be a simple matter to adjust the equilibrium constant for reaction 1 in Table 11.4 (or any of reactions 1 – 5) to achieve a better fit to the data. However, it seems advisable to limit adjustments to log K values as much as possible. (While it is attractive achieve a perfect fit to one's own experimental data by "refining" log K values, such changes may result in an inability to model the published data that were used to derive the previous log K values).

It will be observed that the systems containing citrate shown in Figure 11.15A also contained trace amounts of U. It is assumed that this trace U has no effect on the dissolution of the ferrihydrite when the amounts of both ΣFe and ΣCIT are orders of magnitude higher.

For the experimental system with the lower amount of citrate (100 μmol/L rather than 10 mmol/L), the dissolution of ferrihydrite at pH > 4 could be modelled fairly well, again without any adjustments to equilibrium constants (Figure 11.15B). In this case, there is some scatter, and this may be because most of the Fe in this system is associated with the solid (rather than the aqueous phase). However, it does appear that the solid is less soluble than

predicted in the low pH range (i.e. pH < 4). The predicted solubility (model curve) increases rapidly with decreasing pH in this pH range, due to the mechanism of acid dissolution (rather than Fe-citrate complexation which is responsible for the dissolution in the pH range 4 to 7).

It appears that the presence of citrate in the system may retard this acid-dissolution process. This would be consistent with the results reported by Cornell [1987], who found that citrate reduced the rate of transformation of ferrihydrite to more crystalline products, and led to more hematite, rather than goethite. Goethite forms by dissolution of ferrihydrite, followed by re-precipitation. In contrast, hematite forms via internal aggregation and rearrangement. Thus, it is reasonable that the presence of citrate may retard the acid dissolution step and this may explain the lower measured ferrihydrite solubility at low pH values.

TABLE 11.4 Reactions in the Fe^{3+} – UO_2^{2+} – citrate system

	Reaction	log K (I = 0)
1.	$Fe^{3+} + 3H_2O \Leftrightarrow Fe(OH)_3 + 3H^+$	-4.9 [a]
2.	$Fe^{3+} + CIT^{3-} \Leftrightarrow Fe(CIT)^0$	13.2 [b]
3.	$Fe^{3+} + H^+ + CIT^{3-} \Leftrightarrow Fe(HCIT)^+$	14.4 [b]
4.	$Fe^{3+} + H_2O + CIT^{3-} \Leftrightarrow FeOH(CIT)^- + H^+$	10.4 [b]
5.	$2Fe^{3+} + 2H_2O + 2CIT^{3-} \Leftrightarrow Fe_2(OH)_2(CIT)_2^{2-} + 2H^+$	6.2 [b]
6.	$UO_2^{2+} + CIT^{3-} \Leftrightarrow UO_2CIT^-$	8.7[b]
7.	$2UO_2^{2+} + 2CIT^{3-} \Leftrightarrow (UO_2)_2(CIT)_2^{2-}$	21.3[b]
8.	$Fe^{3+} + UO_2^{2+} + 2CIT^{3-} + 2H_2O \Leftrightarrow Fe(OH)_2(CIT)_2UO_2^{3-} + 2H^+$	20.4[c]

[a] Langmuir [1997]

[b] Smith and Martell [1993]

[c] This complex suggested by Manzurola [1989]. Log K chosen for best fit to experimental data (see text).

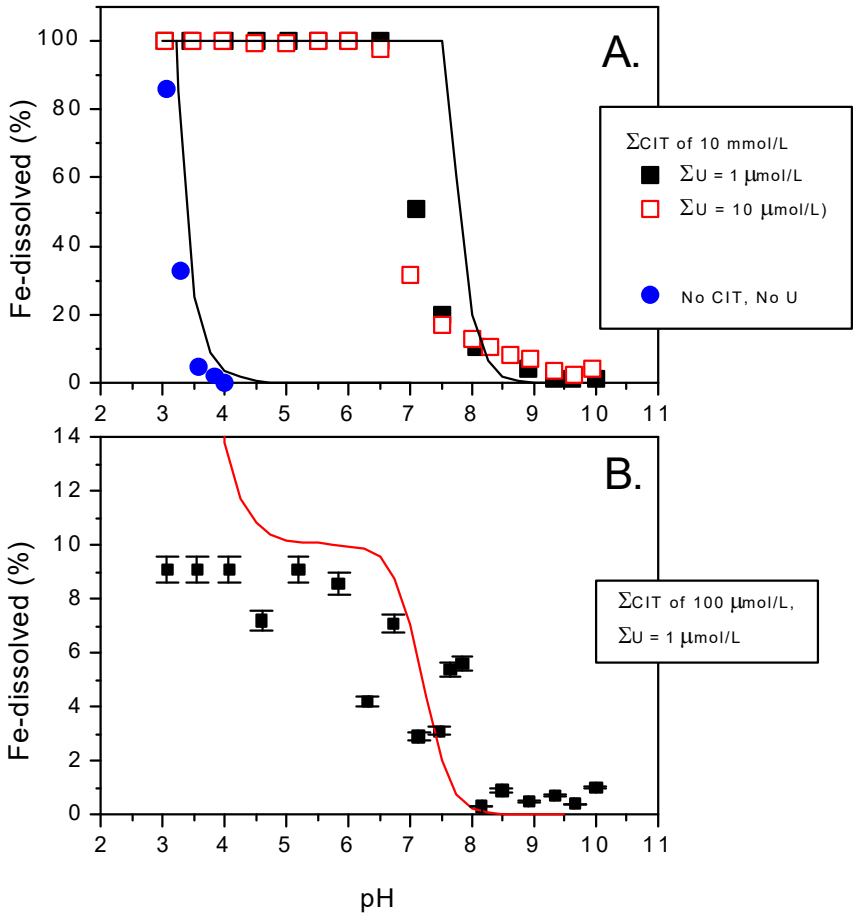


FIGURE 11.15 A) Dissolution of ferrihydrite (ΣFe = 1 mmol/L) in the presence and absence of citrate (0.01 mol/L).
B) Dissolution of ferrihydrite with citrate of 100 µmol/L.
Experimental systems contained U as indicated.
The curves are based on the thermodynamic data in Table 11.4.

Adsorption model of U on ferrihydrite in the presence of citrate – Model 1 with Fe^{3+}-citrate and UO_2^{2+}-citrate complexes

The first approach to modelling U uptake on ferrihydrite in the presence of citrate was to assume that the effect of citrate is restricted to the formation of aqueous complexes of CIT with UO_2^{2+} or Fe^{3+}. The U adsorption reactions were then assumed to be the same as in the citrate-free system (Table 11.2). Reactions 1 to 5 in Table 11.4 were therefore included to simulate the dissolution of ferrihydrite and the formation of Fe^{3+}/CIT complexes, and reactions 6 and 7 were added to account for complexation between uranyl and citrate. This simple sorption model will be referred to as 'Model 1'.

The only modification to the previous modelling approach was to account for the change in the amount of adsorbing surface that results from ferrihydrite dissolution. In the previous simulations of citrate-free systems, with ΣFe of 1 mmol, the amount of solid was fixed at 89 mg/L. In the systems containing citrate, the amount of ferrihydrite present at the pH value of each simulation was calculated using MINTEQA2 (the results of these calculations are shown in Figure 11.15), and this amount was added to the input set for the sorption simulation.

In the systems with ΣCIT of 10 mmol/L, the amount of solid ranged from 0 to 89 mg/L, since up to 100 % of the ferrihydrite dissolved (Figure 11.15A). In the experiments with ΣCIT of 100 μmol/L, a maximum of 10% of the solid dissolved in the presence of CIT. In this case, the calculated amount of solid (shown in Figure 11.15B) was used at pH values above 5.0. However, a constant value of 80 mg/L was used for the experiments below pH 5.0, since in this pH range the MINTEQA2 simulation clearly over-predicted the solubility. The amount of solid in these simulations therefore ranged from 80 to 89 mg/L.

The results of Model 1 for the U-ferrihydrite-citrate system (with 0.01 mol/L of added citrate) were not entirely satisfactory (Figure 11.16). The model correctly predicted zero U adsorption across a wide pH range in the presence of citrate, which can be explained by the dissolution of the ferrihydrite, and the large excess of CIT available to complex UO_2^{2+}. However, significant U

adsorption was still predicted in the pH range between about 7.5 and 9.0. In principle, this should have been experimentally observed if Model 1 is valid. As noted above, arbitrary re-adjustment of adsorption or complexation constants is an unappealing way to solve this problem.

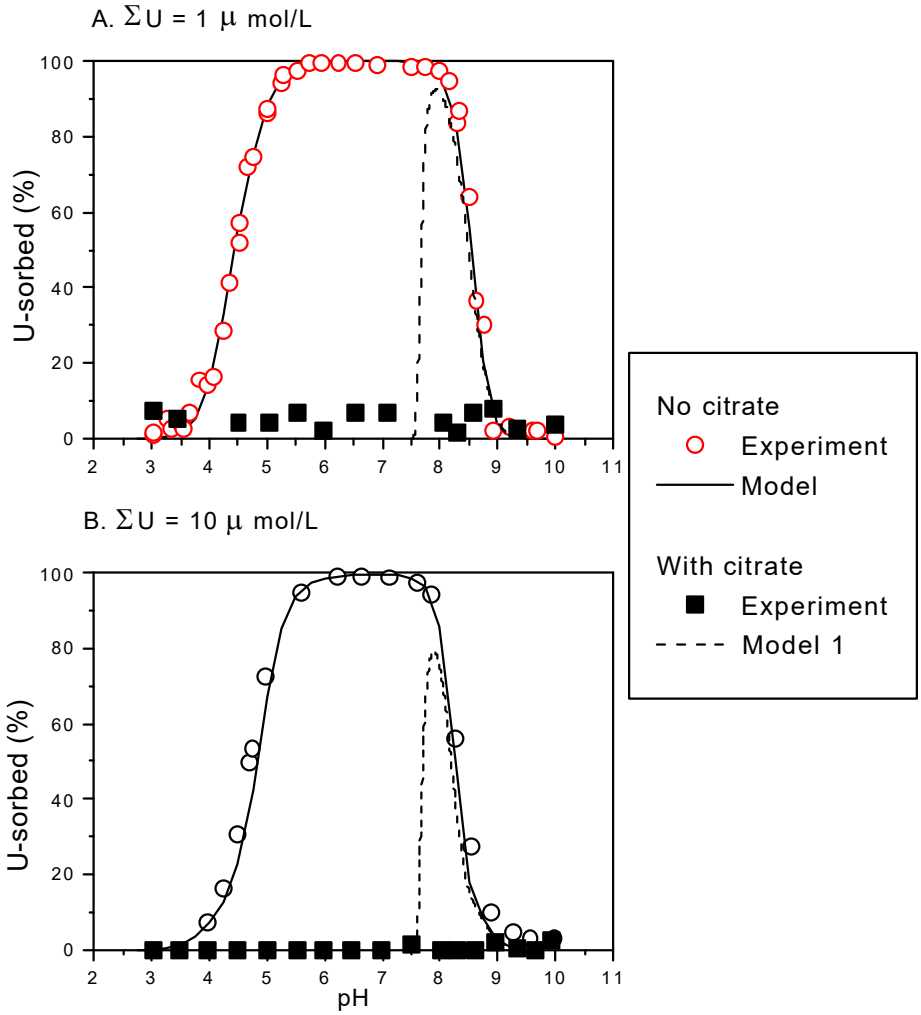


FIGURE 11.16 Modelling U adsorption in the Fe-U-citrate system (ΣFe of 1 mmol/L) using Model 1 (containing only Fe^{3+} – citrate and UO_2^{2+} - citrate complexes). Experimental results are for systems with 0 or 10 mmol/L of citrate. A) ΣU = 1 μmol/L. B) ΣU = 10 μmol/L. For both systems, Model 2 (which has a mixed metal complex) predicts negligible sorption across the entire pH range (see text).

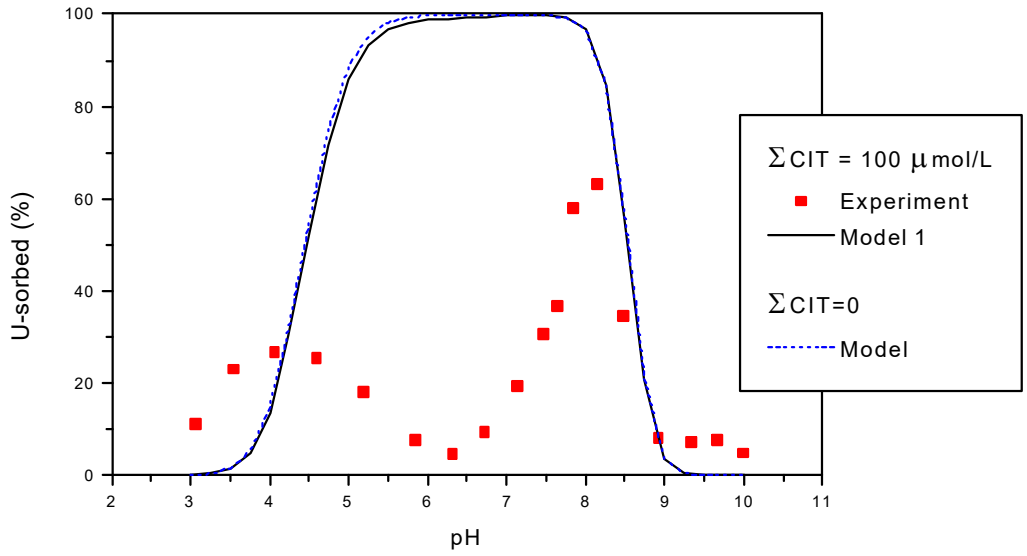


FIGURE 11.17 Modelling U adsorption in the Fe-U-citrate system. Experimental results for ΣCIT = 100 µmol/L with simulation results from Model 1 (containing only Fe-citrate and U-citrate complexes). The Model 1 curve fits the data poorly and is almost identical to the model curve for the citrate-free system. (ΣU = 1 µmol/L, ΣFe = 1 mmol/L)

The modelling results obtained for the system with ΣCIT of 100 µmol/L showed that there is a more serious shortcoming in Model 1. Whereas the experimental results comprise an unusual two-humped U adsorption curve, the model predictions for this system were virtually indistinguishable from the citrate-free system (Figure 11.17). At first this seemed counter-intuitive, since the presence of citrate was expected to strongly complex U and decrease its adsorption (Figure 3.7). However, examination of the MINTEQA2 output files provided the reason for this effect. In this system, there is a large excess of Fe^{3+} relative to CIT. The Fe^{3+} strongly complexed virtually all the citrate in the system, and the uranyl was ineffective in competing against Fe^{3+} for citrate. As a result, the adsorption of U was not significantly lower than for the citrate-free system. In fact, the barely-discernible decrease in U sorption predicted by Model 1 (Figure 11.17) is due to the decrease in the amount of sorbing solid rather than complexation between U and citrate.

Adsorption model of U on ferrihydrite in presence of citrate. Model 2 with Fe^{3+}-citrate complexes, UO_2^{2+}-citrate complexes and mixed–metal complex

In order to explain the data shown in Figure 11.16 and (particularly) Figure 11.17, a number of possibilities were examined. These included arbitrary changes to log K values for the reactions 6 and 7 in Table 11.4, and invoking competition for surface sites between adsorbed citrate and uranyl. The latter possibility was quickly excluded, because there is insufficient citrate to populate a high proportion of the sorbing sites in the system shown in Figure 11.17. The adjustment of reaction log K values appears unattractive for the reasons mentioned earlier, particularly as all these reactions have been well studied in the past.

It was decided that the most likely possibility is that there is an additional aqueous phase uranyl complexation reaction that maintains UO_2^{2+} in solution in the mid-pH range. The only candidate reaction that could be found after an extensive literature search was the following one proposed by Manzurola [1989]:

$$UO_2^{2+} + Fe^{3+} + 2H_4L \Leftrightarrow FeUO_2L_2^{3-} + 8H^+ \qquad (11.12)$$

Here H_4L is citric acid and L^{4-} is the fully deprotonated tetraprotic ligand $CO^-(COO^-)(CH_2COO^-)_2^{4-}$. This corresponds to a citrate ion that has lost the proton from the hydroxyl group, as well as from all three carboxylic acid groups. These authors also proposed analogous mixed metal complexes for similar systems including uranyl Al(III) citrate, uranyl indium citrate and uranyl copper citrate. Furthermore, they suggested the existence of similar mixed metal complexes with other ligands such as malate and tartrate. The possibility of a mixed metal complex was by no means unprecedented. In fact, the uranyl Al(III) citrate complex was proposed in 1959 by Booman and Holbrook.

By analogy with reactions 4 and 5 in Table 11.4 (and in accordance with common convention for this type of reaction where OH^-CIT^{3-} is used in place of L^{4-}), reaction 11.12 can be re-expressed in terms of MINTEQ components as follows:

$$UO_2^{2+} + Fe^{3+} + 2CIT^{3-} + 2H_2O \Leftrightarrow FeUO_2(OH)_2CIT_2^{3-} + 2H^+ \qquad (11.13)$$

This reaction appears quite reasonable given that both Fe and U form similar binuclear complexes with citrate (Figure 11.14, Table 11.4). It will also observed from Figure 11.14 that the source of the hydroxyl may be from the hydration sheath of the Fe^{3+} rather than by deprotonation of the hydroxyl (as envisaged by Manzurola *et al.* [1989]). However, differences about this point do not affect the equilibrium constant of reaction 11.13.

Manzurola *et al.* [1989] proposed an equilibrium constant for the mixed metal complex (reaction 11.12) of log K = -2.45, which, after correction to zero ionic strength and re-calculation in terms of MINTEQ components yields a value of log $K_{\mu=0}$ of 26.9 for reaction 11.13. Preliminary calculations showed that this log K would decrease U sorption to zero in all systems studied. However, analysis of the paper by Manzurola *et al.* [1989] shows that the speciation schemes for uranyl and Fe-citrate were quite different to the set of reactions shown in Table 11.4. This, together with the different assumptions about the source of the fourth proton, suggested that in this case optimisation of the log K for reaction 11.13 would be warranted. Based on the present literature, the value of this equilibrium constant is clearly not well-known.

Reaction 11.13 was then added to the suite of U sorption and complexation reactions used in Model 1. (This comprised the set of sorption reactions in Table 11.2, together with reactions 1 to 7 in Table 11.4). An equilibrium constant for reaction 11.13 (log K = 20.4) was then selected by trial-and-error to simulate the experimental sorption data. This revised model was denoted Model 2.

The resulting model fit (Figure 11.18) is quite good. This is considered to be a satisfactory outcome, because only the one reaction (reaction 8 in Table 11.4) was added to the existing suite of reactions for this system. The experimental data in Figure 11.18 appear complex, but are adequately simulated by a model in which only one constant (log K for reaction 11.13) was used as a fitting parameter.

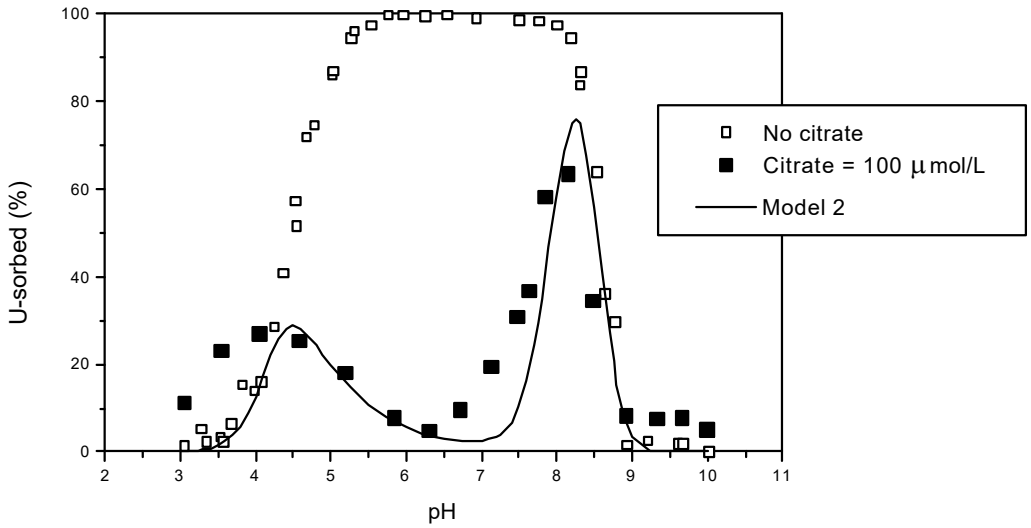


FIGURE 11.18 Sorption data for the U-citrate-ferrihydrite system together with predictions for Model 2. This model has all the reactions in Tables 11.2 and 11.4. However, only the equilibrium constant for reaction 8 in Table 11.4 was used as a fitting parameter for this data-set.

The model simulations for the systems containing ΣCIT of 10 mmol/L were then repeated, this time with the mixed metal complex included. As indicated in Figure 11.16, the model now simulated the experimental data correctly, with negligible sorption predicted across the entire pH range in these systems.

The calculated speciation of U, for the experimental system shown in Figure 11.18, is given in Figure 11.19. It can be seen that the $FeUO_2(OH)_2CIT_2^{3-}$ species dominates U speciation in the mid pH range, and effectively divides the uptake of U into two pH ranges. These comprise a low pH region in which surface speciation is dominated by the surface species $>SO_2UO_2^0$, and a high pH region in which the surface species is $>SO_2UO_2CO_3^{2-}$. This computed speciation provides support for the inclusion of the ternary surface complex $>SO_2UO_2CO_3^{2-}$ in the U adsorption scheme, since it seems unlikely that the double-humped sorption curve would occur if one U surface complex was dominant across the full pH range.

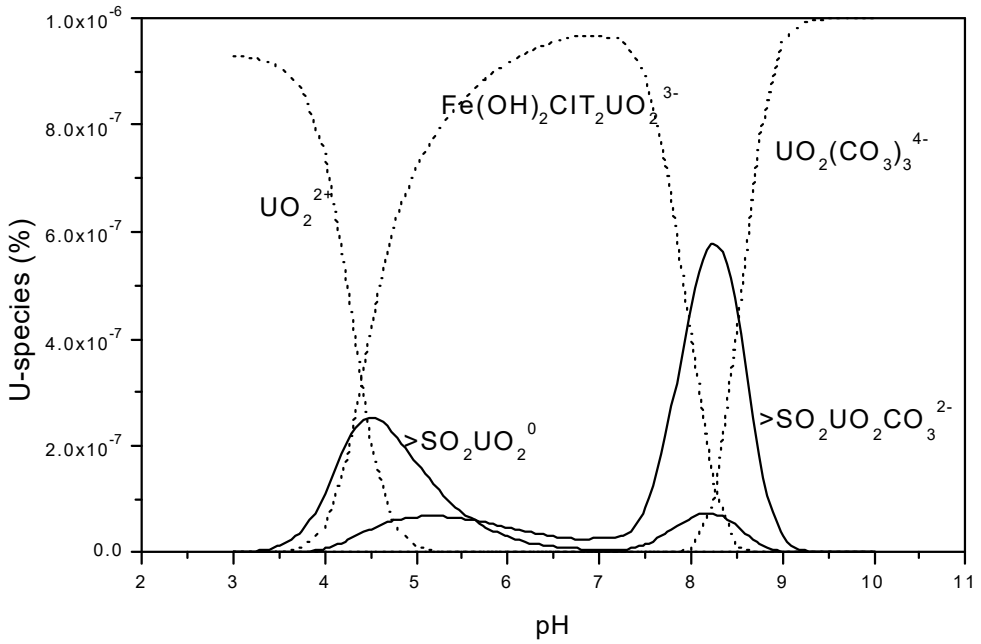


FIGURE 11.19 Computed uranium surface and aqueous speciation for the system shown in Figure 11.17.

The calculations described above provide support for the inclusion of a mixed complex between Fe^{3+}, UO_2^{2+} and citrate in the suite of reactions to describe the experimental system. The structure for this aqueous complex may resemble that for the similar complex involving UO_2^{2+} and Al^{3+} (as suggested by Manzurola *et al.* [1989]). This structure is shown in Figure 11.20.

While it was not expected that a mixed uranyl / ferric complex would play such an important role, it has been previously found that ferric citrate is unusual in terms of its chelating power. Smith [1965], who studied a similar system involving Fe^{3+} and Sn^{2+}, expressed this conundrum as follows: 'It is not obvious why ferric citrate should be so much more effective in chelating tin(II) compared with the citrate anion itself." A similar statement may apply to the analogous uranyl / ferric / citrate complex.

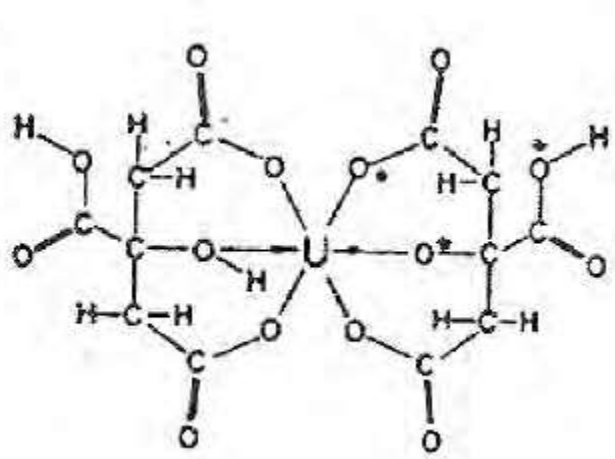


FIGURE 11.20 Possible structure for the mixed metal complex uranyl aluminium citrate. Aluminium bonding positions marked by *. Uranyl oxygen atoms are perpendicular to the plane of the paper. By analogy, the structure of $FeOH_2CIT_2UO_2^{3-}$ may be similar [Manzurola *et al.,* 1989]. Another possibility is that the complex has a similar structure to $(UO_2)_2(CIT)_2^{2-}$ (Figure 11.14e) with the Fe atom in the place of one of the uranium atoms .

Summary of modelling the U-Fe-citrate system

Three experimental systems were studied, involving various amounts of U and citrate. The system involving ΣCIT of 100 μmol/L, ΣU of 1 μmol/L and ΣFe of 1 mmol/L provided the most interesting data-set which could be used to constrain the U sorption model. The most successful model for all experimental systems studied was derived on the following basis:

- All reactions for U sorption on ferrihydrite were the same as found in the citrate-free system (Table 11.2).
- Ferrihydrite dissolution in the presence of citrate was included in the model. The literature value for this solubility was considered to be adequate.
- Selected literature values [Smith and Martell, 1993] for UO_2^{2+}-citrate and Fe^{3+}-citrate interactions were used.
- A mixed metal U-Fe-citrate complex (proposed by Manzurola *et al.* [1989]) was required to model the experimental data.
- The log K value for this complex was adjusted to fit the data.

Note that the log K value required *downward* adjustment to fit the data, which indicates that this complex does not even need to be as strong as proposed by Manzurola *et al.* [1989] in order to adequately fit the data.

This approach provided a good fit to the data obtained in all three systems studied, in particular fitting the interesting double-humped sorption curve obtained in the system with ΣCIT of 100 μmol/L. Only one equilibrium constant (log K) was adjusted in order to fit all three data-sets.

11.8 Summary of SCM for U sorption on ferrihydrite

In this chapter a considerable amount of modelling has been undertaken. The modelling has confirmed the validity of the model reported by Waite *et al.* [1994] and applied it to a comprehensive data-set for U sorption on ferrihydrite in $NaNO_3/CO_2$ systems. The model was implemented using the popular speciation code MINTEQA2.

The model was then extended to include the effects of sulfate and citrate. These systems are summarised as follows:

- There is some aqueous complexation between UO_2^{2+} and SO_4^{2-}. However, it is insufficient to explain the small but significant decrease in U sorption in systems that contain sulfate. It is necessary to also consider competition between sulfate and uranyl for surface sites. The sorption of sulfate was modelled after re-calculation of sorption constants from the literature. Published log K values for sorption reactions could not be used directly because they must be re-derived at the correct site density. The code FITEQL was used for this purpose. Surface competition between sulfate and uranyl is the main reason for decreased U uptake on ferrihydrite in the presence of sulfate.
- Uranyl sorption in the citrate-containing system required the optimisation of a formation constant for a mixed metal (U/Fe/citrate) aqueous complex, previously proposed by Manzurola *et al*. [1989]. Apart from this, all aqueous complexation reactions and ferrihydrite solubility were taken from the literature. U sorption reactions were exactly as given in Table 11.2, and did not require further optimisation. Although the system is complicated, this model is rather simple.

Uranyl was not represented in the comprehensive survey of surface complexation modelling on HFO by Dzombak and Morel [1990]. However, we now have a U sorption model that can simulate U sorption on ferrihydrite across a wide range of conditions, and in the presence of various ligands.

12 MODELLING INTERACTIONS OF URANYL WITH MODEL KAOLINITES

12.1 Modelling approach

Before modelling the data for U sorption on the Georgia kaolinites that were presented in Chapter 7, the entire collection of experimental data obtained in this thesis (on all substrates) was considered. As described in Chapter 10, it appears that the ferrihydrite, kaolinite and natural substrates are rather similar in their sorption behaviour, particularly in terms of the general shapes of the low- and high-pH edges, the effect of ΣU, and the ionic strength dependence. This suggests that the modelling approach for kaolinite should be similar to the one used for ferrihydrite.

Another factor which was taken into account when developing the kaolinite model was the proposed standardisation of approaches to surface complexation modelling which has been advocated by various authors [Dzombak and Morel, 1990; Davis and Kent, 1990; Turner and Sassman, 1996]. These authors have suggested that models should be as simple as possible, have a common surface site density and (in particular) should require a minimum number of adjustable parameters. As put by Turner and Sassman [1996], “while this approach may not represent the exact processes occurring at the interface, it limits the number of adjustable parameters and serves as a baseline for future comparison of modelling results”.

Thus, the modelling approach for kaolinite aimed to be as simple as possible. Given the similarities between the different substrates, it appeared that the best way forward was to attempt to model the kaolinite data using the SCM and similar types of reactions as used for ferrihydrite.

At the same time, however, it was required that the model should reflect the major conclusions of the experimental program. Therefore, the TiO_2 impurity phase in the model kaolinites needed to be taken into account. As discussed in Chapter 7, uranyl is preferentially adsorbed by this phase. Many authors have previously reported that TiO_2 is a strong U adsorber, and Ti-oxide has been suggested for concentrating U from sea-water (Chapter 3). As such, it was essential to model U sorption on the TiO_2 phase in the KGa-1 and KGa-1B

samples. This required a divergence from previous modelling approaches, which have not considered this possibility.

It must be emphasised that the omission of TiO_2 would not necessarily invalidate previous modelling of trace metal uptake on kaolinite, since the Ti-oxide may not be present in all kaolinites (although it appears to be ubiquitous in the Georgia kaolinites[1] which are commonly used as model sorbents). Furthermore, it may be that other metal ions do not show the same affinity as uranyl for the TiO_2 phase. However, considering the outcome of the experimental program, the TiO_2 must be accounted for in the present work, since ignoring its presence would inevitably lead to an incomplete model. The model to be developed for the KGa-1 and KGa-1B materials will therefore diverge significantly from models for similar systems reported in the literature. As such, the main criteria for model success will be restricted to its ability to model the experimental data obtained in the present study.

12.2 Stoichiometry and sites of surface reactions

Kurbatov plot

Although there are similarities between the sorption behaviour of ferrihydrite and kaolinite, they differ in one very significant respect. That is, the pH edge for ferrihydrite is much steeper (as mentioned in section 7.4), which indicates that the proton stoichiometry is not the same as for kaolinite.

Consider the surface reaction involving surface sites (>XOH) and uranyl:

$$n\ >XOH \quad + \quad UO_2^{2+} \Leftrightarrow (>XO)_n\ UO_2^{(2-n)} + n\ H^+ \qquad (12.1)$$

with an associated mass action equilibrium constant β. Here 'n' is the number of surface sites occupied by the adsorbing uranyl species. The following equation [Stumm, 1992] relates the concentration of occupied surface sites (U_{ads}) to the dissolved uranyl concentration:

[1] Jepson and Rowse [1975] reported that Georgia kaolinite and Cornwall (U.K.) kaolinite contained 1.21% and 0.09 wt.% of TiO_2, respectively. The composition reported for the Georgia kaolinite was very similar to the composition of the KGa-1 material given in Table 7.1.

$$\log [U_{ads}] / [U_{diss}] = \log \beta + n \log [>XOH] + n\ pH \qquad (12.2)$$

Assuming that the sorbent is present in large excess, the slope of the curve of $[U_{ads}] / [U_{diss}]$ against pH gives an indication of n, although this is only valid in circumstances where dissolved U is solely the UO_2^{2+} species. For the systems considered in this thesis, the hydrolysis and carbonate complexation of U become more important with increasing pH (Figure 3.1), making this simple graphical analysis inappropriate in the higher pH range.

For an adsorbing metal (Me), the curve of $[Me_{ads}] / [Me^{2+}]$ versus pH is known as a Kurbatov plot, and it is conveniently plotted as log D against pH, where D is equal to (%sorbed) / (100 - %sorbed) [Kinniburgh and Jackson, 1981]. These authors emphasise that the quantitative validity of the method is limited and the procedure is 'known to be suspect under certain conditions'. However, it can yield useful information about the surface reaction stoichiometry. The Kurbatov plot is most successful when the surface sites are present in a large excess (i.e. sorbate concentrations in the micromolar range if possible).

Figure 12.1 shows the experimental U sorption data for ferrihydrite and kaolinite (KGa-1B) in the form of pH-edges and Kurbatov plots. The Kurbatov plot is linear in both cases. The slopes of the curves are 0.85 ± 0.05 for kaolinite and 1.51 ± 0.05 for ferrihydrite. Kinniburgh and Jackson [1981] reported that the slope is often between 0.8 and 1.2 for alkaline earth cations, indicating that the exchange is closer to being equimolar than equivalent (i.e. n=1 rather than n=2). Considering the slope found for the kaolinite in this case, it seems reasonable to commence modelling U sorption on the basis that one uranyl is taken up by each kaolinite surface site. This contrasts with the bidentate surface complexes (occupying two sites) used for modelling U sorption on ferrihydrite. Thus, it appears that the surface reaction that seems most promising for the kaolinite is the following reaction of a single uranyl on a surface site (>XOH):

$$> XOH + UO_2^{2+} \Leftrightarrow > XOUO_2^{+} + H^{+} \qquad (12.3)$$

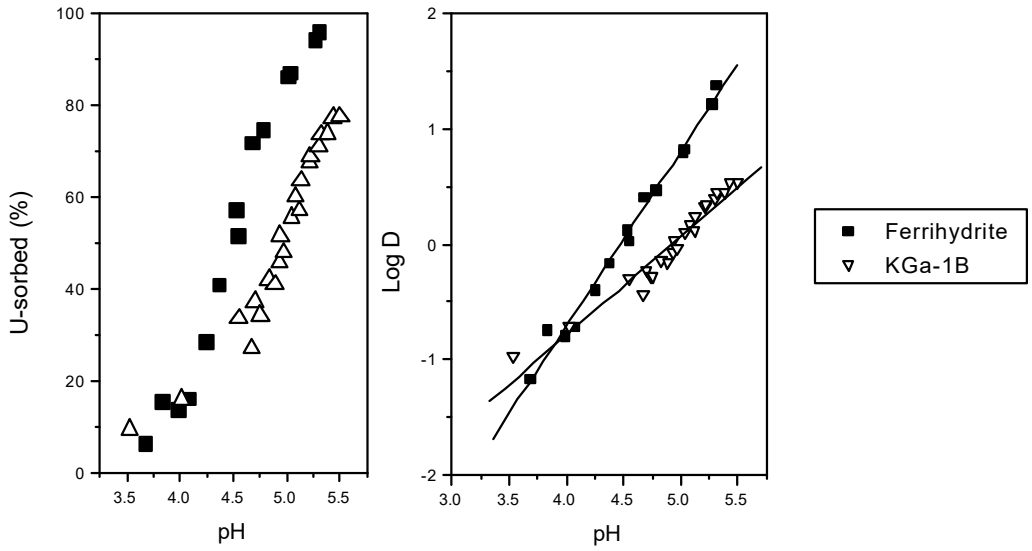


FIGURE 12.1 Adsorption edges and Kurbatov plots for uranyl adsorption on ferrihydrite and KGa-1B kaolinite (ΣU = 1 μmol/L, ferrihydrite mass loading 89 mg/L, kaolinite 4 g/L)

As well as indicating that the stoichiometry of reactions on the ferrihydrite and kaolinite surfaces are different, the Kurbatov plot also suggests that minor Fe impurity phases do not have a strong influence on U sorption by the Georgia kaolinites. This can be inferred from the dissimilarity of the U sorption results for the two materials. In some previous studies, chemical extractions have been used to remove any Fe-rich phases. Although no chemical extractions were carried out on the kaolinites used in the present study, the role of the TiO_2 phase (which has not been previously recognised) seems to be much more important than that of the Fe-oxides in the Georgia kaolinites.

Surface sites on the Georgia kaolinite samples

Kaolinite is a layer silicate, with the simple chemical formula $Si_2Al_2O_5(OH)_4$. Figure 12.2 shows its structure in schematic form. Three morphological planes of different chemical compositions exist at the surface: a

gibbsite layer, a siloxane layer and an edge surface which is a complex Al / Si oxide [Stumm, 1992].

As noted above, the U sorption model for the Georgia kaolinites should involve a set of surface reactions on a titanol (>TiOH) surface site. A further three types of sites would give the model a minimum of four sets of surface reactions, which appears to be too many for an initial modelling exercise. Furthermore, FITEQL cannot simultaneously optimise more than two unknown log K values. Therefore some simplifications to the system were required for modelling purposes.

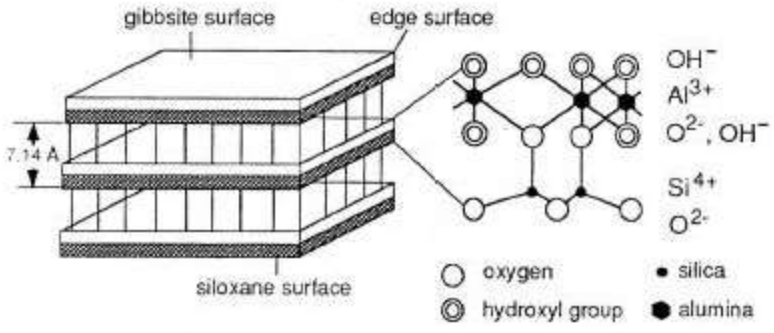


FIGURE 12.2 Schematic structure of kaolinite, showing the alternating silica-type (black) and gibbsite-type (white) layers. Aluminol and silanol groups are exposed at the edge surface [Stumm, 1992]

Previous modelling approaches for kaolinite have involved various simplifications. For example, Kohler *et al.* [1992] assumed that actinide binding on kaolinite only occurred on edge surface sites, which were modelled as aluminol (>AlOH) sites. This assumption was based on the outcome of parallel experiments with gibbsite (which only contains >AlOH sites) and quartz (only >SiOH sites), which showed that actinide uptake on the quartz was much weaker. The approach of Turner and Sassman [1996] was to assume that the kaolinite surface comprised stoichiometric proportions of silanol (>SiOH) and aluminol sites. This approach appeared promising, however the inclusion of U

sorption reactions (with unknown log K values) on both site types would still leave three log K values to be optimised with FITEQL.

The silanol sites are reported to undergo ion-exchange type reactions, particularly at low pH values [Stumm, 1992]. Given that an increase of ionic strength did not result in decreased adsorption of U in the region of the low pH edge (see Figure 7.7), ion-exchange reactions do not appear to be important for uranyl on kaolinite. As noted above, studies of U sorption have reported very little affinity of U for Si-oxide surfaces [Kohler *et al.,* 1992; Borovec, 1981]. Thus, it appeared reasonable to exclude U adsorption on silanol sites in the first instance.

Thus, the model adopted for the initial simulations of U sorption on the Georgia kaolinites assumed the presence of just two types of surface sites: titanol (>TiOH) and aluminol (>AlOH).

The aim was to optimise the log K values (using FITEQL) for the proposed surface reactions on the >TiOH and >AlOH sites, which satisfied the reaction stoichiometry suggested by the Kurbatov plot. Thus, the two reactions that were initially considered were:

$$> TiOH + UO_2^{2+} \Leftrightarrow > TiOUO_2^{+} + H^{+} \qquad (12.4)$$

$$> AlOH + UO_2^{2+} \Leftrightarrow > AlOUO_2^{+} + H^{+} \qquad (12.5)$$

12.3 Modelling U sorption on kaolinite with FITEQL and MINTEQA2

FITEQL model input

In order to model the surface reactions with the SCM, surface acidity constants and populations of the aluminol and titanol sites were required. Stumm [1992] gave the intrinsic acidity constants (pK^{s}_{a1} and pK^{s}_{a2}) of the groups at the edge surface as being 6.3 and 8.7, respectively, and noted that these are comparable to those of γ-Al_2O_3 (7.4 and 10). These values were adopted for the aluminol site. Acidity constants for the more acidic titanol site were taken from the same source (Table 12.1).

The estimation of the amounts of the two types of surface sites (>AlOH and >TiOH) was clearly a critical part of the modelling. One obvious approach was to make both site densities adjustable parameters, and optimise them using FITEQL (as was done for ferrihydrite). Although the results had been satisfactory in that case, this would increase the number of adjustable parameters for the kaolinite model to a minimum of four, even with only one reaction on each site. (Two more adjustable parameters would be needed if the weak and strong site densities were separately optimised on both Ti-oxide and kaolinite phases).

Another method which was considered for estimating the number of titanol type sites in the KGa-1 and KGa-1B kaolinites was to utilise the surface area of the two clays and their titanium content (Table 12.2). It was then proposed to estimate the proportion of the surface area contributed by the anatase phase, using a Ti-oxide surface area taken from the literature. The remainder of the surface area (which could not be accounted for by Ti-oxide) would then be attributed to kaolinite grains. In principle, the population of titanol sites and aluminol sites could then be estimated using the standard site density advocated by Davis and Kent [1990], i.e. 3.84 μmol/m^2.

TABLE 12.1 Kaolinite model input parameters
(pK values are corrected to I = 0.1)

	KGa-1	**KGa-1B**
U-binding >TiOH sites	0.42 μmol/g	0.49 μmol/g
pK^s_{a1} (I=0.1)	**4.81**	**4.81**
pK^s_{a2} (I=0.1)	**7.47**	**7.47**
U-binding >AlOH sites	2.49 μmol/g	2.48 μmol/g
pK^s_{a1} (I=0.1)	**6.19**	**6.19**
pK^s_{a2} (I=0.1)	**8.59**	**8.59**

The problem with this approach was that the surface area of the TiO_2 component of Georgia kaolinites was difficult to either measure or estimate. A brief survey of relevant literature uncovered a range of values for the surface area of TiO_2, including 59 m^2/g [Chang *et al.*, 1987] and 247 m^2/g [Mahal *et al.*, 1981]. It became obvious that this approach was going to involve a large number of poorly constrained or adjustable parameters.

After considering these options, it was decided to attempt to use the outcome of the AEM study to estimate the number of U-binding sites associated with the Ti-oxide and kaolinite grains in the KGa-1 kaolinite, and to use these estimates as input for the sorption modelling.

Estimation of >TiOH and >AlOH site densities for FITEQL input file

The data used in the following discussion were presented in Table 7.2. These data referred to the electron microscope examination of the KGa-1 material, which had been equilibrated with an aqueous phase containing a high concentration of U (100 μmol/L). It seems reasonable that surfaces of the Ti-oxide phase and the kaolinite grains were at (or near) saturation with adsorbed U, since a precipitated uranyl hydroxide phase was observed. Thus, one can use these data to estimate the amount of U-sorbing sites associated with the TiO_2 phase and the kaolinite grains in this sample.

Consider first the Ti-oxide phase, which comprises 1.39 wt % of the KGa-1 sample (i.e. 13.9 mg/g). The Ti-oxide was found to contain 0.71 wt % of adsorbed U, which means that about 98.7 μg of U was adsorbed to the TiO_2 contained in each gram of KGa-1. Assuming that one U is adsorbed to each surface site, this implies that there are 0.415 μmol of U-binding >TiOH sites per gram of KGa-1. Similarly, the kaolinite grains contain 0.06% by weight of U, and make up 98.61% of the solid by weight. Therefore, a gram of KGa-1 contains 2.49 μmol of U-sorbing >AlOH sites on the kaolinite grains.

The site populations on the KGa-1B were then estimated. The KGa-1B contains a higher proportion of TiO_2 than KGa-1, and it was assumed that the number of >TiOH sites would be proportional to the Ti content (there was no

AEM examination of this sample). Because kaolinite grains are assumed to make up the balance of the sample, the KGa-1B sample contains (relative to KGa-1) slightly fewer >AlOH sites associated with kaolinite grains (although this difference is very small). The U-sorbing site populations deduced for the KGa-1B sample were 0.49 μmol/g of >TiOH sites, and 2.48 μmol/g of >AlOH sites, per gram of sample.

Apart from making use of the AEM data, this approach had the significant advantage that none of the parameters in Table 12.1 were optimised by FITEQL. All were either estimated from the AEM results, or taken from the literature. Thus, the number of degrees of freedom of the model was minimised. This approach therefore meets the criteria of minimising the number of adjustable parameters, which was mentioned at the start of this section.

Choice of double layer model

The next stage of the modelling approach was to optimise the log K values for reactions 12.4 and 12.5 using FITEQL. It was originally planned to use the DDLM for electrostatic corrections throughout the FITEQL optimisation procedure. (The DDLM had previously been used in the case of ferrihydrite). However, FITEQL is not configured for this problem, as the proposed U sorption reactions on the titanol and aluminol sites are associated with different surfaces. FITEQL does not accommodate mixtures of two different types of sorbing minerals. The algorithms in FITEQL presuppose that only one solid phase is present and the surface potential of all site types is identical. This might be a realistic model for the present system if the titanol sites were spread uniformly through the kaolinite grains, in which case the surface potential would be the same for all sites. However, the SEM results indicated that the Ti-oxide is largely present as a discrete anatase phase.

A possible solution to this problem was to model the system using a non-electrostatic surface complexation model. In this approach, the electrostatic terms are excluded from the mass law equations for surface equilibria [Davis and Kent, 1990]. Consequently, surface functional groups are treated computationally in the same manner as dissolved ligands (without activity corrections) which FITEQL can readily accommodate. This approach is also

justifiable because for moderately or strongly sorbing ions, the chemical contribution to the free energy of adsorption dominates over the electrostatic contribution [Davis and Kent, 1990].

As in the case of the ferrihydrite modelling, it was intended to subsequently implement the proposed sorption model using MINTEQA2 (see below). The adequacy of the modelling approach will therefore be assessed on the basis of the proximity of the MINTEQA2 outcome to the experimental data points. Under these circumstances, it was expected that any inconsistencies developed during the parameter optimisation phase would become be obvious in the simulation phase.

FITEQL optimisation and modelling

For the first optimisation using FITEQL, an attempt was made to simultaneously derive the log K values for reactions 12.4 and 12.5, which refer to the adsorption of UO_2^{2+} on both the >TiOH and >AlOH sites. The Tableau used for this procedure is given in Table 12.2. It will be observed that the input tableau includes the parameters given in Table 12.1, together with all U species playing a major role in the low pH range. The complexity of the FITEQL optimisation was reduced by only considering the data for the low pH edge (pH < 6.5) and omitting uranyl carbonate complexes, which are not significant in the low pH range. The experimental data used in the optimisation procedure ('serial data' in FITEQL terminology) were the data-sets given in Appendix 1 for experiments with KGa-1 and KGa-1B (4 g/L loading), with ΣU of 1 μmol/L and 10 μmol/L.

It was soon found that model did not converge for all four data-sets, with particular difficulties associated with optimising log K for the postulated $>AlOUO_2^+$ surface species. Examination of the modelling outcomes indicated that the >TiOH site adsorbed strongly at lower pH values, whereas the >AlOH became more prominent in the higher pH range, in which the aqueous uranyl ion becomes hydrolysed (see also section 12.6). The U sorption reaction on the aluminol site was therefore modified to the following reaction:

$$>AlOH + UO_2^{2+} + H_2O \Leftrightarrow >AlOUO_2OH + 2H^+ \qquad (12.6)$$

Many authors have assumed that hydrolysed uranyl species are adsorbed [Tripathi, 1983; Turner and Sassman, 1996], and this appears reasonable, because hydrolysis and adsorption occur in the same pH range. It has also been suggested that the proximity of the surface actually favours or induces uranyl hydrolysis [Tripathi, 1983]. Therefore, the inclusion of reaction 12.6 in place of reaction 12.5 appeared justifiable. When this reaction was included, the model converged for all the data sets. The model outcomes are summarised in Table 12.3, which gives FITEQL estimates of the log K values for reactions 12.4 and 12.6 as determined separately for each data-set.

TABLE 12.2 Tableau for FITEQL input for experimental data with KGa-1B, mass loading of 4 g/L, ΣU of 1 µmol/L. Note that the serial adsorption data consisted of all data points below pH 6.5 (see Appendix 1).

A. FITEQL components and input values

ID	Name	log X	T	Type
1	UO_2[+2]	-6.0	1.00E-06	T(I)
2	TiOH	-5.0	1.96E-06	T(I)
3	AlOH	-4.0	9.92E-06	T(I)
4	NO_3[-]	-1.0	1.00E-01	T(I)
5	UO_2(ads)	0.0	0.00E+00	X&T(II)
6	H[+]	0.0	0.00E+00	X(III)

X – free concentration

T – total concentration

Type I - components for which only T is known

Type II – components for which both X and T are known

Type III – components for which only X is known

TABLE 12.2 (continued)

B. FITEQL species and stoichiometry matrix

ID	Name	log K[##]	UO2	TiOH	AlOH	NO3	UO2(ads)	H[+]
1	H [+]	0.0	0	0	0	0	0	1
2	OH [-]	-13.78	0	0	0	0	0	-1
3	UO_2 [+2]	0.0	1	0	0	0	0	0
4	UO_2OH [+]	-4.98	1	0	0	0	0	-1
5	$(UO2)_2(OH)_2$ [+2]	-5.85	2	0	0	0	0	-2
6	$(UO2)_3(OH)_5$ [+]	-16.22	3	0	0	0	0	-5
7	UO_2NO_3 [+]	-0.14	1	0	0	1	0	0
8	NO_3 [-]	0.0	0	0	0	1	0	0
9	$TiOH_2$ [+]	4.81	0	1	0	0	0	1
10	TiOH	0	0	1	0	0	0	0
11	TiO [-]	-7.47	0	1	0	0	0	-1
12	$AlOH_2$ [+]	6.19	0	0	1	0	0	1
13	AlOH	0	0	0	1	0	0	0
14	AlO [-]	-8.59	0	0	1	0	0	-1
15 [#]	$AlOUO_2$ [+]	-2 (fit*)	1	0	1	0	1	-1
16	$TiOUO_2$ [+]	-2 (fit*)	1	1	0	0	1	-1
15a [#]	$AlOUO_2OH$ [0]	-2 (fit*)	1	0	1	0	1	-2

* value to be optimised

[#] note that the model failed to converge with reaction 15 included. Consequently reaction 15a was substituted for reaction 15. See text.

[##] log K values are for I = 0.1

TABLE 12.3 Derivation of average values of log K for surface complexes

Data-set (see Appendix 1)		Data points	$TiOUO_2^{[+]}$	$AlOUO_2OH^{[0]}$
Clay	ΣU		log K (I=0.1)	log K (I=0.1)
KGa-1B	1 μmol/L	26	1.35	- 4.25
KGa-1B	10 μmol/L	9	1.19	- 4.34
KGa-1	1 μmol/L	9	1.68	- 4.35
KGa-1	10 μmol/L	8	1.48	- 4.49
Average			1.43 ± 0.21	- 4.36 ± 0.10

Table 12.3 shows that, as well as convergence being achieved for all four experimental data-sets, the individual derived equilibrium constants were in good agreement. It seemed pointless to use slightly different log K values for identical reactions on the two different clay materials. Consequently, average log K values for the two proposed surface reactions were determined by simple averaging of the data, which yielded log K values of 1.43 and –4.36 for reactions 12.4 and 12.6 respectively.

The next step was to check that the optimised log K values obtained from the FITEQL output were consistent with the experimental data. This was undertaken by running FITEQL again with a slightly modified input file. In this case, the log K values for the two reactions were entered as fixed parameters, and the amount of U adsorbed was determined. (In this mode, FITEQL is operating in a similar way as MINTEQA2). The outcomes of these simulations are shown in Figures 12.3 and 12.4.

The modelling results shown in these figures were considered to be quite promising. At this stage, only two log K values had been optimised. In comparison, the work by Sassman and Turner [1996] had resulted in a total of six optimised log K values for U adsorption on kaolinite (as discussed in more detail below).

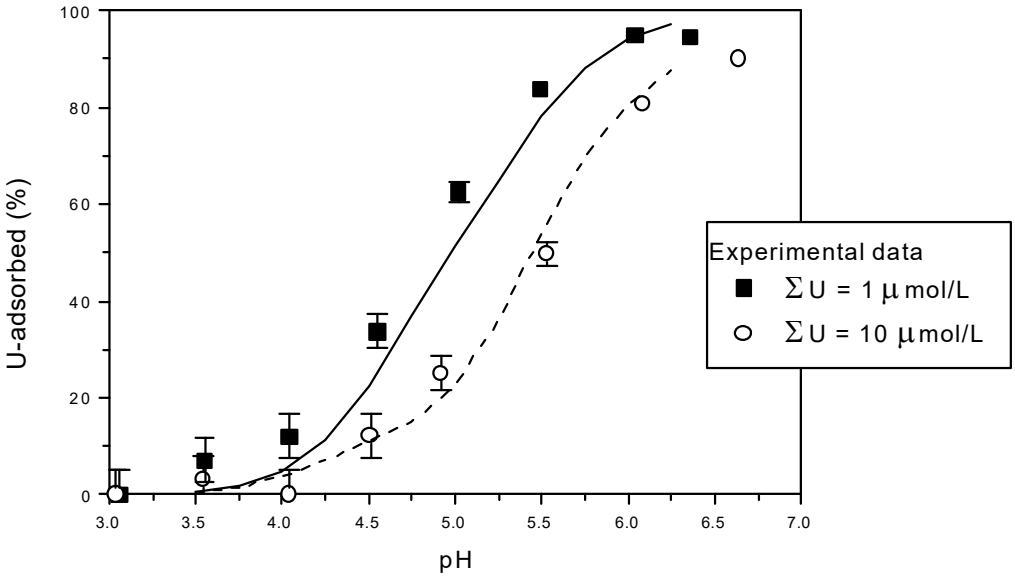


FIGURE 12.3 FITEQL model for KGa-1 data. Mass loading of KGa-1 was 4 g/L (ΣU of 1 μmol/L and 10 μmol/L).

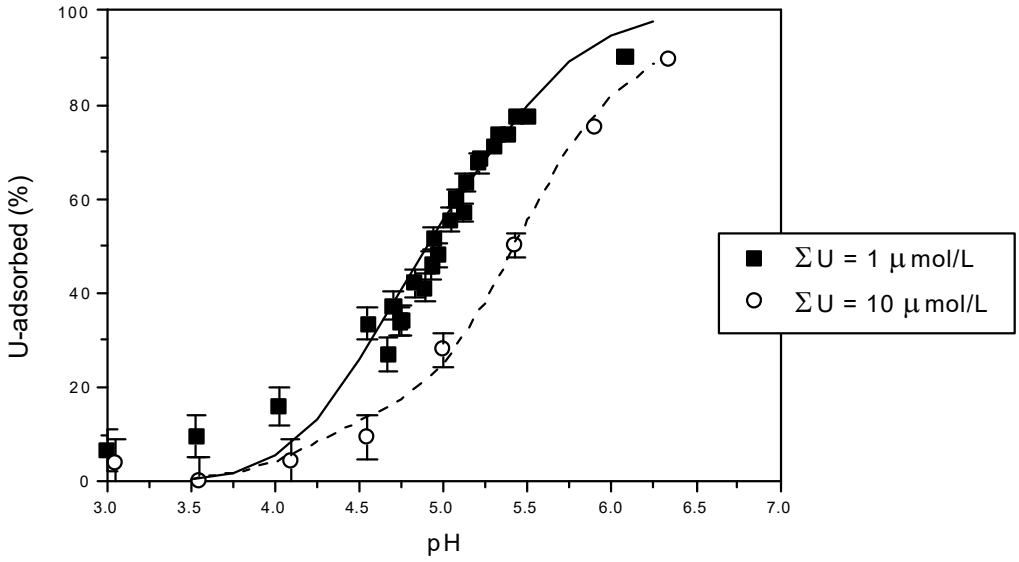


FIGURE 12.4 FITEQL model for KGa-1B data. Mass loading of KGa-1B was 4 g/L (ΣU of 1 μmol/L and 10 μmol/L).

MINTEQA2 modelling

The MINTEQA2 code was now applied to modelling the experimental data obtained across the entire pH range. These simulations used all the available thermodynamic data (Table 3.1) rather than the abbreviated version used in the FITEQL input for the low pH-edge (Table 12.2). In particular, all the carbonate-containing species, and equilibration with atmospheric CO_2, were now incorporated in the model. The two surface reactions (12.4 and 12.6) were also included, with the log K values shown in Table 12.3 (after adjustment to I = 0 as required for MINTEQA2 input).

The model implementation now resembled that used in the analogous modelling with ferrihydrite, with the exception that no electrostatic corrections were made for the log K values of surface reactions. This is because (as discussed above) a non-electrostatic model was used during the FITEQL optimisation procedure. Thus, the >TiOH and >AlOH sites were, in the model, computationally equivalent to uncharged aqueous ligands.

The model outcomes for data sets with the model kaolinites KGa-1 and KGa-1B (ΣU of 1 μmol/L and 10 μmol/L) are shown in Figures 12.5 and 12.6. For the data obtained for pH < 6.5 (used for the FITEQL optimisation), the results of the MINTEQA2 and FITEQL computation are virtually identical. Overall, the fits of the model curves to the experimental data are quite good, considering that the model contains only two optimised parameters. However, there was some inadequacy of the model to accurately simulate the data in the high pH range.

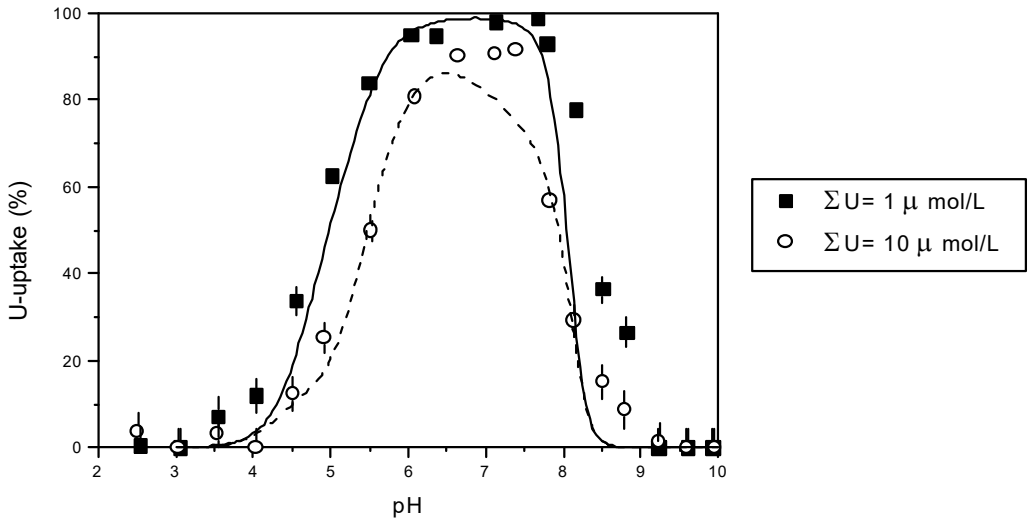


FIGURE 12.5 MINTEQA2 model for KGa-1 data over the pH range 2 to 10, using the log K values for surface species on the >TiOH and >AlOH sites shown in Table 12.3. Mass loading of clay was 4 g/L, background electrolyte 0.1 M $NaNO_3$.

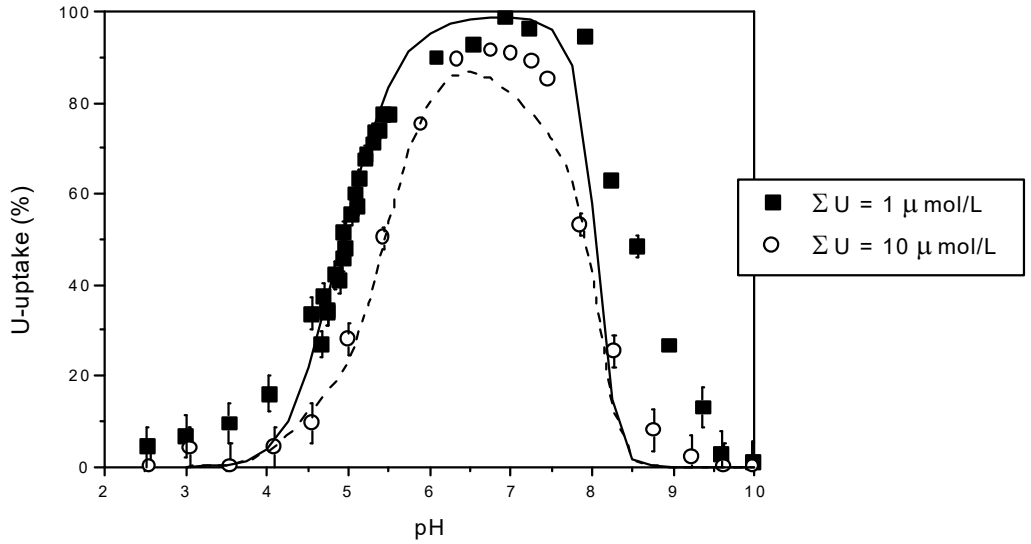


FIGURE 12.6 MINTEQA2 model for KGa-1B data. Experimental conditions similar to Figure 12.5.

12.4 Ternary uranyl-carbonato surface complex

Although the model simulations in Figures 12.5 and 12.6 fit the experimental data fairly well, the model failed to accurately simulate the U-sorption data obtained at higher pH values. For both sets of model simulations, the model high-pH edge for ΣU of 1 μmol/L was at a slightly lower pH value than the experimental data, Also, the sorption maximum with ΣU of 10 μmol/L was under-predicted and occurred at a slightly lower pH value than measured experimentally. In addition, examination of the MINTEQA2 output files (which indicates the relative proportions of individual surface species) showed that, in the model simulation, the >TiOH sites only adsorbed U across a limited pH range in the region of the low pH U sorption edge (see section 12.6). The AEM study indicated that these sites should be populated with adsorbed U in the neutral pH range.

Previously, a good fit to the ferrihydrite U-sorption data in the high pH range had been achieved by postulating a uranyl-carbonato surface complex (Chapter 11). Furthermore, Lieser and Thybusch [1988] had proposed that U-carbonato species were sorbed on TiO_2, because simultaneous adsorption of carbonate and U was observed. Finally, some early studies (discussed in Section 4.1) reported that TiO_2 was an optimal sorbent for concentrating U from seawater (which has a pH around 8). These observations implied that there could be an affinity between U-carbonate complexes and the TiO_2 surface. This suggested that the inclusion of a uranyl carbonate surface complex on the >TiOH sites would be warranted. Therefore, a ternary U carbonate surface complex was postulated for the >TiOH site, analogous to the type of complex that was used to fit the ferrihydrite data (Section 11.2).

The following reaction on the titanol site was therefore added to the suite of surface reactions:

$$> TiOH + UO_2^{2+} + CO_3^{2-} \Leftrightarrow > TiOUO_2CO_3^- + H^+ \qquad (12.7)$$

An appropriate log K value for this reaction was then estimated by running MINTEQA2 with various log K values and examining the model output. Based on its ability to simulate the experimental data, the log K value for

reaction 12.7 was estimated to be 12.0. The resulting model simulations are shown in Figures 12.7 and 12.8.

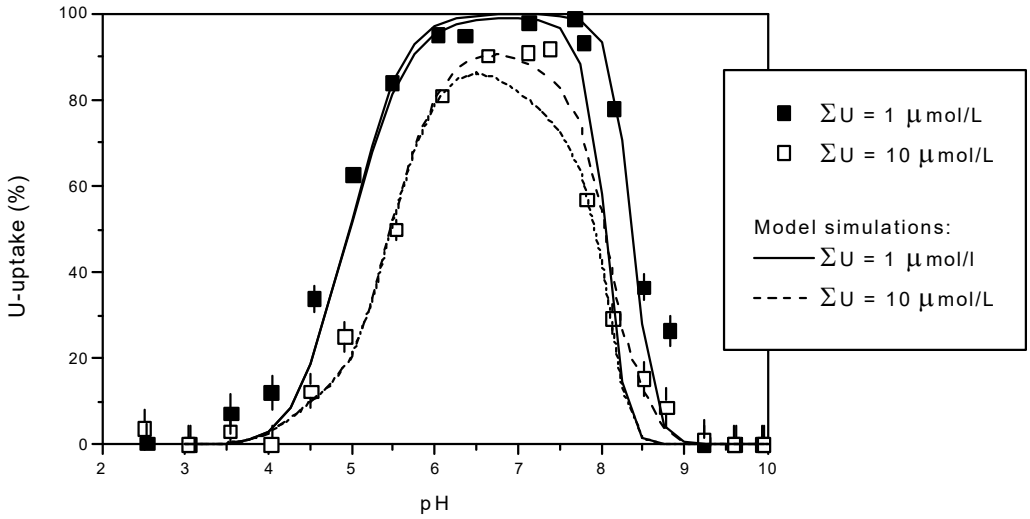


FIGURE 12.7 Model simulations for sorption data with KGa-1, showing the effect of the ternary uranyl carbonate complex on the >TiOH site (log K of 12.0 for reaction 12.7). Simulations including this complex are shown with bold lines or bold dashes. The previous simulations are shown with thinner lines and dashes.

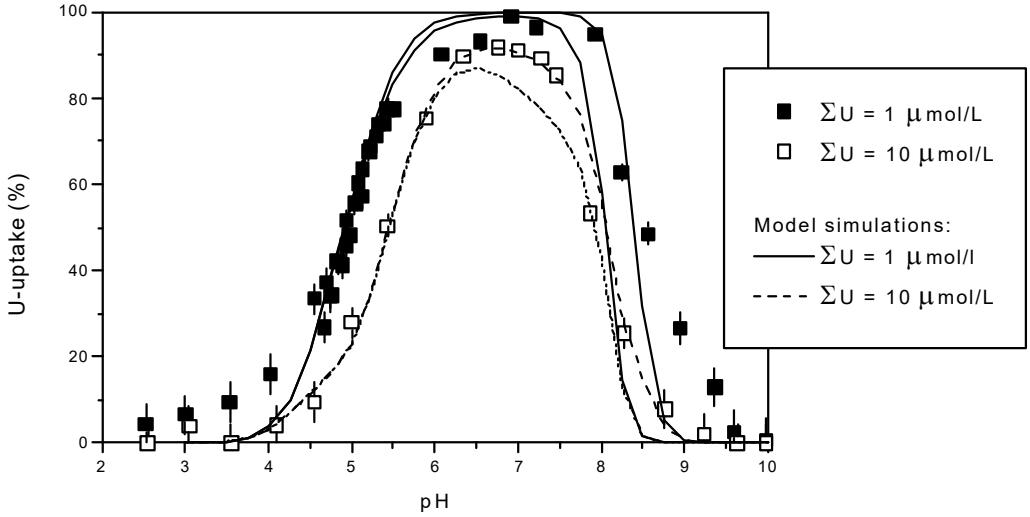


FIGURE 12.8 Model simulations for sorption data with KGa-1B showing the effect of the ternary uranyl carbonate complex on the >TiOH site (Reaction 12.7). Simulations including this complex are shown with thicker lines and dashes.

12.5 Comparison of model output with experimental data

The model simulations shown in Figures 12.7 and 12.8 indicate that the three adsorption reactions in Table 12.4 provide a good simulation of the experimental U-sorption data. The inclusion of the $TiOUO_2CO_3^-$ surface species significantly improves the fit of the model curves to the experimental data. The three proposed surface reactions, together with:

- the surface acidity constants and site populations given in Table 12.1, and,
- the full set of aqueous phase reactions in Table 3.1,

were then used to implement a MINTEQA2 model of all the experimental systems described in Chapter 7. In implementing this model, surface adsorbing sites were treated as uncharged ligands and the adsorption sub-routines in MINTEQA2 were not used. This is because there are no electrostatic terms in the model (as described above).

Figures 12.9 and 12.10 show the same data-sets discussed above, however only model curves for the final sorption model summarised in Table 12.4 are now included. Considering the range of pH and used in these experiments, and the associated change in U-speciation (as well as the different clay materials and ΣU) these model fits appear to be quite adequate.

The sorption data obtained with higher mass loadings were also adequately simulated by the model curves (Figures 12.11 and 12.12). There are slight discrepancies with the higher loadings, and another site on the >TiOH or kaolinite surface could be included to further improve the model. This could be justified on the basis that the model only contains three reactions on the two postulated sites, but this possibility is not further explored here.

TABLE 12. 4 Surface complexation reactions used to describe the experimental sorption data obtained with kaolinites KGa-1 and KGa-1B.

Surface	Reaction	Log K (I=0)
Ti-oxide	$>TiOH + UO_2^{2+} \Leftrightarrow >TiOUO_2^+ + H^+$	1.76
Kaolinite grain	$>AlOH + UO_2^{2+} + H_2O \Leftrightarrow >AlOUO_2OH + 2H^+$	-4.14
Ti-oxide	$>TiOH + UO_2^{2+} + CO_3^{2-} \Leftrightarrow >TiOUO_2CO_3^- + H^+$	12.0

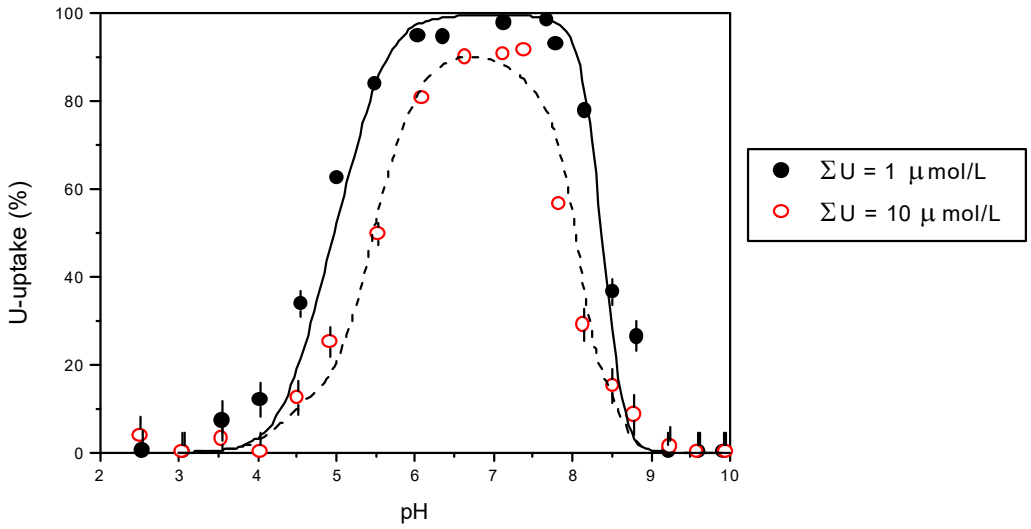


FIGURE 12.9 Model simulation of KGa-1 uranyl sorption data using reactions in Table 12.4.

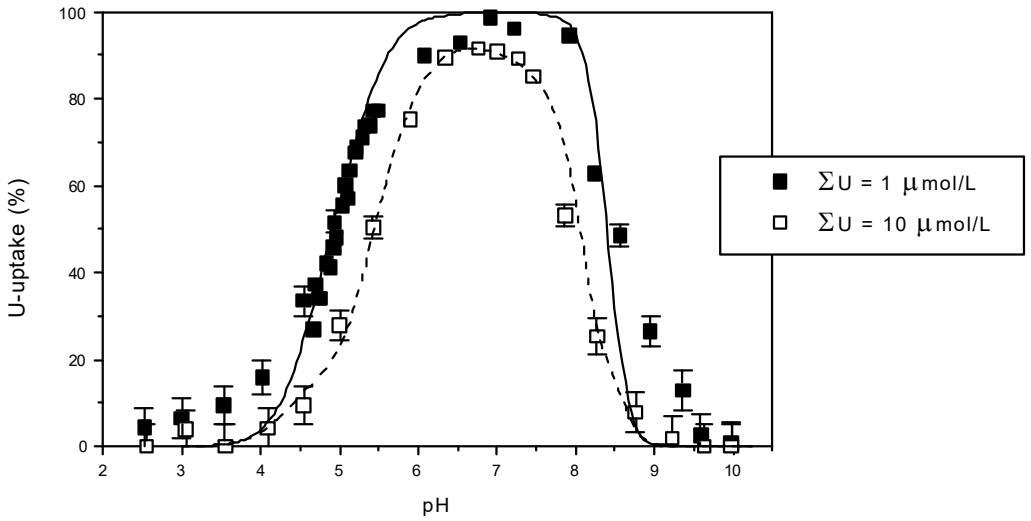


FIGURE 12.10 Model simulation of KGa-1B uranyl sorption data using reactions in Table 12.4.

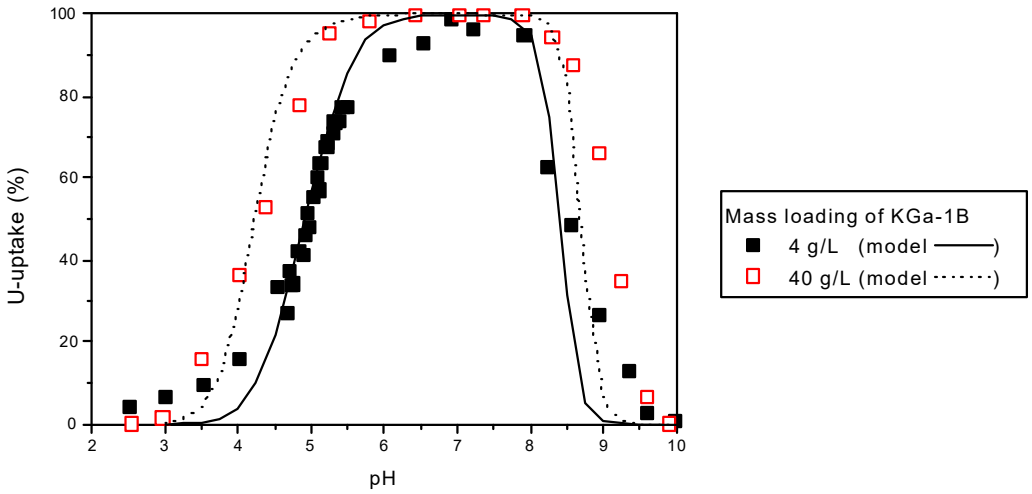


FIGURE 12.11 Modelling the effect of variable mass loading of the KGa-1B kaolinite in experiments with total U of 1 µmol/L.

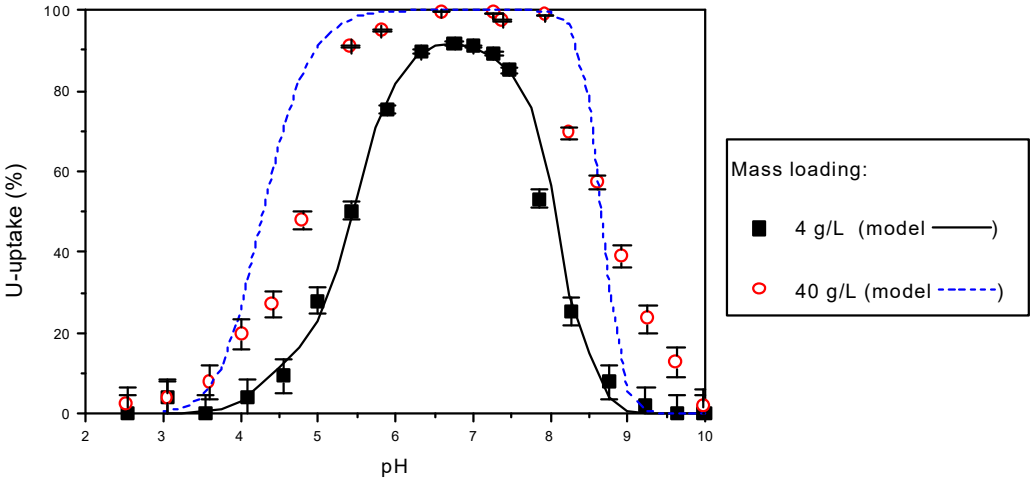


FIGURE 12.12 Modelling the effect of variable mass loading of the KGa-1B kaolinite in experiments with total U of 10 µmol/L.

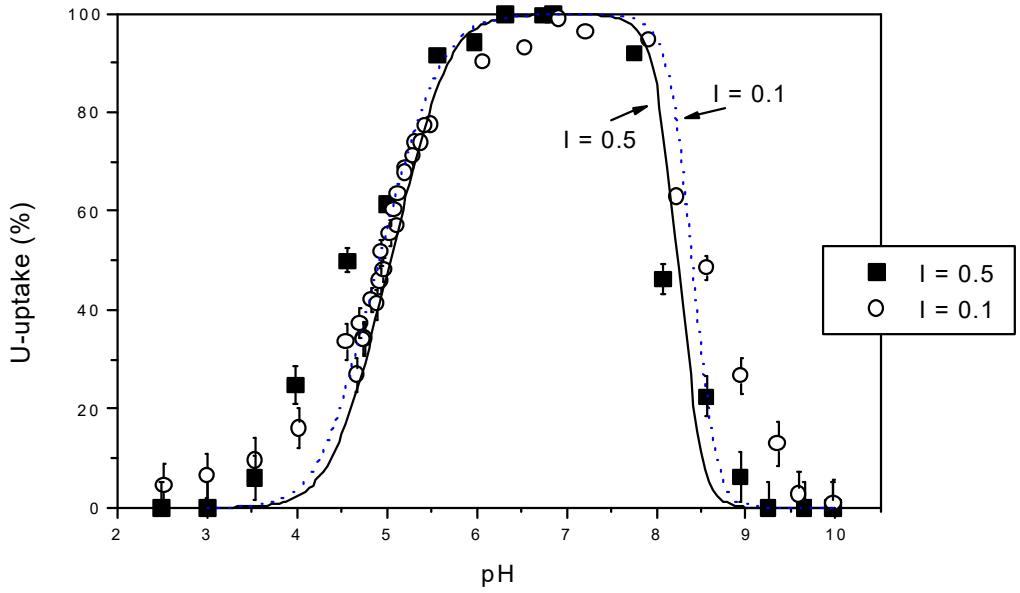


FIGURE 12.13 Modelling the effect of ionic strength on U sorption by the KGa-1B kaolinite. The model predicts a small decrease in U adsorption at high pH values, and this is reflected by the experimental data. However, the effect is small and the data set is inconclusive.

Figure 12.13 shows that a small decrease in sorption is predicted in the region of the high pH edge at higher ionic strength. As with the ferrihydrite model (discussed in Chapter 11), it appears that this effect is related to the aqueous phase activity of the highly charged uranyl-carbonate complexes. Another possible mechanism affecting the experimental U uptake could be competing sorption reactions, perhaps involving carbonate (similar to the carbonate or sulfate adsorption reactions on ferrihydrite). These reactions could be added to the simple non-electrostatic sorption model used for the kaolinite, but much more experimental data would be required to constrain the additional surface reactions.

The simulations of the results obtained with higher ΣU (100 μmol/L or 1 mmol/L) showed conclusively that the U-removal from the aqueous phase in these systems is dominated by precipitation rather than adsorption (Figure 12.14). In principle, the model fits could be further improved by adjusting the

solubility of uranyl hydroxide, which is poorly known (Section 3.3). However, the experiments were not designed with this in mind. The model fit is adequate to establish that the two processes occurring in the system (sorption and precipitation) are relatively well quantified and can now be readily differentiated from each other. As discussed in Chapter 7, the much steeper slope of the 'pH edge' appears to be a characteristic of precipitation of uranyl hydroxide. This sudden change in slope is well replicated in the model for the data obtained with ΣU of 100 μmol/L.

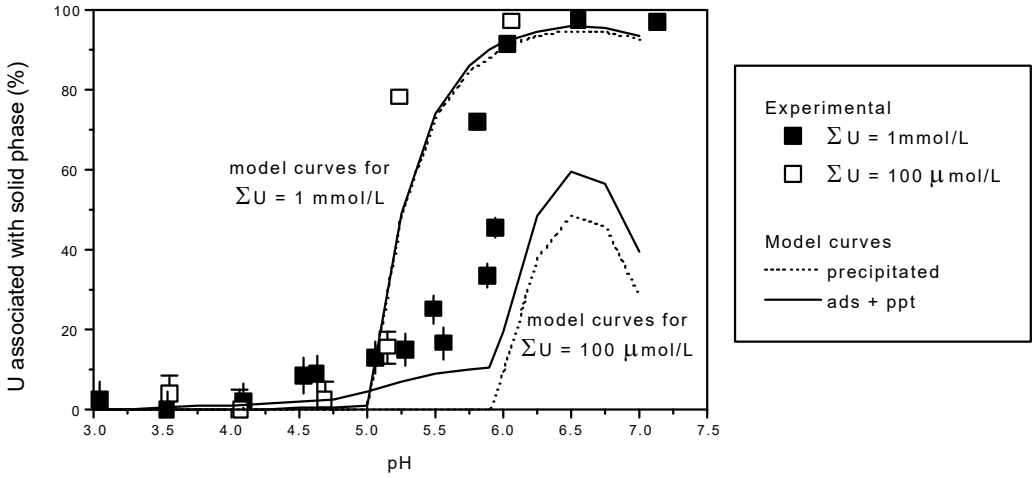


FIGURE 12.14 Simulation results for experiments with ΣU of 100 μmol/L and 1 mmol/L. Model curves are based on precipitation only (·····) and by adsorption and precipitation together (——). In the experiments with ΣU of 1 mmol/L, sorption plays no role in removing U from solution. In the experiments with ΣU of 100 μmol/L, a small amount of sorption occurs between pH 4.5 and 6.0, at which point a steep edge due to precipitation occurs. The model fit could be improved by adjusting the log K for the precipitation of amorphous $UO_2(OH)_2$.

12.6 Surface speciation of adsorbed U

The calculated speciation of surface-bound U provides some insight into the mode of binding of uranyl at the surface. At lower U concentrations (Figure 12.15), the >TiOH site is relatively more important than the aluminol site in adsorbing U, particularly at high and lower pH values. In contrast, the U binding with higher ΣU (Figure 12.16) is dominated by the weaker aluminol site.

The speciation diagrams show that the surface speciation of adsorbed U changes from adsorption of UO_2^{2+} at low pH, through UO_2OH^+ at intermediate pH values, to $UO_2CO_3^0$ at higher pH values. As such, the speciation reflects the changes in aqueous phase speciation.

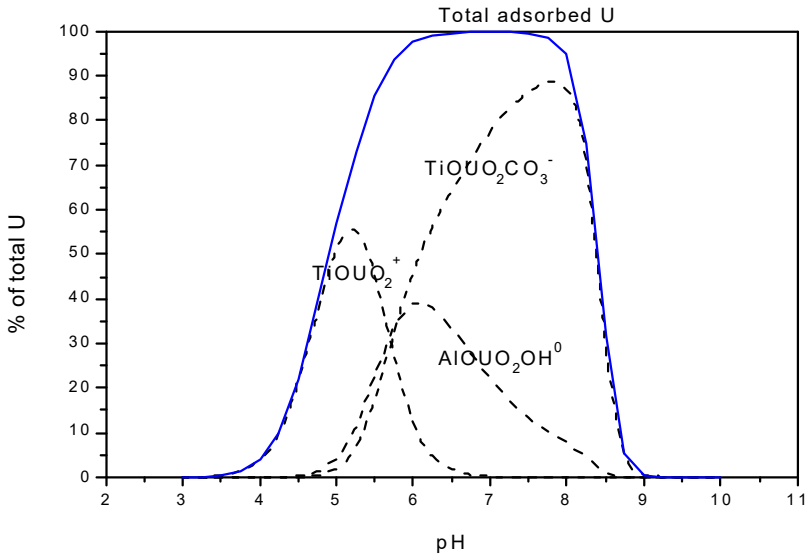


FIGURE 12.15 Surface speciation of adsorbed U in system containing 4 g/L of KGa-1B, with ΣU of 1 µmol/L.

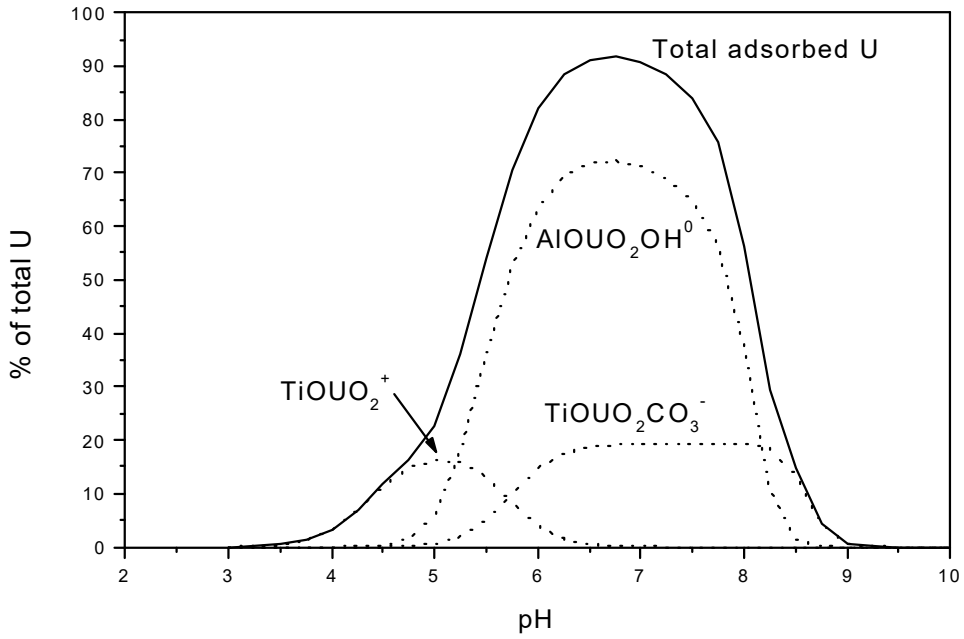


FIGURE 12.16 Surface speciation of adsorbed U in system containing 4 g/L of KGa-1B, with ΣU of 10 µmol/L.

The preference of uranyl for the stronger, less abundant >TiOH site could be quite significant. This is particularly noticeable with lower ΣU, when both the >TiOH and >AlOH sites are available in excess (Figure 12.15) In many experiments with relatively small amounts of U, the uptake of U on the kaolinite grains may be minor compared to the uptake on the TiO_2 phase. This observation may require some re-examination of the significance of kaolinite as a U-adsorber in the environment. An important role for kaolinite has been proposed by various authors including Thompson *et al.* [1994] and Giblin [1980]. The latter author gave few details of the clay material used in the experimental study. Thompson *et al.* [1994] studied a Georgia clay material denoted KGa-2. They reported its TiO_2 content as being 2.08%, which is higher than the two clays used in the present study. It is unclear how much this TiO_2 phase may have contributed to the promising sorption behaviour which they attributed to the kaolinite.

12.7 Comparison of U sorption models

As has been noted above, few previous detailed models for U sorption on kaolinite have been put forward. The model of Turner and Sassman [1996] contained six surface adsorption reactions with associated log K values optimised by FITEQL (Table 12.5). They assumed that the kaolinite surface consisted of stoichiometric proportions of $AlOH^0$ and $SiOH^0$ sites (i.e. a ratio of 1:1). It is possible that some of the proposed surface reactions would not play a significant role in the surface speciation of adsorbed U (this was not reported), in which case the model could be simplified by omitting some surface species. However, Turner and Sassman [1996] noted that the effects of carbonate would complicate the interpretation of the results, and more reactions would presumably be required to simulate the type of systems considered in the present work.

TABLE 12.5 Suite of uranyl surface co-ordination reactions and associated log K values for kaolinite [Turner and Sassman, 1996]. In their study, only the low-pH adsorption edge was modelled.

Surface complex	DDLM Log K
$SiO - UO_2^+$	0.96 ± 0.04
$AlO - UO_2^+$	2.18 ± 0.10
$SiO - UO_2OH^0$	-5.84 ± 0.44
$AlO - UO_2OH^0$	-4.74 ± 0.59
$SiOH - UO_2^{2+}$	5.73 ± 0.16
$AlOH - UO_2^{2+}$	9.20 ± 0.03

The log K values for the adsorption of UO_2^{2+} on a surface site to yield either >SiO-UO_2^+ or >AlO-UO_2^+ were 0.96 and 2.18 respectively (Table 12.5). These values are comparable to the log K for the analogous reaction on the >TiOH site in the present study (log K of 1.76). Similarly, the log K value of Turner and Sassman [1996] for the adsorption of the UO_2OH^+ species on the aluminol site (-4.74) is not dissimilar to the value of –4.14 deduced for the same reaction in the present study. However, these similarities may be of limited significance, as the modelling approaches were somewhat different.

It is also of interest to compare the U-sorption models used for ferrihydrite and kaolinite in the present study. This comparison is summarised in Table 12.6. The differences in modelling approach stem mainly from the available information about the surface sites. This information was derived from EXAFS in the ferrihydrite study, and relied mainly on AEM in the kaolinite work. While Table 12.6 tends to highlight the differences between the model outcomes for the two substrates, it should be borne in mind that there are many areas of similarity between the two models. These include the types of experimental sorption data available, the basic SCM approach, and the FITEQL optimisation procedure.

It is worth commenting on the site density used in this model. Based on the AEM results, the total site population of the KGa-1 sample was estimated to be 2.91 μmol/g (Table 12.1). However, a calculation based on the reported surface area of KGa-1 (8.7 m^2/g), and assuming a site density of 3.84 μmol/m^2 (as suggested by Davis and Kent [1990]), would give a total site population of about 33 μmol/g. A mass loading of 4 g/L would therefore correspond to about 134 μmol/L. of sorbing sites. When this mass loading was used in experiments with ΣU of 100 μmol/L, only a small proportion of the U was adsorbed, and precipitation of U occurred (Figure 7.4). In similar experiments with ΣP of 100 μmol/L, only a small proportion of P (10 - 20%) was taken up (Figure 7.10). If this system contained about 130 μmol/L of active sites, site saturation should not occur in these experiments, and more sorption (of both U and P) might be expected. This suggests that there may be considerably fewer U-sorbing sites sites on the KGa-1 surface than would be expected on the basis of the BET

surface area. Thus, the AEM estimate of site density appears more reasonable than normalisation on the basis of BET surface area in this case.

TABLE 12.6 Comparison of models for U sorption on ferrihydrite and model kaolinites.

	Ferrihydrite model	**Model of KGa-1 and KGa-1B**
Number of surfaces	1	2 (anatase and kaolinite)
Number of sites	2	2
Origin of strong site density	Optimised	Ti-site density derived from AEM examination
Origin of weak site density	Optimised	Al-site density derived from AEM examination
Presence of ternary carbonate complex	Inferred on both strong and weak FeOH sites	Inferred on strong (TiOH) site
Structure of weak-site surface complex	Outcome of EXAFS	Inferred from FITEQL computations
Stoichiometry of strong-site surface complex	Kurbatov plot, and assumed to be the same as the weak complex.	Kurbatov plot
Types of complexes	2	3
Optimised log K values	• strong-site surface U complex ($SO_2UO_2^0$) • weak-site surface U complex ($WO_2UO_2^0$) • strong-site surface U-carbonate complex ($SO_2UO_2CO_3^{2-}$) • weak-site U carbonate complex ($WO_2UO_2CO_3^{2-}$)	• strong-site surface U complex ($TiOUO_2^+$) • weak-site surface U complex ($AlOUO_2OH^0$) • strong-site surface U-carbonate complex ($TiOUO_2CO_3^-$)
Number of optimised parameters	6	3

12.8 Modelling the effect of sulfate and citrate on U sorption by kaolinite

As was discussed in Chapter 7, the effect of sulfate on U sorption by kaolinite was very minor. The U-sulfate-kaolinite systems were simulated by adding the complexation reactions between uranyl and sulfate to the model (Table 12.4). The computational results indicated while some aqueous complexation between SO_4^{2-} and UO_2^{2+} occurs, the presence of sulfate in the experimental system does not significantly influence the adsorption of uranyl (Figure 12.17). Thus, the model and experimental results were in agreement.

Modelling the phenomena involving citrate is a more complex undertaking. The complexation reactions between citrate and uranyl were included in Table 3.1. As shown in Figure 3.7, citrate complexation significantly affects U speciation (ΣU of 1 μmol/L) up to a pH of about 8 (for ΣCIT of 10 mmol/L) or pH 7 (ΣCIT of 100 μmol/L). In the sorption experiments, the presence of 10 mmol/L citrate completely suppressed U sorption over the entire experimental pH range (2 - 10), as shown in Figure 12.18.

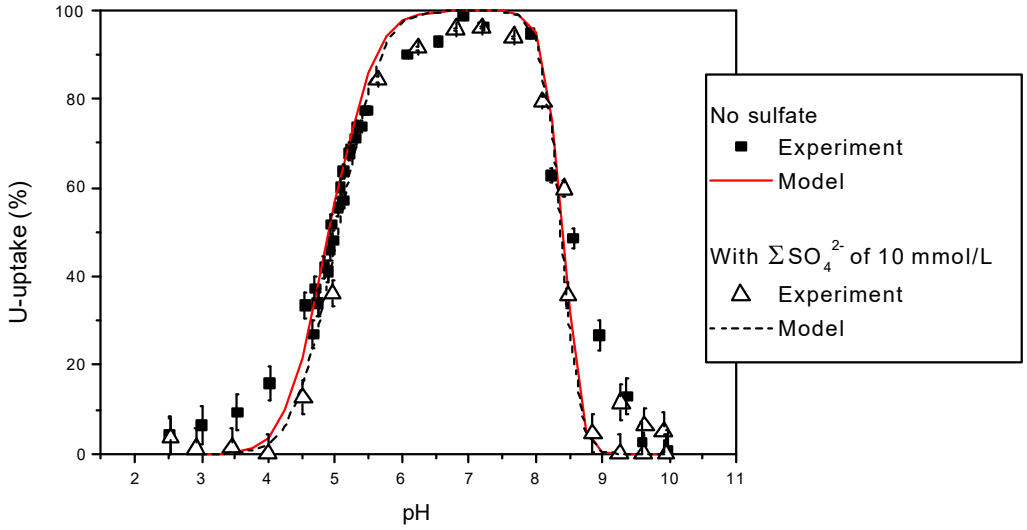


FIGURE 12.17 Modelling the effect of sulfate (10 mmol/L) on U sorption by kaolinite. Sulfate complexation of uranyl is weak, and neither the model nor the experimental data show any significant effect of the presence of sulfate.

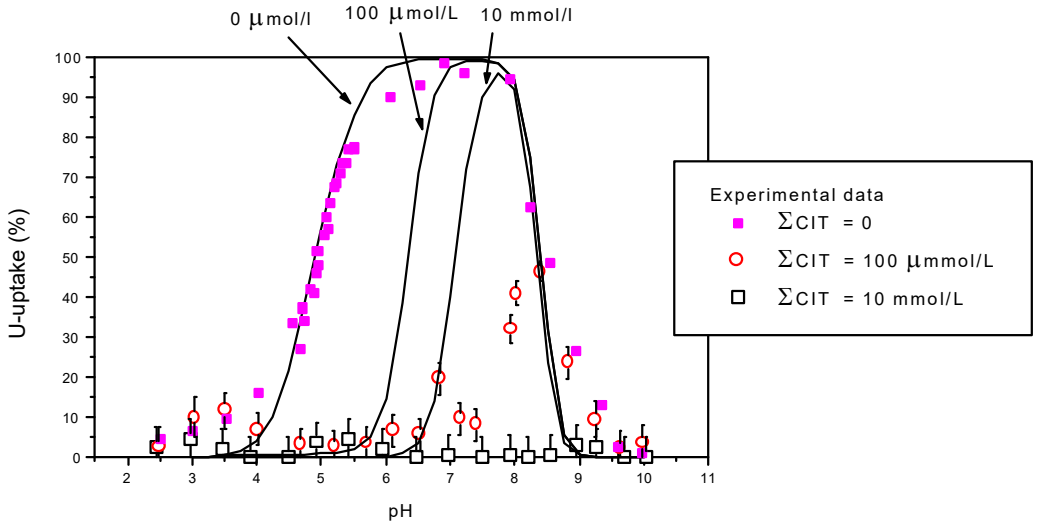


FIGURE 12.18 Modelling the effect of citrate on U sorption. In this simulation, only U-citrate complexation was considered. The poor model fits indicate that the experimental decrease in U sorption in the presence of citrate cannot be solely attributed to aqueous phase uranyl-citrate complexation. As with the analogous ferrihydrite system, other interactions would need to be included.

Given that the effect of citrate on U sorption occurs over this wide pH range, it might be expected that complexation between aqueous uranyl and CIT^{3-} would not, by itself, fully explain the large decrease in U uptake. This was confirmed by the model simulations, which predicted that even with complexation between citrate and uranyl included, some sorption of U should occur between pH 7 and 9 in the presence of 10 mmol/L citrate (Figure 12.18). Similarly, with ΣCIT of 100 µmol/L, a substantial decrease in U sorption was predicted, but the predicted U uptake was still greater than that found experimentally.

The U / kaolinite / citrate system is a complex one, and insufficient data are available to model it at present. Many of the reactions discussed in the analogous U / ferrihydrite / citrate system are relevant. In particular, one would need to model the possible competition for surface sites between uranyl and citrate, which would be expected to reduce U sorption. The amount of citrate in these systems is 10 mmol/L, which is greater than the combined number of

aluminol and titanol surface sites (about 10 μmol/L). With such an excess of citrate, it is very likely that the measured decrease in U sorption is partly due to competition for surface sites between citrate and uranyl. However, other interactions are conceivable, including adsorption of ternary uranyl citrate complexes, and the possible presence of mixed metal Al-U-citrate complexes (a detailed discussion of the analogous U-Fe-citrate aqueous complex was given in section 11.7). It is possible (but less likely) that some impurity Fe may also be desorbed by citrate and a mixed metal (U-Fe-citrate) complex could form by this route.

In summary, the experimental data for the uranyl / citrate / kaolinite systems provide a useful insight into the mechanisms affecting U sorption at the kaolinite surface in the presence of organic ligands. It appears that the observed decrease in adsorption results from complexation between U and citrate in the aqueous phase, and competition between U and citrate for surface sites. However, in this case, only a qualitative explanation is possible. Modelling this system fully would require detailed data on the amount of aqueous citrate, Al and possibly Fe across a wide range of experimental conditions.

12.9 Summary of SCM for U sorption on kaolinite

The model for uranyl sorption on model kaolinites (KGa-1 and KGa-1B) was fairly simple, compared to the model for ferrihydrite and to previous models for the U-kaolinite system. Despite its simplicity, the model accounted for U sorption under a wide range of experimental conditions. The presence of the TiO_2 impurity in the model kaolinites was taken into account, and the system was modelled as a combination of titanol and aluminol sites, using a simple non-electrostatic surface complexation model involving only three surface reactions. The relative amounts of U-binding >TiOH and >AlOH sites were estimated from the AEM results. Precipitation was taken into account in modelling the experimental data obtained with high U concentrations.

The model contained only three optimised log K values, and no other optimised parameters. The types of surface reactions were initially based on a Kurbatov plot of the low pH adsorption edge, with other surface species added subsequently to improve the model simulations at higher pH values. The

proposed hydrolysed surface species was in agreement with several claims in the literature that hydrolysed uranyl species are adsorbed to form surface complexes. There was also a literature precedent for the inclusion of ternary uranyl carbonato complex on a titanol site, and this further improved the fit of the model to the experimental data.

Sulfate had a small effect on U sorption, which may be explained by complexation in the aqueous phase. Citrate had a greater effect, and this was not wholly explained by complexation to form aqueous U-citrate complexes. The most likely explanation would also involve competition for surface sites between U and citrate. A mixed metal (Al-U-citrate) complex, analogous to the one suggested for Fe-U-citrate, may play a role in this system. It would be profitable to carry out a detailed study of citrate sorption on model clays as a precursor to metal adsorption studies in ternary systems.

This is believed to be the first time that the AEM technique has been applied in a study of metal sorption on a mixed phase. The AEM examination provided the first indication that the minor Ti-oxide phase in the model kaolinites plays an important role in U-sorption. Consequently, the titanol site was included in the modelling. The relative numbers of U-sorbing titanol sites and aluminol sites were estimated from the AEM data. This technique will be applied to more complex natural substrates such as the Koongarra materials in the future.

The presence of the TiO_2 phase in the Georgia kaolinites has been noted since the 1960's. Titanium oxide is known to be a strong U sorbent, and at one time was favoured for the purpose of concentrating U from sea waters. Despite this, the Georgia kaolinites have been widely used as model sorbents. One study with this material led to the conclusion that kaolinite is a very strong U adsorber, thereby ignoring the possible role of the TiO_2 phase. The >TiOH sites probably play an increasingly important role at lower uranyl concentrations

The abundant Ti-oxide grains in the Georgia kaolinites may limit the applicability of these materials as model minerals in trace metal sorption experiments. The use of these materials as reference clays for sorption work needs to be re-evaluated.

13 URANYL SORPTION IN PHOSPHATE-CONTAINING SYSTEMS

13.1 Possible mechanisms of surface interactions between uranyl and phosphate

In addition to carbonate, which is ubiquitous in experimental systems equilibrated with air, four complexing ligands were systematically studied in the experimental work described in this thesis. These were phosphate, sulfate, citrate and humic acid. The effects of citrate and sulfate were discussed and modelled in Chapters 11 and 12. A relatively small amount of data for systems containing humic acid was obtained. The subject of humic acid (and other forms of natural organic matter) and its effects on metal complexation and sorption is a vast area into which this thesis will not probe further.

This chapter, which concludes the modelling part of this thesis, addresses the subject of phosphate. As noted in Section 6.4, phosphate is of potential significance in the migration of U at the Koongarra deposit. A considerable amount of data for U sorption on both kaolinite and ferrihydrite was obtained in phosphate-containing systems. The similarities of the results obtained with kaolinite and ferrihydrite suggested that these substrates should be discussed together. This parallel treatment enables some possible mechanisms of interactions to be validly excluded from consideration, as will be shown below.

The objective of this chapter is to therefore to modify the sorption models for uranyl on ferrihydrite and kaolinite (Tables 11.2 and 12.4) to incorporate the phenomena involving phosphate (discussed in detail in Sections 6.4.1 and 7.5.1). Several mechanisms of uranyl-phosphate interactions were considered as being possible contributors to the observed increase in U uptake in the presence of phosphate, and these possible processes are considered in the following sections.

Precipitation of U-phosphate minerals

The first possibility considered was that precipitation may have occurred in these experiments. Precipitation of uranyl hydroxide at high ΣU was

previously taken into account in modelling U uptake on kaolinite in ligand-free systems (see Figure 12.14). Therefore, it was feasible that precipitation of uranyl phosphates could play a role in systems in which phosphate was present (see Section 3.3). Calculations using MINTEQA2, together with the uranyl / phosphate complexes and solids from the NEA data base [Grenthe *et al.,* 1992], showed that precipitation of $(UO_2)_3(PO_4)_2.4H_2O$ was possible between pH values of approximately 4.75 and 7.25 for systems with ΣU of 10^{-6} mol/L and ΣPO_4 of 10^{-4} mol/L, if no sorbing solids were present (see Figure 3.9).

The solubility calculations are more readily compared to experimental data when presented in the standard sorption-edge format used throughout this thesis. The calculated percentage removal of U due to precipitation of $(UO_2)_3(PO_4)_2.4H_2O$ is shown in Figure 13.1, together with experimental data for the uranyl-phosphate-ferrihydrite system. The general trends in the experimental results were similar to the phosphate-free systems, in which U uptake was attributed to adsorption. In particular, the curves do not exhibit the sharp edge predicted for precipitation, but rather the typical S-shaped sorption edge. As with the phosphate-free systems, the curves move to the right with increasing ΣU (i.e a decreasing percentage of U uptake with higher ΣU). Therefore, the experimental data show the same trends as found in phosphate-free systems, in which sorption was the dominant process.

If precipitation is occurring, increasing ΣU by a factor of 100 would greatly increase the proportion of U lost from the aqueous phase, and the edges would move to the left (Figure 13.1). This would be analogous to the movement of the precipitation 'edges' in Figure 12.14, where the curve for ΣU of 1 mmol/L is to the left of that found for ΣU of 100 μml/L. However, this is the opposite to the observed trend in the experimental data in Figure 13.1, indicating that sorption is a more likely mechanism of U removal from the aqueous phase.

Figure 13.1 was calculated on the basis that no removal of U from the aqueous phase occurred by adsorption. When ferrihydrite is present (and the equilibrium concentrations of U and phosphate are greatly reduced by sorption) precipitation is even less likely. In fact, no super-saturation was predicted across the full pH range for experiments with ΣU of 1 μmol/L when ferrihydrite was present.

Figure 6.12 showed that, for ΣU of 1 μmol/L, the presence of phosphate increased U sorption in the pH range below 4.5, in which no precipitation is possible, even in the absence of ferrihydrite. Further evidence that precipitation of U-phosphate phases is not responsible for removing U from solution in these experiments comes from the similar experiments with kaolinite (particularly the data shown in Figure 7.11) in which much higher equilibrium concentrations of both U and phosphate were measured for pH values below 6. This would not be expected if precipitation was occurring in the experiments with ferrihydrite.

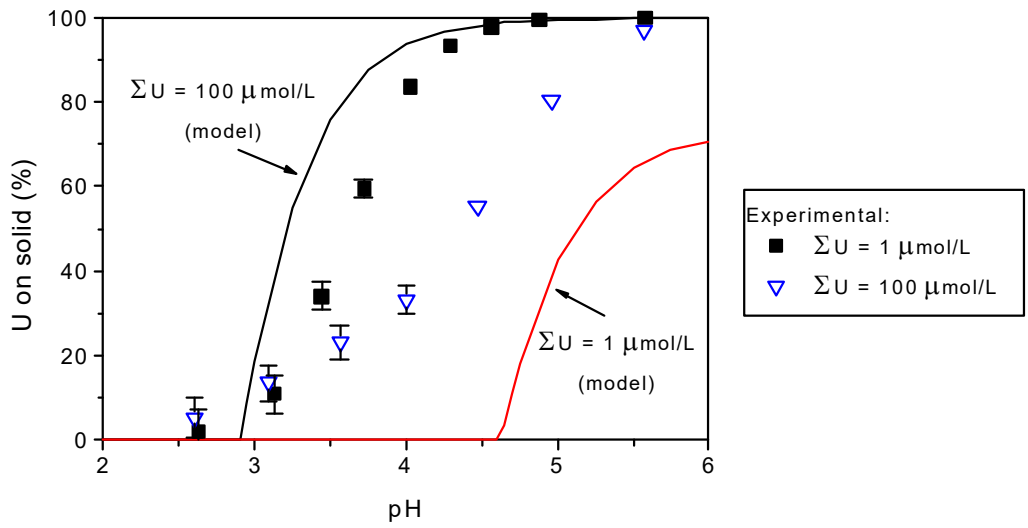


FIGURE 13.1 U uptake on ferrihydrite with added ΣP of 100 μmol/L. Data are presented as U associated with the solid as a function of pH. The model curves were calculated on the basis that U removal from solution occurs by precipitation of $(UO_2)_3(PO_4)_2.4H_2O$. The curves provide a poor fit to the data. Whereas the experimental curve for ΣU of 100 μmol/L is to the right of the curve for ΣU of 1 μmol/L, the precipitation model predicts the opposite. In addition, the distinctive S –shaped sorption curve of the data is absent in the model. (ΣFe = 1mmol/L).

Figure 3.9 indicated that precipitation of sodium autunite is hypothetically possible in some experimental systems. However, the precipitation of this phase is considered to be very unlikely for kinetic reasons. As discussed in Section 10.2, this possibility can also be readily excluded because the loss of U from the aqueous phase is not greater at higher sodium concentrations. In many experiments, an increase in Na concentration actually decreased the amount of U removed from the aqueous phase.

Further evidence that precipitation of uranyl phosphate minerals cannot explain the results is that the enhancing affect of phosphate on U removal from solution occurs at very low concentrations of dissolved uranyl. Figure 6.16 showed that P increased U removal from the aqueous phase at pH 4.5, with dissolved U of 10^{-8} mol/L. At this low concentration of U, none of the minerals in Figure 3.9 would be expected to precipitate.

Finally, according to literature surveyed in Section 3.3, the more soluble phase $UO_2HPO_4.4H_2O(s)$ is generally the first precipitate to form, rather than the sodium autunite or sodium orthophosphate phases. The soluibility of $UO_2HPO_4.4H_2O(s)$ was not generally exceeded in the experimental systems. The accumulated evidence therefore shows that precipitation of U-phosphate minerals can be excluded as an explanation of the experimental phenomena.

Surface precipitation

Another possible mechanism of surface interactions between phosphate and metals has been suggested by Benjamin and Bloom [1981], who studied adsorption of Zn on ferrihydrite. Their experimental system contained equal amounts of phosphate and Fe (10^{-3} mol/L), and it was proposed that a secondary surface phase formed in the presence of strongly sorbing anions (such as phosphate), and that this phase adsorbed trace metals more strongly than the original ferrihydrite. Benjamin and Bloom [1981] hypothesised that adsorption was the dominant mechanism at low surface coverage and that there was some surface density at which an iron-anion surface precipitate starts forming.

The U-PO_4-ferrihydrite systems studied in the present work contain an order of magnitude more Fe than phosphate, and it appears that the uptake of

phosphate could be explained by sorption alone, particularly as the number of available surface sites on the ferrihydrite considerably exceeds the total P concentration. Examination of Figure 6.17 shows that when the P concentration was increased (in the absence of U) site saturation was approached, and the uptake of P consequently decreased. In systems containing approximately equal amounts of P and Fe (i.e. $\Sigma P = \Sigma Fe = 1mmol/L$) there was only a small proportion of P associated with the solid. This observation strongly suggests that there was not a significant amount of P precipitating as ferric phosphate.

Nonetheless, surface precipitation of a second solid phase (such as ferric phosphate) could influence the experimental results, particularly if it bound uranyl very strongly. The possibility of surface precipitation was discussed by Dzombak and Morel [1990], who included it in their overall SCM for adsorption at the ferrihydrite surface.

It would appear that precipitation of ferric phosphate can not explain the enhanced U removal from the aqueous phase in the sorption experiments with kaolinite. This means that in this case another explanation is required. Given that other possibilities have now been excluded, it would be reasonable to invoke a ternary surface complex of the type proposed by Davis and co-workers [Davis and Leckie, 1978; Davis and Kent, 1990]. While this reasoning does not prove that the same type of mechanism also operates in the ferrihydrite-U-phosphate system, it would be consistent to assume that a similar type of ternary surface complex is present in that case also.

Ternary surface complex

The most likely cause of the shift in the low pH edge to the right with increasing ΣU is that sorption plays a major role in the systems containing phosphate. With this mechanism of U removal from solution, uptake at low ΣU occurs on energetically favorable sites, and on less favoured sites with increasing ΣU, both in the presence and absence of phosphate. This would be a reasonable explanation of the data shown in Figure 13.1, and is based on a sorption mechanism.

A ternary surface complex involving both U and phosphate is therefore a reasonable explanation of the experimental results with both ferrihydrite and kaolinite. It is possible to speculate as to the nature of the surface complex. As observed by Leckie [1994], the presence of complexing ligands can cause the formation of 'metal-like' or 'ligand-like' ternary complexes. The U sorption phenomena obtained in the presence of phosphate (Section 6.4.1) were similar to the trends already established for uranyl sorption, although the edges were slightly displaced along the pH scale. Another relevant observation is that phosphate was only weakly attracted to the kaolinite surface, yet U-sorption was strongly increased by the presence of P (see Figure 7.10). These considerations suggest that the binding of the ternary complex at the surface would be via the uranyl ion, that is, a metal-like ternary complex.

While the exact structure of the complex at the surface is uncertain, this does not directly affect the FITEQL calculations discussed below, as these computations relate to the stoichiometry. However, these considerations give some indication of the best way to proceed in terms of postulating surface complexes, and it will be assumed in the first instance that the structure of a surface complex in the presence of phosphate would involve similar U-Fe surface co-ordination to the ligand-free case.

13.2 Modelling the U-phosphate-ferrihydrite system

Phosphate sorption on ferrihydrite

The first step in modelling the U-PO_4-ferrihydrite system is to model the uptake of phosphate on the ferrihydrite. It must be noted at the outset that the experimental data obtained in the present study are not sufficient to provide the level of model detail that has been accomplished in the case of U sorption. Nonetheless, it is clearly desirable to have the phosphate model as realistic as possible. This is because the behaviour of the two species are inter-linked through aqueous complexation and by possible competition for surface sites, as well as by the formation of any ternary surface complexes.

It was hoped to use an existing model for the P-ferrihydrite system taken from the literature. Unfortunately, there is no consensus about how to model P

sorption on ferrihydrite. Another problem was that the experimental systems in the present study are somewhat different from those described in the literature, in terms of the ferrihydrite preparation, the concentration of phosphate, the equilibration with air and the presence of uranyl. There is also the model constraint (previously encountered with modelling sulfate) that the site density used in the U-ferrihydrite model was optimised to fit the U sorption data. Therefore, it does not conform to the standard density advocated by Dzombak and Morel [1990]. As such, re-derivation of log K values associated with any previous model would be required before it could be applied to the present experimental systems. Therefore, it was decided to develop a simple P sorption model that would explain the data. In this process, it was recognised that the data set is not sufficient for a detailed model similar to the one developed for uranyl sorption.

There has been some debate in the literature about whether the surface complex of phosphate on the Fe-oxide surface is bidentate or monodentate. Dzombak and Morel [1990] assumed the latter surface co-ordination, and proposed the following three reactions:

$$>FeOH + PO_4^{3-} + 3H^+ \Leftrightarrow >FeH_2PO_4 + H_2O \qquad K_1 \quad (13.1)$$

$$>FeOH + PO_4^{3-} + 2H^+ \Leftrightarrow >FeHPO_4^- + H_2O \qquad K_2 \quad (13.2)$$

$$>FeOH + PO_4^{3-} + H^+ \Leftrightarrow >FePO_4^{2-} + H_2O \qquad K_3 \quad (13.3)$$

Hawke *et al.* [1989] and several other authors have proposed a similar set of surface reactions. However, Stumm [1992] considered phosphate sorption to be bidentate and proposed the following type of reaction:

$$2 > FeOH + H_2PO_4^- \Leftrightarrow >Fe_2PO_4^- + 2H_2O \qquad (13.4)$$

The data set selected for FITEQL modelling was the phosphate uptake data for the uranyl-free system shown in Figure 6.14. These data were similar (although not identical) to data obtained for P uptake in systems containing uranyl. Although the uranyl concentration in most experiments was low and probably had little effect on P sorption, the uranyl-free system is clearly simpler

and preferable for the present purpose. The first attempt was to develop a FITEQL model of the system using reactions 13.1, 13.2 and 13.3. This modelling was carried out with the log K values for all relevant aqueous complexes corrected to I = 0.1. The carbonate species, which were only expected to play a minor role, were excluded during this phase of model development.

Initially, attempts were made to optimise the constants in pairs (i.e. include at least two surface reactions in the postulated model). It was found that two separately-optimised log K values were not required and a single-species model would be adequate. Of the three reactions, it was found that reaction 13.3 gave the best model fit, as indicated by the WSOS/DOF parameter provided by FITEQL. Log K_3 for reaction 13.3 was estimated to be 16.93 (I = 0.1). For comparison, Dzombak and Morel [1990] derived a log K of 17.72 for the same reaction, with I = 0 and a lower site density.

It was not expected that only one reaction would be needed, but the calculations indicated that reactions 13.1 and 13.2 were not required. The situation was somewhat analogous to the sorption of uranyl on ferrihydrite, where only uptake of the UO_2^{2+} species was included in the optimised model. However, in the present case, the data are too sparse to rule out the possibility of the other surface reactions. Rather, it should be interpreted that the data set is insufficient to constrain the log K values of the other reactions, or to definitively support their presence in the model.

After this initial modelling exercise, the set of reactions used in the optimisation was refined to include reactions involving carbonate species. (Surface reactions involving carbonate had been previously considered in the adsorption model for U). This was done by including H_2CO_3 as a fixed activity species, and adding the carbonate adsorption reactions in Table 11.1 to the FITEQL input file. The inclusion of these reactions caused a very small change of 0.02 in the log K for the reaction 13.3, which was adjusted to 16.95 (I=0.1). Dzombak and Morel [1990] considered that HCO_3^- and CO_3^{2-} were “inert with respect to surface complexation formation” and these species certainly make little difference in this instance.

The proposed phosphate sorption model was then implemented with MINTEQA2, and the fit of the model to the experimental data was assessed and

deemed to be satisfactory (Figure 13.2). Subsequently, the FITEQL computations were repeated assuming the formation of a bidentate surface complex as proposed by Stumm [1992]. This required some slight modifications to the FITEQL input file, in particular different stoichiometries for the relevant reactions in mass-action and mass-balance equations. (Thus the 'B-matrix' in FITEQL differed in this case from the 'A-matrix'. See Herbelin and Westall [1994] for more details). This effort proved to be unprofitable, as the resulting model gave a significantly poorer fit to the data (Figure 13.2).

The conclusions regarding the sorption of phosphate in the present study may be compared to those reached by Balistrieri and Chao [1990] in a modelling study of phosphate adsorption on HFO. These authors also found that only the $FePO_4^{2-}$ surface species was required, and demonstrated that "model curves using a binuclear complex were too steep to fit the data". As such, their experimental and modelling results were very similar to those shown in Figure 13.2.

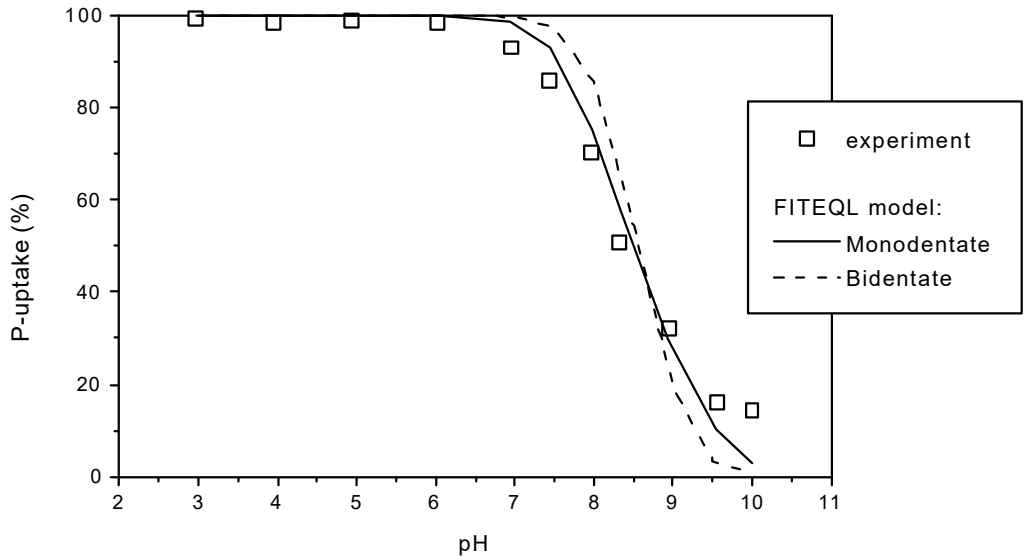


FIGURE 13.2 Modelling the ferrihydrite-phosphate system with FITEQL. The solid curve is the model containing only the monodentate species $>FePO_4^{2-}$. The dotted curve is the best model fit obtained using a bidentate surface-coordination reaction.

The outcome of the present study of phosphate adsorption was that the following reactions, occurring on both strong (S) and weak (W) surface sites, were added to the suite of reactions used for modelling the phosphate-ferrihydrite-uranyl system:

$$>WOH + PO_4^{3-} + H^+ \Leftrightarrow >WPO_4^{2-} + H_2O \qquad \log K = 18.05\ (I=0) \quad (13.5)$$

$$>SOH + PO_4^{3-} + H^+ \Leftrightarrow >SPO_4^{2-} + H_2O \qquad \log K = 18.05\ (I=0) \quad (13.6)$$

FITEQL optimisation of uranyl-phosphate surface complex on ferrihydrite

Having developed a model for the adsorption of phosphate, the next step was to postulate and optimise the log K value for the formation of a ternary surface complex between uranyl and phosphate. This is a more complex system than previously considered, and it was decided to simplify the computations by restricting attention to the low pH edge, and omitting carbonate species and their surface reactions.

The FITEQL file required non-identical 'A' (mass action) and 'B' (mass balance) matrixes, because the existing suite of surface reactions in the phosphate-free system included bidentate uranyl surface complexes (see Table 11.1). As discussed above, it appears that the ternary complex is metal-like rather than ligand-like (using the terminology of Leckie [1994]), in which case it should resemble the bidentate uranyl surface complex rather than the monodentate phosphate surface complex. Thus, the ternary uranyl–phosphate surface complex was also represented by different stoichiometric coefficients in the 'B-matrix'.

Some consideration was then given to the stoichiometry of the proposed ternary surface complex. As the dominant U-phosphate aqueous species involved a single uranyl and a single phosphate ion (with various proton stoichiometries), it seemed sensible to use a uranyl phosphate surface complex such as $Fe_2O_2UO_2PO_4^{3-}$, $FeO_2UO_2HPO_4^{2-}$ or $FeO_2UO_2H_2PO_4^{-}$. The surface reaction to form the first of these is:

$$>Fe(OH)_2 + UO_2^{2+} + PO_4^{3-} \Leftrightarrow FeO_2UO_2PO_4^{3-} + 2H^+ \qquad (13.7)$$

Possibly, the inclusion of surface complexes $FeO_2UO_2HPO_4^{2-}$ or $FeO_2UO_2H_2PO_4^-$ would also be warranted. However, the models for both phosphate and uranyl surface species had not involved protonated surface species, and it was decided to omit these two surface species in the first instance. This decision was partly based on pragmatic grounds, in that there are both weak and strong surface sites in the model, therefore each type of surface species would immediately add two adjustable formation constants. It will by now be clear that the modelling process involves numerous steps. At each point the number of unconstrained variables must be minimised as much as possible to prevent the number of optimised parameters becoming so great as to make the entire exercise meaningless.

As well as the U sorption reactions on both weak and strong sites, the UO_2^{2+} speciation reactions (including those with phosphate) and the deprotonation reactions of phosphoric acid were added to the FITEQL simulation. The log K values for these reactions were shown in Table 3.1. The values were adjusted to I = 0.1 for the FITEQL optimisation. The final FITEQL input file is given in Table 13.1. This input file also contained the diffuse double layer model as indicated by component 160. The experimental results for U uptake in the presence of phosphate (ΣU = 1 μmol/L, data shown in Figure 13.3) were entered as 'serial' data in the FITEQL input file.

The model proposed in Table 13.1 converged for both surface species on weak (W) and strong (S) sites, giving the following log K values (corrected to I = 0):

$$>W(OH)_2 + UO_2^{2+} + PO_4^{3-} \Leftrightarrow WO_2UO_2PO_4^{3-} + 2H^+ \qquad \log K_{\mu=0} = 7.57 \quad (13.8)$$

$$>S(OH)_2 + UO_2^{2+} + PO_4^{3-} \Leftrightarrow SO_2UO_2PO_4^{3-} + 2H^+ \qquad \log K_{\mu=0} = 11.56 \quad (13.9)$$

The corresponding FITEQL model simulation is shown in Figure 13.3. The model provides a good fit to the data. It is worth establishing that this is indeed due to the presence of the ternary complex. If no ternary complex was included, the combined effects of competition for surface sites and aqueous complexation of uranyl would be decreased sorption, as shown by the model simulation (Model (b) in Figure 13.3).

TABLE 13.1 Input file for FITEQL optimisation of proposed ternary uranyl-phosphate surface complexes on ferrihydrite.

id	Name	log X	T	Type
160	X(Psi)	-1.0	0.00	T(I)
2	PO_4[3-]	-5.0	1.00 E-4	T(I)
3	WOH	-3.0	8.73 E-4	T(I)
4	UO_2[2+]	-7.0	1.00 E-6	T(I)
5	NO_3[-]	-1.0	1.00 E-1	T(I)
6	SOH	-5.0	1.80 E-6	T(I)
7	UO_2(ads)	0.0.	0.00	X&T(II)
8	H[+]	0.0	0.00	X(III)

Species

Name	log K	X(Psi)	PO_4[3-]	WOH	UO_2[2+]	NO_3[-]	SOH	UO_2ads	H[+]
H[+]	0.00	0	0	0	0	0	0	0	1
OH[-]	-13.78	0	0	0	0	0	0	0	-1
PO_4[3-]	0.00	0	1	0	0	0	0	0	0
HPO_4[2-]	11.69	0	1	0	0	0	0	0	1
H_2PO4[-]	18.45	0	1	0	0	0	0	0	2
H_3PO_4	20.38	0	1	0	0	0	0	0	3
WOH_2[+]	6.51	1	0	1	0	0	0	0	1
WOH	0.00	0	0	1	0	0	0	0	0
WO[-]	-9.13	-1	0	1	0	0	0	0	-1
WPO_4[-2]	16.95	-2	1	1	0	0	0	0	0
SOH_2[+]	6.51	1	0	0	0	0	1	0	1
SOH	0.00	0	0	0	0	0	1	0	0
SO[-]	-9.13	-1	0	0	0	0	1	0	-1
SPO_4[-2]	16.95	-2	1	0	0	0	1	0	0
WO_2UO_2	-6.28	0	0	1#	1	0	0	1	-2
SO_2UO_2	-2.57	0	0	0	1	0	1#	1	-2
NO_3[-]	0.00	0	0	0	0	1	0	0	0
UO_2NO_3+	-0.14	0	0	0	1	1	0	0	0
UO_2OH[+]	-4.98	0	0	0	1	0	0	0	-1
$(UO_2)_2(OH)_2$[2+]	-5.85	0	0	0	2	0	0	0	-2
$(UO_2)_3(OH)_5$[+]	-16.22	0	0	0	3	0	0	0	-5
UO_2[+2]	0.00	0	0	0	1	0	0	0	0
UO_2PO_4[-]	11.91	0	1	0	1	0	0	0	0
UO_2HPO_4	18.05	0	1	0	1	0	0	0	1
$UO_2H_2PO_4$[+]	21.28	0	1	0	1	0	0	0	2
$WO_2UO_2PO_4$[3-]	*	-3	1	1#	1	0	0	1	-2
$SO_2UO_2PO_4$[-3]	*	-3	1	0	1	0	1#	1	-2

* - to be optimised.

- bidentate surface species for which the stoichiometry in the 'B matrix' differs.

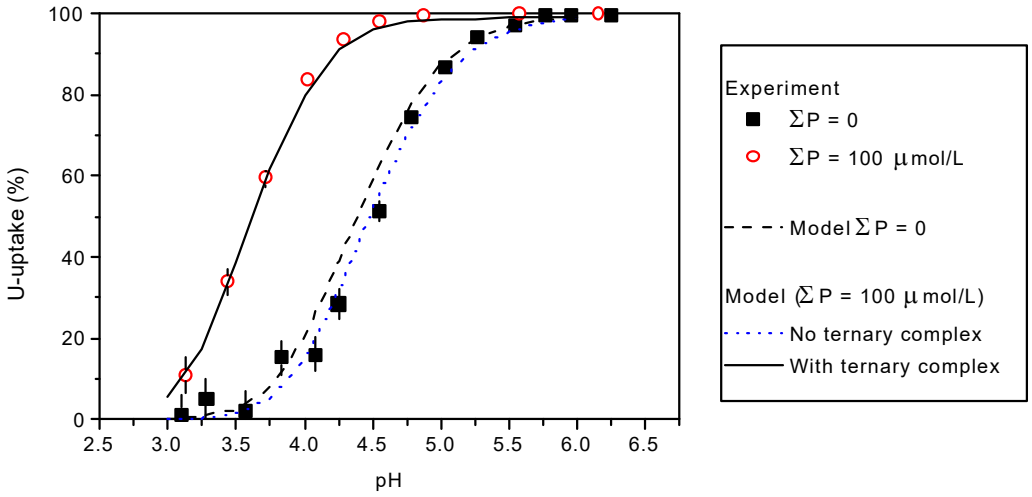


FIGURE 13.3 Modelling U sorption on ferrihydrite in the presence of phosphate using FITEQL. Three model simulations are shown – a) Standard model for ΣP = 0. b) Model with competing P sorption reaction and aqueous uranyl-phosphate complexation (no ternary complex). c) Model (b) plus ternary surface complexes (equations 13.8 and 13.9). The ternary complex is clearly required to simulate the experimental data. (ΣU = 1 µmol/, ΣFe = 1 mmol/L, 0.1 $NaNO_3$ in equilibrium with air)

Implementation with MINTEQA2

As noted above, the model summarised in Table 13.1 is simplified in that carbonate species are omitted. This does not create significant error for the low pH edge, which occurs in the pH region where carbonate species play only a minor role in uranyl speciation. The testing of the proposed model over the entire pH range requires that various complexation and competitive sorption reactions involving carbonate be included. The next step was therefore to implement the proposed model using MINTEQA2 over the pH range 3 to 10, with all these reactions included. This exercise also provided the opportunity to check for possible errors during the computations. (This parallel use of MINTEQA2 and FITEQL proved to be extremely useful in validating the models of these more complex systems).

The outcome of the MINTEQA2 simulation of the data obtained with ΣU of 1 μmol/L appears to be satisfactory (Figure 13.4). The model predicts that the presence of P should increase U uptake in the region of the low pH edge (as was shown in the FITEQL modelling). A small increase in the region of the high pH edge is also predicted. However, the experimental data points in the region of the high pH edge are inconclusive. Figure 13.4 suggests that further refinements to the model are not necessary to adequately simulate the full experimental pH range.

The simulation results for ΣU of 100 μmol/L are given in Figure 13.5, together with the experimental data. The model fit in this case is particularly encouraging, since this data set was not used to derive the model. In fact, the model predictions in Figures 13.4 and 13.5, which cover ΣU of 1 μmol/L and 100 μmol/L (and the pH range from 2 – 10), are based on FITEQL analysis only of the 1 μmol/L data-set in the pH range below 6.5. The model predicts an increase of U sorption in the presence of phosphate in the region of the high pH edge for ΣU of 100 μmol/L, and in this case this is supported by the experimental data.

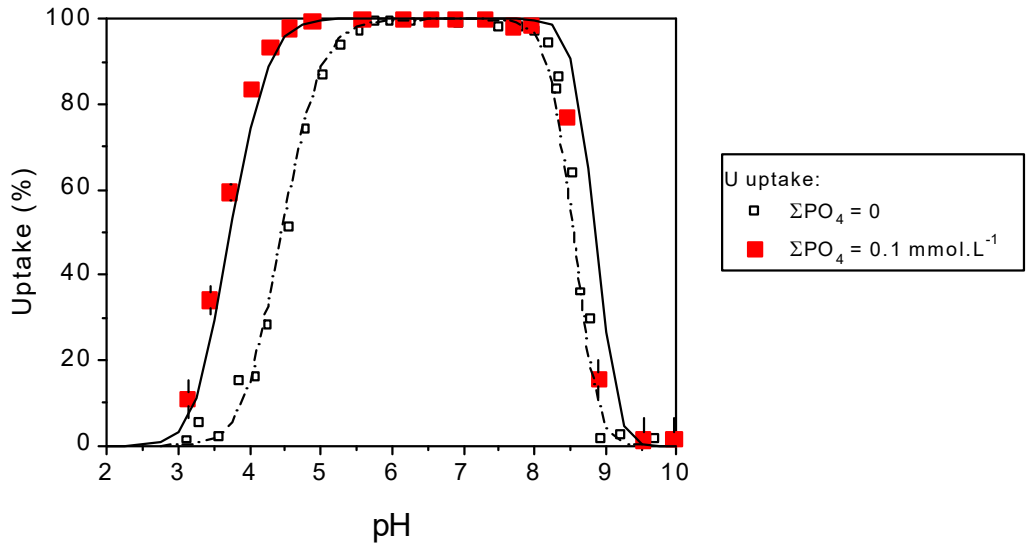


FIGURE 13.4 Sorption model with ternary uranyl phosphate surface complex as implemented by MINTEQA2 for ΣU of 1 μmol/L. The model is indicated by the solid line. Experimental data and model (dotted curve) in the absence of phosphate are also shown.

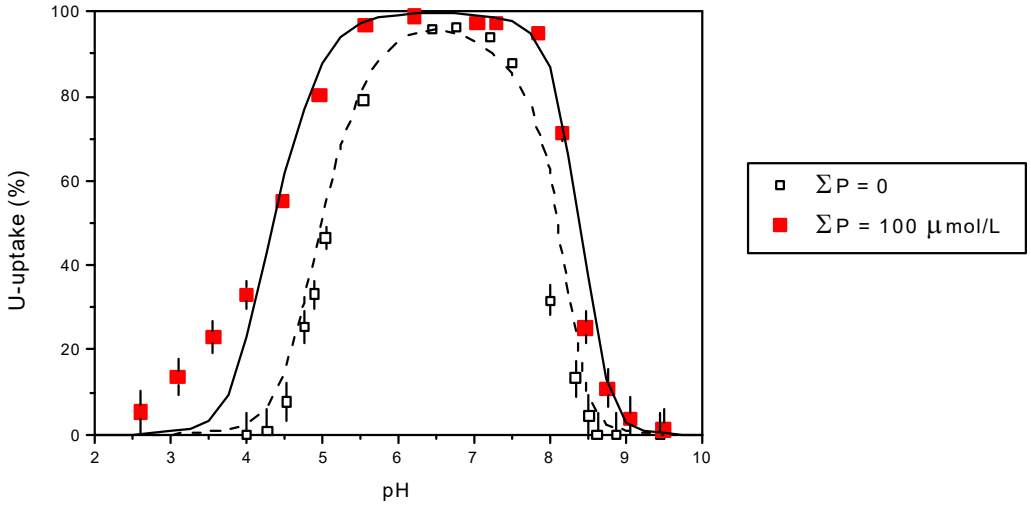


FIGURE 13.5 Sorption model with ternary uranyl phosphate surface complex as implemented by MINTEQA2 for ΣU of 100 μmol/L. Model is indicated by the solid line. Experimental data and model (dashed curve) in the absence of phosphate are also shown.

The increased sorption at the very low pH values (Figure 13.5) appears to slightly deviate from the model curve. This effect may be associated with ferrihydrite transformation, but further model refinements were not attempted to simulate this.

The model simulations in Figures 13.4 and 13.5 indicate that the model is able to simulate experimental data across the entire pH range. As noted in Section 6.4.1, it is an interesting that the high pH edge for ΣU of 100 μmol/L was affected by the presence of phosphate, whereas the 1 μmol/L edge showed little effect. (This was considered to be slightly surprising because there is a larger excess of phosphate to uranyl in the latter system). In Section 6.4.1 it was speculated that this was because the ratio of carbonate to phosphate increases as the pH becomes higher, thus causing the edge for ΣU of 100 μmol/L (which occurs at lower pH) to be more greatly affected. This qualitative explanation remains quite reasonable, and underlies the model outcome. However, the model simulation is probably more convincing.

The next part of the modelling was to simulate the experiments in which ΣU was varied at constant pH. As noted above, these experiments assisted in excluding possible precipitation, since the effect of phosphate on U uptake extended to very low U concentrations. However, these results were not used to develop the model, and were carried out at a lower ionic strength than the pH edge experiments. Figures 13.6 and 13.7 show that the model simulates the results adequately across a wide range of ΣU. The experimental data and modelling results once again highlight the very large increase in U sorption on ferrihydrite which is associated with the addition of phosphate to the system.

A final interesting feature of the model is its prediction that the adsorption of phosphate should be enhanced by the presence of uranyl across a limited pH range (Figure 13.8). It was suggested in Section 6.4.1 that this could be discerned in the experimental data (a close inspection of Figure 6.14 is warranted). Although the data are inadequate to quantify this feature, the results support the assertion that the presence of metals at the Fe-oxide surface would enhance the uptake of phosphate [Boland *et al.,* 1977], in a similar way that the presence of phosphate increased the uptake of uranyl. While this observation is peripheral to the present work, it raises some interesting insights about the behaviour of adsorbed species at mineral surfaces.

As has been emphasised by several authors, this type of modelling generally proceeds in the absence of conclusive information about surface structures from techniques such as EXAFS. Even with such structural information, it is difficult to be sure about the degree of protonation of surface species. This inevitably means that the question of uniqueness becomes an issue in surface complexation modelling. In the present case, it is possible that other selections of surface species could accommodate the data. However, this would not affect the main conclusion of this modelling exercise, which has been to establish the likely existence of a ternary uranyl-phosphate complex on the ferrihydrite surface. While the exact stoichiometry of this complex may remain problematic, the model appears to work satisfactorily and have some predictive power.

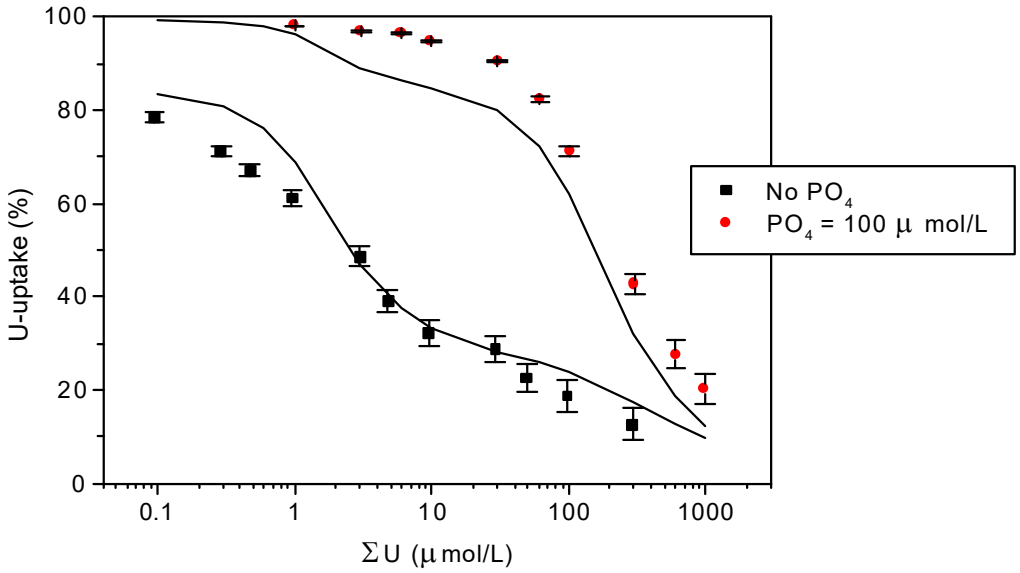


FIGURE 13.6 Simulation of U adsorption in the presence of phosphate at fixed pH of 4.5 (I = 0.02). These data were not used to derive the model. Although not an exact fit, the model simulates the enhancing effect of phosphate on U sorption across a wide range of ΣU (as well as a wide pH range as already shown).

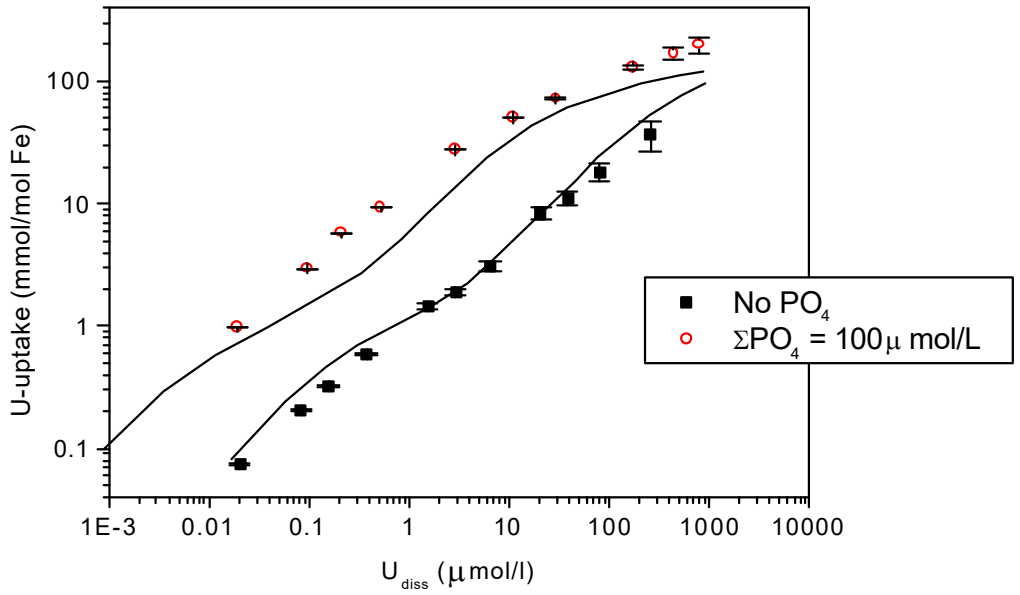


FIGURE 13.7 Experimental data and model simulations from Figure 13.6 in isotherm format. Background electrolyte was 0.02 M $NaNO_3$ equilibrated with air.

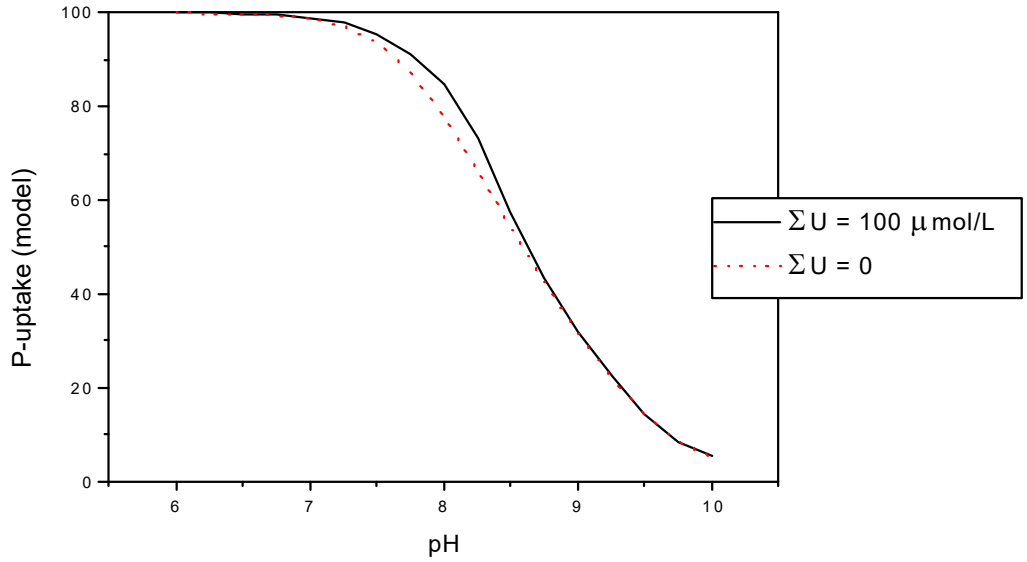


FIGURE 13.8 The model predicts that the presence of uranyl should slightly increase the uptake of phosphate on the ferrihydrite surface. In a qualitative sense, this does reflect the experimental data. This supports the conceptual basis of the model.

13.3 Modelling the U-phosphate-kaolinite system

Modelling phosphate uptake

The first objective in simulating the uranyl-phosphate-kaolinite system was to model the uptake of phosphate. In the absence of any further model-constraining information, it seemed reasonable to use the same site density for P sorption as was derived from the AEM data (Table 12.1), even though the latter data were obtained for U rather than P. Based on this work, the total site density of the KGa-1B material is 2.97 μmol/g, of which 84% is aluminol sites.

As with the experiments with ferrihydrite, the U-sorption experiments with kaolinite (KGa-1B) were undertaken with added ΣP of 100 μmol/L. The kaolinite mass loadings were 4 g/L and 40 g/L. Assuming the site density given above, the total number of sites in the experiments with 4 g/L loading was about 12 μmol/L. It is therefore not surprising that only a small proportion of the phosphate was adsorbed by the clay for this mass loading (see Figure 7.10). It

would be difficult to achieve successful modelling under these circumstances. Therefore, attention was restricted to the data obtained with the 40 g/L loading of KGa-1B (Figure 13.9). Here the number of available sites is about 120 μmol/L, of which about 100 μmol/L are aluminol sites.

The main uncertainty in fitting a model to these data is that there is no obvious method of assessing the relative affinity of P for titanol and aluminol sites. This is a contrast to the situation with U, where the AEM provided evidence of the preference of uranyl for the titanol site, as well as a means of quantifying this. (AEM data for the association of P with the anatase and kaolinite phases would have been useful).

The following reactions were considered for the system:

$$>AlOH + PO_4^{3-} + H^+ \Leftrightarrow >AlPO_4^{2-} + H_2O \quad (13.10)$$

$$>AlOH + PO_4^{3-} + 2H^+ \Leftrightarrow >AlHPO_4^{-} + H_2O \quad (13.11)$$

$$>AlOH + PO_4^{3-} + 3H^+ \Leftrightarrow >AlH_2PO_4 + H_2O \quad (13.12)$$

The same set of surface reactions was also considered for the titanol (>TiOH) site. As there are two sites, there are a total of six potential reactions to investigate. The initial modelling proceeded on the basis that both sites contribute to the observed P uptake, but there were difficulties in achieving convergence, even with one or more of reactions 13.10 to 13.12 omitted. There was not enough data to constrain the model. In particular, the relative importance of >TiOH and >AlOH sites was unknown. Various simulations were tried, but it became clear that the >TiOH sites were not significant in fitting any models. This is because the aluminol sites comprise about 85% of the total sites, whereas the less numerous >TiOH sites can only adsorb a maximum of about 20% the phosphate in the system. Therefore, regardless of the log K for the sorption reactions on the titanol site, the majority of the uptake would have to be on the aluminol sites. It was therefore decided that P uptake would be modelled as occurring only on the aluminol site.

The model simulation then proceeded in a straightforward fashion with only the aluminol site included, and it was soon established that reaction 13.10 was unimportant. With both of the two other surface species (reactions 13.11

and 13.12) included, the goodness of fit parameter WSOS/DOF improved. As only one site was now in the model, both log K's could be optimised together with FITEQL. The log K values (I=0) were 25.93 for reaction 13.10 and 30.19 for reaction 13.12. The resulting model simulation and the main surface species are shown in Figure 13.9. It appears that the model provides a reasonable simulation of the data.

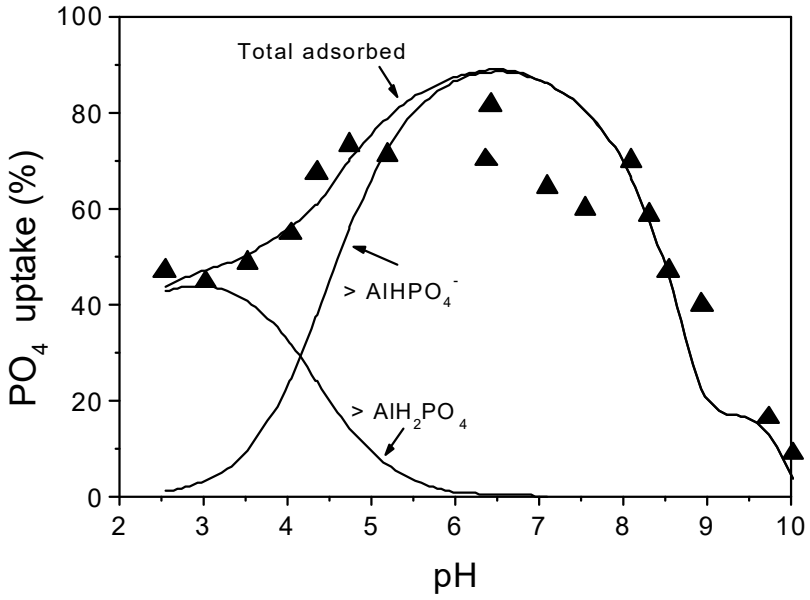


FIGURE 13.9 Model simulation of the uptake of phosphate on Georgia kaolinite KGa-1B.

FITEQL analysis of the ternary surface complex for the KGa-1B sample

The final task was to postulate a log K value for the proposed ternary uranyl phosphate surface complex on the KGa-1B model substrate. Given the strong preference of uranyl for the titanol site (see Figure 12.15), it was expected that the titanol site would be of much greater significance than the aluminol site in U uptake on this sample, particularly for experiments with the 40 g/L loading. In this case, the number of titanol sites (19.6 μmol/L) is greatly in excess of the ΣU. Therefore, modelling proceeded on the basis that the >AlOH site made no significant contribution to the adsorption of the proposed ternary complex. This is obviously a substantial simplification. However, there does not

appear to be any way of constraining the adsorption of the proposed ternary complex on the aluminol site with the available data-sets.

The following surface reactions involving both uranyl and phosphate were therefore considered on the titanol site:

$$> TiOH + PO_4^{3-} + UO_2^{2+} \Leftrightarrow > TiOUO_2PO_4^{2-} + H^+ \quad (13.13)$$

$$> TiOH + PO_4^{3-} + UO_2^{2+} \Leftrightarrow > TiOUO_2HPO_4^- \quad (13.14)$$

$$> TiOH + PO_4^{3-} + UO_2^{2+} + H^+ \Leftrightarrow > TiOUO_2H_2PO_4 \quad (13.15)$$

$$> TiOH + PO_4^{3-} + UO_2^{2+} + 2H^+ \Leftrightarrow > TiOUO_2H_3PO_4^+ \quad (13.16)$$

The models were implemented using FITEQL input files that included the adsorption reactions for U on the titanol and aluminol sites derived for the phosphate-free systems (Chapter 12). These were entered with fixed log K values, and attempts were made to optimise only the log K values for reactions 13.13 to 13.16. The FITEQL simulations did not converge for reaction 13.13, and while FITEQL would produce a log K for reaction 13.14 in some simulations, this did not greatly improve the fit of the model to the data. However, models which included both the $>TiOUO_2H_2PO_4$ and $>TiOUO_2H_3PO_4^+$ surface species were more promising. Therefore, a FITEQL model including both species was developed for the data sets obtained with the two different loadings of kaolinite. Six simulations were considered, with the models comprising:

a) only reaction 13.15
b) only reaction 13.16
c) reactions 13.15 and 13.16.

Log K values were derived in each case, and the model outcomes were then computed using MINTEQA2 and compared with the experimental data. The simulations of model (a) with only the $> TiOUO_2H_2PO_4$ species provided a poor model fit at the lowest pH values at the start of the pH edge. Model (b) was adequate for the higher loading data set, but over-predicted U sorption at low pH in the case of the 4 g/L loading. It also had the significant problem that the log K values for reaction 13.16 derived from the two data sets differed by more

than 1.0 unit, which was not considered to be acceptable. Model (c) proved to be satisfactory for both data sets, and was therefore preferred on this basis. The two simulations gave consistent log K values of 28.75 and 29.15 for reaction 13.16. A simple average value log $K_{\mu=0.1}$ of 28.95 was chosen for this reaction.

However, the log K values for reaction 13.15 did not agree satisfactorily between the two data-sets even for model (c). As noted above, model (b) had worked for the higher loading data set, indicating that reaction 13.15 was not essential for the simulation in that case. Therefore, it was decided that the log K for reaction 13.15 should be chosen so as to ensure an adequate fit of model (c) to the lower loading data. As noted by Dzombak and Morel [1990] there is no simple way of selecting log K values. The selection in this case was influenced by the satisfactory outcome of the model simulations. The selected log $K_{\mu=0.1}$ for reaction 13.15 was 25.48.

MINTEQA2 modelling of kaolinite – phosphate system

The model for the system was now implemented using MINTEQA2, with the following two surface reactions added:

$$> TiOH + PO_4^{3-} + UO_2^{2+} + H^+ \Leftrightarrow > TiOUO_2H_2PO_4 \quad \log K_{\mu=0} = 27.02 \qquad (13.15)$$

$$> TiOH + PO_4^{3-} + UO_2^{2+} + 2H^+ \Leftrightarrow > TiOUO_2H_3PO_4^+ \quad \log K_{\mu=0} = 30.60 \qquad (13.16)$$

As previously noted, the kaolinite U-sorption model is a non-electrostatic model, and therefore does not contain any corrections for the electrical double layer effects. The MINTEQA2 simulation of the U sorption data obtained in the presence of phosphate was adequate (Figures 13.10 and 13.11). The model correctly simulated the increase in U sorption in the region of the low pH edge, and indicated that there is little or no effect on the high pH edge. It is likely that more detailed modelling with a greater amount of experimental data could further increase the accuracy of the predictions. However, the main conclusion is that, as with ferrihydrite, the effect of phosphate on U uptake is due to a ternary surface complex of the type proposed in reactions 13.15 and 13.16.

In this case, the experimental data set is not sufficient to completely constrain the model, particularly in terms of the relative contributions of the titanol and aluminol sites to P sorption, and to the binding of the proposed ternary complex. This system has not been previously studied, and the data required to constrain the model far exceed what was expected when the work commenced. Nonetheless, it appears that the general framework of the model for U sorption on kaolinite is now in place, and this model can accommodate the effects of various ligands.

An unusual aspect of the model is that the ternary uranyl phosphate complex is adsorbed on the titanol site and P on the aluminol site. However, this results from the fact that micromolar amounts of U will preferentially sorb on the stronger, lower abundance titanol site. The population of these sites is inadequate to adsorb the phosphate, and there appears to be no option but to model the phosphate uptake as occurring only on the aluminol site.

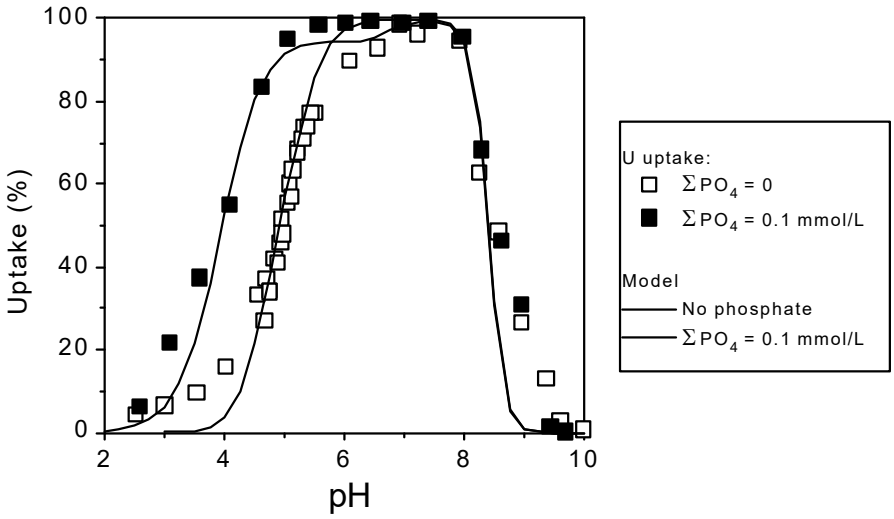


FIGURE 13.10 Modelling U uptake on kaolinite (4 g/L) in the presence and absence of 100 μmol/L phosphate (ΣU = 1 μmol/L). The model includes a ternary uranyl-phosphate surface complex on the titanol site. The model fit is quite good, however a slight discrepancy exists in the neutral pH range. In this pH range, about 5% of the total U is present as the aqueous species UO_2HPO_4(aq) and $UO_2PO_4^-$. The fit could be improved by including another surface complex, however this log K cannot be well-constrained by the available data.

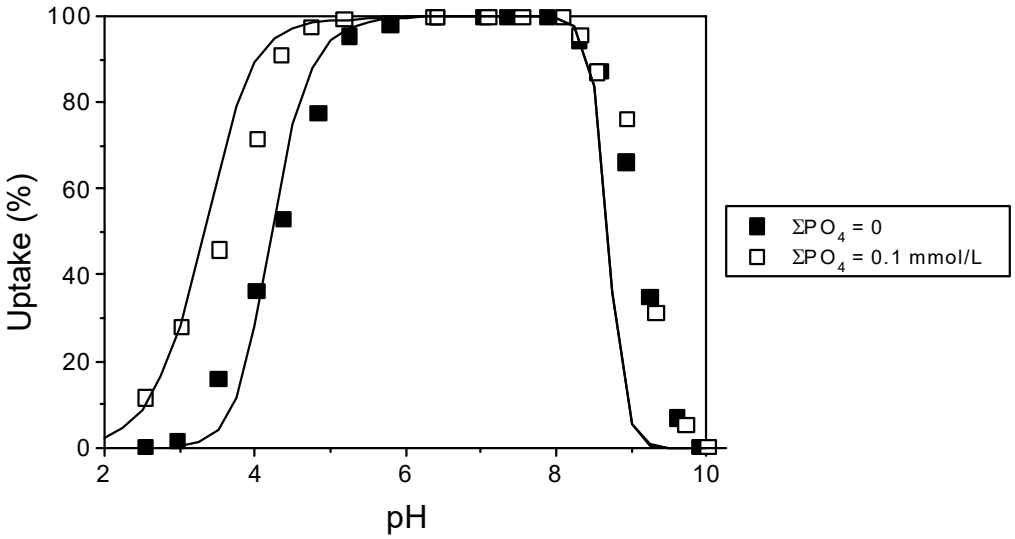


FIGURE 13.11 Modelling U uptake on kaolinite in the presence and absence of 100 μmol/L phosphate (mass loading of 40 g/L, ΣU = 1 μmol/L). The curves are model simulations.

13.4 Modelling the effects of phosphate on U sorption by model minerals

The considerable increase in U sorption on ferrihydrite and kaolinite when phosphate is present can be attributed to the formation of ternary uranyl-phosphate surface complexes on the mineral surfaces. There is some model uncertainty introduced from the interdependence of the calculated parameters with the phosphate sorption data. This latter data-set lacked the degree of detail of the corresponding data-sets for uranyl, and it would be desirable for the suite of surface reactions for phosphate to be better constrained.

The main conclusion is that sorption involving a ternary surface complex is the major mechanism responsible for the increased uranyl uptake by both kaolinite and ferrihydrite when phosphate is present. In the absence of the proposed ternary complexes, the combination of aqueous uranyl-phosphate complexation and adsorption of phosphate on surface sites causes a slight decrease in predicted uranyl sorption.

Thus, the surface complexation modelling of the experimental systems has been able to explain all the experimental results. At the commencement of the experimental work, it was considered likely that phosphate would decrease uptake of uranyl due to aqueous complexation and competition. The experimental outcome was entirely contrary to this expectation, and it was demonstrated that this was not due to precipitation. While the details of surface species and log K values are still somewhat conjectural, the model appears to be based on a realistic premise, that ternary surface complexes occur in the system and have a significant role in uranyl uptake. It may be observed in conclusion that the proposed ternary uranyl-phosphate surface complexes are analogous to those previously proposed for carbonate in both the ferrihydrite and model kaolinite systems.

PART IV.

Conclusions

14 OUTCOMES OF THE U-SORPTION STUDY

14.1 Conclusions

14.1.1 Chemical influences on uranium sorption

The adsorption of U on ferrihydrite, kaolinite and the Koongarra natural substrates has been investigated under a wide range of conditions. The most important chemical factors which affected U adsorption in these experiments were the:

- pH, which affects U sorption by determining aqueous U speciation, and also via the protonation or de-protonation of surface sites,
- ionic strength, which significantly reduces U uptake at higher pH values,
- ΣU, which indicates the presence of multiple surface sites and possible precipitation, and
- presence of complexing ligands, which can increase or decrease adsorption.

14.1.2 Modelling of U adsorption

Ferrihydrite

A surface complexation model with two sites (weak and strong) was used for uranyl adsorption on ferrihydrite. A single type of reaction was able to simulate uranyl adsorption in the low pH range. This reaction involved the formation of a mononuclear, bidentate surface complex on weak and strong sites:

$$>Fe(OH)_2 + UO_2^{2+} = (>FeO_2)UO_2^0 + 2H^+$$

The following uranyl carbonate surface complex was required to adequately simulate sorption data at higher pH values:

$$>Fe(OH)_2 + UO_2^{2+} + CO_3^{2-} = (>FeO_2)UO_2CO_3^{2-} + 2H^+$$

The populations of weak and strong sites, and the log K values for the above reactions, were optimised using FITEQL, giving a total of six fitted parameters in the ferrihydrite model.

The substantial effect of citrate on U sorption was modelled without any change or addition to the suite of U sorption reactions. However, the sorption reactions were supplemented by a set of U-citrate and Fe-citrate interactions that were taken from the literature. The most significant outcome of the modelling was that an aqueous mixed metal (U-Fe-citrate) complex was also required to simulate the experimental sorption data:

$$Fe^{3+} + UO_2^{2+} + 2CIT^{3-} + 2H_2O \Leftrightarrow Fe(OH)_2(CIT)_2UO_2^{3-} + 2H^+$$

It was necessary to optimise the log K value for the above reaction, which has not been adequately studied in the past.

The effect of sulfate comprised weak aqueous uranyl-sulfate complexation and competition between sulfate and uranyl for surface sites.

The presence of phosphate substantially increased uranyl sorption by ferrihydrite, particularly in the low pH range. These systems were modelled using the same set of sorption reactions on the ferrihydrite surface, supplemented by a ternary surface complex reaction on both weak and strong sites:

$$>Fe(OH)_2 + UO_2^{2+} + PO_4^{3-} \Leftrightarrow > FeO_2UO_2PO_4^{3-} + 2H^+$$

The sorption reactions mentioned in this section were able to simulate the extensive suite of U sorption data collected in this project. This data-set is one of the most comprehensive available for U interactions with a model substrate. The surface complexation model covered a wide pH range, ΣU, ligand effects, ionic strength and pCO_2.

Kaolinite

In this work, standard kaolinites from Georgia were used as model substrates. These materials contain an anatase impurity phase, which appears to play a substantial role in the uptake of uranyl. The model of this system included two sorption sites, comprising a titanol site and an aluminol site. The surface reactions on these sites were:

$$>TiOH + UO_2^{2+} \Leftrightarrow >TiOUO_2^{+} + H^{+}$$
$$>TiOH + UO_2^{2+} + CO_3^{2-} \Leftrightarrow >TiOUO_2CO_3^{-} + H^{+}$$
$$>AlOH + UO_2^{2+} + H_2O \Leftrightarrow >AlOUO_2OH + 2H^{+}$$

The site density for the titanol and aluminol sites were estimated from the AEM examination, and the log K values for the three postulated reactions were optimised using FITEQL.

The addition of phosphate to the uranyl / kaolinite system caused a similar increase in uranyl sorption to that observed in the case of ferrihydrite. The U sorption model was modified by the addition of two ternary surface complexation reactions on the titanol site:

$$> TiOH + PO_4^{3-} + UO_2^{2+} + H^{+} \Leftrightarrow > TiOUO_2H_2PO_4$$
$$> TiOH + PO_4^{3-} + UO_2^{2+} + 2H^{+} \Leftrightarrow > TiOUO_2H_3PO_4^{+}$$

While a ternary surface complex would probably also form on the aluminol site, this reaction was not required to simulate the sorption data, and the corresponding log K value was not constrained by the experimental results.

Kaolinite is a comparatively weak adsorbing substrate for uranyl. In circumstances with high total U (ΣU), the precipitation of the uranyl hydroxide needed to be taken into account to adequately simulate the experimental results. However, precipitation did not appear to play a role in the experiments with the U-phosphate-kaolinite systems, which were carried out with lower ΣU.

14.1.3 Sorption phenomena in the natural environment

As has been previously recognised, iron oxides have a strong influence on U retention by Koongarra weathered schist samples. This was shown by a decrease in U sorption on samples that had been subjected to a CDB extraction. This extraction removed strongly sorbing Fe-oxides (and other oxides) with an associated reduction in surface area.

The potential importance of iron mineral transformations in influencing U mobility was demonstrated. These transformations have two important effects. Firstly, they produce a more stable solid substrate with a lower tendency to sorb U than fresh ferrihydrite. Secondly, some uranium can be incorporated into the solid during the transformation (aging) process, and thereby isolated from interactions with the aqueous phase. Thus, Fe oxide transformations have a complex effect on U mobility. Whilst transformations provide a mechanism for U immobilisation by incorporation in the solid, the transformed solid has less ability to sorb U directly from solution.

Sorption phenomena in experiments with natural materials from the Koongarra uranium deposit were similar to those observed in model systems. The mineralogy of the Koongarra samples is fairly uniform, and this was reflected in similar adsorption of uranyl. The differences in sorption were largely attributed to different accessible U contents. In addition, complexing species present in the samples (e.g. humic acid and phosphate) may affect the outcome of the experiments. Humic materials appear to be important in the Koongarra system, and this was demonstrated by sorption experiments with the model minerals in systems containing humic acid.

The intrinsic accessible U content, which contributes to the total U (ΣU) in experiments with the natural substrates, must be taken into account when interpreting the sorption data on the natural materials. Two methods of estimating this quantity were considered: sequential extraction or isotope exchange. The isotope exchange results have the advantage that they do not involve chemical extractions and assumptions about their effects.

Uranyl sorption on the natural materials was broadly similar to the model substrates, including the effects of pH, mass loading, ionic strength, pCO_2, and total uranium. This implies that the chemistry of the aqueous phase must be well understood in order to model U sorption in environmental systems. It also suggests that a successful model for U sorption on the model minerals will be a major step forward towards a quantitative understanding of U mobility at Koongarra.

14.2 Summary of the work

The work described in this thesis was part of a project involving several participants from organisations including ANSTO, UNSW, and the USGS. During this project, numerous U sorption experiments on model and natural substrates were undertaken. The sorption database was combined with experimental and modelling activities of several other workers to produce the model for sorption on ferrihydrite [Waite *et al.,* 1994]. The specific contribution of the author was to collect and interpret a large amount of experimental sorption data, with an emphasis on testing proposed models. This data-set is summarised in Appendix 1.

The experimental work described in this thesis formed the basis of the papers about the following subjects:

- The U concentration dependence, effect of pCO_2 and effect of ionic strength on U sorption by ferrihydrite [Waite *et al.,* 1994]
- The effects of phosphate and humic acid on U sorption by ferrihydrite [Payne *et al.,* 1996]
- Uranium (VI) adsorption on kaolinite and ferrihydrite [Payne *et al.,* 1998]
- The role of Fe-minerals and their transformations [Payne *et al.,* 1994].

The modelling undertaken during this thesis employed both the FITEQL and MINTEQA2 geochemical codes. Both of these codes are very valuable in this type of study. The parallel use of both computer codes was useful in validating the modelling approach and reducing the incidence of error in the models.

The model put forward by Waite *et al.* [1994] has now been extended to include:

- precipitation and solubility limits in sorption experiments with kaolinite [Payne *et al.,* 1998]
- the role of the TiO_2 impurity phase in experiments with Georgia kaolinites [Payne *et al.,* 1998]
- the effect of sulfate (Chapter 11)
- interactions in the uranyl-citrate-ferrihydrite system, particularly the role of the proposed aqueous mixed-metal complex (Chapter 11)
- a model for uranyl sorption on kaolinite (Chapter 12)
- models of the effect of phosphate on uranyl sorption (Chapter 13)

14.3 Possible further work

Numerous areas for further investigation have arisen during this work. Many of the systems studied in this thesis would benefit from further modelling with additional experimental data. The modelling of the natural Koongarra materials was not attempted in this thesis, and the experimental data are being modelled in a related PhD thesis[1]. Uranyl sorption in systems containing humic materials was not modelled, and would be a study in its own right.

The analytical electron microscopy (AEM) work proved to be very useful in the present study, and provided a means to understand the surface chemistry occurring in the U-kaolinite system. This technique should now be applied in the U-kaolinite-phosphate system and in studies of U sorption on the more complex natural materials. Similarly, further EXAFS work would assist in unravelling the co-ordination of uranyl at mineral surfaces. Detailed studies of citrate sorption on kaolinite and ferrihydrite would also be useful.

It is also necessary to independently measure the log K value for the aqueous mixed metal uranyl-ferric-citrate complex. This should be fairly straightforward in systems that do not contain sorbing materials. This work is already planned for commencement at ANSTO in 1999.

[1] Brett Fenton, PhD Thesis, University of NSW, in preparation

The experience derived from the present study suggests that several issues should be emphasised in the design phase of future sorption studies. The main factors for consideration are:

- to be aware of possible precipitation and how to distinguish it from sorption
- to vary the total metal concentration
- to consider the possible effects of impurity phases, even in popular standard ‘model’ materials
- in experiments involving ligands, to obtain detailed data on ligand sorption as well as of the radionuclide or metals of primary interest
- to obtain the largest possible ‘multi-dimensional’ data-base with the type of detail obtained here under controlled, fixed conditions.

Further studies along these lines should contribute to further advancement of the rapidly expanding field of sorption modelling.

PART V.

References and appendices

15 REFERENCES

P.L. Airey, 1986, 'Radionuclide migration around uranium ore bodies in the Alligator Rivers Region of the Northern Territory of Australia – analogue of radioactive waste repositories – a review', *Chemical Geology,* **55:** 255-268.

P.L. Airey, C. Golian and D.A. Lever, 1986. *An Approach to the Mathematical Modelling of Uranium Series Redistribution Within Ore Bodies*. Report AAEC/C49, AAEC, Lucas Heights.

B. Allard, U. Olofsson and B. Torstenfelt, 1984, 'Environmental actinide chemistry', *Inorganica Chimica Acta,* **94:** 205-221.

L.E. Allison, 1965, 'Organic Carbon'. In: *Methods of Soil Analys*is (C.A. Black, ed.). American Society of Agronomy, Madison.

J.D. Allison, D.S. Brown, and K.J. Novo-Gradec, 1990. *MINTEQA2, A Geochemical Assessment Model for Environmental Systems*. USEPA, Athens.

S. Altmann, 1997. *Using Chemical Thermodynamic Models for Guiding Radio Element K_d Investigations for Performance Assessment*. Status Report for OECD/NEA, Paris (draft version).

L.L. Ames, J.E. McGarrah, B.A. Walker and P.F. Salter, 1982, 'Sorption of uranium and cesium by Hanford basalts and associated secondary smectite', *Chemical Geology,* **35:** 205-225.

L.L. Ames, J.E. McGarrah and B.A. Walker, 1983a, 'Sorption of trace constituents from aqueous solutions onto secondary minerals. I. Uranium', *Clays and Clay Minerals,* **31:** 321-334.

L.L. Ames, J.E. McGarrah, B.A. Walker and P.F. Salter, 1983b, 'Uranium and radium sorption on amorphous ferric oxyhydroxide', *Chemical Geology,* **40:** 135-148.

APHA, 1985*. Standard Methods for the Examination of Water and Wastewater.*

Sixteenth edition. American Public Health Association.

L.S. Balistrieri and T.T. Chao, 1990, 'Adsorption of selenium by amorphous iron oxyhydroxide and manganese dioxide', *Geochimica et Cosmochimica Acta,* **54,** 739-751.

P. Benes, K. Kratzer, S. Vlckova and E. Sebestova, 1998, 'Adsorption of uranium on clay and the effect of humic substances', *Radiochimica Acta,* **82:** 367-373.

M.M. Benjamin and N.S. Bloom, 1981, 'Effects of strong binding of anionic adsorbates on adsorption of trace metals on amorphous iron oxyhydroxide'. In: *Adsorption from Aqueous Solution* (P.H. Tewari, ed.), pp. 41-60, Plenum Press, New York.

M.D.A. Bolland, A.M. Posner and J.P. Quirk, 1977, 'Zinc adsorption by goethite in the absence and presence of phosphate', *Australian Journal of Soil Research,* **15:** 279-286.

G.L. Booman and W.B. Holbrook, 1959, 'An extraction, controlled-potential coulometric method specific for uranium(VI)', *Analytical Chemistry,* **31:** 10-16.

O.K. Borgaard, 1982, 'The Influence of Iron Oxides on the Surface Area of Soil', *Journal of Soil Science,* **33:** 443-449.

Z. Borovec, 1981, 'The adsorption of uranyl species by fine clay', *Chemical Geology,* **32:** 45-58.

J.W. Bowden, A.M. Posner and J.P. Quirk, 1977, 'Ionic adsorption on variable charge mineral surfaces. Theoretical-charge development and titration curves'. *Australian Journal of Soil Research,* **15:** 121-136.

J. Bruno, J. de Pablo, L. Duro and E. Figuerola, 1995, 'Experimental study and modeling of the U(VI) – $Fe(OH)_3$ surface precipitation/coprecipitation equilibria', *Geochimica et Cosmochimica Acta,* **59:** 4113-4123.

S.A. Brusilovskii, 1958, 'Investigation of the precipitation of hexavalent uranium hydroxide', *Proceedings of the USSR Academy of Science,* **120:** 343-347.

C.C.Y. Chang, J.A. Davis and J.S. Kuwabara, 1987, 'A study of metal ion adsorption at low suspended-solid concentrations', *Estuarine, Coastal and Shelf Science,* **24:** 419-424.

Chemchek, 1990, *Kinetic Phosphorescence Analyser, Operation and Service Manual.* Chemchek Instruments Inc., Richland, USA.

C. Chisholm-Brause, S.D. Conradson, C.Y. Buscher, P.G. Eller and D.E. Morris, 1994, 'Speciation of uranyl sorbed at multiple binding sites on montmorillonite', *Geochimica et Cosmochimica Acta,* **58:** 3625-3631.

G.R. Choppin, H.R. Erten, and Y-X Xia, 1996, 'Variation of stability constants of thorium citrate complexes with ionic strength', *Radiochimica Acta,* **74:** 123-127.

R.M. Cornell, 1987, 'Comparison and classification of the effects of simple ions and molecules upon the transformation of ferrihydrite into more crystalline products', *Z. Pflanzenernahr. Bodenk.* **150:** 304-307.

J-P. Crine, 1987, 'Ionic impurities in water contained in plastic and pyrex bottles', *Polymer Engineering Science,* **27:** 611-614.

R.V. Davies, J. Kennedy, R.W. McIlroy, R. Spence and K.M. Hill, 1964, 'Extraction of uranium from sea water', *Nature,* **203:** 1110-1115.

J.A. Davis, R.O. James and J.O. Leckie, 1978, 'Surface ionization and complexation at the oxide / water interface', *Journal of Colloid and Interface Science,* **63:** 480-499.

J.A. Davis and D.B. Kent, 1990, 'Surface complexation modeling in aqueous geochemistry'. Chapter 5 in: *Reviews in MIneralogy Vol. 23: Mineral-Water Interface Geochemistry* (M.F. Hochella and A.F. White, Eds.). Mineralogical Society of America, Washington.

J.A. Davis and J.O. Leckie, 1978, 'Effect of adsorbed complexing ligands on trace metal uptake by hydrous oxides', *Environmental Science and Technology*, **12:** 1309-1315.

J.A. Davis and J.O. Leckie, 1980, 'Surface ionisation and complexation at the

oxide/water interface. 3. Adsorption of anions', *Journal of Colloid and Interface Science,* **74:** 32-43.

A.J. Dent, J.D.F. Ramsey and S.W. Swanton, 1992, 'An EXAFS study of uranyl ion in solution and sorbed onto silica and montmorillonite clay colloids', *Journal of Colloid and Interface Science,* **150: 45-60.**

G. Dongarra and D. Langmuir, 1980, 'The stability of UO_2OH^+ and $UO_2(HPO_4)_2^{2-}$ complexes at 25°C', *Geochimica et Cosmochimica Acta,* **44:** 1747-1751.

P. Duerden, 1992, 'The Alligator Rivers Analogue Project – characterisation of the development of the uranium dispersion fan', *Materials Research Society Symposium Proceedings*, **257:** 529-536.

M.C. Duff and C. Amrhein, 1996, 'Uranium (VI) adsorption on goethite and soil in carbonate solutions', *Soil Science Society of America Journal,* **60:** 1393-1400.

D.A. Dzombak and F.M.M. Morel, 1990*. Surface Complexation Modeling - Hydrous Ferric Oxide.* Wiley-Interscience, New York.

R. Edis, T. Murakami, N. Yanase, A. Koppi, D. Klessa, T.E. Payne, A. Snelling, L. Cao, T. Nightingale, J. Cashion, J. Brown, D. Emerson and D. Sverjensky, 1994. *Chemistry and Mineralogy of Rocks and Soil.* Alligator Rivers Analogue Project, Final Report, Volume 8. ANSTO, Menai, Australia.

H.A. Elliott, M.R. Liberati and C.P. Huang, 1986, 'Effect of Iron Oxide Removal on Heavy Metal Sorption by Acid Subsoils', *Water, Air and Soil Pollution,* **27:** 379-389.

H.T. Evans, Jr., 1963, 'Uranyl ion coordination', *Science,* **141:** 154-158.

A.J. Francis and C.J. Dodge, 1993, 'Influence of complex structure on the biodegradation of iron-citrate complexes', Applied and Environmental Microbiology, **59:** 109-113.

A.J. Francis, C.J. Dodge and J.B. Gillow, 1992, 'Biodegradation of metal citrate complexes and implications for toxic-metal mobility', *Nature,* **356:** 140-142.

R.A. Freeze and J.A. Cherry, 1979. *Groundwater*. Prentice Hall, New Jersey.

C.C. Fuller, J.A. Davis abd G.A. Waychunas, 1993. 'Surface chemistry of ferrihydrite: Part 2. Kinetics of arsenate adsorption and coprecipitation', *Geochimica et Cosmochimica Acta,* **57:** 2271-2282.

R.R. Gadde and H.A. Laitinen, 1974, 'Studies of heavy metal adsorption by hydrous iron and manganese oxides', *Analytical Chemistry,* **46**: 2022-2026.

A.M. Giblin, 1980, 'The role of clay adsorption in genesis of uranium ores'. In: *Uranium in the Pine Creek Geosyncline* (J. Ferguson and A.B Goleby, Eds.). IAEA, Vienna.

A.M. Giblin, B.D. Batts and D.J. Swaine, 1981, 'Laboratory simulation studies of uranium mobility in natural waters', *Geochimica et Cosmochimica Acta,* **45:** 699-709.

I. Grenthe, J. Fuger, R.J.M. Konings, R.J. Lemire, A.B. Muller, C. Nguyen-Trung and H. Wanner, 1992. *Chemical Thermodynamics of Uranium.* Elsevier, Amsterdam.

I. Grenthe, I. Puigdomenech, M.C.A. Sandino and M.H. Rand, 1995, '*Corrections to the uranium NEA-TDB review'.* In: Chemical Thermodynamics of Americium (Ed: R.J. Silva). Elsevier, Amsterdam.

A.R. Gupta and B. Venkataramani, 1988, 'Sorption of uranyl ions on hydrous oxides: A new surface hydrolysis model', *Bulletin of the Chemical Society of Japan,* **61:** 1357-1362.

D. Hawke, P.D. Carpenter and K.A. Hunter, 1989, 'Competitive adsorption of phosphate on goethite in marine electrolytes', *Environmental Science and Technology,* **23**: 187-191.

K.F. Hayes, G. Redden, W. Ela and J.O. Leckie, 1991, 'Surface complexation models: an evaluation of model parameter estimation using FITEQL and oxide mineral titration data', *Journal of colloid and Interface Science,* **142:** 448-469.

A. Herbelin and J. Westall, 1994. *FITEQL - A Computer Program for*

Determination of Chemical Equilibrium Constants from Experimental Data. Oregon State University, Corvallis.

C.H. Ho and D.C. Doern, 1985, 'The sorption of uranyl species on a hematite sol', *Canadian Journal of Chemistry,* **63:** 1100-1104.

C.H. Ho and N.H. Miller, 1985, 'Effect of humic acid on uranium uptake by hematite particles', *Journal of Colloid and Interface Science,* **106:** 281-288.

C.H. Ho and N.H. Miller, 1986, 'Adsorption of uranyl species from bicarbonate solution onto hematite particles', *Journal of Colloid and Interface Science,* **110:** 165-171.

P.B. Hostetler and R.M. Garrels, 1962, 'Transportation and precipitation of uranium and vanadium at low temperatures, with special reference to sandstone-type uranium deposits'. *Economic Geology,* **57:** 137-167.

C.K. Hsi and D. Langmuir, 1985, 'Adsorption of uranyl onto ferric oxyhydroxides: Application of the surface complexation site-binding model', *Geochimica et Cosmochimica Acta,* **49:** 1931-1941.

E.A. Jenne, 1968, 'Controls on Mn, Fe, Co, Ni, Cu and Zn concentrations in soils and water: the significant role of hydrous Mn and Fe oxides'. In: *Trace Inorganics in Water (Ed: R.A. Baker)*. ACS Symposium Series, Washington.

B.S. Jensen, 1982. *Migration Phenomena of Radionuclides into the Geosphere*. Harwood Academic Publishers for the Commission of the European Communities, Brussels.

W. B. Jepson and J.B. Rowse, 1975, 'The composition of kaolinite – an electron microscope microprobe study', *Clays and Clay Minerals,* **23:** 310-317.

J.H. Johnston and D.G. Lewis, 1983, 'A detailed study of the transformation of ferrihydrite to hematite in an aqueous medium at 92°C', *Geochimica et Cosmochimica Acta,* **47:** 1823-1831.

N.J. Keen, 1968, 'Studies on the extraction of uranium from sea water', *Journal of the British Nuclear Society,* **7:** 178-183.

D.G. Kinniburgh, 1986, 'General purpose adsorption isotherms', *Environmental Science and Technology,* **20:** 895-904.

D.G. Kinniburgh and M.L. Jackson, 1981, 'Cation adsorption by hydrous metal oxides and clay'. In: *Adsorption of Inorganics at Solid-Liquid Interfaces (Eds: M.A. Anderson and A.J. Rubin).* Ann Arbor Science Publishers, Michigan.

M. Kohler, E. Wieland and J.O. Leckie, 1992, 'Metal-ligand-surface interactions during sorption of uranyl and neptunyl on oxides and silicates'. pp 51-54 In: *Water-Rock Interaction (Eds: Kharaka and Maest).* Balkema, Rotterdam.

K.B. Krauskopf, 1967. *Introduction to Geochemistry*. McGraw-Hill, New York.

K.S. Kung and I.R. Triay, 1994, 'Effect of natural organics on Cs and Np sorption'*, Radiochimica Acta,* **66/67**: 421-426.

D. Langmuir, 1978, 'Uranium solution – mineral equilibria at low temperatures with applications to sedimentary ore deposits', *Geochimica et Cosmochimica Acta,* **42:** 547-569.

D. Langmuir, 1997. *Aqueous Environmental Geochemistry.* Prentice-Hall, New Jersey.

J.O Leckie, 1994, 'Ternary complex formation at mineral / solution interfaces'. pp181-212 In: *Binding Models Concerning Natural Organic Substances in Performance Assessment (NEA / OECD Workshop Proceedings).* OECD Documents, Paris.

K.H. Lieser, S. Quandt-Klenk and B. Thybusch, 1992, 'Sorption of uranyl ions on hydrous silicon dioxide', *Radiochimica Acta,* **57:** 45-50.

K.H. Lieser and B. Thybusch, 1988, 'Sorption of uranyl ions on hydrous titanium dioxide', *Fresenius'-Zeitschrift-fuer-Analytische-Chemie,* **332:** 351-357.

R.T. Lowson, S.A. Short, B.G. Davey and D.J. Gray, 1986, $^{234}U/^{238}U$ and $^{230}Th/^{234}U$ activity ratios in mineral phases of a lateritic weathered zone', *Geochimica et Cosmochimica Acta*, **50**: 1697-1702.

H.S. Mahal, B. Venkataramani and K.S. Venkateswarlu, 1981, 'Sorption properties of oxides VIII: Sorption of uranium on hydrous oxides', *Journal of Inorganic and Nuclear Chemistry,* **43:** 3335-3342.

R.L. Malcolm and P. MacCarthy, 1986, 'Limitations in the use of commercial humic acids in water and soil research', *Environmental Science and Technology,* **20:** 904-911.

E. Manzurola, A. Apelblat, G. Markovits and O. Levy, 1989, 'Mixed-metal hydroxycarboxylic acid complexes – formation constants of U^{VI} with Fe^{III}, Al^{III}, In^{III} and Cu^{II}', *Journal of the Chemical Society, Faraday Transactions 1*, **85:** 373-379.

K. Masuda and T. Yamamoto, 1971, 'Studies on environmental contamination by uranium 2. Adsorption of uranium on soil and its desorption', *Journal of Radiation Research,* **12-3-4:** 94-99.

L. Maya, 1982, 'Sorbed uranium (VI) species on hydrous titania, zirconia and silica gel', *Radiochimica Acta,* **31:** 147-151.

J.P. McKinley, J.M. Zachara, S.C. Smith and G.D. Turner, 1995, 'The influence of uranyl hydrolysis and multiple site-binding reactions on adsorption of U(VI) to montmorillonite', *Clays and Clay Minerals,* **43:** 586-598.

W. Miller, R. Alexander, N. Chapman, I. McKinley and J. Smellie, 1994. *Natural Analogue Studies in the Geological Disposal of Radioactive Wastes*. Elsevier, Amsterdam.

G.M. Milton and R.M. Brown, 1987, 'Adsorption of uranium from groundwater by common fracture secondary minerals', *Canadian Journal of Earth Sciences,* **24:** 1321-1328.

F.M.M. Morel and J.G. Hering, 1993. *Principles and Applications of Aquatic Chemistry,* John Wiley, New York.

A.I. Moskvin, A.M. Shelyakina and P.S. Perminov, 1967, 'Solubility product of uranyl phosphate and the composition and dissociation constants of uranyl phosphato-complexes', *Russian Journal of Inorganic Chemistry,* **12:** 1756-1760.

V. Moulin and G. Ouzounian, 1992, 'Role of colloids and humic substances in the transport of radio-elements through the geosphere', *Applied Geochemistry Supplement,* **1**: 179-186.

T. Murakami, H. Isobe, T. Ohnuki, N. Yanase, T. Sato, H. Kimura, K. Sekine, R. Edis, A.J. Koppi, D.A. Klessa, C. Conoley, T. Nagano, S. Nakashima and R. C. Ewing, 1994. *Weathering and its Effects on Uranium Redistribution*. Alligator Rivers Analogue Project, Final Report, Volume 9. ANSTO, Menai.

T. Nomizu, M. Sanji, M. Hiraide and A. Mizuike, 1989, 'Determination of humic and fulvic acids in river waters by concentration with anion exchanger followed by centrifugation'*, Analytical Sciences,* **5:** 363-365.

R.T. Pabalan, D.R. Turner, and F.P. Bertetti, 1994. 'Sorption modelling for HLW performance assessment'. In: *NRC High-level Radioactive Waste Research at CNWRA, January-June 1994* (B. Sagar, ed.), pp. 77-96, Center for Nuclear Waste Regulatory Analyses, San Antonio.

G.A. Parks, 1967, 'Aqueous surface chemistry of oxides and complex oxide minerals'. Chapter 6 in: *Equilibrium Concepts in Natural Water Systems* (R.F. Gould, Ed.). American Chemical Society, Washington.

G.A. Parks and P.L. DeBruyn, 1962, 'The zero point of charge of oxides', *Journal of Physical Chemistry,* **66:** 967-973.

T.E. Payne and T.D. Waite, 1991, 'Surface complexation modelling of uranium sorption data obtained by isotope exchange techniques', *Radiochimica Acta*, **52/53**: 487-493.

T.E. Payne, R. Edis, A.L. Herczeg, K. Sekine, T. Seo, T.D. Waite and N. Yanase, 1994. *Groundwater Chemistry*. Alligator Rivers Analogue Project, Final Report, Volume 7. 185pp. Australian Nuclear Science and Technology Organisation, Menai.

T.E. Payne, J.A. Davis and T.D. Waite, 1996, 'Uranium adsorption on ferrihydrite – effects of phosphate and humic acid', *Radiochimica Acta,* **74:** 239-243.

T.E. Payne, G.R. Lumpkin and T.D. Waite, 1998, 'Uranium^{VI} adsorption on model minerals: controlling factors and surface complexation modeling'. Chapter 2 in: *Adsorption of Metals by Geomedia: Variables, Mechanisms and Models* (E.A. Jenne, Ed.). Academic Press. San Diego. pp 75-97.

R.J. Pruett and H.L. Webb, 1993, 'Sampling and Analysis of KGa-1B Well Crystallized Kaolin Source Clay'. *Clays and Clay Minerals*, **41:** 514-519.

G.D. Redden, J. Li and J.O. Leckie, 1996, 'Ternary uranyl-citrate surface complex formation on goethite, gibbsite and phylosilicate minerals', Book of Abstracts, ACS National Meeting, New Orleans. American Chemical Society, Washington, D. C.

R. Reitmeyer, J.R. Bargar and J.A. Davis, 1999, 'A spectroscopic approach to surface complexation modeling of uranyl-carbonates on iron-oxide surfaces', Book of Abstracts, ACS National Meeting, Anaheim. American Chemical Society, Washington, D. C.

B. Salbu, H.E. Bjornstad, N.S. Lindstrom, E. Lydersen, E.M. Brevik, J.P.Rambaek and P.E. Paus, 1985, 'Size fractionation techniques in the determination of elements associated with particulate or colloidal material in natural fresh waters', *Talanta,* **32:** 907-913.

A. Sandino and J. Bruno, 1992, 'The solubility of $(UO_2)_3(PO_4)_2.4H_2O$ (s) and the formation of U(VI) phosphate complexes; Their influence on uranium speciation in natural waters', *Geochimica et Cosmochimica Acta,* **56:** 4135-4145.

J.M. Schreyer and C.F. Baes, 1954, 'The solubility of Uranium (VI) orthophosphates in phosphoric acid solutions', *Journal of the American Chemical Society,* **76:** 354-357.

U. Schwertmann and R.M. Cornell, 1991. *Iron Oxides in the Laboratory*. VCH Publishers, New York.

U. Schwertmann and E. Murad, 1983, 'Effect of pH on the formation of goethite and hematite from ferrihydrite', *Clays and Clay Minerals,* **31:** 277-284.

K. Sekine, T. Payne, T.D. Waite and J. Davis, 1990, 'Experimental study of uranium sorption'. Section 10 in: *Alligator Rivers Analogue Project, Progress Report, 1 September 1990 – 30 November 1990.* ANSTO, Menai.

S.M. Serkiz, J.D. Allison, E.M. Perdue, H.E. Allen and D.S. Brown, 1996, 'Correcting errors in the thermodynamic database for the equilibrium speciation model MINTEQA2'. *Water Research,* **30:** 1930-1933.

L.M. Shuman, 1977, 'Adsorption of Zn by Fe and Al hydrous oxides as influenced by aging and pH', *Soil Science Society of America Journal,* **41:** 703-706.

T.D. Smith, 1965, 'Chelates formed by Tin(II) with citric and tartaric acids, and their interaction with certain transition metal ions', *Journal of the Chemical Society,* **1965:** 2145-2150.

R.M. Smith and A.E. Martell, 1993. *NIST Critical Stability Constants of Metal Complexes Database, NIST Standard Reference Database 46.* US Department of Commerce, Gaithersburg MD.

A.A. Snelling, 1994. *Geologic Setting*. Alligator Rivers Analogue Project, Final Report, Volume 2. ANSTO, Lucas Heights.

A.G. Solomah, 1983, 'Effects of temperature on the leaching behavior of sintered modified Synroc-B waste form', *Nuclear Technology,* **62:** 311-316.

G. Sposito, 1989. *The Chemistry of Soils.* Oxford University Press, New York, 277pp.

I.E. Starik, F.E. Starik and A.N. Apollonova, 1958, 'Adsorption of microquantities of uranium by iron hydroxides and its desorption by the carbonate method', *USSR Journal of Inorganic Chemistry,* **3:** 121-128.

W. Stumm, 1992. *Chemistry of the Solid-Water Interface.* Wiley-Interscience, New York.

W. Stumm, H. Hohl and F. Dalang, 1976, 'Interaction of metal ions with hydrous oxide surfaces'. *Croatica Chemica Acta,* **48:** 491-504.

R.M. Taylor, 1990, 'Some observations on the formation and transformation of iron oxides'. In: *Soil Colloids and their Associations in Aggregates* (M.F. de Boodt, Ed.). Plenum Press, New York.

A. Tessier, P.G.C. Campbell and M. Bisson, 1979, 'Sequential Extraction Procedure for the Speciation of Particulate Trace Metals'. *Analytical Chemistry,* **51**: 844-850.

H.A. Thompson, G.A. Parks and G.E. Brown, Jr., 1994. **Spectroscopic Studies of U(VI) Sorption at the Kaolinite-Water Interface*. Report LA-SUB-95-177. Los Alamos National Laboratory.***

E. Tipping, 1993, 'Modelling the binding of Europium and the Actinides by Humic Substances', *Radiochimica Acta,* **62:** 141-152.

V.S. Tripathi, 1983. *Uranium (VI) Transport Modeling: Geochemical Data and Submodels.* PhD Thesis. Stanford University.

D.R. Turner, 1993. *Mechanistic Approaches to Radionuclide Sorption Modeling.* Report CNWRA 93-019. Center for Nuclear Waste Regulatory Analyses. San Antonio.

D.R. Turner and S.A. Sassman, 1996, 'Approaches to sorption modeling for high-level waste performance assessment', *Journal of Contaminant Hydrology,* **21:** 311-332.

C.H. Van Der Weijden, R.C. Arthur and D. Langmuir, 1976, 'Sorption of uranyl by hematite: Theoretical and geochemical implications'. *Geological Society of America, Abstracts.* p1152.

C.H. Van Der Weijden, M. Van Leeuwen and A.F. Peters, 1985, 'The adsorption of U(VI) onto precipitating amorphous ferric hydroxide'. *Uranium*, **2:** 53-58.

H. Van Olphen and J.J. Fripiat, 1979. *Data Handbook for Clay Materials and Other Non-metallic Minerals.* Pergamon, Oxford.

B. Venkataramani and A.R. Gupta, 1991, 'Effect of anions on the sorption of uranyl ions on hydrous oxides: Application of the surface hydrolysis model'.

Colloids and Surfaces, **53:** 1-19.

T.D. Waite, 1989, 'Mathematical modeling of trace element speciation'. Chapter 5 in: *Trace Element Speciation: Analytical Methods and Problems* (G.E. Batley, Ed.). CRC Press, Boca Raton.

T.D. Waite, J.A. Davis, T.E. Payne, G.A. Waychunas and N. Xu, 1994, 'Uranium(VI) Adsorption to Ferrihydrite: Application of a Surface Complexation Model'. *Geochimica et Cosmochimica Acta,* **58:** 5465-5478.

E. Warnecke, A. Hollman and G. Stier-Friedland, 1984, 'Migration of radionuclides: experiments within the site investigation program at Gorleben', *Materials Research Society Symposium Proceedings,* **26:** 41-48.

C.E. Weaver, 1976, 'The nature of TiO_2 in kaolinite', *Clays and Clay Minerals,* **24**: 215-218.

J. Westall and H. Hohl, 1980, 'A comparison of electrostatic models for the oxide / solution interface'. *Advances in Colloid and Interface Science,* **12:** 265-294.

N. Yanase, T. Nightingale, T. Payne and P. Duerden, 1991, 'Uranium distribution in mineral phases of rock by sequential extraction procedure', *Radiochimica Acta,* **52/53**: 387-393.

N. Yanase, T.E. Payne, and K. Sekine, 1995, 'Groundwater geochemistry in the Koongarra Ore Deposit, Australia (I): Implications for uranium migration', *Geochemical Journal*, 29: 1-29.

Appendix 1

U-sorption data sets

Data obtained in 0.1M NaNO3, equilibrated with air (unless otherwise indicated)

Experiments with various total U

U=1e-6 Fe=1mmol/L	
pH	U-sorbed(%)
3.04	0.7
3.06	1.4
3.28	5.2
3.35	2.3
3.53	3.5
3.57	2.2
3.68	6.3
3.83	15.3
3.99	13.8
4.08	16.0
4.25	28.5
4.37	40.8
4.53	57.1
4.55	51.5
4.68	71.7
4.78	74.5
5.02	86.1
5.03	86.9
5.27	94.2
5.31	96.0
5.54	97.3
5.76	99.5
5.96	99.5
6.25	99.4
6.55	99.5
6.93	98.9
7.50	98.4
7.77	98.1
8.00	97.2
8.19	94.3
8.31	83.6
8.33	86.5
8.53	63.8
8.64	36.1
8.78	29.7
8.93	1.6
9.21	2.6
9.61	1.8
9.68	1.8
10.02	0.0

These are the standard conditions

U=1e-5 Fe=1mmol/L	
pH	U-sorbed(%)
3.99	7.1
4.25	16.2
4.49	30.1
4.71	49.4
4.76	53.0
4.99	72.3
5.61	94.4
6.22	98.9
6.65	98.9
7.15	98.5
7.62	97.2
7.87	93.7
8.29	56.0
8.57	27.1
8.91	9.5
9.29	4.6
9.58	2.8
9.99	3.0

Higher Fe loading

U=1e-6 Fe=20mmol/L	
pH	U-sorbed(%)
2.58	0.0
2.97	0.8
3.32	9.0
3.69	42.4
3.99	71.1
4.28	91.4
4.63	98.3
4.89	99.5
5.38	99.8
5.96	99.9
6.55	99.9
7.20	99.9
7.58	99.9
7.94	99.9
8.18	99.8
8.62	97.4
8.98	77.8
9.26	34.5
9.65	0.0
9.97	0.0

U=1e-4 Fe=1mmol/L	
pH	U-sorbed(%)
4.00	0.0
4.27	0.9
4.52	7.7
4.76	25.5
4.89	33.2
5.04	46.4
5.54	79.1
6.45	95.9
6.76	96.3
7.21	94.1
7.50	87.9
8.01	31.7
8.34	13.3
8.52	4.4
8.63	0.0
8.88	0.0
9.46	0.0

U=1e-8 Fe=1mmol/L	
pH	U-sorbed(%)
4.02	28.2
4.29	43.4
4.50	70.1
4.78	88.3
5.06	95.9

Experiments on this page
0.1 M NaNO3
Air equilibration
Total U - indicated
Total Fe - indicated

Elevated pCO2

Elevated pCO2
=1e-2atm
I=0.1
U=1e-6 Fe=1mmol/L

pH	U-sorbed(%)
3.65	3.1
4.23	37.6
4.84	91.6
5.18	96.6
5.60	95.6
5.98	99.3
6.40	99.2
6.85	97.9
7.32	71.5
7.51	36.0
7.85	0.0
8.21	0.0
8.49	0.0
8.87	0.0
9.29	0.0

Ionic strength varied

Air equilibrated

I=0.004
U=1e-6 Fe=1mmol/L

pH	U-sorbed(%)
3.60	0.7
4.16	36.4
4.39	56.5
4.52	60.5
4.73	78.0
5.08	93.1
5.29	94.1

I=0.02
U=1e-6 Fe=1mmol/L

pH	U-sorbed(%)
3.58	5.2
4.09	25.3
4.35	39.8
4.52	50.9
4.83	82.5
5.03	90.6
5.38	96.6

I=0.02 (cont)

7.74	98.9
7.96	97.1
8.10	97.1
8.23	96.9
8.43	90.1
8.50	84.6
8.64	76.6
8.75	51.8
8.80	53.2
9.12	11.3
9.55	0.0

I=0.1
U=1e-6 Fe=1mmol/L

pH	U-sorbed(%)
3.04	0.7
3.06	1.4
3.28	5.2
3.35	2.3
3.53	3.5
3.57	2.2
3.68	6.3
3.83	15.3
3.99	13.8
4.08	16.0
4.25	28.5
4.37	40.8
4.53	57.1
4.55	51.5
4.68	71.7
4.78	74.5
5.02	86.1
5.03	86.9
5.27	94.2
5.31	96.0
5.54	97.3
5.76	99.5
5.96	99.5
6.25	99.4
6.55	99.5
6.93	98.9
7.50	98.4
7.77	98.1
8.00	97.2
8.19	94.3
8.31	83.6
8.33	86.5
8.53	63.8
8.64	36.1
8.78	29.7
8.93	1.6
9.21	2.6
9.61	1.8
9.68	1.8
10.02	0

Standard conditions

I=1.0
U=1e-6 Fe=1mmol/L

pH	U-sorbed(%)
3.63	4.7
4.06	13.4
4.35	36.8
4.48	51.1
4.91	78.4
5.20	91.2

I=0.5
U=1e-6 Fe=1mmol/L

pH	U-sorbed(%)
7.43	98.9
7.77	91.6
8.00	79.0
8.15	70.6
8.23	62.1
8.29	44.7
8.48	29.0
8.59	22.8
8.72	10.7
9.04	4.8
9.60	0.0
10.07	0.0

I=2.5
U=1e-6 Fe=1mmol/L

pH	U-sorbed(%)
7.95	45.6
8.22	25.6
8.40	4.9
8.67	2.3

FERRIHYDRITE / PHOSPHATE SYSTEM

I=0.1 U=1umol/L P=100umol/L		
pH	U-sorb(%)	P-sorb(%)
2.63	2.1	97.0
3.13	10.9	99.4
3.44	34.0	99.4
3.72	59.4	99.2
4.03	83.5	
4.29	93.2	99.0
4.56	97.7	98.7
4.88	99.3	98.9
5.58	99.9	96.7
6.16	99.9	93.9
6.55	99.8	91.7
6.89	99.9	88.0
7.31	99.8	78.8
7.70	98.2	82.8
7.96	98.5	77.4
8.46	76.8	61.3
8.90	15.4	53.8
9.53	1.2	38.6
9.96	1.3	17.9

I=0.02 U=1umol/L P=100umol/L		
pH	U-sorb(%)	P-sorb(%)
3.03	12.5	96.8
3.49	45.9	99.1
4.03	84.0	99.5
4.60	98.1	97.0
5.11	99.9	96.1
6.10	100.0	96.6
7.16	100.0	88.0
7.97	95.6	68.0
8.28	95.3	55.8
8.62	72.4	43.7
8.97	21.4	32.5
9.36	0.0	21.3
9.68	0.0	19.0

I=0.5 U=1umol/L P=100umol/L		
pH	U-sorb(%)	P-sorb(%)
3.04	12.3	94.2
3.37	29.1	93.7
3.75	67.0	97.2
4.04	86.9	97.8
4.49	96.6	97.0
5.01	99.3	92.5
6.04	99.6	91.3
7.11	99.9	89.5
7.41	100.0	
7.49	99.9	
7.84	97.3	
7.97	96.2	68.5
8.14	76.6	
8.23	69.6	57.6
8.27	59.8	
8.57	24.7	49.2
8.92	4.9	37.0
9.30	0.3	25.4
9.62	2.6	18.9

I=0.1 U=100umol/L P=100umol/L		
pH	U-sorb(%)	P-sorb(%)
2.60	5.3	98.4
3.09	13.5	99.0
3.56	23.0	99.0
4.00	33.1	98.2
4.47	55.2	99.0
4.96	80.4	98.8
5.57	96.7	98.2
6.21	99.0	98.0
7.04	97.2	96.1
7.30	97.3	97.0
7.85	94.8	93.8
8.17	71.2	84.6
8.47	25.2	65.1
8.76	10.9	54.2
9.07	3.7	45.8
9.50	1.1	29.6

I=0.1 No U P=100umol/L	
pH	P-sorb(%)
2.97	99.4
3.94	98.2
4.94	98.9
6.03	98.4
6.95	93.0
7.44	85.7
7.97	70.2
8.33	50.8
8.95	32.1
9.55	16.2
10.00	14.5

Total Fe = 1 mmol/L
Air equilibration
Ionic strength is indicated

FERRIHYDRITE / CITRATE SYSTEM

0.1M NaNO3, 1 mmol/L Fe; 0.01 M citrate

U=1umol/L

pH	% U on solid	% Fe on solid
3.03	7.4	0
3.44	5.4	0
3.99	-2.4	0
4.50	4.0	0
5.02	3.9	0
5.51	7.0	0
5.99	1.8	0
6.52	6.6	0
7.10	6.8	49.2
7.52	-2.0	80.2
8.06	4.1	89.5
8.30	1.4	82.1
8.57	6.7	--
8.90	7.6	95.7
9.32	2.6	98.7
9.63	-2.8	98.5
10.01	3.4	98.8

U=10 umol/L

pH	% U on solid	% Fe on solid
3.03	0	0.2
3.49	0	0
3.95	0	0
4.47	0	0.7
4.99	0	0.6
5.51	0	0.2
5.99	0	0.1
6.46	0	2.6
6.97	0	68.5
7.50	1.4	82.9
8.03	0	86.9
8.30	0	89.4
8.62	0	91.6
8.94	1.9	92.6
9.32	0.5	96.3
9.64	0	97.5
9.93	2.4	96

Citrate not present

pH	Fe on solid (%)
3.06	14.3
3.28	67.6
3.57	95.4
3.83	98.0
4.00	100.0

Citrate = 1 e-4 U=1e-6 Fe=1e-3

U			Fe	
pH	% Sorbed	Abs. Error	% Dissolve	Abs. Error
3.06	11.1	4	9.1	0.4
3.55	23.1	3	9.1	0.4
4.06	26.8	3	9.1	0.4
4.59	25.4	3	7.2	0.3
5.19	18.1	3	9.1	0.4
5.84	7.8	4	8.6	0.3
6.31	4.7	4	4.2	0.2
6.72	9.5	4	7.1	0.3
7.13	19.3	3	2.9	0.1
7.47	30.8	3	3.1	0.1
7.64	36.6	3	5.4	0.2
7.84	58.1	2	5.6	0.2
8.15	63.3	1	0.3	0.01
8.48	34.5	3	0.9	0.03
8.92	8.3	4	0.5	0.02
9.33	7.4	4	0.7	0.03
9.66	7.7	4	0.4	0.02
10.00	4.9	4	1.0	0.04

FERRIHYDRITE / HUMIC ACID SYSTEM

0.1 M $NaNO_3$, air equilibrated, Fe=1mmol/L

	U = 1 umo/L	
pH	U-sorb(%)	HA-sorb(%)
3.07	8.4	
3.08	0.0	
3.30	7.5	
3.42	6.4	
3.56	22.2	85.8
3.76	26.2	--
3.84	25.2	--
3.99	33.3	--
4.06	47.4	81.8
4.29	57.0	--
4.57	77.5	87.5
4.61	81.8	--
4.92	91.7	--
5.08	92.4	93.5
5.24	96.9	--
5.45	96.8	--
5.96	98.7	90.3
6.48	98.2	--
7.03	--	81.6
7.06	98.3	--
7.26	97.1	--
8.00	98.3	80.8
8.22	88.2	--
8.27	93.9	90.7
8.60	68.8	73.4
8.64	45.9	--
8.92	18.5	81.8
9.28	4.0	--
9.48	18.5	66.9
9.75	--	--
10.00	0.0	50.7

FERRIHYDRITE / SULFATE SYSTEM

SULFATE = 0.01 mol/L

U = 1 umol/L		U=10 umol/L	
pH	U-sorb(%)	pH	U-sorb(%)
2.99	3.6	2.95	2.1
3.44	0.0	3.53	4.6
4.00	1.6	4.11	6.2
4.54	25.8	4.53	15.3
4.95	67.4	5.01	43.9
5.55	93.9	5.48	78.7
6.01	97.6	6.05	94.4
6.48	98.8	6.55	97.8
6.97	98.4	6.92	98.1
7.56	96.6	7.29	97.0
7.87	95.0	7.75	93.5
8.27	76.4	8.18	65.3
8.50	48.7	8.48	21.9
8.89	16.7	8.82	9.1
9.26	8.4	9.20	3.1
		9.58	5.8
		9.95	3.6

Isotherm data used in Figure 6.4 I = 0.1

[U] mol/L	U ads mol/mol Fe	total U mol/L	% ads	exact pH
	pH ~4.52			
2.99E-09	7.01E-06	1.0E-08	70.1	4.50
4.29E-07	5.71E-04	1.0E-06	57.1	4.53
4.85E-07	5.15E-04	1.0E-06	51.5	4.55
6.99E-06	3.00E-03	1.0E-05	30.0	4.49
9.23E-05	7.70E-03	1.0E-04	7.7	4.52
	pH ~4.78			
1.17E-09	8.83E-06	1.0E-08	88.3	4.78
2.55E-07	7.45E-04	1.0E-06	74.5	4.78
4.70E-06	5.30E-03	1.0E-05	53.0	4.76
7.45E-05	2.55E-02	1.0E-04	25.5	4.76
	pH ~5.02			
1.31E-07	8.69E-04	1.0E-06	86.9	5.03
1.39E-07	8.61E-04	1.0E-06	86.1	5.02
2.77E-06	7.20E-03	1.0E-05	72.3	4.99
5.36E-05	4.64E-02	1.0E-04	46.4	5.04
	pH ~5.57			
2.70E-08	9.73E-04	1.0E-06	97.3	5.54
5.60E-07	9.40E-03	1.0E-05	94.4	5.61
2.09E-05	7.91E-02	1.0E-04	79.1	5.54

U sorption isotherm at pH 4.5 No phosphate present I=0.02

Final pH	Total U (μM)	% Sorbed	Abs. Error	U in sol. (μM)	U sorbed (mmol/mol Fe)	Abs. Error
4.52	0.095	78.5	0.9	0.0205	0.075	0.0008
4.51	0.289	71.2	1.2	0.0832	0.206	0.003
4.50	0.474	67.0	1.3	0.156	0.318	0.006
4.50	0.962	61.1	1.6	0.374	0.588	0.01
4.48	3.00	48.6	2.1	1.54	1.46	0.06
4.50	4.81	39.2	2.4	2.92	1.89	0.1
4.51	9.52	32.2	2.7	6.46	3.06	0.3
4.51	29.11	28.7	2.9	20.77	8.34	0.8
4.50	49.24	22.6	3.1	38.13	11.12	2
4.49	97.43	18.7	3.3	79.25	18.18	3
4.50	292.59	12.6	3.5	255.79	36.80	10

U sorption isotherm at pH 5.25 No phosphate present I = 0.02

Final pH	Init. Conc (μM)	% Sorbed	Abs. Error	U in sol. (μM)	U sorbed (mmol/mol Fe)	Abs. Error
5.23	0.299	96.7	0.13	0.00997	0.289	0.0004
5.22	0.457	94.5	0.22	0.0253	0.432	0.001
5.24	0.975	94.6	0.22	0.0526	0.922	0.002
5.24	2.96	90.9	0.36	0.268	2.69	0.01
5.23	4.87	92.4	0.30	0.371	4.50	0.01
5.25	9.62	90.3	0.39	0.931	8.69	0.04
5.21	30.20	84.1	0.63	4.79	25.41	0.2
5.21	50.94	82.3	0.71	9.01	41.94	0.4
5.20	99.48	73.1	1.07	26.73	72.75	1
5.22	298.18	45.4	2.18	162.81	135.38	7
5.24	491.82	34.6	2.61	321.53	170.30	13
5.24	967.54	22.6	3.10	749.15	218.39	30
5.26	949.97	20.8	3.17	752.74	197.23	30

U sorption data Ferrihydrite

U sorption isotherm in presence of phosphate (100 umol/L)
Figure 6.15 and 6.16 Fe = 1 mmol/L I=0.02

U						
Final pH	Init. Conc (μM)	% Sorbed	Abs. Error	U in sol. (μM)	U sorbed (mmol/mol Fe)	Abs. Error
4.53	0.999	98.1	0.1	0.0191	0.980	0.001
4.52	3.04	96.8	0.1	0.0962	2.95	0.004
4.53	5.99	96.5	0.1	0.210	5.78	0.008
4.52	9.88	94.7	0.2	0.522	9.36	0.02
4.54	30.45	90.5	0.4	2.90	27.55	0.1
4.54	61.63	82.2	0.7	10.98	50.65	0.4
4.55	101.55	71.2	1	29.22	72.32	1
4.52	303.54	42.7	2	173.95	129.59	7
4.50	606.38	27.6	3	438.96	167.41	18
4.50	982.20	20.2	3	783.91	198.29	31

Adsorption of P. No U present (isotherm)
Figure 6.17 Fe = 1 mmol/L I=0.02

Final pH	Init. Conc (μM)	% Sorbed	Abs. Error	P in sol. (μM)	P sorbed (mmol/mol Fe)	Abs. Error
5.26	0.978	99.7	0.01	0.00277	0.975	0.0001
5.24	2.00	98.8	0.05	0.0230	1.98	0.001
5.24	2.96	98.5	0.06	0.0457	2.92	0.002
5.24	5.93	98.1	0.08	0.115	5.81	0.005
5.27	9.84	97.6	0.1	0.234	9.61	0.009
5.24	20.00	96.8	0.1	0.647	19.35	0.03
5.26	31.21	97.3	0.1	0.835	30.37	0.03
5.20	60.30	99.6	0.02	0.237	60.07	0.01
5.19	96.79	97.8	0.09	2.15	94.64	0.09
5.21	97.11	96.5	0.1	3.38	93.73	0.1
5.29	191.80	73.2	1	51.39	140.41	2.1
5.30	283.93	54.3	2	129.71	154.22	5
5.29	587.05	32.0	3	399.08	187.96	16
5.25	958.49	20.3	3	764.02	194.47	31

Adsorption of P (isotherm) No U present Fe = 1 mmol/L
Figure 6.17 I=0.02

Final pH	Init. Conc (μM)	% Sorbed	Abs. Error	P in sol. (μM)	P sorbed (mmol/mol Fe)	Abs. Error
8.23	2.93	99.1	0.03	0.0251	2.90	0.001
8.23	5.69	97.6	0.1	0.136	5.55	0.01
8.23	9.42	96.8	0.1	0.303	9.11	0.01
8.23	19.25	92.8	0.3	1.38	17.87	0.1
8.23	28.95	90.8	0.4	2.66	26.29	0.1
8.24	55.34	75.8	1	13.40	41.94	1
8.25	95.07	57.2	2	40.71	54.36	2
8.23	190.42	35.8	3	122.27	68.15	5
8.25	284.05	25.3	3	212.22	71.83	8
8.27	578.34	9.0	4	526.33	52.01	21
8.27	943.23	3.3	4	911.68	31.55	36
8.27	1984.02	4.9	4	1887.54	96.48	76
8.26	2940.43	3.1	4	2848.60	91.83	114

SUMMARY OF SORPTION DATA - KAOLINITE KGa-1

0.1 M NaNO3, air equilibration, 4 g/L
Percentage uptake of U on the solid

Total U 1umol/L	
pH	U-sorbed (%)
2.54	0.3
3.06	0.0
3.55	7.1
4.04	12.0
4.55	33.7
5.02	62.5
5.49	83.9
6.04	95.0
6.36	94.6
7.13	97.8
7.68	98.6
7.79	93.0
8.16	77.8
8.51	36.4
8.82	26.4
9.23	0.0
9.61	0.0
9.93	0.0

Total U 10 umol/L	
pH	U-sorbed (%)
2.51	3.6
3.04	0.0
3.54	3.0
4.04	0.0
4.51	12.3
4.92	25.1
5.53	49.8
6.09	80.7
6.64	90.0
7.12	90.7
7.39	91.6
7.83	56.7
8.14	29.1
8.51	15.2
8.79	8.6
9.24	1.2
9.59	0.0
9.95	0.0

Total U 100 umol/L	
pH	U-sorbed (%)
2.54	1.5
3.04	2.6
3.53	0.0
4.09	2.2
4.53	8.6
4.63	9.0
5.06	12.9
5.28	14.9
5.49	25.2
5.56	16.7
5.81	72.1
5.88	33.5
5.94	45.5
6.03	91.7
6.55	97.8
7.13	97.1

Total U 0.01 umol/L	
pH	U-sorbed (%)
2.49	1.6
3.01	6.3
3.34	11.5
3.84	19.0
4.05	40.4
4.53	70.8
5.03	90.4
5.45	96.2
6.14	99.5

Total U 1 mmol/L	
pH	U-sorbed (%)
3.55	4.0
4.07	0.0
4.69	2.4
5.15	15.7
5.24	78.4
6.06	97.5

SUMMARY OF SORPTION DATA - KAOLINITE KGa-1B

(standard conditions) Mass loading 4 g/L, air equilibration, 0.1 M NaNO3

total U 1e-8		total U 1e-6		total U 1e-5		total U 1e-4		total U 1e-3	
pH	%	pH	%	pH	%	pH	%	pH	%
2.55	1.5	2.52	4.3	2.55	0.0	7.34	79.7	8.07	88.9
3.11	2.3	3.00	6.6	3.05	4.0	7.90	62.6	8.20	75.6
3.53	16.3	3.53	9.5	3.55	0.0	8.16	18.2	8.28	57.6
4.07	34.1	4.02	16.0	4.09	4.2	8.49	13.5	8.72	10.6
4.55	72.1	4.55	33.5	4.55	9.4	8.87	10.6		
5.03	90.9	4.67	26.9	5.00	27.9	9.27	8.9		
5.46	97.6	4.70	37.3	5.43	50.3	9.60	7.6		
5.99	99.8	4.74	34.0	5.90	75.3	9.94	8.3		
		4.75	34.2	6.34	89.5				
		4.83	42.1	6.76	91.6				
		4.89	41.1	7.00	90.9				
		4.93	45.9	7.27	89.2				
		4.94	51.6	7.46	85.1				
		4.97	48.1	7.86	53.2				
		5.04	55.5	8.27	25.4				
		5.08	60.1	8.76	7.9				
		5.12	57.1	9.23	2.0				
		5.13	63.5	9.63	0.0				
		5.21	67.6	9.98	0.0				
		5.22	68.7						
		5.30	71.1						
		5.32	73.7						
		5.38	73.8						
		5.43	77.3						
		5.50	77.4						
		6.08	90.0						
		6.54	93.0						
		6.92	98.8						
		7.22	96.3						
		7.92	94.7						
		8.24	62.8						
		8.56	48.5						
		8.95	26.6						
		9.36	13.0						
		9.59	2.6						
		9.98	0.7						

KGa-1B higher mass loading		40 g/L	
total U = 1e-6		total U = 1e-5	
pH	%	pH	%
2.54	0.0	2.54	2.3
2.97	1.5	3.06	3.7
3.51	15.9	3.60	7.9
4.02	36.2	4.02	19.7
4.38	53.0	4.42	27.3
4.84	77.6	4.80	47.9
5.25	95.4	5.42	90.9
5.80	98.2	5.83	94.7
6.43	99.8	6.60	99.4
7.03	99.9	7.27	99.2
7.35	99.8	7.38	97.3
7.89	99.8	7.93	98.7
8.30	94.3	8.24	69.5
8.59	87.4	8.61	57.2
8.93	66.2	8.92	39.0
9.25	34.8	9.26	23.6
9.60	6.8	9.62	12.8
9.91	0.0	9.98	1.7
air equilibration, 0.1 M NaNO3			

Ionic strength of 0.5 Mass loading 4g/L	
Total U = 1e-6	
2.49	0.0
3.00	0.0
3.53	6.0
3.98	24.8
4.56	50.0
5.00	61.4
5.56	91.5
5.97	94.1
6.32	99.8
6.73	99.7
6.85	99.8
7.75	92.0
8.08	46.3
8.56	22.5
8.94	6.2
9.25	0.0
9.65	0.0
9.97	0.0

Phosphate experiments			Total P of 100 u mol/L		
	4 g/L	KGa-1B		40 g/L	KGa-1B
	U ads	Pads		U ads	P ads
2.59	6.4	5.3	2.54	11.5	46.9
3.08	21.8	8.1	3.03	27.9	44.7
3.59	37.4	6.6	3.53	45.7	48.5
4.09	55.2	10.4	4.04	71.6	54.7
4.62	83.7	12.6	4.35	91.0	67.5
5.04	95.0	12.7	4.75	97.3	73.3
5.56	98.5	14.8	5.19	99.2	71.2
6.01	99.0	13.2	6.37	99.8	70.1
6.43	99.6	13.5	6.42	99.9	81.7
6.96	99.1	13.7	7.10	99.9	64.6
7.39	99.4	12.4	7.55	99.7	59.9
7.96	95.8	10.1	8.10	99.8	70.0
8.28	68.3	8.0	8.32	95.7	58.8
8.61	46.3	5.1	8.54	87.1	47.0
8.94	30.8	2.5	8.94	76.1	40.0
9.42	1.4	1.3	9.33	31.1	--
9.68	0.3	0.0	9.73	5.1	16.4
10.04	0.0	0.0	10.02	0.0	8.9
U=1e-6, 0.1 M NaNO3			U=1e-6, 0.1 M NaNO3		

Humic acid experiments	
KGa-1B 4 g/l	
pH	U ads (%)
2.59	6.6
3.10	18.4
3.53	32.3
4.08	55.3
4.59	78.3
5.06	91.4
5.67	97.7
6.05	99.2
6.66	99.1
7.05	99.0
7.60	98.6
8.00	91.6
8.26	67.9
8.61	35.2
8.96	12.6
9.32	5.9
9.69	0.0
10.02	0.7
U=1e-6, 0.1 M NaNO3	

Sulfate experiments
Sulfate 0f 0.01 M, KGa-1B loading of 4 g/L, 0.1 M NaNO3

Total U 1e-6	
pH	U-ads
2.53	3.7
2.91	1.2
3.45	1.3
3.99	0.0
4.52	12.7
4.96	36.1
5.63	84.3
6.23	91.4
6.80	95.7
7.19	95.9
7.67	93.8
8.11	79.4
8.42	59.6
8.48	35.6
8.86	4.5
9.25	0.0
9.27	11.5
9.61	0.0
9.63	6.3
9.91	4.9
9.95	0.0

Total U 1 e-5	
pH	Uads
2.43	6.2
2.89	7.4
3.52	8.2
3.97	9.6
4.52	18.5
4.90	23.6
4.96	23.9
5.38	43.5
5.78	45.8
6.03	61.3
6.10	65.4
6.67	78.9
7.11	85.0
7.14	77.6
7.47	80.3
7.58	75.5
7.68	73.4
7.99	49.3
8.01	34.2
8.03	53.2
8.21	38.7
8.52	23.5
8.89	14.3
9.26	10.7
9.63	8.6
9.98	0.5

SUMMARY OF SORPTION DATA - KAOLINITE KGa-1B

CITRATE EXPERIMENTS

1. Total CIT -= 0.01 M
Kga-1B, 4 g/L, 0.1 M NaNO3, air equilibrium

total U = 1e-6		total U = 1e-5	
pH	% Sorbed	pH	% Sorbed
2.44	2.3	2.44	4.1
2.97	4.4	2.94	2.7
3.46	2.1	3.47	2.6
3.9	0.0	3.95	2.4
4.49	0.0	4.48	0.0
4.93	3.7	4.99	0.4
5.43	4.6	5.48	2.8
5.95	2.0	5.94	0.0
6.46	0.0	6.47	0.0
6.98	0.4	6.94	0.0
7.49	0.0	7.49	2.0
7.92	0.6	7.94	0.0
8.19	0.0	8.23	2.1
8.55	0.4	8.57	0.0
8.95	2.8	8.92	0.0
9.26	2.2	9.26	0.0
9.69	0.0	9.65	1.5
10.03	0.0		

2. Citrate=1e-4
U=1e-6

pH	% Sorbed
2.49	2.5
3.04	9.8
3.51	11.7
4.02	6.9
4.68	3.1
5.20	2.6
5.70	3.5
6.11	6.7
6.53	5.6
6.83	19.6
7.15	9.6
7.40	8.2
7.94	32.0
8.02	40.8
8.39	46.4
8.82	23.7
9.24	9.3
9.63	2.1
9.98	3.4

SUMMARY OF SORPTION DATA - NATURAL SUBSTRATES

W1 SAMPLE

Mass loading of 4 g/L (air-equilibrated)

Spike added		Effect of DCB	
pH	U-sorb(%)	pH	U-sorb(%)
1.19	5.6	1.26	8.0
1.85	10.5	1.83	0.0
2.41	15.6	2.65	12.0
3.00	25	3.19	10.0
3.64	48	3.78	29.3
4.19	66.5	4.04	37.2
4.50	82.6	4.26	47.5
5.05	93.1	4.64	66.3
5.21	95.7	5.30	90.2
6.20	99.5	6.29	97.6
7.05	99.3		
Isotope exchange not determined		(air)	

Mass loading of 20 g/L (elevated CO2)

pCO2 = 1 %		Isotope exchange	
Spike added		%	ug/g
pH	U-sorb(%)	236 (sol)	238 (sol)
1.24	11.50	88.50	40.9
2.08	20.80	79.20	34.7
3.14	48.90	51.10	17.6
4.06	84.90	15.10	4.4
5.19	97.92	2.08	1.0
6.05	99.09	0.91	0.4
6.58	98.51	1.49	0.7
6.79	97.85	2.15	1.1
6.93	96.35	3.65	1.5
7.54	75.00	25.00	7.7
8.06	36.00	64.00	23.6
8.53	12.00	88.00	34.1
8.93	6.40	93.60	38.6
9.24	0.00	100.00	44.9

Mass loading of 20 g/L (air)

Spike added		Isotope exchange	
		%	ug/g
pH	U-sorb(%)	236 (sol)	238 (sol)
1.57	14	86	39.4
2.08	23	77	32.4
2.56	32	68	24
3.04	41	59	17.6
3.55	57	43	11.2
4.13	78.9	21.1	3.88
4.64	95.6	4.4	1.18
5.29	99.1	0.9	0.5
5.68	99.1	0.9	<0.4
6.77	99.4	0.6	<0.4
6.83	99.6	0.4	<0.4
7.54	98.6	1.4	<0.4
8.14	91.4	8.6	1.4
8.23	85.1	14.9	1.52
8.37	84	16	2.72
8.71	59	41	6.4
8.88	62	38	10.2
9.26	40	60	19.4
9.63	21	79	28.4
9.93	8	92	35.6

U = 1e-4 added (air)

Mass loading 20 g/L	
pH	U-sorb(%)
1.56	4.2
2.08	7.4
2.59	11.9
3.10	11.1
3.60	27
4.14	38.6
4.49	50.2
4.95	69.5
5.62	90.6
5.92	96
6.91	98.1
7.28	97.4
7.46	97.7
8.08	74.4
8.25	44
8.57	25.4
8.84	11.7
9.27	10
9.70	6.2
10.09	8.2

SUMMARY OF SORPTION DATA - NATURAL SUBSTRATES

W2 SAMPLE

Mass loading of 4 g/L	

Spike added		Isotope exchange %	ug/g
pH	U-sorb(%)	236 (sol)	238 (sol)
1.56	4.0	96.0	240
2.14	5.7	94.3	273
2.57	16.2	83.8	204
2.84	21.2	78.8	200
3.22	32.1	67.9	160
3.59	45.1	54.9	128
3.77	50.7	49.3	115
3.92	57.3	42.7	95
4.2	68.4	31.6	68
4.46	77.3	22.7	53
4.6	84.3	15.7	34
4.96	93.3	6.7	18
5.32	97.3	2.7	6
5.89	99.0	1.0	2
6.01	99.2	0.8	
6.62	99.3	0.7	
6.79	99.5	0.5	
7.23	98.9	1.1	2
7.38	99.1	0.9	2
7.48	98.6	1.4	3
8.31	76.0	24.0	47
8.62	48.8	51.2	99
8.89	20.9	79.1	155
9.23	8.4	91.6	187
9.64	5.9	94.1	191
9.98	1.4	98.6	198

Effect of DCB	
pH	U-sorb(%)
1.61	2.2
2.21	0.3
2.45	5.6
2.87	7.3
3.25	0.0
3.75	14.2
4.36	47.1
4.84	73.4
5.37	94.9
6.39	98.5

Added U of 1e-4 M	
pH	U-sorb(%)
1.69	0.9
2.41	5.9
3.01	4.9
3.56	7.3
3.90	17.3
4.11	18
4.69	29.1
5.48	53.9
6.37	90.8

Elevated CO2

pCO2=1%

Mass loading of 4 g/L Spike added		Isotope exchange		
pH	U-sorb(%)	% 236 (sol)	ug/g 238 (sol)	234U/238U
1.14	7.0	93.0	266	0.61
2	9.7	90.3	225	0.68
3.08	33.0	67.0	161	0.66
3.93	63.6	36.4	78	0.64
4.76	91.0	9.0	19	
5.76	97.9	2.2	8	
6.31	97.6	2.4	8	
6.58	96.8	3.3	8.5	
7.08	84.2	15.8	34	0.68
7.5	41.6	58.4	129	0.66
8.02	10.3	89.7	198	0.65
8.65	0.0	100.0	216	0.71
9.05	2.0	98.0	225	0.65
9.38	3.4	96.6	221	0.66

W2 (continued)

Other ionic strengths

0.02M

pH	U-sorb(%)	236(sol)	ug/g 238U(sol)
2.05	12	88.0	226
2.63	26	74.0	183
3.12	41	59.0	134
3.56	53	47.0	94
3.91	69	31.0	62
4.26	79	21.0	44
4.65	90.3	9.7	21

0.2M

pH	U-sorb(%)	236(sol)	238U(sol)
2.08	2	98.0	220
2.52	21	79.0	211
3.13	34	66.0	168
3.52	44	56.0	128
3.97	66	34.0	92
4.53	85	15.0	36
4.99	92.9	7.1	14

2.2M

pH	U-sorb(%)	236(sol)	238U(sol)
2.04	4	96.0	204
2.49	24	76.0	173
3.06	44	56.0	134
3.63	63	37.0	95
4.17	83	17.0	35
4.89	96	4.0	10

SUMMARY OF SORPTION DATA - NATURAL SUBSTRATES

W2c SAMPLE Mass loading of 4 g/L

Spike added			0.1 M NaNO3		
pH	U-sorb(%)	236U(aq)	238U(aq)	234U/238U	error
1.58	1.4	98.6	104.0	0.64	0.04
2.12	7.4	92.6	98.3	0.64	0.03
2.65	17.7	82.3	81.3	0.68	0.05
3.14	24.7	75.3	68.2	0.70	0.05
3.70	48.1	51.9	44.2	0.68	0.04
4.32	77.6	22.4	18.9	0.71	0.05
4.57	87.4	12.6	10.7	0.64	0.07
5.36	98.2	1.8	1.8		
5.88	98.6	1.4	1.7		
6.77	99.6	0.4	<1		
6.63	99.9	0.1	<1		
7.29	99.3	0.7	<1		
8.09	93.2	6.8	6.0		
8.26	81.8	18.2	13.5	0.67	0.09
8.30	76.0	24.0	16.3	0.66	0.08
8.47	54.7	45.3	38.1	0.59	0.07
8.61	47.9	52.1	45.5	0.64	0.06
8.98	14.0	86.0	65.4	0.68	0.04
9.24	5.0	95.0	68.7	0.74	0.03
9.67	6.6	93.4	79.7	0.70	0.04
9.99	5.1	94.9	78.3	0.77	0.06

0.02 M NaNO3			ug/g
pH	U-sorb(%)	236U(aq)	238U(aq)
8.04	95.8	4.2	4.0
8.24	85.1	14.9	11.3
8.60	59.5	40.5	31.8
8.95	29.2	70.8	52.7
9.25	12.6	87.4	64.2
9.67	7.6	92.4	72.1
10.06	-0.7	100.7	82.0

0.5 M NaNO3			ug/g
pH	U-sorb(%)	236U(aq)	238U(aq)
7.49	98.9	1.1	0.7
7.87	83.9	16.1	9.9
8.15	60.0	40.0	28.6
8.50	21.2	78.8	55.0
8.86	13.7	86.3	67.2
9.46	5.5	94.5	86.5

2.5 M NaNO3			ug/g
pH	U-sorb(%)	236U(aq)	238U(aq)
7.39	89.3	10.7	9.1
7.82	58.5	41.5	33.4
8.06	33.2	66.8	57.2
8.40	10.0	90.0	89.0
8.81	3.6	96.4	89.2
9.43	0.05	99.95	90.9

With 10 mmol/L Mg		
0.1M NaNO3		
pH	U-sorb(%)	Mg(aq %)
1.63	3.0	102
2.21	11.1	99
2.72	13.8	99
3.15	23.5	96
3.61	44.9	96
4.10	61.1	95
4.33	71.6	94
4.86	89.5	93
5.73	99.2	94
6.04	99.3	93
6.70	99.6	94
7.03	98.7	94
7.93	89.9	92
8.00	89.9	95
8.30	59.4	96
8.64	31.5	94
8.84	22.1	107
9.20	16.4	94
9.63	6.0	91
9.93	-0.8	89

SUMMARY OF SORPTION DATA - NATURAL SUBSTRATES

W7 SAMPLE

Mass loading of 4g/L

Spike added	
Total U = 3e-8	
pH	U-sorb(%)
1.61	4.7
2.29	10.7
2.89	46.6
3.35	78.2
3.66	90.5
4.14	97.3
4.96	99.3
5.42	99.5

Total U = 1e-6	
pH	U-sorb(%)
1.64	9.4
2.30	18.2
2.80	27.0
3.32	43.2
3.74	61.7
4.28	84.7
4.74	94.9
5.59	98.0
6.44	98.0

Total U = 1e-4	
pH	U-sorb(%)
1.68	4.7
2.41	1.6
2.85	4.7
3.60	10.0
4.21	22.1
4.59	30.9
5.30	55.1
5.93	81.2
6.58	94.9

Appendix 2

List of selected publications by the author

1. **P.L. Airey, P. Duerden, D. Roman, C. Golian, T. Nightingale, T. Payne, B.G. Davey, D. Gray, A. Snelling and D. Lever, 1987,** 'The Prediction of the Long-term Migration of Radionuclides in the Far-field of High Level Waste Repositories: Results from the Alligator Rivers Natural Analogue Study', in *The Geological Disposal of High Level Radioactive Wastes*, (Ed. D.G. Brookins), Theophrastus Publications S.A., Athens, Greece, pp 507-524.

2. **T.E. Payne and T.D. Waite, 1991,** 'Uranium and Thorium Migration in Koongarra Groundwater - Implications to Nuclear Waste Disposal', *Chemistry in Australia,* **58:** 281-283.

3. **T.E. Payne and T.D. Waite, 1991,** 'Surface Complexation Modelling of Uranium Sorption Data Obtained by Isotope Exchange Techniques', *Radiochimica Acta,* **52/53:** 487-493.

4. **N. Yanase, T. Nightingale, T. Payne and P. Duerden, 1991,** 'Uranium Distribution in Mineral Phases of Rock by Sequential Extraction Procedure', *Radiochimica Acta,* **52/53:** 387-393.

5. **T.E. Payne, R. Edis and T. Seo, 1992,** 'Radionuclide Transport by Groundwater Colloids at the Koongarra Uranium Deposit', in *XV International Symposium on the Scientific Basis for Nuclear Waste Management* (C.G. Sombret, Ed.), Materials Research Society Symposium Proceedings, **257:** 481-488.

6. **Andrew L. Herczeg and Timothy E. Payne, 1992,** 'Recharge and Weathering Processes in Fractured Rock Aquifers in Northern Australia', 7th International Conference on Water-Rock Interaction, International Association for Geochemistry and Cosmochemistry. Published in: *Water-Rock Interaction - VII* (Y. Kharaka and A.E. Maest, Eds.) Balkema, Rotterdam, pp 561-564.

7. **T.D. Waite and T.E. Payne, 1993,** 'Uranium Transport in the Sub-surface Environment. Koongarra - A Case Study', in *Metals in Groundwater,* (Eds: H.E. Allen, E.M. Perdue and D.S. Brown). Lewis Publications, Chelsea, Michigan, pp 349-410. ISBN 0-87371-277-3.

8. **T.D. Waite, J.A. Davis, T.E. Payne, G.A. Waychunas, and N. Xu, 1994,** 'Uranium(VI) adsorption to ferrihydrite: Application of a surface complexation model', *Geochimica et Cosmochimica Acta*, **58:** 5465-5478.

9. **K.P. Hart, T.E. Payne, B.J. Robinson and P. Van Iseghem, 1994,** 'Neptunium Uptake on Boom Clay - Time Dependence and Association of Np with Fine Particles', *Radiochimica Acta*, **66/67:** 19-22.

10. **T. E. Payne, J.A. Davis and T.D. Waite, 1994,** 'Uranium Retention by Weathered Schists - The Role of Iron Minerals', *Radiochimica Acta*, **66/67:** 297-303.

11. **G.R. Lumpkin, K.P. Hart, P.J. McGlinn, T.E. Payne, R. Giere and C.T. Williams, 1994,** 'Retention of Actinides in Natural Pyrochlores and Zirconolites', *Radiochimica Acta*, **66/67:** 469-474.

12. **K.P. Hart, B.J. Robinson, T.E. Payne, P. van Iseghem and K. Lemmens, 1995,** 'Interactions Between Np-doped Synroc and Boom Clay', in *XVIII International Symposium on the Scientific Basis for Nuclear Waste Management* (T. Murakami and R. Ewing, Eds.), Materials Research Society Symposium Proceedings, **353:** 841-845.

13. **N. Yanase, T.E. Payne and K. Sekine, 1995,** 'Groundwater Geochemistry in the Koongarra Ore Deposit, Australia (I): Implications for Uranium Migration', *Geochemical Journal,* **29:** 1-29.

14. **N. Yanase, T.E. Payne and K. Sekine, 1995,** 'Groundwater Geochemistry in the Koongarra Ore Deposit, Australia (II): Activity ratios and Migration Mechanisms of Uranium Series Radionuclides', *Geochemical Journal,* **29:** 31-54.

15. **T.E. Payne, G.R. Lumpkin, P.J. McGlinn and K.P. Hart, 1995,** 'Application of a Selective Phase Extraction Procedure to Samples from the Adamello Contact Aureole', in *XVIII International Symposium on the Scientific Basis for Nuclear Waste Management* (T. Murakami and R. Ewing, Eds.), Materials Research Society Symposium Proceedings, **353:** 1259-1266.

16. **K.P. Hart, G.R. Lumpkin, R. Giere, C.T. Williams, P.J. McGlinn and T.E. Payne, 1996,** 'Naturally-Occurring Zirconolites - Analogues for the Long-term Encapsulation of Actinides in Synroc', *Radiochimica Acta,* **74:** 309-312.

17. **T.E. Payne, J.A. Davis and T.D. Waite, 1996,** 'Uranium Adsorption on Ferrihydrite - Effects of Phosphate and Humic Acid', *Radiochimica Acta,* **74:** 239-243.

18. **T. Sato, T. Murakami, N. Yanase, H. Isobe, T.E. Payne and P.L. Airey, 1997,** 'Iron Nodules Scavenging Uranium from Groundwater', *Environmental Science and Technology*, **31,** 2854-2858.

19. **Payne, T.E., Szymczak, R., and Waite, T.D., 1998.** 'Interactions between dissolved phosphorus and suspended sediments in a tropical estuary'. Published in: *Second International Conference on Environmental Problems in Coastal Regions* (C. A. Brebbia, Ed.). WIT Press / Computational Mechanics Publications, Southampton. pp 219-230. ISBN 1 85312 527 X.

20. **T.E. Payne, S. Shinners and J.R. Twining, 1998,** 'Uranium sorption on tropical wetland sediments. Published in: *Uranium Mining and Hydrogeology II,* (B. Merkel and C. Helling, Eds.). Verlag Sven von Loga, Koln. pp 298-307. ISBN 3 87361 267 4.

21. **T.E. Payne, G.R. Lumpkin and T.D. Waite, 1998,** 'Uranium^{VI} adsorption on model minerals: controlling factors and surface complexation modeling'. Chapter 2 in: *Adsorption of Metals by Geomedia: Variables, mechanisms and models* (E.A. Jenne, Ed.). Academic Press. San Diego. pp 75-97.

Appendix 3

List of papers based on the U-sorption data described in this thesis

T. E. Payne, J.A. Davis and T.D. Waite, 1994, 'Uranium Retention by Weathered Schists - The Role of Iron Minerals', *Radiochimica Acta,* **66/67:** 297-303.

T.E. Payne, J.A. Davis and T.D. Waite, 1996, 'Uranium Adsorption on Ferrihydrite - Effects of Phosphate and Humic Acid', *Radiochimica Acta,* **74:** 239-243.

T.E. Payne, G.R. Lumpkin and T.D. Waite, 1998, 'Uranium^{VI} adsorption on model minerals: controlling factors and surface complexation modeling'. Chapter 2 in: *Adsorption of Metals by Geomedia: Variables, Mechanisms and Models* (E.A. Jenne, Ed.). Academic Press. San Diego. pp 75-97.

Copies of these papers may be obtained from :

Dr T.E. Payne
Australian Nuclear Science and Technology Organisation
PMB #1
Menai
NSW 2234
Australia